Using *Caenorhabditis elegans* to Fight Human Neurodegenerative Diseases

Xi Chen

Thesis submitted in accordance with the requirements of the University of Liverpool for the degree of Doctor in Philosophy

September 2014

ABSTRACT

Debilitating age-associated neurodegenerative disorders (NDs) are a major public health challenge in increasingly ageing societies. Currently approved therapeutics are successful in slowing the progression of NDs but not in reversing or preventing the symptoms. A major goal of neurodegeneration research is therefore to identify potential new therapies for these devastating and eventually fatal disorders.

In this study, multiple well-defined *C. elegans* neurodegeneration models were integrated to uncover effective therapeutic interventions that target shared pathogenic pathways. Using locomotion behaviour and lifespan as phenotypic readouts, the well-established anti-epileptic drug ethosuximide was identified as a promising compound with the potential to combat more than one ND. It not only rescued the short lifespan and chemosensory defects of a *C. elegans* null mutant model of the rare autosomal dominant human ND known as adult-onset neuronal ceroid lipofuscinosis (ANCL), but also ameliorated the mobility defect and short lifespan of worm tauopathy and polyglutamine models based on transgenic expression of mutant human disease proteins. The ability of ethosuximide to rescue these phenotypes did not correlate well with levels of aggregated Tau and polyglutamine protein, suggesting that ethosuximide suppresses proteotoxicity without preventing protein aggregation. Although the main proposed therapeutic target of ethosuximide in epilepsy is the T-type calcium channel, deletion of its worm homologue, *cca-1*, did not affect the increase in locomotion and lifespan in the tauopathy model. This suggests that ethosuximide counteracts proteotoxicity via a novel mechanism.

To further investigate how ethosuximide might exert its neuroprotective properties, we conducted global gene expression analyses using the Affymetrix *C. elegans* whole genome microarray platform and compared the transcriptome of ethosuximide-treated ANCL models and wild-type worms to that of unexposed controls. Various downstream bioinformatic investigations including gene ontology analyses, regulatory motif discovery, publication enrichment analysis, comparative analyses with curated data sources and literature were performed and revealed a wide range of DAF-16-dependent transcriptional alterations. *C. elegans* DAF-16 is the sole orthologue of the mammalian FOXO family of transcription factors (TFs) that are implicated in the regulation of a wide range of physiological processes. Genes commonly regulated in ethosuximide-treated animals have varied roles in lipid metabolism, redox homeostasis, longevity/ageing, chromatin remodelling and ubiquitination. Many ethosuximide-responsive genes also contained DAF-16 regulatory elements within their promoter regions and were known to be among the top most responsive DAF-16 TF targets. The importance of DAF-16 in ethosuximide-mediated protection was further substantiated by RNA interference and cell culture experiments. Ethosuximide was shown to consistently induce the transcriptional activity of a subset of mammalian FOXO target genes and conferred protection against expanded polyglutamine peptides-induced aggregation in mammalian neuronal cells. These findings should encourage further screening and characterisation of other neuroprotective compounds, and ultimately may assist in expediting translational drug research and clinical testing for new therapeutic targets to combat protein conformational disorders in general.

ACKNOWLEDGEMENTS

First and foremost I must express my profound gratitude to my PI, Professor Alan Morgan. I would especially like to thank him for his guidance, motivation, patience and for trusting my capabilities, giving me the freedom to be independent, whilst always being there to provide excellent advice when required. His enthusiasm and constant willingness to discuss the project, research and life in general, and career prospects will always be greatly appreciated.

Along with a great supervisor, comes a great lab. Red Block is a unique place and I have spent a very content four years in this laboratory. There are many from the lab that have guided my progress in protocols and provided experimental support and encouragements during the process of completing my Ph.D. I would like to thank in particular Dr. James Johnson (guru of worm knowledge, technical issues and things in general), Dr. Lee Haynes, Dr. Hannah McCue and Dr. Matthew Edmonds for their good humour and for putting up with my constant nagging questions and took time out to answer each one of them patiently. My thanks and sincere gratitude also goes to Professor Bob Burgoyne and Dr. Jeff Barclay for their guidance and advice. I extend my gratitude to Dayani Rajamanoharan, Hannah McCue and Paul Todd for their friendship, scientific discussions, feedback, and constant support – you guys are AWESOME!!!! Thank you for sharing my taste in films and for always being there to listen, advise and cheer me on, and for making lab life even more fun by bringing in homemade cakes, biscuits and endless supply of chocolates and sweets. I will miss working with all of you. Special thanks to all the Red Blockers past and present for

making the lab such a great environment to work in and for all the great laughs and fun we had on lab outings and parties - Dr. Sudhanva Kashyap, Dr.Vicky Martin, Dr. Leanne Bloxam, Dr. Pryank Patel, Mimi Ayala, Joanna Wardyn, Jennifer Mak, Steven Dodd, Sarah Darling, Joe Zeguer, Marie Cawkwell and Dr. Andy Herbert. To honorary Red Blockers Dr. Martin Smith, Ailsa Dermody for being relentlessly enthusiastic and always taking the time to go through talks, posters and writing with me; Emmanuel Oke for his insights and help on confocal microscopy. Thanks to those people who kindly read and commented on draft chapters of this thesis: Hannah McCue, Matthew Edmonds, Jeff Barclay, Vicky Martin and of course Alan Morgan.

I express my gratitude towards all my wonderful friends near and far who I confided in, laughed and travelled with during my graduate studies. Special thanks to Phoedi, Tim, Angela, Alan and Sam for listening to my many rants and giving me excuses to take days off.

I would also like to take this opportunity to say how immensely grateful I am to my family for their unwavering love and support. A HUGE thank you to Mum and Dad for giving me strength and perseverance throughout my PhD and for always asking how my worms are getting on and pretend to feign interest when I get excited about a major result involving worms. Last but not least I would like to acknowledge those worms that have been sacrificed for the purpose of this project.

TABLE OF CONTENTS

ABBREVIATIONS

6-OHDA	6-hydroxydopamine
AA	Ascorbic acid
AD	Alzheimer's Disease
AEDs	Antiepileptic drugs
aex-3	Aboc EXpulsion defective-3
AKT/PKB	Protein kinase B
ALS	Amyotrophic Lateral Sclerosis
ANCL	Adult-onset Neuronal Ceroid Lipofuscinosis
APOE4	APOlipoprotein E-4
APP	Amyloid Precursor Protein
ASM	Acid sphingomyelinases
ATP	Adenosine TriPhosphate
ATXN3	ATAXIN-3
Aβ	Amyloid-beta
BACE	Beta-site APP Cleaving Enzyme
BDNF	Brain-derived neurotrophic factor
BSA	Bovine serum albumin
cAMP	Cyclic adenosine monophosphate
CAG	Cytosine–adenine–guanine
CDC7	Cell division cycle kinase 7
CGC	Caenorhabditis Genetics Centre
CHIP	C terminus of the Hsc70-interacting protein
ChIP-Seq	Chromatin Immunoprecipitation & Next Generation Sequencing
CLN	Ceroid-Lipofuscinosis, Neuronal
CREB	cAMP response element-binding protein
CSF	Cerebrospinal fluid
CSPα	Cysteine String Protein alpha
CTD	Comparative Toxicogenomic Database
CTSD	Cathepsin D
CYP	Cytochromes P450
DAE	DAF-16-associated element
DAergic	Dopaminergic
daf	Abnormal DAuer Formation
dat-1	Dopamine active transporter 1
DAVID	Database for Annotation, Visualization and Integrated Discovery
DBE	DAF-16-binding element
DE	Differential expression
DEGs	Differentially expressed genes
DEPC	Diethylpyrocarbonate-treated
DMEM	Dulbecco's Modified Eagle Medium
DMSO	Dimethyl Sulphoxide
DNA	Deoxyribonucleic Acid
DNAJC5	DnaJ homolog subfamily C member 5
DNJ	DnaJ domain-containing protein
dnj-14	DNaJ domain
DRPLA	Dentatorubral pallidoluysian atrophy

EAK	Enhancer-of-akt-1
ECL	Enhanced chemiluminescence
EIF4G1	Eukaryotic translation initiation factor 4 gamma 1
ELT	Erythroid-like transcription factor family
ER	Endoplasmic Reticulum
ERK	Extracellular signal-regulated kinases
FA	Formic acid
FC	Fold change
FDR	False discovery rate
FOXL1	Forkhead box L1
FOXO	Forkhead Box Class O
FTDP	Frontotemporal Dementia and Parkinsonism
FUS	Fused in Sarcoma
GABA	Gamma-Aminobutyric Acid
GAD	Glutamic Acid Decarboxylase
GBA	Glucosidase, Beta, Acid
GFP	Green fluorescent protein
glit-1	GLIoTactin homolog-1
GO	Gene Ontology
GST	Glutathione S-transferase
GWAS	Genome-wide association studies
HD	Huntingtin's Disease
HDAC	Histone deacetylases
HIP-1	Huntingtin Interacting Protein-1
hipr-1	Huntington Interacting Protein Related-1
hop-1	Homolog Of Presenilin-1
HRP	Horseradish peroxidise
Hsc70	Heat Shock Cognate 70
Hsf-1	Heat Shock Factor-1
Hsp-16	Heat Shock Protein-16
Hsp40	Heat Shock Protein-40
Hsp70	Heat Shock Protein-70
HTS	High-throughput screening
Htt	Huntingtin
IBM	Inclusion Body Myositis
IGF-1	Insulin like Growth Factor-1
IIS	Insulin like Growth Factor-1 like Signalling
IL	Inner Labial
IPTG	Isopropyl β-D-1-thiogalactopyranoside
KCNJ	Potassium inwardly-rectifying channel
KEGG	Kyoto Encyclopedia of Genes and Genomes
KLF	Kruppel-like factor
LB	Luria-Bertani broth
LRRK2	Leucine-rich repeat kinase-2
LVA	Low voltage activated
MAPK	Mitogen-activated protein kinase
MAPT	Microtubule-associated protein Tau
mec	MEChanosensory abnormality

MEF2A	Myocyte specific enhancer factor
Mib1	Mind bomb 1
MJD	Machado-Joseph disease
Mn^{2+}	Manganese
MPTP	1-methyl 4-phenyl 1,2,3,6-tetrahydropyridine
mTOR	Mammalian Target Of Rapamycin
N2A	Neuro2A
NAD	Nicotinamide adenine dinucleotide
NCL	Neuronal Ceroid Lipofuscinosis
NDs	Neurodegenerative disorders
NFT	Neurofibrillary Tangles
NGF	Neuronal growth factor
NGM	Nematode Growth Media
NINDS	National Institute of Neurological Disorders and Stroke
NMJ	Neuromuscular Junction
Nrf2	Nuclear factor (erythroid-derived 2)-like-2
OASIS	Online Application for the Survival Analysis of Lifespan Assays
PBS	Phosphate Buffered Saline
PCA	Principal components analysis
PCR	Polymerase Chain Reaction
PD	Parkinson's disease
PDE	PhosphoDiEsterase
PEG	Polyethylene Glycol
PI 3-kinase	Phosphatidylinositol 3-kinase
PINK1	PTEN induced putative kinase-1
polyQ	Polyglutamine
PPT-1	Palmitoyl protein thioesterase
pqe-1	PolyQ toxicity Enhancer
PSEN1/2	Presenilin-1/ Presenilin-2
PTL-1	Protein with tau-like repeats
qRT-PCR	Real-time quantitative PCR
RAB	Reassembly
REST	Repressor element 1-silencing transcription factor
ric	Resistance to Inhibitors of Cholinesterase
RIPA	Radio-immunoprecipitation assay
RNAi	Ribose Nucleic Acid Interference
ROS	Reactive oxygen species
rpm	Revolutions per minute
RSAT	Regulatory Sequence Analysis Tools
SBMA	Spinobulbar muscular atrophy
SCA	Spinocerebellar ataxia
SCF	Skp1-Cullin-F-box
SDR	Short-chain dehydrogenase
SDS	Sodium dodecyl sulphate
SDS-PAGE	Sodium dodecyl sulphate polyacrylamide gel electrophoresis
sel-12	Suppressor/Enhancer of Lin-12
SEM	Standard Error of the Mean
SGT	Small glutamine-rich TPR-containing protein

sir-2.1	Silent Information Regulator-2.1
SK	Small conductance Ca^{2+}-activated K^{+} channels
skn-1	SKiNhead
SMA	Spinal Muscular Atrophy
SMN	Survival Motor Neuron
SNAP-25	Synaptosomal-associated protein 25
SNARE	Soluble NSF Attachment Protein REceptor
snb-1	SyNaptoBrevin related-1
sng-1	Synaptogyrin
snRNP	Small nucleolar ribonucleoprotein
SOC	Super optimal broth with catabolite suppression
SOD	Superoxide dismutase
spe-4	Defective SPErmatogenesis-4
SPELL	Serial Pattern of Expression Levels Locator
SUT	Suppressor of Tau Pathology
SWI/SNF	SWItch/sucrose non-fermentable
TBP	TATA-binding protein
TDP-43	TAR DNA binding protein 43
TFBS	Transcription factor binding sites
TFs	Transcription factors
TGF-β	Transforming growth factor beta
TOR-2	Human TORsin related-2
TPP1	Tripeptidyl peptidase-1
TSA	Trichostatin A
TSSs	Transcription start sites
TTR	TransThyretin-Related
UCH-L1	Ubiquitin carboxy-terminal hydrolase L1
UDP	Uridine diphosphate
UGTs	UDP-glucuronosyl/glucosyl transferases
unc	UNCoordinated phenotype
UPS	Ubiquitin-proteasome system
UTR	Untranslated region
UV	Ultraviolet
VA	Valproic acid
VPS35	Vacuolar protein sorting 35
WASH	Wiskott-Aldrich syndrome and SCAR homolog complex
YFP	Yellow Fluorescent Protein

CHAPTER 1: INTRODUCTION

1.1 OVERVIEW OF HUMAN NEURODEGENERATIVE DISEASES

Despite two decades of intense molecular research and the identification of many specific causative mutations, debilitating neurodegenerative diseases (NDs) including the common and renowned disorders such as Alzheimer's disease (AD) and Parkinson's disease (PD), and other less frequent forms such as Hungtinton's disease (HD), spinocerebellar ataxia (SCA), amyotrophic lateral sclerosis (ALS) and prion diseases afflict millions worldwide and remain a significant and unresolved financial and social burden facing ageing populations. Therapies for these devastating and eventually fatal disorders are lacking and pharmaceutical research on new potential treatments has been one of the main fields of investigation.

NDs are characterised by progressive neuropsychiatric dysfunction and the loss of structure and function of specific neuronal circuitry that in turn result in behavioural symptoms. NDs can occur either on a completely hereditary basis (e.g. HD) or sporadically in the majority of cases (e.g. AD, PD, ALS). In spite of the diversity in the underlying genes involved, inheritance patterns, clinical manifestation and exact sites of neuropathology, the rare, early onset familial (also known as Mendelian) forms and the more prevalent late-onset sporadic forms of different NDs share some common genetic origins and pathological hallmarks such as the progressive and chronic nature of the disease, the extensive loss of specific neuronal subtypes, synaptic dysfunctions, the formation and deposition of misfolded protein aggregates (Muchowski, 2002, Taylor *et al.*, 2002, Soto and Estrada, 2008). Research and technological innovations over the past 10 years have

made considerable progress in the elucidation of mechanisms of ND initiation and progression that lead to neurodegeneration. Emerging common themes in the pathogenesis of neurodegeneration include: aberrant phosphorylation, palmitoylation and acetylation of disease-causing proteins, protein misfolding, deficient ubiquitin–proteasome system (UPS) or autophagic process to clear disease-causing proteins, altered RNA metabolism, oxidative stress, mitochondrial dysfunction, excitotoxicity, disrupted axonal transport, neuroinflammation and microglial activation (Ehrnhoefer *et al.*, 2011). Linkage analysis, high-throughput sequencing and genome-wide association studies (GWAS) have also identified susceptibility genes in many NDs (Table 1.1) with the promise to help unravel even more genes, novel loci and common genetic variants associated with the diverse collection of human NDs. Thus developments of therapeutic interventions that are applicable across the broad spectrum of NDs and target the shared pathogenic mechanisms may offer the best hope for a future neuroprotective therapy.

1.1.1 Alzheimer's disease

AD is the most common ND, affecting 35 million patients worldwide. Clinically, it is characterised by progressive loss of short-term memory and cognitive domains toward a state of profound dementia. AD is pathologically characterised by neuronal loss and the formation of extracellular amyloid plaques and intracellular neurofibrillary tangles (NFTs) due to aggregation of two proteins, amyloid-β (Aβ) and Tau, respectively (Gandhi and Wood, 2010). AD is genetically heterogeneous, and can be caused by one or more of several genes as well as environmental factors. There are two different forms of AD. The first is early-onset familial AD (< 40 years), which accounts

for less than 5% of all AD cases (Campion *et al.*, 1999), and is caused by rare single dominant mutations in genes encoding amyloid precursor protein (APP), and/or the enzymes involved in APP processing: γ-secretase components presenilins (PSEN), PSEN1 and PSEN2 (Shastry, 1998). Missense mutations in these three genes favour the aberrant proteolytic processing of APP by the amyloidogenic pathway as well as increasing the self-aggregation of Aβ into amyloid fibrils. The sequential cleavage of APP is mediated by the concerted action of both β-secretase [β-site APP-cleaving enzyme, BACE] and γ-secretase complex which consists of PSEN1 or PSEN2, anterior pharynx defective 1, presenilin enhancer 2 and nicastrin which lead to the generation of the extracellular Aβ peptide (Takasugi *et al.*, 2003, Turner *et al.*, 2003). This peptide fragment is prone to aggregation and is a primary component of amyloid senile plaques which are fundamental to the pathogenesis of AD and can be detected in the post-mortem brain samples of patients with AD. Aβ has also been found to accumulate in muscles of patients with inclusion body myositis (IBM). The causes of the more common sporadic late-onset AD (> 65 years) are genetically complex with heritability estimates up to 80%, and are clinically and pathologically similar to familial cases. Its complex aetiology is attributed to interactions between susceptibility genes involved in lipid homeostasis (*APOE, CLU/APOJ, ABC1, ABCA7*), endocytosis (*BIN1, PICALM, CR1, CD2AP*), membrane-spanning 4 domains family proteins (*MS4A6A, MS4A4E*), and environmental risk factors such as age, hypertension, oestrogen supplements, smoking, stroke, heart disease, depression, arthritis, and diabetes (Bertram *et al.*, 2010, Ridge *et al.*, 2013). The inheritance of the ε4

allele of apolipoprotein is the single strongest genetic risk factor for sporadic AD (Maioli *et al.*, 2012).

In addition to amyloid plaques, AD, Pick's disease, corticobasal degeneration, Down's syndrome and specific types of frontotemporal dementia (FTD): frontotemporal dementia with parkinsonism chromosome 17 type (FTDP-17) and frontotemporal lobar dementia (FTLD) are associated with intraneuronal accumulation of NFTs. There is a strong clinical and pathologic overlap between FTD, AD and ALS. NFTs are composed of the microtubule-associated protein Tau which aggregates into insoluble fibrillar deposits when it is hyperphosphorylated (Mandelkow and Mandelkow, 1998) and is detectable in post-mortem brain samples of patients with AD. Mutations in genes encoding Tau (*MAPT*), progranulin (*GRN*), and chromatin-modifying protein 2B (*CHMP2B*) have been identified in FTD. Certain mutations in Tau (missense and deletions) including: G272V, delK280, P301L, P301S, V337M, G389R, and R406W may lead to reduced microtubule binding and an increased propensity to aggregate (Ingram and Spillantini, 2002). Other proposed pathogenic mechanisms include inflammation and cerebral hypoperfusion. Together, these are all important targets for disease-modifying therapies (Ehrnhoefer *et al.*, 2011).

1.1.2 Neuronal ceroid lipofuscinoses

The neuronal ceroid lipofuscinoses (NCLs) represent the most common group of diverse hereditary NDs of children (Haltia, 2006), distinguished from other NDs by an excess accumulation of autofluorescent, electron dense storage materials ceroid and lipofuscin in multiple tissues including neurons (Jalanko and Braulke, 2009). Another quintessential feature shared by these

genetically distinct types of NCLs is the progressive and selective loss of neurons particularly in cerebral and cerebellar cortex and, less constantly in retina, leading to dementia, epilepsy, blindness and motor deterioration (Schulz *et al.*, 2013). Despite being lesser studied than other major NDs, our understanding of the molecular basis of different NCLs has advanced significantly in recent years as defective NCL genes and the corresponding proteins have been established for all major typical and atypical NCL forms by using various early clinical, neuropathological, biochemical and molecular genetic studies (Haltia, 2006), as well as animal models (canines, sheep, mice) (Goebel *et al.*, 1982, Mayhew *et al.*, 1985, Pardo *et al.*, 1994, Koike *et al.*, 2000). To date, mutations that cause NCL have been found in at least 14 human genes (*CLN1/PPT1, CLN2/TPP1, CLN3, CLN4/DNAJC5, CLN5, CLN6, CLN7/MFSD8, CLN8, CLN10/CTSD, CLN11/GRN, CLN12/ATP13A2, CLN13/CTSF, CLN14/KCTD7, CLCN6*, *CLCN7* and *SGSH*) (Peltonen *et al.*, 2000, Siintola *et al.*, 2006a, Kmoch *et al.*, 2013). Over 260 causative mutations were identified and multiple sets of molecular data have also shown that different mutations in a single NCL gene can give rise to different forms of NCLs (Mitchison and Mole, 2001).

The typical NCL symptoms and characteristic lysosomal storage material have been shown to be caused by defects in either lysosomal enzymes (*CLN1/PPT1, CLN2/TPP1, CLN10/CTSD, CLN13/CTSF*) or in novel transmembrane proteins of unknown function (*CLN3, CLN6, CLN7/MFSD8, CLN8*) (Boustany, 2013, Schulz *et al.*, 2013). More recent work has shown that mutations in a synaptic chaperone gene (*CLN4/DNAJC5*) (Noskova *et al.*, 2011), a granulin precursor gene

(*CLN11/GRN*) (Smith *et al.*, 2012a), ATPase gene (*CLN12/ATP13A2)* (Bras *et al.*, 2012) and a potassium channel gene (*CLN14/KCTD7*) (Staropoli *et al.*, 2012) also cause NCLs.

Depending on the age at onset of symptoms, characteristic clinical features, histological findings, and genetic loci, these genetically distinct subtypes of NCLs are classified as congenital, infantile, late infantile, juvenile or adult. A mutation in the *CLN10/CTSD* gene causes lysosomal enzyme cathepsin D deficiency and results in the congenital NCL form where accumulation occurs in the majority of tissues and starts as early as the first semester and death occurs in early infancy (Siintola *et al.*, 2006b). Infantile onset NCL is associated with the deficiency of the lysosomal enzyme palmitoyl protein thioesterase 1 (*PPT1*) and mutation in a potassium channel gene (*KCTD7)* (Vesa *et al.*, 1995, Staropoli *et al.*, 2012). Late infantile-onset NCL is the most genetically heterogeneous form. While classical late infantile-onset NCL is associated with the deficiency of the lysosomal enzyme tripeptidyl peptidase 1 (*CLN2/TPP1*), causative mutations for variant late infantile-onset NCL are found in *CLN1/PPT1*, *CLN5, CLN6, CLN7/MFSD8* and *CLN8* genes (Kousi *et al.*, 2009). Juvenile onset NCL is caused due to many mutations and polymorphisms in the *CLN3* and *CLN1* genes (Palmer *et al.*, 2013).

Adult-onset NCL which is also known as Kufs and Parry disease has an autosomal recessive and an autosomal dominant form (Mimura *et al.*, 1992, Burneo *et al.*, 2003, Ivan *et al.*, 2005). Onset is usually in the fourth decade of life but earlier presentations have also been reported (Schulz *et al.*, 2013). While autosomal recessive mutations in *CLN3, CLN5*, *CLN6*,

CLN10/CTSD *CLN11/GRN*, *CLN13/CTSF* and *PPT1* genes have been observed in the Kufs variant forms of ANCL (Siintola *et al.*, 2006a, Smith *et al.*, 2013), the genetic and molecular basis of ANCL with dominant inheritance (Parry's disease) was not known until recently. Using a combination of linkage analysis, copy-number analysis, gene-expression analysis, and exome sequencing, several independent groups have discovered that *CLN4B*, autosomal-dominant adult-onset NCL, is caused by mutations in the *DNAJC5* gene encoding the cysteine-string protein alpha, (CSPα) (Benitez *et al.*, 2011, Noskova *et al.*, 2011, Velinov *et al.*, 2012, Cadieux-Dion *et al.*, 2013). CSPα is a neuroprotective presynaptic co-chaperone with an essential physiological role in presynaptic proteostasis and the maintenance of exocytotic release of neurotransmitter, hormones and enzyme precursors. Numerous studies have also provided critical insights into the neuroprotective role of CSPα in NDs. CSPα has been linked to both HD and PD as it was shown to not only interact with mutant huntingtin *in vitro* (Miller *et al.*, 2003), but also functionally overlap *in vivo* with α-synuclein, for preventing neurodegeneration (Chandra *et al.*, 2005). Deletion of CSPα in flies and mice impairs synaptic function and results in neurodegeneration, behavioural deficits and premature death (Zinsmaier *et al.*, 1994, Fernandez-Chacon *et al.*, 2004).

1.1.3 Polyglutamine disorders

Among the dynamic repeat expansion diseases, the diverse polyglutamine (polyQ) disorders represent the most common class of hereditary NDs, encompassing nine NDs: HD, spinobulbar muscular atrophy (SBMA), dentatorubral pallidoluysian atrophy (DRPLA) as well as SCA types 1, 2, 3, 6,

7 and 17 (Kakizuka, 1998, Kopito and Ron, 2000, Stefani and Dobson, 2003). With the exception of SBMA, an X-linked recessive disease, all other polyQ disorders are autosomal dominantly inherited. Each of these disorders is caused by abnormal exonic trinucleotide cytosine–adenine–guanine (CAG) repeat expansions, within disease-causative genes in different chromosomes and exhibits ageing- and CAG tract length-dependent onset, selective neuronal vulnerability, and a progressive, usually fatal, clinical course. Each disorder has a characteristic pathological threshold polyQ length below which disease does not occur (Gusella and MacDonald, 2000, Zoghbi and Orr, 2000). HD, the most common and a fully penetrant polyQ disease, is triggered by the expression of at least 36 CAG repeats located in exon 1 of the *HTT* gene, which encodes the large and multifunctional huntingtin protein (Htt). SCA1, an inherited cerebellar ataxia, arises as a result of at least 39 CAG repeats present in exon 8 of the *ATXN1* gene on chromosome 6p23, which codes for the ataxin-1 protein involved in RNA metabolism and transcriptional regulation, and SCA3 (also known as Machado-Joseph disease, MJD) is induced by a CAG expansion repeat of at least 60 or more in exon 10 of the *ATXN3* gene (14q32.1) encoding the ataxin-3 protein with deubiquitinating activity (Fiszer and Krzyzosiak, 2013). A hallmark of polyQ-expansion diseases is the intranuclear, intracellular and/or extracellular aggregation of expanded polyQ proteins which is a well-conserved pathological feature and has been the focus of extensive investigation (Stefani and Dobson, 2003). Studies from mouse models of polyQ diseases have demonstrated that the onset of apparent symptomatic impairment often precedes detectable neuropathology (Figiel *et al.*, 2012). Common themes

that emerge from studies of pathogenesis and neuronal dysfunction in polyQ diseases include transcriptional dysregulation of intracellular Ca^{2+} homeostasis, impairment of the UPS, decreased axonal transport, alterations in levels of brain-derived neurotrophic factor (BDNF) and neuronal growth factor (NGF), RNA toxicity, altered intracellular trafficking, sequestration of critical cellular proteins in aggregates, aberrant caspase activation, altered energy metabolism, and synaptic and mitochondrial dysfunction (La Spada *et al.*, 2011). PolyQ pathogenesis has been attributed to a gain of function due to the toxicity of the proteins carrying a polyQ expansion (Orr and Zoghbi, 2007). However, the exact mechanisms underlying expanded polyQ toxicity, neuronal dysfunction, progression of symptoms, and, ultimately, neuronal death remain unclear.

1.1.4 Parkinson's disease

PD belongs to the family of synucleopathies and is the second most common ND after AD (Lesage and Brice, 2009). Clinically, it is characterised by a progressive motor syndrome comprising bradykinesia, postural instability, rigidity, resting tremor which have been long attributed to the selective degeneration of nigral-striatal dopaminergic (DAergic) neurons, as well as non-motor features of cognitive decline, neuropsychiatric symptoms, sleep disturbance and autonomic dysfunction (Chaudhuri *et al.*, 2006). Pathologically, PD is characterised by the loss of DAergic neurons in the substantia nigra pars compacta, and the presence of intraneuronal cytoplasmic inclusions called Lewy bodies in surviving neurons of affected brain regions, which are rich in α-synuclein. As with AD, the prevalence of PD increases with age and it is largely a late-onset sporadic

neurodegenerative condition (Gandhi and Wood, 2010). Rare and early-onset familial PD, which accounts for 5-10% of all cases is usually monogenic in origin, and is caused by either autosomal-dominantly (*SNCA/PARK1/4, UCHL1/PARK5, LRRK2/PARK8, PARK11, VPS35/PARK17, EIF4G1/PARK18*) or autosomal-recessively (*Parkin/PARK2, PINK/PARK6, DJ-1/PARK7, ATP13A2/PARK9, PLA2G6/PARK14, FBX07/PARK15*) inherited mutations (Table 1.1) (Gandhi and Wood, 2010). These genetic mutations were shown to converge onto several main cellular pathways which are associated with mitochondrial metabolism, synaptic transmission (exocytosis and endocytosis), sorting and recycling of endosomal receptors, and autophagy–lysosomal pathways. A number of genes such as α-synuclein (*SNCA/PARK1*) and leucine-rich repeat kinase 2 (*LRRK2*/*PARK8*) which account for a substantial proportion of autosomal-dominant PD cases, have also provided insight into the sporadic forms of PD. Mutations in *LRRK2* are the most frequent genetic cause of familial PD (Zimprich *et al.*, 2004). Almost 80 *LRRK2* gene variants have been reported worldwide, at least seven are proven pathogenic mutations and appear to cause PD pathogenesis by enhancing the kinase activity, inhibiting the GTPase activity, and altering the dimerisation, subcellular localisation or distinct protein interactions of LRRK2 (Gómez-Suaga *et al.*, 2014). These include: N1437H, R1441C/G/H, Y1699C, S1761R, G2019S, I2012T and I2020T (Cookson, 2010). Genomic multiplications (duplications, triplications) and missense mutations in the *SNCA* gene, including A53T, A30P, H50Q, G51D, E46K, though extremely rare in sporadic PD, are the second most common cause of dominantly

inherited PD. The *SNCA* gene product α-synuclein is abundantly expressed in the central nervous system and is the primary structural component of Lewy bodies. Recent work provided important evidence for a gain of function by α-synuclein to underlie PD pathophysiology and mechanisms leading to pathogenic function of α-synuclein may include formation of membranous pores that permeabilise cellular membranes (Martin *et al.*, 2011), neuroinflammation, prion-like spreading, sequestration in Lewy bodies, and interplay between Tau, microtubule dysfunction and metal dyshomeostasis (Chege and McColl, 2014).

However, incomplete penetrance of these mutations suggests additional genetic risk factors and interactions with the environment are crucial for developing disease. Indeed, recent genetic findings have identified rarer causes of familial PD or parkinsonism, which include mutations in: *DNAJ* genes (*DNAJC6, DNAJC13)*, inflammation genes (*HLA-DRA),* glucocerebrosidas (*GBA*)*,* GTP cyclohydrolase 1 (*GCH1),* membrane-associated genes (*GAK–DGKQ, RAB7L1, BST1)*, vacuolar protein sorting 35 (*VPS35*) and eukaryotic translation initiation factor 4 gamma 1 (*EIF4G1*) (Trinh and Farrer, 2013). *VPS35* is an essential component of the retromer cargo-recognition complex involved in endosomal-lysosomal trafficking. The identification of an aspartate to asparagine substitution (D620N) in *VPS35* by multiple groups thus provides a compelling genetic link for retromer dysfunction in familial autosomal dominant and sporadic PD (Vilarino-Guell *et al.*, 2011, Zimprich *et al.*, 2011), and most recent work further suggested that perturbed endosome-to-trans-Golgi network (TGN) transport and impaired association with the actin-polymerising Wiskott-Aldrich syndrome and SCAR

homolog (WASH) complex caused by D620N mutation could contribute to PD aetiology (McGough *et al.*, 2014).

Furthermore, mutations in Parkin (*PARK2*), PINK1 (*PARK6*) and DJ1 (*PARK7*) have been linked to autosomal recessive juvenile onset parkinsonism (Gandhi and Wood, 2010) and were shown to affect mitochondrial biogenesis and induction of autophagy. More rarely, recessively inherited forms of atypical parkinsonism are caused by mutations in the ATPase type 13A2 (*ATP13A2*), phospholipase A2, group VI (*PLA2G6*), pantothenate kinase (*PANK2*) and F-box only protein 7 (*FBXO7*) genes (Trinh and Farrer, 2013). Supporting the hypothesis that dysfunction of mitochondrial complex I, oxidative stress and compromised energy level of DAergic neurons are implicated in the pathogenesis of PD, exposing worms, rodents or primates to compounds which inhibit mitochondrial complex I activity and induce oxidative stress, such as methyl 4-phenyl 1,2,3,6-tetrahydropyridine (MPTP), paraquat, and rotenone, caused selective DAergic neuronal loss, neuronal dysfunction as well as protein accumulations immunopositive for α-synuclein (Hisahara and Shimohama, 2010). Taken together, these discoveries have highlighted the importance of the UPS, mitochondrial metabolism, oxidative stress, synaptic transmission, endosomal trafficking and autophagy–lysosomal pathways in PD pathogenesis. Other genes, such as ubiquitin *UCHL1/PARK5*, probable nuclear receptor *NR4A2*/*NURR1* and serine protease *HTRA2*/*OMI*, have also been associated with PD, although their roles remain unclear (Gandhi and Wood, 2010).

Disease name	Human gene	Function	*C. elegans* gene
AD GENES			
EOFAD	*APP*	Neuronal development and synaptic formation and repair	*apl-1*
	PSEN1/2	Gamma-secretase activity	*sel-12, hop-1 and spe-4*
	APH1/2		*aph-1, pen-2 and aph-2*
AD, FTD	*MAPT*	Microtubule stabilisation	*ptl-1*
LOAD	*APOE* (ε4-allele)	Lipid/cholesterol metabolism	–
ALS GENES			
Familial and sporadic ALS with or without FTD	*SOD1*	Superoxide metabolism	*sod-1*
	TARDBP	RNA metabolism	*tdp-1*
	FUS	RNA metabolism	*fust-1*
	OPTN	Vesicular transport	–
	VCP	Vesicular transport	*cdc-48.1/2*
	UBQLN2	Proteasome	*ubqnl-1*
	C9ORF72	regulate endosomal trafficking and autophagy in neuronal cells	*alfa-1*
	SQSTM1	Autophagy	*sqst-2*
	PFN1	Cytoskeleton dynamics	*pfn-1*
Rare causes of ALS or ALS-like syndromes	*DCTN1*	Cytoskeleton dynamics	*dnc-1*
	ALS2	Endocytosis	–
Familial and sporadic ALS with or without FTD	*CHMP2B*	Vesicular transport	
	FIG4	Vesicular transport	*C34B7.2*
	HNRNPA2B1	RNA metabolism	*hrp-1*
Sporadic ALS	*ELP3*	–	–
Juvenile ALS	*SETX*	RNA processing	
Typical ALS	*HNRNPA1*	RNA processing	*hrp-1*
Sporadic ALS	*ATXN2*	–	*atx-2*
Familial and sporadic ALS	*ANG*	Blood vessels formation	–
Juvenile ALS	*SPG11*	DNA damage	
Typical and atypical ALS	*VAPB*	Vesicular transport	*vpr-1*
	NEFH	Cytoskeleton dynamics	*H39E23.3*
Familial ALS	*ARHGEF28*	RNA metabolism	*rhgf-1*
NCL GENES			
Infantile NCL	*CLN1/PPT1*	Palmitoyl-protein thioesterase 1 precursor	*F44C4.5/ppt-1*
Congenital ovine NCL	*CLN10/CTSD*	Cathepsin D precursor	*R12H7.2b/asp-4*
Late infantile NCL	*CLN2/TPP1*	Tripeptidyl-peptidase 1 precursor	–
	CLN5, CLN6, CLN8	–	
Juvenile NCL	*CLN3*		*F07B10.1/cln-3.1*
			C01G8.2/cln-3.2
			ZC190.1/cln-3.3
Adult-onset NCL	*CLN4/DNAJC5*	neuroprotective presynaptic co-chaperone	*dnj-14*
PD GENES			
EOPD	*PARK1/PARK4/SNCA*	Neurotransmitter release	–

Disease name	Human gene	Function	*C. elegans* gene
	PARK2/Parkin	Target proteins for degradation, maintenance mitochondrial function	*pdr-1*
Classical PD	*PARK3*	–	–
	PARK5/UCHL1		*ubh-1*
EOPD	*PARK6/PINK1*	Oxidative stress response, maintenance mitochondrial function	*pink-1*
	PARK7/DJ-1	Redox sensor, antioxidant	*djr-1.1, djr-1.2*
Classical PD	*PARK8/LRRK2*	Mixed lineage kinase	*lrk-1*
Atypical PD with dementia, spasticity, and supranuclear gaze palsy	*PARK9/ATP13A2*	–	*capt-6*
Classical PD	*PARK10*		–
Late-onset PD	*PARK11*		
Classical PD	*PARK12*		
	PARK13/HTRA2	Mitochondrial serine protease	
Early-onset dystonia-parkinsonism	*PARK14/PLA2G6*	–	
Early-onset parkinsonian-pyramidal syndrome	*PARK15/FBX07*		
Classical PD	*PARK16*		
	PARK17/VPS35	Autophagy; endosome-to-Golgi retrieval	*vps-35*
	PARK18/EIF4G1	–	–
Late-onset PD	*GBA*	Lysosome	*F11E6.1, TO4A8.7*
POLYQ GENES			
HD	*HTT*	Transcriptial repressor, membrane trafficking, endocytosis	–
SBMA	*AR*	Nuclear receptor, androgen response	
DRPLA	*ATN1*	Nuclear receptor corepressor, transcriptional corepressor	
SCA1	*ATXN1*	RNA processing, transcription factor, transcriptional corepressor, general repressor of transcription	*K04F10.1*
SCA2 and ALS	*ATXN2*	RNA binding protein.	*D2045.1/atx-2*
SCA3, MJD	*ATXN3*	Transcription factor, transcriptional coactivator, transcriptional repressor, histone H2B deubiquitinase	*atx-3*
SCA6	*CACNA1 A*	Voltage-gated calcium channel, transcription factor	–
SCA7	*ATXN7*	Integral member of SAGA complex, regulation of histone acetylation and ubiquitination	
SCA17	*ATXN17*	General transcription factor, member of TFIID complex	
SMA GENES			
SMA	*SMN1/2*	spliceosomal snRNP assembly and in pre-mRNA splicing	*smn-1*

Table 1.1: Known human neurodegenerative disease (ND) associated-genes and their *C. elegans* orthologues. Human NDs: AD, Alzheimer's disease; ALS, Amyotrophic lateral sclerosis; DRPLA, dentatorubral pallidoluysian atrophy; EOFAD, early-onset familial Alzheimer's disease; EOPD, early-onset Parkinson's disease; FTD, Frontotemporal dementia; HD, Huntington's disease; LOAD, late-onset Alzheimer's disease; MJD, Machado–Joseph disease; NCL, neuronal ceroid lipofuscinosis; PD, Parkinson's disease; SBMA, spinobulbar muscular atrophy; SCA, spinocerebellar ataxias; SMA, Spinal muscular atrophy.

1.1.5 Amyotrophic lateral sclerosis

ALS, also known as Lou Gehrig's disease, is the most common late-onset motor neuron disease characterised by the progressive degeneration of upper (cortical) and lower motor neurons (spinal cord), the loss of myelin in the spinal cord, the presence of neuroinflammation, muscle dysfunction, and eventually paralysis (Pasinelli and Brown, 2006). The vast majority (90-95%) of ALS cases are sporadic (Boillée *et al.*, 2006), however, a small percentage is familial in origin, exhibiting an autosomal dominant mode of inheritance. Mutations in the copper/zinc superoxide dismutase (*SOD1*) gene (Rosen *et al.*, 1993) has been identified as the most common source of familial ALS causing approximately 20% of cases (Barber and Shaw, 2010). As a result, the majority of ALS research has focused on the role of *SOD1* mutations in disease pathogenesis. The widely expressed homodimeric, cytosolic enzyme, SOD1 catalyses the conversion of unstable superoxide radicals ($\bullet O_2^-$) to oxygen (O_2) and hydrogen peroxide (H_2O_2), providing an important antioxidant defence. Since overexpression of mutant human SOD1 in mice causes a motor neuropathy similar to ALS, whereas knockout of endogenous murine SOD1 has no such effect, it was hypothesised that *SOD1* mutations resulting in familial ALS are due to a toxic gain of function. The proposed mechanisms of SOD1 toxicity include mitochondrial dysfunction, axonal dysfunction, excitotoxicity and neuroinflammation (Chen *et al.*, 2013).

In recent years, key developments have revealed a novel ND spectrum with ALS overlapping clinically and pathologically with other neurodegenerative conditions including FTD. Identification of additional genes predisposing for familial ALS and/or ALS-FTLD including

transactivating response element DNA binding protein-43 (*TDP-43*) (Sreedharan *et al.*, 2008), Fused-in-sarcoma (*FUS*) (Dormann *et al.*, 2010), *C9ORF72*, vesicle-associated membrane protein (*VAMP*)/synaptobrevin-associated membrane protein B (*VAPB/ALS8*), Ataxin 2 (*ATAX2)*, Ubiquitin-like protein ubiquilin2 (*UBQLN2*), Optineurin (*OPTN*), D-amino acid oxidase (*DAO*), Amyotrophic lateral sclerosis 2 (*ALS2*), Valosin-containing protein (*VCP*), *MAPT*, Dynactin 1 (*DCTN1*), Angiogenin and Senataxin (*SETX*) have facilitated better understanding of ALS pathogenesis (Gros-Louis *et al.*, 2006, Hardiman, 2011). The common molecular pathways associated with these different ALS related genes mainly involve intracellular trafficking (axonal transport, vesicle docking and transport, microtubule and neurofilament stabilisation) and RNA metabolism (alternative splicing abnormalities, RNA binding) (Chen *et al.*, 2013). Attention has been devoted specifically to the ubiquitously expressed DNA/RNA binding protein (TDP-43), which is implicated in repression of gene transcription, alternative exon splicing and mRNA stability (Fiesel *et al.*, 2012). It has been increasingly associated with multiple NDs, primarily in the pathogenesis of ALS with cognitive impairments spectrum of diseases because of consistent deposition of ubiquitinated TDP-43 inclusions in these diseases. Dominant mutations in the *TARDBP* gene, encoding TDP-43, were repeatedly reported as a primary cause of ALS in about 3% of familial cases and 1.5% of sporadic cases (Swarup *et al.*, 2011).

In 2011, two groups (DeJesus-Hernandez *et al.*, 2011, Renton *et al.*, 2011) simultaneously and independently reported that a heterozygous expanded hexanucleotide repeat (GGGGCC) located in the first intron or promoter region of the *C9ORF72* gene is a major contributing factor to the

chromosome 9p21-linked diseases ALS and FTD. This initial discovery was quickly followed by further research on independent cohorts of patients from all over the world to uncover potential disease mechanisms and *C9ORF72* mutations are increasingly associated with other human NDs such as AD and PD with a broad phenotypic spectrum. Accumulating evidence strongly implicates both a loss-of-function disease mechanism due to decreased level of C9ORF72 transcript and a toxic RNA gain-of-function mechanism in the pathogenesis of *C9ORF72*-related diseases. Repeat expansion may generate insoluble and toxic dipeptide repeat (DPR) proteins through repeat-associated non-ATG (RAN) translation (Ash *et al.*, 2013), and formation of G-quadruplex by GGGGCC-repeating RNA and DNA was also shown to cause abortive transcription which in turn affects efficient C9ORF72 protein production (Haeusler *et al.*, 2014). Despite the observation that the hexanucleotide repeat expansion is the most common genetic abnormality of sporadic and familial ALS and FTD in European countries, accounting for 60% of familial ALS/FTD, up to 21.0% of sporadic ALS and 7–10% sporadic FTD, the pathogenic repeat expansion was rarely present in patients from Asian countries, such as Korea, China and Japan (Liu *et al.*, 2014).

1.1.6 Spinal muscular atrophy

Spinal muscular atrophy (SMA) is an autosomal recessive neuromuscular disease caused by the homozygous deletion, rearrangement, or mutation of the ubiquitously expressed telomeric Survival Motor Neuron gene *SMN1,* which predominantly produces a full-length functional SMN protein, coupled with the inability of centromeric homologue *SMN2* which only produces low levels of functional full-length SMN to compensate for the loss of *SMN1*,

resulting in a deficiency of the SMN protein. The multifunctional SMN has an essential housekeeping role in all cells to facilitate small nucleolar ribonucleoprotein (snRNP) biogenesis, pre-mRNA splicing, transcription, translation, signal transduction, stress granule formation, intra-cellular trafficking, axonal transport and postnatal muscle nerve terminal maturation (Seo *et al.*, 2013). SMA remains one of the most frequent genetic causes of infant mortality. Degeneration and loss of anterior horn lower motor neurons in the spinal cord and cranial nerve nuclei, the classic hallmark of SMA, leads to progressive denervation of skeletal and intercostal muscles, proximal muscle weakness, with subsequent atrophy of the corresponding muscles, paralysis and premature death in more severe cases due to respiratory failure (Crawford and Pardo, 1996). Based on the age of onset and the level of motor function, SMA has been classified as four clinical types ranging from congenital forms to asymptomatic cases. Although *SMN1* is the pathogenic gene for SMA, *SMN2* also participates in the pathogenesis of SMA as a critical mutation in *SMN2* was shown to cause aberrant splicing of the majority of transcripts, leading to the production of a truncated and rapidly degraded protein (SMNΔ7) (Mitrpant *et al.*, 2013). Furthermore, the copy number of *SMN2* modifies and correlates with the clinical severity of SMA and therefore can be potentially targeted for therapy. Despite intense research and increased knowledge of the cellular roles of SMN, the specific molecular pathways involved in SMA pathogenesis are still largely unknown, and there is currently no curative therapy available for SMA (Ling *et al.*, 2012). Preclinical research to elucidate key pathogenic events and identify promising treatments for SMA has relied heavily upon murine models.

Recent work has suggested that SMA is a multi-system disorder, affecting a range of cells and tissues (liver, lung, bones, blood vessels, heart, gastrointestinal, pancreas) other than neuromuscular system (Hamilton and Gillingwater, 2013). Genetic and pharmacological modifiers capable of correcting aberrant splicing and stabilising mRNA, SMN and SMNΔ7, and/or increasing the abundance specific activity of SMN have also been proposed as promising therapeutic targets (Seo *et al.*, 2013).

1.2 ATTRIBUTES OF *CAENORHABDITIS ELEGANS* AS A MODEL FOR HUMAN NEURODEGENERATIVE DISEASE

The inherent intricacies and neurological complexity of the human brain have hampered faster advances in understanding the molecular mechanisms behind NDs. Much of our current understanding of the molecular basis and the pathophysiology of NDs is offered by the studies in cultured cells and diverse animal models such as yeast (*Saccharomyces cerevisiae*), worm (*Caenorhabditis elegans*), fly (*Drosophila melanogaster*) and mouse (*Mus muluscus*) which have been constructed over the years to try to mimic the pathogenesis of NDs. None have been totally successful as the models available so far do not reproduce the full constellation of changes that compose the characteristic neuropathological phenotype seen in human NDs, due to the unique complexities of the human brain. While studies on unicellular models such as yeast or bacteria, as well as immortalised cell lines, primary neuronal cultures have been carried out (Hall and Yao, 2005, Falkenburger and Schulz, 2006, Winderickx *et al.*, 2008), these systems lack intercellular physiological pathways (e.g., neurotransmitter circuitry). In

contrast, vertebrate disease models offer *in vivo* opportunities and extensive similarity to the human brain. However, testing the therapeutic value of small molecules in mice and other mammalian model systems are expensive and require time-consuming experimental designs which can be prohibitive. Recent interests have turned to invertebrate models which bridge the gap between the simplicity of *in vitro* studies and the complexity of the human brain, and they allow for a more high-throughput and mechanistic approach. *C. elegans*, in particular, is a powerful model as it lacks many of the complexities of mammalian systems but retains the advantages of an intact organism. It excels in its simplicity, ability to reproduce asexually, fully sequenced genome, short generation time (≈ 3 days) and lifespan (≈ 3 weeks), considerable reproductive capacity (250-300 offspring), economy of testing susceptibility to RNA interference (RNAi), ability to self or cross-fertilise, distinctive behavioural and neuropathological defects, coupled with a surprisingly high degree of biochemical conservation.

Such experimental malleability is particularly advantageous, as *C. elegans* nervous system maturation and subsequent progressive stages of neuronal degeneration occur over a matter of days and can be assessed in large isogenic populations. The transparency of worms also facilitates the visualisation of any desired neurons and fluorescently-tagged proteins and assessment of the impact of pathogenic proteins within an intact animal in both temporal- and tissue-specific fashions. Recently, optogenetic techniques have been adapted to *C. elegans,* such that the neuronal activity can be measured by monitoring calcium levels and neurons can be activated by blue light stimulation of channelrhodopsin (Husson *et al.*, 2013). The cell lineage

and location of each of the 959 somatic cells which constitute this organism, including the morphology and the complete wiring diagram of the physical and chemical connections between *C. elegans*' 302 neurons (White *et al.*, 1976, White *et al.*, 1986, Hall and Russell, 1991), have been fully determined, thereby allowing the dissection of simple and complex behaviours at the level of individual cells and genes (Hobert *et al.*, 2002). Together, the 302 neurons make approximately 5000 chemical synapses, 600 gap junctions, and 2000 neuromuscular junctions (White *et al.*, 1986), thus conferring unparalleled precision and control in the identification and manipulation of neuronal cells (Pouya *et al.*, 2011). Extensive characterisations of whole *C. elegans* genome have also revealed remarkable homology with the human genome and physiology, with about 70% of human disease-related genes having a clear *C. elegans* homologue (Kuwabara and O'Neil, 2001), including many that have been implicated in NDs (Table 1.1). Remarkable similarities exist at the molecular and cellular levels between nematodes and vertebrates neurons. For example, ion channels, receptors, classic neurotransmitters [acetylcholine, glutamate, γ-aminobutyric acid (GABA), serotonin, and dopamine (DA)] and vesicular transporters are similar in both structure and function between vertebrate and *C. elegans* (Hardaway *et al.*, 2012). Physiological processes and signalling pathways such as formation, trafficking, and release of synaptic vesicles, and regulation of nervous system development by common guidance and polarity cues i.e. Netrin, Slt, Wnt, and Par protein complexes (Cáceres *et al.*, 2012) are also highly conserved between the nematode and vertebrates. In addition, *C. elegans* lacks a vascular system which enables the studying of

neuronal damage independently of vascular damage (Duan and Sesti, 2013). *C. elegans* also mainly encodes a single functional orthologue of the corresponding human gene, thus bypassing the complications of extensive functional redundancy observed among many mammalian proteins to model and shed important light on the specific biological functions of any gene of interest.

Despite its relative neuronal simplicity, *C. elegans* has different neuronal classes that constitute its rudimentary nervous system, including interneurons, chemosensory, mechanosensory, and thermosensory types; 75 motor neurons innervate the body wall muscles (excluding the head); 56 of these are cholinergic and 19 are GABAergic (Teschendorf and Link, 2009). These neurons enable *C. elegans* to exhibit a repertoire of simple and well-characterised behaviours which can be experimentally assessed to study specific neuronal dysfunction and degeneration (Figure 1.1), as certain NDs confer differential vulnerability of specific neuronal populations which lead to distinct clinical phenotypes expression; and when combined with biophysical assays can also facilitate the examination of protein solubility in neurons of interest (Teixeira-Castro *et al.*, 2011). Much debate has surrounded the mechanisms underlying age-dependent motor activity decline in *C. elegans*. Initial detailed examination of representative sensory and motor neurons have previously demonstrated that during neuronal ageing, there is little, if any, neuronal cell death and no signs of any neuronal degeneration despite advanced age and extensive behavioural decline. Instead, *C. elegans* senescence was attributed to widespread deterioration of surrounding somatic tissues which parallels sarcopenia in vertebrates (Herndon *et al.*,

2002). Recent reports have described progressive morphological changes in *C. elegans* neurons such as aberrant outgrowths and beading along neuron processes and age associated synaptic deterioration (Tank *et al.*, 2011, Toth *et al.*, 2012). Further functional analysis of the aging nervous system and muscles revealed that motor neurons, not body-wall muscles exhibit progressive functional deterioration, beginning in early life. Lifespan-extending mutations and pharmacological stimulation of synaptic transmission in the aging nervous system was also shown to slow down the rate of functional aging and potentiate locomotion activity in aged worms (Liu *et al.*, 2013). In light of these observations, it is clear that the impact of different challenges i.e. genetic perturbations or exposure to drugs and various external stimuli on the survival and function of defined neuronal populations in *C. elegans* nervous system can be readily studied. For example, inhibitory GABAergic and excitatory cholinergic motor functions can be assessed by quantifying the motility (amplitude and frequency of body bends on solid surface or in liquid) and foraging behaviour of the worm, respectively. Behaviours such as reduced motility is a typical characteristic of neuromuscular disease and have already been automated to allow for higher throughput analysis (Helmcke *et al.*, 2010). Motor, mechanosensory, chemosensory, DAergic and serotoninergic functions can be evaluated by measuring the pharyngeal pumping rate and behavioural changes in response to mechanical, osmotic, and chemical stimuli. In addition, the ability to generate primary *C. elegans* neuronal cultures can also expedite the functional analysis of neuron subtypes and allow direct assessment of their

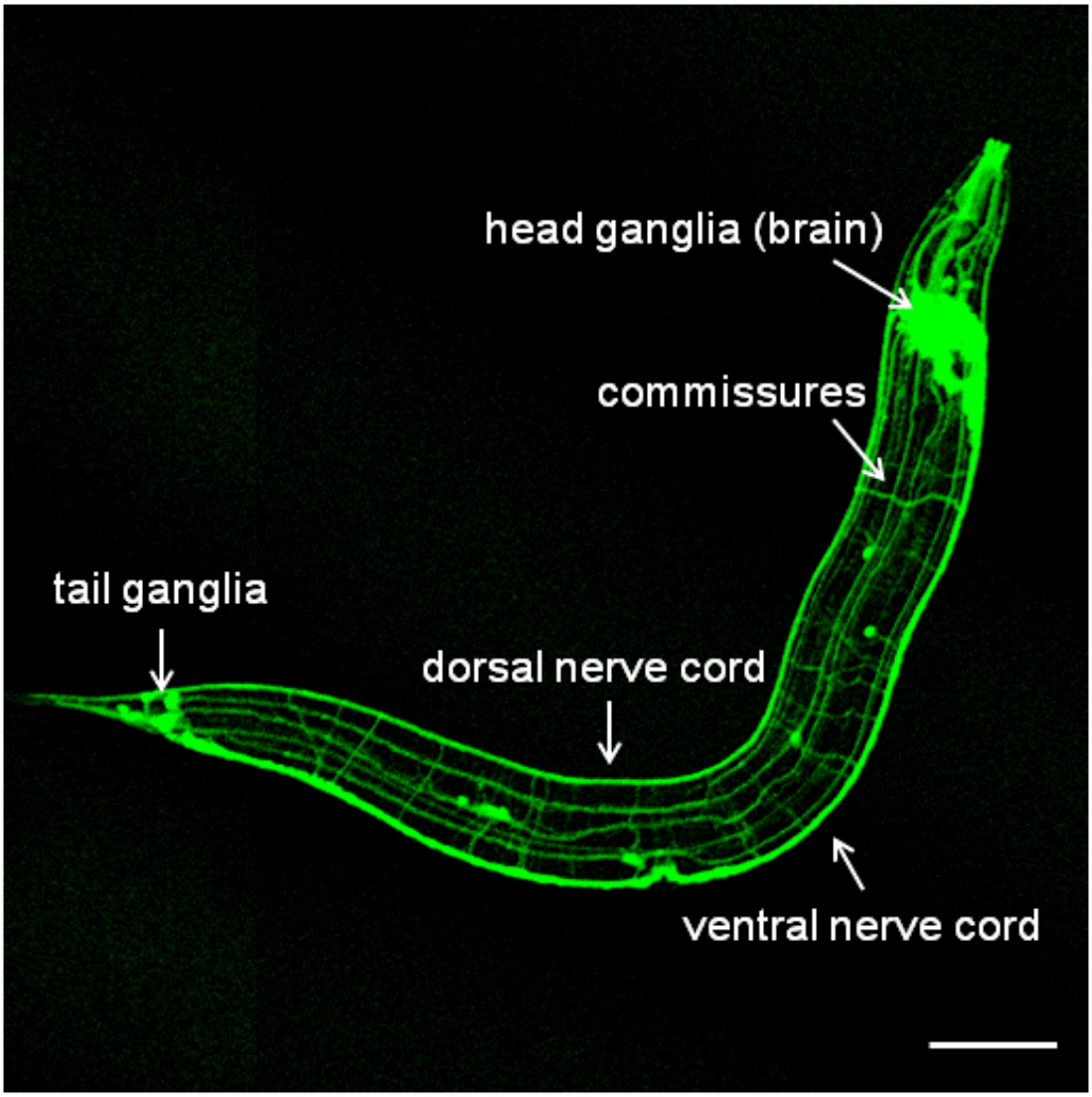

Figure 1.1: *C. elegans* nervous system marked by enhanced green fluorescent protein (EGFP) expression (driven by *rab-3* promoter) in all worm neurons. Scale bar, 100 μm

responses to toxic insults. For all these reasons, *C. elegans* is a powerful model that can translate findings from basic behavioural and cognitive neuroscience into an improved understanding of NDs in humans, and to assist in expediting translational drug research and clinical testing for the development of new therapeutic interventions against NDs (Leung *et al.*, 2008).

1.3 OVERVIEW OF *C. ELEGANS* NEURODEGENERATIVE DISEASE MODELS

C. elegans is frequently among the first animal models generated for newly identified ND genes and is useful for rapidly addressing mechanistic questions and testing therapeutic options. A large number of *C. elegans* models for ND have been developed by knocking-out, knocking-down and over-expression of many human ND-associated proteins (plus and minus mutations) or the equivalent worm orthologues. Appendix Table A1 displays a summary table illustrating the available human ND models of *C. elegans.* Strong parallels were especially observed in the genotype-to-phenotype correlations between the human NDs and the phenotypes of transgenic *C. elegans* ND models, which therefore support the validity of the approach as expression of mutant human proteins in *C. elegans* can closely model a fundamental property of these mutations in humans.

1.3.1 Modeling the pathophysiology of Alzheimer's disease

1.3.1.1 Aβ and presenilin

Investigation of mechanisms underpinning AD has been facilitated by the development of both mutant and transgenic *C*. *elegans* AD models of Aβ toxicity. The *C. elegans* genome encodes genes in which mutations are correlated with AD (Table 1.1). These include: an APP-related gene, *apl-1*, which encodes APL-1 (amyloid precursor-like protein) that lacks the Aβ peptide; a Tau orthologue (*ptl-1*), three presenilin orthologues (*sel-12, hop-1* and *spe-4*) and three genes whose product proteins combine to form the canonical functional γ-secretase complex (*aph-1, pen-2* and *aph-2)*. However, *C. elegans* does not appear to encode a β-secretase orthologue, and therefore lacks BACE1-like activity which is required to generate Aβ from its precursor, APP. Nevertheless, characterisations of these *C. elegans* orthologues via AD-related gene deletions or RNAi knockdown have provided significant functional insights into the role and regulation of the mammalian counterparts (Dimitriadi and Hart, 2010, Ewald and Li, 2012).

The inability of *C. elegans* to generate Aβ has been circumvented by Christopher Link who pioneered the modeling of β-amyloidosis in nematodes by expressing the human Aβ gene in the worm muscle cells (Link, 1995). To date, Link and colleagues have generated multiple convincing *C. elegans* Aβ peptide models, amongst which the constitutive (*unc-54*) and inducible Aβ muscle-specific expression (*myo-3*) have been used extensively for mechanistic studies of Aβ toxicity (Link, 1995, Link *et al.*, 2003, Wu *et al.*, 2006) due to their significant methodological advantages (ease of phenotypic scoring and sensitivity of muscle cells to RNAi) (Dimitriadi and Hart, 2010).

The constitutive Aβ model displayed an age-dependent paralysis phenotype and intramuscular Aβ accumulations that co-localised with amyloid specific dyes (thioflavin S and Congo Red) (Link, 1995, Fay *et al.*, 1998, Link *et al.*, 2001). Subsequent models were engineered to inducibly express Aβ upon temperature upshift, either in muscle (Link *et al.*, 2003) or pan-neuronally (Dosanjh *et al.*, 2010), with distinct differences in the severity of phenotypes. While a fully penetrant paralysis phenotype independent of amyloid deposition was obtained in worms with inducible Aβ muscle expression (Link, 2006), inducible, pan-neuronal expression of the Aβ resulted in intraneuronal deposition of Aβ along with relatively mild dysfunctions in chemotaxis to benzaldehyde, serotonergic transmission, associative learning and experience-dependent learning, and no overt locomotion defects were found (Link, 2006, Wu *et al.*, 2006, Dosanjh *et al.*, 2010). This temperature inducibility was engineered following introduction of temperature-inducible Aβ transcript into worms harbouring a temperature-sensitive mutation in a gene essential for mRNA surveillance (*smg-1*). Upshifting temperature from the permissive (16°C) to non-permissive/restrictive (23°C) conditions induces Aβ production by inactivating the nonsense-mediated decay pathway, which result in stabilisation of the $A\beta_{1-42}$ mRNA and substantial translation of transgenic transcripts (~5-fold increase). Recently developed transgenic Aβ models include a novel model that expresses Aβ in the secretory pathway of glutamatergic neurons (a neuronal subtype particularly susceptible to AD) using the *eat-4* promoter (Treusch *et al.*, 2011). While this transgenic strain was not reported to have any gross visible phenotypes, visualisation of the glutamatergic neurons with a P_{eat-4}::GFP construct demonstrated that Aβ

expression led to an age-dependent glutamatergic neurodegeneration. Furthermore, following demonstration that the existing *C. elegans* Aβ models are in fact predominately expressing amino-truncated $A\beta_{3\text{-}42}$ instead of the more disease relevant form, $A\beta_{1\text{-}42}$, McColl *et al.* (McColl *et al.*, 2012) generated a new transgenic model of *C. elegans* that expresses and accumulates full-length human-$A\beta_{1\text{-}42}$ peptide which aggregates and results in more severe and fully penetrant age progressive-paralysis.

1.3.1.2 Tau

Intraneuronal accumulation of NFTs composed of the microtubule binding protein Tau in cell bodies is the second hallmark of AD and other NDs, such as Pick's disease, Down's syndrome, and FTDP-17. Protein with Tau-like repeats (PTL-1) is the sole *C. elegans* orthologue of members of the mammalian MAPT(Tau)/MAP2/MAP4 family and regulates both organismal and neuronal ageing in a cell-autonomous manner (Goedert, 1996, McDermott *et al.*, 1996, Chew *et al.*, 2014). Like the case of *apl-1* in AD, *ptl-1* loss-of-function does not appear to recapitulate the human Tau pathology, since mutations in *ptl-1* resulted in only touch insensitivity, premature touch neuron aging and shortened life span (Chew *et al.*, 2013). Various transgenic Tau models expressing human Tau have therefore been generated. Despite using different isoforms of human *MAPT* and FTDP-17 mutations, these models yielded complementary findings in regards to the effects of neuronal Tau expression (Kraemer *et al.*, 2003, Miyasaka *et al.*, 2005, Brandt *et al.*, 2009). While Kraemer *et al.* (Kraemer *et al.*, 2003) employed the *aex-3* promoter to drive pan-neuronal expression of the most abundant human brain Tau isoform (1N4R) and FTDP-17- mutant Tau sequences (V337M and

P301L), Miyasaka *et al.* (Miyasaka *et al.*, 2005) drove expression of human wild-type adult Tau isoforms (0N4R and 0N3R) and FTLD-17-mutant Tau (P301L and R406W) in the mechanosensory neurons using the *mec-7* promoter. In another model, Brandt *et al*. overexpressed wild-type, pseudohyperphosphorylated (PHP) and phosphorylation-resistant human fetal Tau pan-neuronally under the *rgef-1* promoter (Brandt *et al.*, 2009). All these transgenic mutant Tau lines exhibited robust phenotypes and clear biochemical changes that recapitulate key observations of the human disease, including severe locomotion impairments, abnormal neuronal morphology, decreased neurotransmission, accumulation of insoluble, phosphorylated Tau, axonal degeneration, age-dependent neuronal degeneration and loss.

More recently, Fatouros *et al.* (Fatouros *et al.*, 2012) and Di Domenico *et al.* (Di Domenico *et al.*, 2012) utilised the V337M mutant Tau expressing lines to generate new models for further elucidation. Rather than comparing phenotypes of transgenic versus non-transgenic animals, as was done in previous *C. elegans* Tau studies, Fatouros *et al*. established and compared a new Tau model co-expressing either pro-aggregant mutated form of human Tau (deletion of K280) or anti-aggregant mutated forms of human Tau (I277P and I308P) from a *rab-3* pan-neuronal promoter, along with full length human Tau V337M. This resulted in pronounced phenotypic differences with pro-aggregant transgenic line exhibiting high levels of Tau aggregation that in turn caused uncoordinated movement in adults, axonal defects, and alterations in presynaptic structure, while anti-aggregant transgenic lines had low levels of Tau aggregates and displayed only mild phenotypes with

significantly less morphological abnormalities. Di Domenico *et al.* co-expressed human wild-type and mutated PD gene LRRK2 with Tau V337M to elucidate possible contributions of mutated LRRK2 in Tau-dependent neurodegenerative processes since mutations in the *MAPT* have been shown to be associated with FTD and parkinsonism (Hutton *et al.*, 1998) and new studies have demonstrated possible pathophysiological interplay between LRRK2 and Tau or α-synuclein (Di Domenico *et al.*, 2012, McCormick *et al.*, 2013).

1.3.2 *C. elegans* models of neuronal ceroid lipofuscinosis

Interest in NCLs has led to the development of models in diverse organisms. Like the other NDs, NCL research could benefit from work on the worm homologues of human defective NCL genes. Studies have shown that *C. elegans* has orthologues of genes involved in the congenital, infantile, juvenile and adult-onset forms of NCL (Table 1.1) (de Voer *et al.*, 2008).

Worm aspartyl protease gene *asp-4* is the orthologue of the human cathepsin D-encoding *CTSD/CLN10* gene that is mutated in the congenital NCL. Though no worm strains carrying deleterious *asp-4* mutations are available, RNAi knockdown experiments have suggested that *asp-4* mediates neuronal necrosis and is required for neurodegeneration (Syntichaki *et al.*, 2002).

Orthologues of the *PPT1/CLN1* and *CLN3* genes involved in the infantile and the juvenile forms of NCL, respectively, have been identified in *C. elegans*. As mentioned above, mutations in *PPT1* was shown to cause the infantile NCL and to date a disproportionate amount of research has been conducted on the function of *PPT1*. Two different *C. elegans ppt-1* mutant

strains were isolated. However, studies have shown that the phenotypes of both *ppt-1* deletion mutants are too mild to be used in genetic modifier screens. The *ppt-1* mutants do not exhibit neuronal degeneration or accumulation of storage material that are characteristics of infantile NCL. Moreover, despite observations of delayed egg laying, decreased health span and mild mitochondrial defect, most *ppt-1* mutants displayed no morphological, locomotion or neuronal defects (Porter *et al.*, 2005).

In contrast to other model organisms, *C. elegans* has three *CLN3* orthologues, designated *cln-3.1*, *cln-3.2*, and *cln-3.3*. Single mutant worm juvenile NCL models were generated by knocking out *cln-3.1*, *cln-3.2*, or *cln-3.3*. Due to redundancy, all three single mutant models were phenotypically wild-type with only slightly reduced brood-size and lifespan observed. A *cln-3* triple mutant model was also generated and its behaviour and integrity of the nervous system were subsequently explored. However, no functional aberrations or morphological defects were detected, thus indicating that the *cln-3* genes are not essential (de Voer *et al.*, 2008, Bond *et al.*, 2013).

Our lab has recently conducted research on a new and potentially useful *C. elegans* model of the adult-onset NCL to analyse the function of the worm *DNAJC5* homologue. In *C. elegans*, the *dnj-14 gene* is the sole orthologue of human CSP, the product of *DNAJC5,* and two mutant alleles of *dnj-14, ok237* and *tm3223* were isolated and phenotypically characterised. Both mutant strains were shown to be phenotypically similar to CSP knockout mice, and to some extent, CSP knockout *Drosophila*, as they exhibited increased mortality, age-dependent locomotion, neurotransmission and chemosensory neuron defects, with the latter phenotype manifested later as

neurodegeneration in the sensory cilia (Kashyap *et al.*, 2014). This model provided insight into the conservation of CSP function as *dnj-14*, was shown to be a key neuroprotective gene like its mammalian homologue, and its potential for future chemical genetic screening was also demonstrated following identification of pharmacological suppressors that ameliorated *dnj-14* lifespan and neuronal defects, which will be discussed in details below.

1.3.3 *C. elegans* models of polyglutamine repeat diseases

Although *C. elegans* does not possess an Htt orthologue, diverse transgenic models where varying numbers of polyQ tracts are expressed in different sets of neurons, muscle cells and even intestine cells have been widely used to model several aspects of polyQ neurotoxicity to address the mechanisms underlying the impact of aggregation prone proteins on cellular function and to identify novel disease modifiers. The progressive nature of polyQ-mediated toxicity, protein aggregation and general severity of phenotype demonstrated in these models is age and polyQ tract length dependent, recapitulating critical aspects models of polyglutamine expansion diseases have made significant contributions to the field.

Initial studies using *C. elegans* to investigate polyQ pathogenesis have limited the expression of polyQ to small subsets of neurons. The first *C. elegans* model of polyQ-mediated neurotoxicity was established by expressing an N-terminal 171 residue fragment of huntingtin with 150 CAG repeats (Htt171-Q150) (Faber *et al.*, 1999) in the non-essential bilateral pair of chemosensory neurons (ASH, ASI, PHA, and PHB) using the *osm-10* promoter. Htt-Q150 expression was found to induce age-dependent sensory process degeneration (demonstrated by a defective uptake of lipophilic

fluorescent dyes via the endings of chemosensory neurons), formation of Htt-positive cytoplasmic aggregates, perturbed function of the neurons (demonstrated by the defective sensory response to touch which is mediated by ASH sensory neurons) and eventual death of chemosensory neurons. In a similar neuronal HD model (Parker *et al.*, 2001), Htt57-Q128 fused to GFP constructs were expressed in ALM and PLM mechanosensory neurons of the body using the *mec-3* promoter. Expanded polyQ tracts caused increased touch receptor dysfunction and axonal perturbations, without neurodegeneration (Parker *et al.*, 2001). Behavioural and biophysical analyses of a pan-neuronal *C. elegans* polyQ model that broadly expresses expanded polyQ fragments in different subsets of neurons under the *rgef-1* promoter revealed polyQ length-dependent aggregation, neurotoxicity, and a dynamic pathogenic threshold at a length of 35-40 glutamines (Brignull *et al.*, 2006a).

In addition to above mentioned neuronal models, the Morimoto lab sought to delineate mechanisms underlying polyQ aggregation and toxicity through generations of the muscle-specific models (Satyal *et al.*, 2000) that express fluorescent proteins bearing varying numbers of polyQ tracts in pharyngeal and body wall muscles (Nass and Hamza, 2001, Nass *et al.*, 2005) using the *myo-3* and *unc-54* promoters, respectively. The resultant phenotypes were reminiscent of human disease progression. They also explored the effects of polyQ on cellular capacity for protein folding via simultaneous expression of temperature-sensitive (ts) protein mutants and polyQ transgenes. Furthermore, separate *in vivo* models also used the muscle-specific *unc-54* promoter to drive either 17 amino acid residues

derived from the DRPLA protein (DRPLAP) (Yamanaka *et al.*, 2004) or huntingtin exon 1 (Wang *et al.*, 2006) and these models confirmed that protein folding is critical in the toxicity of expanded polyQ fragments.

Despite encoding orthologues for most SCA caused by polyQ expansions, *C. elegans* models have only been generated and characterised for SCA2 and SCA3 (Kiehl *et al.*, 2000, Ciosk *et al.*, 2004, Rodrigues *et al.*, 2011, Teixeira-Castro *et al.*, 2011). Two *C. elegans* MJD/SCA3 pathogenesis models were recently generated and provided important insights regarding the pathogenic mechanisms involving aggregation, proteolysis and toxicity of expanded ataxin 3 (ATXN3). The pan-neuronal MJD model expresses polyQ-expanded ATXN3 protein under the *rgef-1* promoter (Teixeira-Castro *et al.*, 2011), while the new muscle-specific ATXN3 model expresses polyQ-containing C-terminal domain of the ATXN3, with various polyQ lengths (Q45 or Q63) in body wall muscle cells using the *unc-54* promoter (Christie *et al.*, 2014). Both models exhibited polyQ length-dependent aggregation that correlated with toxicity, as demonstrated by overt motor dysfunctions. However, unlike some previously described polyQ models (Morley *et al.*, 2002, Brignull *et al.*, 2006a), neither aging nor proteotoxic stress affect the aggregation and toxicity of this ATXN3 C-terminal fragment in body wall muscle cells.

1.3.4 Modeling the pathophysiology of Parkinson's disease

1.3.4.1 α-synuclein

All established familial PD genes are strictly conserved in the nematode with most residue positions mutated in PD patients encoding identical amino acids in *C. elegans* orthologues: Parkin (*pdr-1*), PINK1 (*pink-1*), UCHL-1 (*ubh-1*),

DJ-1 (*djr-1.1, djr-1.2*), LRRK2 (*lrk-1*), ATP13A2 (*capt-6*), and GBA (*F11E6.1, TO4A8.7*), with the exception of α-synuclein (Table 1.1). Knockout models of these orthologues either exhibited DAergic neurodegeneration, or were sensitised to mitochondrial toxins (Ved *et al.*, 2005, Karpinar *et al.*, 2009, Saha *et al.*, 2009, Sämann *et al.*, 2009), and have produced some important insights into their normal function. A plethora of transgenic models of synucleinopathy have now been established by multiple laboratories with pan-neuronal (*aex-3*), dopaminergic (*dat-1*) and motor-neuron (*unc-30*, *acr-2*)-target expression of both wild-type and mutant human α-synuclein expression and have facilitated the identification of multiple neuroprotective genetic factors that are conserved across species.

While pan-neuronal expression of wild-type, or pathogenic mutant (A53T and/or A30P) human α-synuclein gave rise to variable phenotypes as a result of the specific promoters (*aex-3, unc-51*) used in the transgene constructions, preferential neuronal dysfunctions in DAergic neurons were consistently reported by three groups following their expressions in DAergic neurons driven by the DA-specific *dat-1* promoter. These include reduced dopamine content, age-dependent DAergic neuron degeneration, motor deficits reversible by dopamine administration, defective dopamine-dependent behaviour, intracellular α-synuclein aggregates similar to Lewy bodies, and similar patterns of pharmacological vulnerability as those described above for familial PD genetic knock outs, which is reversed by treatment with antioxidants (Lakso *et al.*, 2003, Ved *et al.*, 2005, Kuwahara *et al.*, 2006).

Following the approach initially developed for polyQ-induced aggregation (Nollen *et al.*, 2004), numerous research groups have also constructed α-synuclein muscle models to uncover regulators of α-synuclein aggregation by expressing α-synuclein::GFP (or YFP) fusion fragments using the *unc-54* promoter (Hamamichi *et al.*, 2008, van Ham *et al.*, 2008). The Caldwell (Caldwell *et al.*, 2010) and Plasterk (Nollen *et al.*, 2004) groups both demonstrated that α-synuclein::GFP (or YFP) fusion protein expressed in body-wall muscles cells leads to the formation of visible fluorescent aggregates, as previously observed for GFP::polyQ (Caldwell *et al.*, 2010). Additionally, Kuwahara *et al.* (Kuwahara *et al.*, 2012) recently studied the role of serine-129 phosphorylation on α-synuclein neurotoxicity by pan-neuronally overexpressing nonphosphorylatable S129A-α-synuclein or phosphorylation mimic S129D-α-synuclein using the *unc-51* promoter, and observed severe motor dysfunction, growth retardation and synaptic abnormality in the transgenic S129A-α-synuclein model.

1.3.4.2 Toxin-induced

Environmental toxin exposure has been extensively linked to increased risk of developing nonhereditary PD. The well-characterised DAegic neurons of *C. elegans* are highly sensitive to many classic neurotoxins previously used to model PD in higher organisms, such as 6-hydroxydopamine (6-OHDA), MPTP, and rotenone (Braungart *et al.*, 2004, Ved *et al.*, 2005, Marvanova and Nichols, 2007, Saha *et al.*, 2009). Exposure to these toxins exclusively degenerates DAergic neurons in *C. elegans* and leads to PD syndromes that share similar features both in humans and mice (Ishiguro *et al.*, 2001, Nass *et al.*, 2001, Cao *et al.*, 2005, Nass *et al.*, 2005, Ved *et al.*, 2005, Marvanova

and Nichols, 2007). 6-OHDA and the reactive, neurotoxic metabolite of MPTP, 1-methyl-4-phenylpyridinium (MPP^+), selectively accumulate in the mitochondria of DAergic neurons and impair mitochondrial respiration by inhibiting complex I of the respiratory chain, and increase reactive oxygen species (ROS) generation and/or mitochondrial dysfunction, thereby inducing DAergic neurodegeneration and cell death. 6-OHDA is structurally similar to dopamine and is actively taken up by DAergic and noradrenergic transporters on DAergic cells (Nass *et al.*, 2001). MPTP is highly lipophilic and readily crosses the mammalian blood-brain barrier and cell membranes. It converts to the active toxic metabolite MPP^+ intracerebrally by the monoamine oxygenase B in astrocytes (Braungart *et al.*, 2004), and is secreted via the extraneural monoamine transporter to be actively taken up by DAergic cells via DA transporters (Aitlhadj *et al.*, 2011). Analogous to the findings with 6-OHDA, MPP^+-induced DAergic neurodegeneration in *C. elegans* is associated with behavioural defects i.e. significantly reducing mobility (Braungart *et al.*, 2004).

Recent studies have shown that in addition to chemical exposure, heavy metals, such as manganese (Mn^{2+}), methylmercury (MeHg), aluminum and other environmental contaminants i.e. fungicides, pesticides, insecticides, can generate potent models of dopamine neuron-cytotoxicity as they caused a wide range of phenotypic abnormalities as well as DAergic neurodegeneration (Aschner *et al.*, 2013).

1.3.4.3 Leucine-rich repeat kinase 2

Although the majority of PD studies conducted in *C. elegans* have focused on α-synuclein models, several LRRK2 neurodegenerative worm models have

recently been generated and are of considerable interest. LRRK2 was reported to play an important role in modulating mitochondrial dysfunction, since deletion and depletion of the *C. elegans* LRRK2 orthologue, *lrk-1* sensitised worms to the ER stress induced by tunicamycin and the mitochondrial toxic rotenone, respectively. To study the possible gain-of-function phenotype acquired by LRRK2 mutations, transgenic *C. elegans* models with pan-neuronal or DAergic neuronal overexpression of human LRRK2 WT, R1441C/G, G2019S and K1347A mutations were developed using either the *snb-1 or dat-1* promoter, and pathogenic mutant forms resulted in an age-dependent degeneration of DAergic neurons, locomotor dysfunction, behavioural abnormalities and dopamine deficiency (Saha *et al.*, 2009).

1.3.5 *C. elegans* amyotrophic lateral sclerosis models

1.3.5.1 Superoxide dimutase (SOD-1)

Just as aforementioned protein-misfolding disorders have been modeled in worms, a number of *C. elegans* models have been developed to study various aspects of ALS pathogenesis. Mutations in SOD1 are the most common known cause of familial ALS. Since both deletion and RNAi knock-down of any of the five forms of SOD in *C. elegans* had relatively little effect on the worm and the resulting phenotypes do not appear to mimic neuromuscular aspects of ALS (Doonan *et al.*, 2008), a number of transgenic lines expressing mutant forms of human SOD1 found in familial ALS patients under a range of promoters have been generated and recapitulated the motor neuron degeneration and paralysis characteristic of ALS patients

(Witan *et al.*, 2008, Gidalevitz *et al.*, 2009, Wang *et al.*, 2009b, Sleigh and Sattelle, 2010, Li *et al.*, 2013).

No morphological abnormalities or discernible phenotypes were observed in the first *C. elegans* model of SOD1 toxicity, which express human wild-type and familial ALS-associated human *SOD1* (A4V, G37R and G93A) constructs under the control of either the muscle-specific *myo-3* promoter or the universal heat-shock inducible *hsp-16.2* promoter (Oeda *et al.*, 2001). However, worms expressing mutant SOD1 were found to be preferentially sensitive to paraquat-induced oxidative stress which in turn significantly reduced the degradation rate of mutant SOD1 protein, and caused aberrant accumulation of mutant human SOD1 proteins in muscle cells. In subsequent studies, transgenic worms expressing dimeric forms of wild-type and misfolding mutant (G85R) human SOD1 behind a pan-neuronal promoter (*sng-1*) were generated. Larvae expressing mutant G85R SOD1 homodimers only displayed a marginal reduction in locomotion, while lifespan in the presence of paraquat was no different to control. In contrast, mutant heterodimer-expressing (with wild-type SOD1) worms showed reduced cellular aggregation, a highly significant decrease in motility and a shortened lifespan when exposed to paraquat (Witan *et al.*, 2008). With another well-characterised model, pan-neuronal expression (*snb-1* promoter) of a mutant form of SOD1 (unfused G85R or fused G85R-YFP), but not wild-type SOD1, resulted in a clear age-dependent impairment of locomotion and neuronal transmission. Interestingly, the observed phenotype correlated with intra-neuronal SOD1 protein aggregation which appeared to be restricted to certain mechanosensory neurons despite the pan-neuronal expression of

SOD1 (Wang *et al.*, 2009b). More recently, a *C. elegans* model was generated to express WT or mutant G93A SOD1 exclusively in GABAergic motor neurons. Mutant G93A SOD1-expressing lines showed an age-dependent paralysis accompanied by significant SOD1 aggregation and axonal guidance defects (Li *et al.*, 2013).

SOD1 toxicity in *C. elegans* muscle cells was also examined by Gidalevitz and co-workers (Gidalevitz *et al.*, 2009) using WT and mutant SOD1-YFP fusion proteins (G85R, G93A, and truncated 127X) driven by the *unc-54* promoter. Consistent with the neuronal aggregation seen by Wang *et al.* (Wang *et al.*, 2009b), only mild cellular dysfunction were evident in the body muscle cells expressing the three distinct SOD1 mutations (Gidalevitz *et al.*, 2009).

1.3.5.2 TDP-43, FUS and C9ORF72

Genes recently shown to be mutated in ALS include the DNA/RNA binding proteins *TDP-43* and *FUS*, and *C9ORF72,* a novel familial and sporadic ALS causative gene. Since very little is currently known about the biological role of *C9ORF72*, work from genetically convenient model organisms such as *C. elegans* could shed light on the molecular pathogenic mechanisms of *C9ORF72* toxicity and provide further insights into the disease state. Parker's group has recently characterised the loss of function of *C. elegans C9ORF72* orthologue *F18A1.6*, also called, *alfa-1* (ALS/FTD associated gene homologue). It was observed that decreased expression of *alfa-1* caused sensitivity to osmotic stress, age-dependent motility defects, leading to paralysis and neurodegeneration specifically of the GABAergic motoneurons (Therrien *et al.*, 2013).

Efforts to understand the mechanism of ALS and Frontotemporal lobar degeneration with ubiquitinated inclusions (FTLD-U) have led to the development of model systems exhibiting some features of RNA-binding proteins pathology. Deletion of *C. elegans* TDP-43 orthologue, TDP-1 caused sensitivity to oxidative and osmotic stresses and discernible defects in fertility, growth, and locomotion. However, paradoxically, worms lacking *tdp-1* have a longer lifespan (Ash *et al.*, 2010, Liachko *et al.*, 2010, Zhang *et al.*, 2012b). Both pan-neuronal (*snb-1* promoter) and motor neuron specific (*unc-25* and *unc-47* promoters) *C. elegans* models of TDP-43 and FUS proteinopathy have been generated and recapitulated various characteristic features seen in ALS and FTLD-U patients. Attention has been specifically devoted to TDP-43 as there are currently only two *C. elegans* FUS transgenic models. In contrast to the aforementioned SOD1 worm models, transgenic expression of the WT form of TDP-43, was highly neurotoxic. Ash *et al.* (Ash *et al.*, 2010) first reported that the pan-neuronal expression of human TDP-43 or its *C. elegans* orthologue TDP-1 caused neurotoxicity and protein aggregation, and further correlated the uncoordinated phenotype with defasciculation of the GABAergic motor neurons. Liachko and colleagues (Liachko *et al.*, 2010) similarly found that pan-neuronal overexpression of WT human TDP-43 caused motor defects. However, overexpression of various human ALS-associated TDP-43 mutants (G290A, A315T, or M337V) caused more severe phenotypes that are analogous to the phenotypes observed in ALS and FTLD-U patients. These include: progressive paralysis, reduced lifespan, and degeneration of motor neurons accompanied by hyperphosphorylation, truncation, and ubiquitination of the TDP-43 protein

that accumulates in detergent insoluble protein deposits. Intriguingly, the severity of motor dysfunction and neurodegeneration was observed to be highly correlated with TDP-43 phosphorylation levels, but not with protein aggregation. However, Zhang and colleagues (Zhang *et al.*, 2012b) demonstrated that TDP-43 misfolding and high aggregation propensity do contribute to its neurotoxicity as pan-neuronal expression of full-length and truncated human TDP-43 variants resulted in robust behavioural phenotypes including the locomotor defects, synaptic transmission abnormalities and formation of insoluble protein aggregates. Parker's group (Vaccaro *et al.*, 2012) further developed models which express human WT or mutant TDP-43 specifically in GABAergic motor neurons using an *unc-47* promoter. Interestingly, the overexpression of mutant TDP-43, but not wild-type TDP-43, caused an adult-onset, progressive paralysis phenotype accompanied by GABAergic neurodegeneration and synaptic transmission impairment.

1.3.6 *C. elegans* model of spinal muscular atrophy

The *C. elegans* genome harbours a single *smn-1* gene, which encodes a highly conserved SMN orthologue (Miguel-Aliaga *et al.*, 1999). The first of two *C. elegans smn-1* alleles generated, *smn-1(ok355)*, is a genetic null that possesses a deletion removing all but 87 bp at the 3′ end of the gene, resulting in SMN-1 loss of function and neuromuscular function deficits. Since *smn-1* deletion is homozygous lethal, the *ok355* allele must be maintained using a balancer chromosome that allows the differentiation of genotypes through expression of GFP (Briese *et al.*, 2009). Like in *Drosophila*, mutant animals proceed through embryogenesis due to maternal SMN-1 contribution from the heterozygous parental generation. Once depleted, the *smn-1*

homozygotes become discernible from wild-type larvae and exhibit pleiotropic defects including late larval arrest, decreased lifespan, defects in motility and pharyngeal pumping. *smn-1(ok355)* animals are indistinguishable from wild-type for up to two days post hatching, suggesting both that muscles are successfully targeted and reached by developing motor neurons and that SMN-1 plays a vital role in later development and adult life, as indicated in a severe mouse model of SMA. Moreover, neuromuscular function rapidly and progressively declines in early larval stages; specifically, both thrashing rate in solution and pharyngeal pumping rate become significantly reduced leading to larval lethality, and few homozygous mutant animals reach adulthood. Interestingly, the mutant displays no cholinergic motor neuron loss or gross defects in nervous system morphology in contrast to humans and mice. *smn-1(ok355)* was also used to show that pan-neuronal SMN-1 expression can partially rescue the phenotype of the mutant, whereas muscle-directed expression has little effect, similar to the situation seen in mice (Briese *et al.*, 2009, Dimitriadi and Hart, 2010, Sleigh and Sattelle, 2010).

Sleigh *et al.* (Sleigh *et al.*, 2011) recently isolated and characterised the second, weaker *C. elegans smn-1* allele, *smn-1(cb131*). This represents a less severe SMA mutant model that obviates the need for a balancer chromosome and expensive equipment required to separate genotypes. The *smn-1(cb131)* worms display a range of mild defects including a minor motility defect caused by reduced synaptic neurotransmission, similar to the null, but remain fertile, thus should greatly facilitate drug screening for compounds that improve motor function.

1.4 *C. ELEGANS* AS A MODEL TO DECIPHER GENETIC ASPECTS OF NEUROTOXICITY

Much of the current knowledge about modifiers of NDs using model organisms has been gathered from candidate approaches and unbiased genetic screens which use induced mutations i.e. knockouts/knockdowns and overexpression, in fixed genetic backgrounds. Though study of *C. elegans* orthologues of human ND-associated genes have produced some important insights into their normal function, most of the knowledge about NDs acquired in *C. elegans* came from transgenic models expressing the human disease proteins. We recently performed an integrated analysis of the data available from genetic screens of regulators of neurodegeneration in various disease models in yeast, fly and worms (Chen and Burgoyne, 2012), but uncovered relatively few shared genetic factors that affect several or all disease models as many of the regulators may be organism or disease-specific. Several of the shared regulators that have been robustly demonstrated in different model systems are chaperones, ubiquitin-related enzymes [including the E3 ligase, C terminus of the Hsc70-interacting protein (CHIP) which directly links the two pathways], histone deacetylases and 14-3-3 proteins. Interestingly, other shared regulators emerged which have not previously been considered as key regulators of neurodegeneration including peroxisomal acyl-CoA oxidase, which suggest novel targets for ND therapy.

1.4.1 Aβ

As mentioned above, studies of AD-related genes and pathways in *C. elegans* have provided important insights into the general function and pathways of AD-related genes and toxicity of specific Aβ species. Using both

deletion mutants and transgenic animals overexpressing APL-1, the importance of maintaining neuronal APL-1 within homeostatic levels was demonstrated, as either loss of APL-1 or overexpression of APL-1 resulted in lethality (Hornsten *et al.*, 2007, Wiese *et al.*, 2010). Follow up studies further revealed a role of APL-1 in *C. elegans* sensory plasticity as pan-neuronal, ectopic and targeted expression of APL-1, were shown to disrupt chemotaxis response, associative and non-associative learning which are mediated via TGF-β signaling and decreased insulin/IGF-1 signaling (Hassan *et al.*, 2009, Ewald *et al.*, 2012). Studies of the *C. elegans* presenilin orthologues *sel-12* and *hop-1* have also linked AD to the apoptotic and Notch-pathway signaling, which were later confirmed in vertebrates (Leung *et al.*, 2008). However, most of the knowledge about molecular processes underlying AD acquired in *C. elegans* came from transgenic worm models with tissue-specific or inducible expression of human Aβ. Using both the constitutive and temperature-inducible muscle Aβ models, a combination of studies has demonstrated that the $A\beta_{1-42}$ toxicity is highly dependent on genes implicated in general protein degradation pathways or longevity (Cohen *et al.*, 2006, Florez-McClure *et al.*, 2007, Fonte *et al.*, 2008). It has been demonstrated that decreased insulin receptor signaling following RNAi knockdown of the insulin/IGF-1 receptor, DAF-2, reduced $A\beta_{1-42}$ toxicity in the *C. elegans* body wall muscles through the opposing activities of two downstream transcription factors (TFs), heat shock factor 1 (HSF-1), which regulates Aβ disaggregation, and DAF-16, which facilitates the formation of larger, less toxic Aβ aggregates. RNAi knockdown of either *daf-16* or *hsf-1* enhanced Aβ toxicity with opposing effects on the $A\beta_{1-42}$ aggregation. Dietary restriction,

which extends lifespan in *C. elegans*, has also been found to reduce Aβ (and polyQ) toxicity in a HSF-dependent manner (Steinkraus *et al.*, 2008). The critical role of endogenous chaperone proteins in regulation of Aβ toxicity was also assessed (Fonte *et al.*, 2002, Fonte *et al.*, 2008). Mass spectrometry revealed that two HSP70 orthologues (C15H9.6 and F26D10.3), three αB-crystallin-related small heat shock proteins (HSP-16s) [T27E4.3 (HSP-16.1), Y46H3A.d (HSP-16.2), and T27E4.3 (HSP-16.48)], and a putative orthologue of a mammalian small glutamine-rich tetratricopeptide repeat-containing protein (SGT) proposed to bind to hsc7C (R05F9.10) co-localise and co-immunoprecipitate with Aβ (Fonte *et al.*, 2002). Further investigation of the biological role of HSP-16.2 on Aβ toxicity in the temperature-inducible transgenic model demonstrated that increased HSP-16.2 protein expression by either ectopic overexpression HSP-16 or a protective heat shock treatment substantially suppressed the Aβ-induced paralysis phenotype and Aβ oligomerisation without affecting the total Aβ protein accumulation (Fonte *et al.*, 2008, Wu *et al.*, 2010). The inducible model has also been used to demonstrate a role for autophagy in countering Aβ toxicity (Florez-McClure *et al.*, 2007) and was also subjected to two microarray studies which revealed up-regulated expression of αB-crystallin, tumour necrosis factor-induced protein 1 (TNFAIP1) and arsenite-inducible protein (AIP-1) upon Aβ induction, and their relevance to AD were further validated by similarly observed functions for their human counterparts (Link *et al.*, 2003, Hassan *et al.*, 2009). Recent findings provided strong genetic evidence that enzymes of O-GlcNAc cycling OGT-1 and OGA-1 are key

regulators of proteostasis and might be the potential targets to treat AD (Wang *et al.*, 2012, Hanover and Wang, 2013).

Using the new AD model with transgenic Aβ expression in glutamatergic neurons, genes involved in clathrin mediated endocytosis, such as *unc-11*, *unc-26*, *Y44E3A.4*, which are known AD risk factors in humans and were originally identified in a yeast modifier screen, suppressed glutamatergic neurodegeneration (Treusch *et al.*, 2011). Furthermore, the protective function of human repressor element 1-silencing transcription factor (REST) is also conserved in worms as mutations in the *C. elegans* functional REST orthologue *spr-4*, which suppressed the *sel-12/PSEN* egg-laying defect (Lakowski *et al.*, 2003), also significantly accelerated glutamatergic neurodegeneration (Lu *et al.*, 2014).

1.4.*2* Tau

The transgenic mutant Tau V337M worms have been subjected to both classic forward genetic and RNAi-based reverse genetic screens to identify modifiers that would exacerbate or alleviate the Tau-induced behavioural defects. Forward genetic screens based on classical chemical mutagenesis and positional cloning identified two novel candidate genes, *sut-1* and *sut-2* (Suppressor of Tau Pathology), whose loss of function strongly ameliorated the Tau-induced neurodegeneration (Kraemer *et al.*, 2003). Follow-up genetic studies and yeast two-hybrid screens further revealed that SUT-1 and SUT-2 may participate in the pathological pathway activated by Tau (Kraemer and Schellenberg, 2007, Guthrie *et al.*, 2009). It was suggested that SUT-1 suppresses Tau pathology defects by modulating actin dynamics, via its interaction with UNC-34, the cytoskeletal regulated protein Enabled

(ENA) (Kraemer and Schellenberg, 2007). It was also hypothesised that SUT-2, a zinc finger-containing protein ameliorates Tau pathology by affecting centrosome and/or aggresome function, via its direct interaction with ZYG-12, a HOOK protein family member and this interaction was further validated *in vitro* as human MSUT-2 also binds HOOK2 (Guthrie *et al.*, 2009). A full genome RNAi feeding screen in which 16,757 RNAi clones were assayed resulted in the identification of six genes that exacerbated only the Tau-induced behavioural defect (Kraemer *et al.*, 2006). These genes encoded proteins with a range of functions, including phosphorylation [e.g. glycogen synthase kinase 3β (*GSK3B*)], chaperone activity [e.g. heat-shock protein 70 (*HSP70*)], neurotransmission and signalling (e.g. *Munc13-4*), nucleic acid function (e.g. *sir-2.3*) and proteolysis [e.g. *CTSE* (cathepsin E)]. Reassuringly, mammalian orthologues of these modifier genes had been previously implicated in human Tauopathies and Tau-mediated pathology in other models. In addition, over-expression of human HSP70 in the Tau model of touch insensitivity significantly improved their touch response, whereas over-expression of the mammalian GSK-3β kinase slightly exacerbated Tau-induced neurodegeneration (Miyasaka *et al.*, 2005), the latter observation being consistent with *Drosophila* studies (Jackson *et al.*, 2002). Furthermore, using the transgenic muscle Tau model (*unc-54*::Tau::GFP), it was reported that RNAi-mediated knock down of the cochaperone CHIP in *C. elegans* promotes accumulation of abnormally phosphorylated Tau, demonstrating an important role of CHIP in the ubiquitin-dependent degradation of Tau (Dickey *et al.*, 2006).

1.4.3 PolyQ

C. elegans is a highly tractable tool for the study of polyQ protein dynamics and toxicity and has been extensively used to determine how polyQ pathogenicity contributes to neurodegeneration. Utilising the *C. elegans* neuronal HD model that expresses Htt-Q150 in ASH sensory neurons (Faber *et al.*, 1999), processes characteristic of apoptotic cell death, histone deacetylases (HDACs), autophagy and cAMP (Cyclic adenosine monophosphate) response element-binding protein (CREB) have been implicated in HD. Loss-of-function mutations and/or RNAi knock down of *C. elegans* genes mediating autophagy (*bec-1, atg-7, atg-18*), CREB (*crh-1*), CREB binding proteins (*cbp-1*), polyQ enhancer-1 (*pqe-1*) and majority *of* HDAC genes (*hda-1, hda-2, hda-4, hda-5, hda-6, hda-10, hda-11, sir-2.1, sir-2.2*), were discovered to exacerbate Htt-Q150 aggregation and neurodegeneration (Faber *et al.*, 2002, Parker *et al.*, 2005, Bates *et al.*, 2006). In contrast, the loss of ASH function was reversed in a *ced-3*/caspase mutant background and *hda-3*/HDAC deletion and depletion significantly reduced Htt-Q150-induced degeneration when *hda-1* activity was not compromised (Bates *et al.*, 2006). Complete loss of *sir-2.3*/HDAC activity also had no effect. The same polyQ toxicity model was also used in conjunction with primary cell culture neurons to demonstrate that posttranslational modification of mutant Htt by increased acetylation at lysine residue 444 (K444) may significantly improve the clearance of accumulated mutant Htt and actively targeting proteins for degradation by autophagy, leading to neuroprotection both *in vitro* and *in vivo* (Jeong *et al.*, 2009). The complex roles of specific HDACs in regulating Htt-polyQ toxicity was further

explored in another neuronal HD model that expresses Htt-Q128 in touch receptor neurons, and increased expression of the *C. elegans* orthologue of silent regulator information 2 (*sir-2.1*), a class III HDAC, was shown to ameliorate Htt-Q128 toxicity through the activity of *daf-16* transcription factor (TF) (Parker *et al.*, 2005). Additionally, Htt-Q128 worms were also utilised in a large-scale functional RNAi screen to identify modifiers of Htt-Q128-induced touch insensitivity. Interestingly, some of the RNAi hits identified from this *C. elegans* screen were up-regulated in the striatum of mouse HD models (Lejeune *et al.*, 2012), thus underscoring the relevance of using *C. elegans* models for the identification of potential therapeutic targets for human NDs. In-depth analysis of positive hits emphasised a role for cell differentiation/survival, metabolic and neurodegenerative disease pathways in the modulation of expanded-polyQ cytotoxicity (Lejeune *et al.*, 2012). Using the same model, *C. elegans* huntingtin-interacting protein 1 orthologue (*hipr-1*) and other synaptic endocytosis proteins were shown to protect against polyQ neuronal dysfunction (Parker *et al.*, 2007). Tauffenberger *et al.* (Tauffenberger *et al.*, 2012) further reported that loss of function mutations in *tdp-1* and *fust-1*, worm orthologues of human TDP-43 and FUS can reduce Htt-Q128-mediated behavioural defects and neurodegeneration, and their neuroprotective effects were further validated in mammalian neurons. However, suppression of Htt-Q128 toxicity by *tdp-1* is independent of *hdac-6*/HDAC6, but dependent on progranulin (*pgrn-1*/PGRN), a known TDP-43 target (Tauffenberger *et al.*, 2012).

PolyQ muscle-specific model systems have also been utilised to screen for modifiers. A dramatic delay of polyQ toxicity and appearance of

protein aggregates by loss of AGE-1, the *C. elegans* orthologue of phosphoinositide 3-kinase (PI3K) (Morley *et al.*, 2002) was observed in a body wall muscle-specific model. The same model was then used in a genome-wide RNAi screen which yielded 186 genes with diverse functions that, when knocked down, caused premature aggregation of polyQ35 aggregates (Nollen *et al.*, 2004). A subsequent RNAi screen of human orthologues of these *C. elegans* modifiers showed a subset that are also suppressors of mHTT aggregation in human cells (HEK293) expressing HTT-Q74-GFP (Teuling *et al.*, 2011). Other independent muscle HD models demonstrated the protective effects of *C. elegans* p97 homologues CDC-48.1 and CDC-48.2 (Yamanaka *et al.*, 2004), and ubiquilin (Wang *et al.*, 2006) in polyQ-induced toxicity, as well as for investigating the role of mitochondria dynamics in relation to expanded polyglutamine HD protein toxicity (Wang *et al.*, 2009a). Most recently, RNAi knockdown of *dnj-27*/ERdj5, an ER luminal protein upregulated in response to ER stress, was shown to exacerbate the impaired mobility of a polyQ40 muscle model, suggesting that *dnj-27* interacts with polyQ and protects against polyQ induced paralysis (Munoz-Lobato *et al.*, 2013). Temperature sensitive mutant proteins (UNC-54, dynamin, Ras, paramyosin) have also been used as probes for the cellular folding environment as studies revealed that transgene-induced polyQ expression in muscles or neurons of animals carrying temperature-sensitive mutations in genes unrelated to polyQ toxicity further exacerbated genetic defects and polyQ aggregation phenotype (Gidalevitz *et al.*, 2009).

1.4.4 PD

Numerous groups have made particular use of transgenic and toxin-induced *C. elegans* PD models for elucidating genetic pathways involved in PD (Lakso *et al.*, 2003, Hamamichi *et al.*, 2008, van Ham *et al.*, 2008). In particular, gene expression changes of α-synuclein expressing nematode lines have been widely monitored and permitted further insights into the neuropathologic mechanisms of α-synuclein. An unifying theme that has arisen from multiple whole genome forward, RNAi knockdown and microarray screenings of *C. elegans* models of α-synuclein overexpression-induced toxicity is a strong connection with mitochondrial function, proteostasis and endomembrane trafficking (Cooper *et al.*, 2006, Vartiainen *et al.*, 2006, Gitler *et al.*, 2008, Hamamichi *et al.*, 2008, Ichibangase *et al.*, 2008). Interestingly, different worm orthologues of known recessive PD genes such as *pink-1(PINK1), pdr-1 (parkin), djr-1.1 (dj-1)* and *capt-6 (ATP13A2)* consistently appear in most modifier screens as suppressors of α-synuclein-induced toxicity (Ved *et al.*, 2005, Gitler *et al.*, 2008, Hamamichi *et al.*, 2008, van Ham *et al.*, 2008). The P_{dat-1}::WT α-synuclein model (Cao *et al.*, 2005) demonstrated the neuroprotective role of an ER-associated chaperone, TorsinA/TOR-2 and a GTPase involved in ER-to-Golgi transport, Rab1A (Cooper *et al.*, 2006). The pan-neuronal α-synuclein models of Kuwahara *et al.* (Kuwahara *et al.*, 2006) that overexpress human α-synuclein (WT, A53T, A30P) under the control of the *unc-51* promoter were utilised in a large-scale RNAi screen, which led to the identification of ten enhancers of α-synuclein-induced neurotoxicity, mostly consisting of components from the endocytic pathway. Phosphorylation of α-synuclein at Ser-129, a characteristic

posttranslational modification evident in synucleinopathy lesions, was also detected in a subset of these transgenic worms (Fujiwara *et al.*, 2002). Recent gene expression profiling of pan-neuronal S129A-transgenic models revealed strong upregulation of *daf-16*/FOXO pathway genes, which the authors proposed to act against the dysfunction caused by the S129A-α-synuclein (Kuwahara *et al.*, 2012). Another whole genome microarray analysis was performed on a transgenic *C. elegans* model overexpressing human α-synuclein under the *aex-3* promoter and demonstrated the effect of pan-neuronal α-synuclein on proteasome, mitochondrial complex and nucleasome gene expression (Vartiainen *et al.*, 2006). These data therefore not only provide support for the role of dysfunctional mitochondria and inhibition of proteasomal function in synucleopathies, but also suggest a novel mechanism of neurodegeneration (i.e. regulation of nuclear protein in mediating neurotoxicity) for future study.

RNAi screening of two similar transgenic lines expressing α-synuclein in body wall muscle cells identified lysosomal trafficking genes (*vps-41*, *W08D2.5/ATP13A2*), lipid- and vesicle-associated genes (W02A11.2, *hgrs-1)* and aging-associated genes (*sir-2.1, lagr-1*) as modifiers that strongly protects against α-synuclein aggregation (Hamamichi *et al.*, 2008, van Ham *et al.*, 2008). The effect of several of these genes has been independently confirmed. Most recent work further substantiated the critical role of lysosomal trafficking in cellular homeostasis, maintenance and pathogenesis of synucleinopathies. While expression of the human orthologue, hVPS41 protected DAergic neurons from both α-synuclein- and 6-OHDA-induced DAergic neurodegeneration in *C. elegans*, as well as human SH-SY5Y

neuroblastoma cells from the toxic effects of the dopamine-specific neurotoxins 6-OHDA and rotenone (Ruan *et al.*, 2010), identified interacting partners of ATP13A2 were also shown to impact α-synuclein aggregation and α-synuclein-induced neurodegeneration (Usenovic *et al.*, 2012).

1.4.5 ALS

Both RNAi screenings and whole genome expression profiling have been performed using the ALS models. While genome-wide RNAi screening of transgenic G85R SOD1 neuronal model (Wang *et al.*, 2009b) and G93A SOD1 muscle aggregation models (Silva *et al.*, 2011b) isolated enhancers (protein chaperones, TGF-β, SUMO and topoisomerase I) and suppressors (which are also Q35 aggregation suppressor modifiers: cytoskeleton components and matrix proteins, posttranslational modifying enzymes, energy, metabolism, gene expression and protein synthesis related modifiers) of mutant SOD1 aggregation, respectively, a comprehensive RNAi screen of over 450 *C. elegans* kinases using a *C. elegans* model of mutant M337V TDP-43 proteinopathy identified twelve kinases that improved TDP-43-driven behavioural phenotypes (Liachko *et al.*, 2013).

Consistently, loss of function mutations of TDP-43 or FUS suppressed neurotoxicity and neurodegeneration in several ALS models (Zhang *et al.*, 2011, Vaccaro *et al.*, 2012, Zhang *et al.*, 2012b) as well as in a *C. elegans* model of HD (Tauffenberger *et al.*, 2012), suggesting that there may be genetic interactions amongst genes linked to neurodegeneration. Interestingly, abnormal ER stress and proteostasis which have been a recurrent theme in the sporadic and familial cases of ALS, was also revealed

as a highly affected biological process in a recent transcriptome analysis of *tdp-1(ok803)* (Zhang *et al.*, 2012b, Therrien and Parker, 2014).

Recent studies have similarly demonstrated that alterations in the IIS pathway which is a well characterised genetic modifier of aging and several aforementioned NDs in *C. elegans*, can also robustly modulate the solubility and neurotoxicity of ALS related proteins i.e. mutant SOD1 and TDP-43 as assessed by mobility, protein aggregation and longevity of transgenic models. Reduced *daf-2* activity was shown to suppress the toxicity and protein aggregation of both G85R SOD1 and TDP-43, an effect that might be due to an increased capacity for clearance/folding in these worms. HSF-1 was not only recovered as an enhancer of G85R SOD1-YFP aggregation/toxicity in a full genome feeding RNAi screen, but also a potent regulator of the TDP-43-induced neurotoxicity (Zhang *et al.*, 2011, Boccitto *et al.*, 2012). Introduction of mildly destabilising temperature-sensitive missense mutations which previously enhanced polyQ aggregation and elevation of environmental temperature strongly exacerbated the phenotypic defects and cellular toxicity of SOD1::YFP and TDP-43::YFP, respectively. This phenomenon seen in distinct models of disease involving protein misfolding and aggregation supports the hypothesis that dysfunction in conformational diseases may not be due to the misfolding/aggregation toxicity of the causative mutant but may be attributed to a global disruption in protein folding homeostasis (Gidalevitz *et al.*, 2009).

1.4.6 SMA

A high-throughput genome-wide RNAi screen using the loss-of-function *smn-1(ok355)* allele explored the genetic circuitry affecting SMN neuromuscular

function. While no suppressors were found, four enhancers *ncbp-2*, *T02G5.3*, *grk-2,* and *flp-4* were uncovered and subsequently tested for function as *smn-1* neuromuscular modifier genes using the pharyngeal pumping assay. Excellent concordance of modifier gene action in both *C. elegans* and *Drosophila* was further demonstrated, since twelve candidate SMN modifier genes that originally enhanced SMN loss of function defects in a previous *Drosophila* screen also enhanced SMN loss of function defects in *C. elegans* and *vice versa*. Bioinformatic analysis of these cross-species modifier genes revealed endocytosis and RNA processing as specific cellular pathways that are critical genetic modulators of SMN function (Dimitriadi and Hart, 2010).

In another study, the human E3 ubiquitin ligase, mind bomb 1 (*Mib1*) was proposed as a novel therapeutic target for SMA as it ubiquitinates and catalyses the degradation of SMN, and was further validated as a conserved cross-species modifier of SMN loss-of-function defects. Depletion of *C. elegans Mib1* orthologue *mib-1* by RNAi knockdown significantly ameliorated the pharyngeal pumping neuromuscular defects of *smn-1*-deficient animals, and MIB-1 was also shown to directly impact SMN-1 function independently of Notch signalling (Kwon *et al.*, 2013).

1.5 EXPLORING THERAPEUTIC STRATEGIES IN *C. ELEGANS* MODELS OF NEURODEGENERATIVE DISEASES

In addition to its value for screening for genetic contributors to diseases, numerous groups have also capitalised on *C. elegans* model system to screen for chemical compounds prior to validation in vertebrate models. Several large-scale, high-throughput drug screens (HTS) utilising recent

technological advances have been performed and identified effective bioactive compounds, novel antimicrobial compounds, specific inhibitors of SKN-1 and drugs that alter misfolded protein accumulation. The efficacy of some compounds such as fluphenazine was further validated in mammalian cell line and mouse models (O'Reilly *et al.*, 2014).

Numerous *C. elegans* neurodegeneration models have been used to test the effects of individual drugs [e.g., resveratrol in a polyQ model (Parker *et al.*, 2005); acetaminophen in multiple PD models (Locke *et al.*, 2008); methylene blue in a ALS model (Vaccaro *et al.*, 2012) and riluzole in a SMA model (Dimitriadi *et al.*, 2013)] or relatively small collections of compounds [e.g., subcomponents of Gingko biloba extracts in Aβ toxicity models (Wu *et al.*, 2006), candidate HD drugs in a polyQ model (Voisine *et al.*, 2007)]. *C. elegans* findings with potential therapeutic relevance are illustrated in Appendix Table A1. Many compounds such as resveratrol (Parker *et al.*, 2005), methylene blue (Vaccaro *et al.*, 2012), PBT2 (Cherny *et al.*, 2012) and clioquinol (Matlack *et al.*, 2014) also displayed protective effects beyond *C. elegans* models, with efficacy in *Drosophila* and zebrafish as well as mouse ND models.

1.5.1 Aβ

The Aβ-induced paralysis observed in the well-characterised muscle-specific strains has provided a valuable phenotype for straightforward quantification of the effects of treatments on Aβ toxicity and validation of potential therapeutic interventions for AD. *C. elegans* strain CL2006 which constitutively expresses human $A\beta_{1\text{-}42}$ has been elegantly used to demonstrate the neuroprotective effects of a diverse range of compounds:

natural products - specific gingkolides (Wu *et al.*, 2006), soya isoflavone glycitein (Gutierrez-Zepeda *et al.*, 2005), green tea component epigallocatechin gallate (Abbas and Wink, 2009, Abbas and Wink, 2010) and coffee extract (Dostal *et al.*, 2010); FDA-approved drugs - tannic acid, bacitracin, rifampicin (Lublin *et al.*, 2011); amyloid-binding dye thioflavin T (Alavez *et al.*, 2011), reserpine (Arya *et al.*, 2009) and antidepressant fluoxetine; polyphenolic compounds – curcumin and ferulic acid (Jagota and Rajadas, 2012) in Aβ toxicity (Keowkase *et al.*, 2010b). These treatments conferred considerable life-span extension and cellular stress tolerance (Gutierrez-Zepeda *et al.*, 2005, Wu *et al.*, 2006), since most compounds were shown to attenuate the rate of toxic human $A\beta_{1-42}$ mediated paralysis, suppress the $A\beta_{1-42}$ induced toxic ROS and hydrogen peroxide levels and inhibit $A\beta_{1-42}$ oligomerisation and deposits (Smith and Luo, 2003, Wu *et al.*, 2006). Recent studies have also demonstrated how the antibiotic tetracycline and its analogues (Diomede *et al.*, 2010), and ethanol extract of Liuwei Dihuang (Sangha *et al.*, 2012) successfully protected the CL4176 inducible $A\beta_{1–42}$ muscle-specific expression model from the $A\beta_{1-42}$ insult and oxidative stress by inhibiting $A\beta_{1-42}$ oligomerisation and reducing superoxide production. Oleuropein aglycone, the main polyphenol in extra virgin olive oil was recently shown to protect against amyloid toxicity in both constitutive and inducible $A\beta_{1-42}$ models (Diomede *et al.*, 2013). In addition, two recent large, unbiased yeast-based screens of pharmacological modifiers identified the 8-hydroxyquinoline chemical scaffold (8-OHQ), a class of clinically relevant bioactive metal chelators as neuroprotective compounds that reduced proteotoxicity associated with the aggregation of several ND-specific

proteins: TDP-43, α-synuclein, polyglutamine proteins, or $A\beta_{1-42}$ (Tardiff *et al.*, 2012, Matlack *et al.*, 2014). Notably, two closely related 8-OHQs - PBT2 and clioquinol, which conferred neuroprotective benefits in mouse models of AD, with the former also effective in improving cognition and reducing Aβ in cerebrospinal fluid in a small Phase IIA trial in AD patients - were further shown to rescue $A\beta_{1-42}$ toxicity in *C. elegans* body wall muscle cells (McColl *et al.*, 2012) and glutamatergic neurons (Matlack *et al.*, 2014) .

1.5.*2* Tau

Using transgenic FTDP-17 tauopathy models, a novel compound belonging to the aminothienopyridazine class, cmp16, was shown to effectively ameliorate the worms' motility and neuronal defects (Fatouros *et al.*, 2012). In a recent screen of a library of FDA-approved compounds, dopamine D2 receptor antagonism was presented as a promising strategy for targeting tau-induced neurotoxicity, as antipsychotics such as azaperone, flupenthixol, perphenazine, and zotepine improved the phenotypic features of Tauopathy in worms. Azaperone, in particular, effectively ameliorated mutant Tau-induced functional defects and reduced the level of insoluble Tau aggregation (McCormick *et al.*, 2013).

1.5.3 PolyQ

Voisine *et al.* (Voisine *et al.*, 2007) screened candidate pharmacological compounds utilising a HD model in which the *pqe-1* genetic mutant background greatly enhanced Htt-Q150-mediated toxicity. Both lithium chloride and mithramycin alleviated neuronal cell death, while trichostatin A, a class I and class II HDAC inhibitor provided significant neuroprotection. Using the same HD model, Varma *et al.* (Varma *et al.*, 2007) discovered that

small molecular inhibitors of metabolism (mitochondrial and glycolytic function) such as rotenone, oligomycin and 4-dinitrophenol rescued neuronal loss and degeneration by activating caspase inhibition and ERK and AKT prosurvival signalling and their efficacy were further validated in cell culture and *Drosophila* HD models. Resveratrol, a demonstrated activator of sirtuin deacetylases, also effectively alleviated Htt-Q128 toxicity in both worm and neuronal culture models (Parker *et al.*, 2005). Recently, treatment of a *C. elegans* model of MJD with 17-(allylamino)-17-demethoxygeldanamycin (17-AAG), an HSP90 inhibitor, successfully decreased the mutant ATXN3 aggregation and improved locomotor activity (Teixeira-Castro *et al.*, 2011). Treatment of the same model with valproic acid (VA), another HDAC inhibitor and a well-known anti-epileptic drug, also led to improved locomotor activity accompanied by a decrease in mutant ATXN3 aggregation. Therefore, HDAC inhibitors which promote histone acetylation over deacetylation and were also known to provide protection against polyQ mediated toxicity in vertebrate and *Drosophila* neurons may hold promise as preventive therapy in polyQ diseases.

Other pan-neuronal or neuron specific HD models facilitated the identification of other potential therapeutic interventions, including the anti-cancer agent β-lapachone (Shin *et al.*, 2013), *D. officinarum* root extracts (Yang *et al.*, 2012) and a phenol glycoside salidroside (Xiao *et al.*, 2014), which conferred protection against polyQ neuronal toxicity. Treating *C. elegans* muscle polyQ models with hydroxylamine, icariin and celecoxib derivatives: NG-094, icariside II and OSU-03012 ameliorated polyQ-mediated protein aggregation and protected against polyQ proteotoxicity (Cai *et al.*,

2011, Ching *et al.*, 2011, Haldimann *et al.*, 2011). Aspirin, an analgesic agent, was also shown to significantly improve polyQ-mediated animal paralysis, reducing the number of Q35-YFP aggregates and delaying polyQ-dependent acceleration of aging (Ayyadevara *et al.*, 2013).

1.5.4 PD

Multiple PD models, notably the toxin-induced models have aided in the discovery and validation of potential pharmacological interventions for PD. Chemical screens have suggested that compounds which protect mitochondria or increase autophagy protect against α-synuclein toxicity (Ved *et al.*, 2005, Wolozin *et al.*, 2011). Braungart *et al.* (Braungart *et al.*, 2004) performed a HTS with the *C. elegans* MPTP model of PD and found that several anti-PD drugs can ameliorate MPTP-induced mobility defects in this model. Notably, lisuride and apomorphine which are dopamine receptor agonists, as well as rottlerin (protein kinase C inhibitor) ameliorated the behavioural defects at low concentration. In addition, nomifensine (dopamine transporter inhibitor), nicotine (nAch receptor antagonist), selegiline (MAO-B inhibitor), MPEP (mGluR-5 inhibitor), amantadine, α-lipoic acid (antioxidant) and ascorbic acid (AA) were useful at higher concentrations (Ved *et al.*, 2005). In another screen, two mammalian DA D2 receptor agonists, bromocriptine and quinpirole, were identified to confer significant neuroprotection independent of DA receptors in a 6-OHDA-induced DAergic neurodegeneration model of PD (Marvanova and Nichols, 2007). Similarly, a low concentration of acetaminophen (analgesic and antipyretic) was reported by Locke *et al*. (Locke *et al.*, 2008) to significantly protect against 6-OHDA toxicity-induced DAergic neurodegeneration in $P_{dat\text{-}1}$::GFP expressing worms.

However, the protection appears to be selective as acetaminophen was not neuroprotective against α-synuclein-induced neurodegeneration at any concentration tested. The anti-epileptic drug, VA provided significant dopaminergic neuroprotection in a *C. elegans* PD model associated with human α-synuclein overproduction which was further shown to be mediated through ERK-MAPK signalling (Kautu *et al.*, 2013). Most recent studies have also demonstrated the neuroprotective effects of phytocompounds such as *n*-butylidenephthalide, curcumin, N-acetylcysteine and vitamin E on 6-OHDA-induced degeneration of DAergic neurons and their ability to attenuate α-synuclein accumulation. *n*-butylidenephthalide, in particular, has the greatest neuroprotective capacity and was shown to also restore food-sensing behaviour and the dopamine level in a pharmacological or transgenic *C. elegans* PD model as well as enhancing the life span of 6-OHDA-treated animals (Fu *et al.*, 2014a). Acetylcorynoline, the major alkaloid component derived from *Corydalis bungeana*, a traditional Chinese medical herb demonstrated the same neuroprotective effects when applied to the same pharmacological and transgenic *C. elegans* PD models (Fu *et al.*, 2014b).

Kinase-targeted inhibition of LRRK2 protein activity was recently established as an effective treatment for PD as LRRK2 kinase inhibitors consistently mitigated pathogenesis caused by different LRRK2 mutations. Liu *et al.* (Liu *et al.*, 2011b) showed that though GW5074, an indoline compound, and sorafenib, a Raf kinase inhibitor, did not have protective effects against α-synuclein- and 6-OHDA-induced toxicity, they increased survival and reduced DAergic neurodegeneration in G2019S-LRRK2 transgenic *C. elegans* and *Drosophila*. Yao *et al.* (Yao *et al.*, 2012) further

demonstrated the potency of kinase inhibitors as they were able to pharmacologically rescue both the behavioural deficit and neurodegeneration manifested by the expression of mutant LRRK2 G2019S and R1441C *in vivo* using two LRRK2 inhibitors, TTT-3002 and LRRK2-IN1, which also potently inhibited *in vitro* kinase activities of LRRK2 wild-type, R1441C and G2019S at nanomolar to low micromolar concentrations when administered either pre-symptomatically or post-symptomatically.

1.5.5 ALS

Treatment with methylene blue (MB), an aggregation inhibitor of the phenothiazine class not only rescued toxic phenotypes (including neuronal dysfunction and oxidative stress) associated with mutant TDP-43 and FUS in *C. elegans* and zebrafish ALS models (Vaccaro *et al.*, 2012), but also ameliorated Tau mediated toxicity in a newly established *C. elegans* model of Tau (Fatouros *et al.*, 2012). Using transgenic TDP-43 models, Tauffenberger *et al.* evaluated 11 compounds previously reported to enhance longevity in *C. elegans* and resveratrol (polyphenol), rolipram (phosphodiesterase 4 inhibitor), reserpine (antihypertensive), ethosuximide (anticonvulsant), trolox and propyl gallate (antioxidants) were revealed as effective candidates that protected against mutant TDP-43 toxicity in motor neurons (Tauffenberger *et al.*, 2013). Recent genetic experiments by Kraemer's group suggested that inhibiting cell division cycle kinase 7 (CDC7) kinase activity reduces phosphorylation of TDP-43 and the consequent neurodegeneration. Small molecule inhibition of CDC-7 by PHA767491 was further shown to robustly reduce TDP-43 phosphorylation and prevent TDP-43 dependent neurodegeneration both *in vitro* and *in vivo* (Liachko *et al.*, 2013).

1.5.6 SMA

Riluzole, an anti-glutamate agent proven to slow the progression of ALS and extend the ALS patients' survival by two to three months, was shown to also improve the neuromuscular function of the *smn-1(ok355)* null mutant model of SMA by activating the small conductance Ca^{2+}-activated K^+ (SK) channels which significantly increase both the motility and pharyngeal pumping rates of worms during feeding, as well as preventing axonal defects in Smn-deficient rat hippocampal neurons (Dimitriadi *et al.*, 2013). Through screening of the National Institute of Neurological Disorders and Stroke (NINDS) collection of chemical compounds with subsequent validation assays in a mutant SMA model with a milder and fertile *smn-1(cb131)* allele, two FDA-approved drugs - 4-aminopyridine (potassium channel blocker) and gaboxadol hydrochloride (agonist of a specific extrasynaptic, *δ*-containing $GABA_A$ receptor subtype, $\alpha_4\beta_3\delta$), and one novel compound - N-acetylneuraminic acid (Neu5Ac) were shown to rescue at least one aspect of *smn-1* phenotypic dysfunction (Sleigh *et al.*, 2011) with potential for further study in vertebrate models for the treatment of SMA.

1.5.7 ANCL

Our recent data indicated that the newly established *dnj-14* null mutant model of ANCL has potential for identifying generic neuroprotective interventions rather than drug targets that are disease specific. A focused chemical screen revealed that the natural polyphenolic compound resveratrol could ameliorate the short lifespan and chemosensory phenotypes of the *dnj-14* mutants. A partial rescue of neurodegeneration phenotype was also observed. The mechanism of resveratrol action was deduced to be PDE4 inhibition-

dependent as the cAMP phosphodiesterase inhibitor, rolipram was shown to mimic resveratrol in rescuing *dnj-14* (Kashyap *et al.*, 2014). In contrast to other worm neurodegeneration models (Parker *et al.*, 2005, Karuppagounder *et al.*, 2009, Bizat *et al.*, 2010, Tauffenberger *et al.*, 2013), resveratrol acted in a *sir-2.1*-dependent manner, as *sir-2.1; dnj-14* double mutants showed full lifespan rescue by resveratrol.

Taken together, *C. elegans* ND models have extensively broadened the research on human NDs and will continue to facilitate the identification of novel pathways and drug targets, and expedite translation to clinical testing. Using a selection of the aforementioned neuronal worm models to screen for generally neuroprotective agents effective in multiple models is a potentially efficient strategy for therapeutic drug discovery for NDs. Neuronal ND models directly capture the neurodegeneration seen in NDs have already been shown to identify neuron-specific regulators as well as generally neuroprotective compounds that alleviate the functional consequences of protein misfolding common to neurodegeneration.

1.6 AIMS AND OBJECTIVES

The specific aims of this study were to:

1. Test the applicability of multiple *C. elegans* ND models for neuroprotective drug screening.

2. Identify generally neuroprotective compounds that alleviate the pathological phenotypes of selected ND models.

3. Investigate the mechanism of action of efficacious drugs.

CHAPTER 2: METHODS

2.1 MATERIAL AND REAGENTS

2.1.1 Chemicals and consumables

If not stated otherwise, enzymes, chemicals, kits and solutions used for molecular and biochemical analysis listed in Table 2.1 were utilised according to manufacturer's instructions.

Table 2.1: Lists of reagents used in this study

Consumables	Manufacturer
Hard-Shell® Low-Profile Thin-Wall 96-Well Skirted PCR Plates	BioRad, Hemel Hempstead, UK
iTaq™ Universal SYBR® Green Supermix Supermix	BioRad, Hemel Hempstead, UK
Ampicillin	Calbiochem, Nottingham, UK
Kanamycin	Calbiochem, Nottingham, UK
Proteinase K	Invitrogen, Paisley, UK
RNase free Dnase I	Invitrogen, Paisley, UK
UltraPure™ DNAse/RNAse-Free Distilled Water	Invitrogen, Paisley, UK
SYBR Safe DNA gel stain	Invitrogen, Paisley, UK
TRIzol® Reagent	Invitrogen, Paisley, UK
Recombinant RNasin® Ribonuclease Inhibitor	Invitrogen, Paisley, UK; Promega UK Ltd., Southampton, UK
Restriction enzymes *ApaI, ApaII, BsrgI*, *NcoI, SacII*	New England Biolabs, Hitchin, UK
M-MuLV Reverse Transcriptase (RNase H-)	New England Biolabs, Hitchin, UK
OneTaq Quick-Load 2X Master Mix with Standard Buffer - 100 rxns	New England Biolabs, Hitchin, UK
Deoxynucleotide (dNTP) Solution Set - 8 µmol of each	New England Biolabs, Hitchin, UK
HighRanger Plus 1kb Ladder 300-10000bp	Norgen Biotek (Thorold, ON, Canada)
Random Primers	Bioline, Taunton, MA; Promega UK Ltd., Southampton, UK
Isopropyl β-D-1-thiogalactopyranoside (IPTG)	Sigma-Aldrich, UK
Ethosuximide	Sigma-Aldrich, UK
Succinimide	Sigma-Aldrich, UK
5-Hydroxy-1,4-naphthoquinone (Juglone)	Sigma-Aldrich, UK
6-Hydroxydopamine hydrobromide	Sigma-Aldrich, UK
Resveratrol (>99%)	Sigma-Aldrich, UK
The PureYield™ Plasmid Midiprep System	Promega UK Ltd., Southampton, UK

Consumables	Manufacturer
Qiagen RNeasy Mini Kit,	Qiagen, Crawley, West Sussex, UK
QIAprep Spin Miniprep Kit	Qiagen, Crawley, West Sussex, UK
Absolutely RNA Microprep Kit	Stratagene, Cambridge, UK
Dulbecco modified Eagle medium (DMEM)	Gibco®, Invitrogen, UK
Fetal Calf Serum (heat-inactivated) (FCS)	Gibco®, Invitrogen, UK
Penicillin-Streptomycin	Gibco®, Invitrogen, UK
Trypsin-EDTA (1×), liquid	Gibco®, Invitrogen, UK
PromoFectin transfecting agent transfection reagent	PromoKine, Heidelberg, Germany
RPMI-1640 medium, with sodium bicarbonate	Sigma-Aldrich, UK
Sytox Orange® nucleic acid dye	Invitrogen, Paisley, UK
NuPAGE® 12% Bis-Tris Gels	Invitrogen, Paisley, UK
NuPAGE® MOPS SDS Running Buffer (for Bis-Tris Gels only)	Invitrogen, Paisley, UK
SeeBlue® Plus2 Pre-Stained protein standard	Invitrogen, Paisley, UK

2.1.2 Oligonucleotides

All oligonucleotides used in this study were synthesised by Sigma-Aldrich.

Table 2.2: Lists of all used oligonucleotides

Oligo Name	Sequence 5' to 3'	Amplicon Size (bp)	Purpose
C. elegans			
pmp-3 F	TGGTGTCGCGATTACTGTAG	283	qRT-PCR
pmp-3 R	GATTTGTTGTCGCAGAGTGG		
act-1 F	CTACGAACTTCCTGACGGACAAG	102	qRT-PCR
act-1 R	CCGGCGGACTCCATACC		
cyp-34A9 F	CGAGACTCTTGCCGTAGACC	149	qRT-PCR
cyp-34A9 R	TTCCACCGGTAACCTCTGTC		
cyp-34A9 F	TAACCGATAGGCCAAAGACG	281	qRT-PCR
cyp-34A9 R	ACAAGATCTCTTCCCGATGC		
cyp-35B1 F	CAAAGATGGAGCAGGAGAGG	131	qRT-PCR
cyp-35B1 R	ATTGAATCCTGCGACCAAAG		
cyp-14A3 F	CAAAGGACCGTTACCATTGC	283	qRT-PCR
cyp-14A3 R	TTGAAGCCTCCAGTTGTCTC		
ugt-25 F	ATGACTCACGGAGGTCTTGG	108	qRT-PCR
ugt-25 R	TGCAAGCATATTCGCATTTC		
gst-4 F	TGCTCAATGTGCCTTACGAG	173	qRT-PCR
gst-4 R	AGTTTTTCCAGCGAGTCCAA		
gst-10 F	AAGAGATTGTGCAGACTGGAG	99	qRT-PCR

Oligo Name	Sequence 5' to 3'	Amplicon Size (bp)	Purpose
gst-10 R	AGAACATGTCGAGGAAGGTTG		
clec-85 F	CCTGATGATAAGTATATTGGAGACCTGT GCTACTC	94	qRT-PCR
clec-85 R	GGTTTTGGCTGTAGCACGCCGACTGAGC ATCC		
ttr-44 F	GACGTCTGATCTGTGGAGAC	301	qRT-PCR
ttr-44 R	TCCAGGTTGAGAACTCCAAG		
dhs-26 F	AACATCTGCAGGATCTTGGG	297	qRT-PCR
dhs-26 R	CACAAAGTGATTGCCCATCC		
dod-6 F	TCCTCGTCATCATGTCTGTC	148	qRT-PCR
dod-6 R	CACTTTCCGCAAGTCTTTGG		
ugt-53 F	AACTTCCCTTTACCCCGAAC	276	qRT-PCR
ugt-53 R	TGTTTCGCTTTACGAATCGC		
ins-2 F	TCTGTCTCCTCTTCACAACTG	203	qRT-PCR
ins-2 R	ACATTCTCCACATGTTGCAAGC		
pph-6 F	ACATGGAGGACTTTCACCTG	307	qRT-PCR
pph-6 R	ATAGCAGTAGTTTGGAGCCG		
dnj-14 (ok237) Full F	GAAAATTGGTGATGATGCTGCAGG	WT 2590, *ok237* 361	*ok237* genotyping PCR
dnj-14 (ok237) Mid F	CGCCAATATCTCCAGTCTCCAATG	WT 1736, *ok237* none	
dnj-14(ok237) R	GTCTCCCAGAGGCAGTCGAACAAC		
daf-16(mu86) F 1	CCCACATTCGTGTGGGTTTTCTAGTCG	WT 11385, *mu86* 405	*mu86* genotyping PCR
daf-16(mu86) out R	CGTTATCAAATGCTCCTTGCATTGAATC		
daf-16(mu86) int R	GCGTCAGTTCCGATCTGATATGAAC	WT 635, *mu86* none	
daf-16(+) F	GCAATGTGGACAGCTCGGCGGAGC	WT 436, *mu86* none	*mu86* homozygotes genotyping
daf-16(+) R	CAGATAAGAGAGAGTCTTATAGGG		
cca-1(ad1650) Avery F	CCGCAATTTGCCCTCCACAT	WT 3310, *ad1650* 930	*ad1650* genotyping PCR
cca-1(ad1650) Avery R	ATGAGGATGGCGAAGAGGACC		
cca-1(ad1650) F	CGGAAATATTAACTGTCATTCTGGA	WT 1350, *ad1650* none	*ad1650* homozygotes genotyping
cca-1(ad1650) R	CGTGCCTTCACAACCGAACTG		
Tau F	CAAGCTCGCATGGTCAGTAA	425	Tau genotyping
Tau R	TTCTCAGTGGAGCCGATCTT		
Mice			
Ccng2 F	AGGGGTTCAGCTTTTCGGATT	112	qRT-PCR
Ccng2 R	AGTGTTATCATTCTCCGGGGTAG		
Cdkn1a F	CCTGGTGATGTCCGACCTG	103	qRT-PCR
Cdkn1a R	CCATGAGCGCATCGCAATC		
Cdkn1b F	TCAAACGTGAGAGTGTCTAACG	103	qRT-PCR
Cdkn1b R	CCGGGCCGAAGAGATTTCTG		
Gadd45a F	AGACCCCGATAACGTGGTACT	318	qRT-PCR
Gadd45a R	TGATCCATGTAGCGACTTTCC		
Sod2 F	CAGACCTGCCTTACGACTATGG	113	qRT-PCR
Sod2 R	CTCGGTGGCGTTGAGATTGTT		

Oligo Name	Sequence 5' to 3'	Amplicon Size (bp)	Purpose
Rbl2 F	AACTTCCCCATGATTAGCGATG	97	qRT-PCR
Rbl2 R	GGTTAGAACACTGAAGGGCATTT		
Cat F	GCGTCCAGTGCGCTGTAGA	199	qRT-PCR
Cat R	TCAGGGTGGACGTCAGTGAA		
Eif4ebp1 F	GGGGACTACAGCACCACTC	171	qRT-PCR
Eif4ebp1 R	CTCATCGCTGGTAGGGCTA		
Bcl2l11 F	CCCGGAGATACGGATTGCAC	96	qRT-PCR
Bcl2l11 R	GCCTCGCGGTAATCATTTGC		
Gapdh F	AGGTCGGTGTGAACGGATTTG	123	qRT-PCR
Gapdh R	TGTAGACCATGTAGTTGAGGTCA		
Actb F	GGCTGTATTCCCCTCCATCG	154	qRT-PCR
Actb R	CCAGTTGGTAACAATGCCATGT		

2.1.3 Nematode strains and materials

Table 2.3: List of all utilised *C. elegans* strains and genotypes.

Strain	Genotype	Origin
N2 DRH	*C. elegans* wild type var. Bristol	CGC
RM2754	*dnj-14(ok237)X*	CGC
	dnj-14(tm3223)X	NBRP
JD21	*cca-1(ad1650)X*	CGC
AM134	*rmIs126* [P_{unc-54}*::Q0::YFP::unc-54 3′-UTR*]	CGC
AM138	*rmIs130* [P_{unc-54}*::Q24::YFP::unc-54 3′-UTR*]	CGC
AM140	*rmIs132* [P_{unc-54}*::Q35::YFP::unc-54 3′-UTR*]	CGC
AM141	*rmIs133* [P_{unc-54}*::Q40::YFP::unc-54 3′-UTR*]	CGC
CZ1200	*lin-25(n756ts)X*; *juIs76*[P_{unc-25}::GFP + *lin-15(+)*]	BC Kraemer
CK10	*bkIs10* [P_{aex-3}*::h4R1N TauV337M* + P_{myo-2}*::*GFP]	BC Kraemer
CK49	CZ1200 *bkIs10* [P_{aex-3}*::h4R1N TauV337M* + P_{myo-2}*::*GFP]	BC Kraemer
CB1370	*daf-2(e1370)III*	CGC
CF1038	*daf-16(mu86)I*	CGC
TJ356	*zIs356* [P_{daf-16}*::daf-16a/b::GFP* + *rol-6*]	CGC
LM99	*smn-1(ok355) I/hT2*[*bli-4(e937)+let-?(q782)+qIs48*P_{myo-2}::GFP]	CGC
HA659	*rtIs11*[P_{osm-10}::GFP + P_{osm-10}*::HttQ150 +dpy-20*(+)]	CGC
HA759	*pqe-1(rt13)*; *rtIs11*[P_{osm-10}::GFP + P_{osm-10}*::HttQ150 +dpy-20*(+)]	CGC
CB112	*cat-2(e1112)*	CGC
PD8120	*smg-1(cc546)*	CGC
	N2 *Ex*[P_{dat-1}::α-syn(WT) + P_{dat-1}::GFP]	CGC
	juIs76 [P_{unc-25}::GFP + *lin-15(+)* + P_{myo-2}*::*GFP]	J Johnson
UA57	*baIn4* [P_{dat-1}::GFP + P_{dat-1}::CAT-2]	RD Blakely
BY250	*vtIs7* [P_{dat-1}::GFP]	RD Blakely
CL2355	*smg-1(cc546) dvIs50* [P_{snb-1}::$A\beta_{1-42}$::long 3'-UTR + P_{mtl-2}::GFP]	CD Link
CL2122	*dvIs15* [P_{unc-54} + P_{mtl-2}::GFP]	CD Link
	P_{snb-1}*::G85R SOD1-YFP*	J Wang
	P_{snb-1}*::WT SOD1-YFP*	J Wang
CL2166	*dvIs19* [(P_{gst-4}*::*GFP*::NLS*]III	CGC
Strains obtained by crossings		
AMG119	*cca-1(ad1650)X ; bkIs10* [P_{aex-3}*::h4R1N TauV337M* + P_{myo-2}*::*GFP]	X Chen

2.2 MOLECULAR BIOLOGY METHODS

2.2.1 Transformation of plasmids into chemically competent *E.coli*

To amplify DNA constructs by plasmid miniprep or midiprep methods, plasmid DNA was transformed into chemically competent *E.coli* strain XL1, prepared in-house, via heat shock treatment. A 50 µl aliquot of bacteria was thawed on ice before incubation with 0.5 µl of DNA in pre-chilled Eppendorf tubes on ice for 30 minutes. After heat shock treatment at 42°C for 45 seconds, the sample was put immediately back on ice for 2 minutes followed by addition of 950 µl super optimal broth with catabolite repression (SOC) medium (2% (w/v) tryptone, 0.5% (w/v) yeast extract, 10 mM NaCl, 2.5 mM KCl, 10 mM $MgCl_2$, 20 mM glucose) and incubation at 37°C for 1 hour with continuous shaking at 220 rpm. 25 µl of the transformed *E.coli* were spread onto LB-agar plates (1% (w/v) tryptone, 0.5% (w/v) yeast extract, 1% (w/v) NaCl, 1% (w/v) agar), containing the required antibiotic (100 µg/ml ampicillin or 50 µg/ml kanamycin) and cultured overnight at 37°C.

2.2.2 Purification of plasmid DNA

Discrete *E. coli* colonies containing the relevant plasmid were picked to inoculate 30 ml of LB media (1% w/v tryptone, 0.5% w/v yeast extract, 8.56 mM NaCl) containing a selection antibiotic and were grown overnight at 37°C, 250 rpm. The cultures were then pelleted by centrifugation (12000 *x g*, 10 minutes) and plasmid DNA were extracted from the bacterial pellet using either a QIAprep Spin Miniprep Kit (Qiagen) or a PureYield Plasmid Midiprep System (Promega) following the manufacturer's guidelines. The plasmid DNA

concentration was determined spectroscopically with the NanoDrop® Lite (Thermo Fisher Scientific, Waltham, MA, USA) at 260 and 280 nm.

2.2.3 DNA digestion with restriction endonucleases

Plasmids were digested with restriction endonucleases (NEB) that were selected using ApE (A plasmid Editor; http://biologylabs.utah.edu/jorgensen/wayned/ape/). 5 µl of miniprep or midiprep DNA was added to 0.5 µl of restriction enzyme, 2 µl of 10x bovine serum albumin (BSA) and 2 µl of 1x reaction buffer (NEB) in 20 µl of total reaction volume. The reaction was incubated at 37°C for at least one hour.

2.2.4 Separation and isolation of DNA fragments

Agarose gel electrophoresis was used to separate DNA fragments according to their size. To load the DNA solution into the gel pockets, DNA fragments were combined with 6x DNA loading buffer (0.35% (w/v) orange G, 0.1% (w/v) bromophenol blue, 30% (w/v) sucrose) and separated by gel electrophoresis using a 2% (w/v) agarose gel containing SYBR® Safe DNA Gel Stain (Life Technologies). Electrophoresis was carried out in Tris-acetate-EDTA buffer (40 mM Tris, 20 mM acetic acid, 1 mM EDTA) at 90 V for 45-60 minutes. 10 µl of HighRanger Plus 100bp DNA ladder (Norgen Biotech) was run alongside the samples as a size reference. The DNA was visualised with UV light in a ChemiDoc XRS (BioRad) with Quantity One software (BioRad; v4.6.3).

2.3 *C. ELEGANS* BASED METHODS

2.3.1 Maintenance and propagation of *C. elegans* strains

C. elegans strains were cultured on 6 cm nematode growth medium agar (NGM; 2% (w/v) agar, 0.3% (w/v) NaCl, 0.25% (w/v) peptone, 1 mM $CaCl_2$, 5 µg/ml cholesterol, 25 mM KH_2PO_4, 1 mM $MgSO_4$) at 20°C, seeded with 50 µl *E. coli* strain OP50 culture as a food source, using standard methods (Brenner, 1974). Worm strains were maintained at 20°C, except for strains CL2355, CL2122 and PD8120 utilised in Chapter 3, which were maintained for 36 hours at 17°C, and upshifted to 25°C to induce transgene expression. *C. elegans* strains used in this study are detailed in Table 2.3, they were either obtained from Caenorhabditis Genetics Center (CGC, University of Minnesota, USA) or generously provided by the labs in which the strain had been constructed. *dnj-14(tm3223)X* was obtained from the National Bioresource Project for the Experimental Animal "Nematode *C. elegans*" based in the lab of Dr Shohei Mitani (Tokyo Women's Medical University, Tokyo, Japan). N2 var. Bristol was used as wild type strain. Worms were transferred from an old plate to a new plate either by picking individual worms with a tungsten wire, or by cutting out a chunk of agar and putting it on a new plate.

2.3.2 Axenisation and decontamination of *C. elegans* cultures

For the decontamination of *C. elegans* strains, worms were subjected to alkaline hypochlorite treatment or by transferring original worms to fresh plates on a daily basis. For bleach sterilisation, a relatively full plate of gravid adults was washed with 3.5 ml sterile H_2O and collected in a 15 ml Falcon

tube. 1.5 ml bleach mixture (two parts commercial bleach to one part 5 M NaOH) was added and the falcon tube was vortexed well every 2 minutes for 10 minute to destroy the cuticle of gravid animals and allow the release of eggs. Axenised eggs were collected by centrifugation at 1300 x *g*, 4°C for 2 minutes and washed twice with 5 ml sterile H_2O. The supernatant was removed and the pellet of eggs was transferred to the edge of a seeded plate.

Sterilisation and synchronisation of stocks by alkaline hypochlorite treatment was essential in Chapter 5 due to the large-scale *C. elegans* culture for the highly sensitive microarray experiment and subsequent RNA interference (RNAi) analyses. Contamination during RNA sample preparations and carrying over of either OP50 bacteria or HT115 RNAi bacteria needs to be avoided.

Limited egg-lay was also applied to age-synchronise nematodes. 5-15 gravid adults were plated to lay eggs for 6 hours and then removed to set the eggs in synchrony. All the eggs released in that time period have been shown to be well synchronised. Some strains are more prolific than other strains, so times and numbers of animals were adjusted accordingly.

2.3.3 Freezing and recovery of *C. elegans* stocks

For indefinite storage *C. elegans* strains were frozen and kept at -80°C. Worms of 2-3 freshly starved 60 mm plates (containing many L1-L2 stage larvae) were washed off plates with 1.5 ml M9 buffer (5 g/l NaCl, 3 g/l KH_2PO_4, 6 g/l Na_2HPO_4, 1 mM $MgSO_4$) and collected in a 15 ml falcon tube. After adding an equal volume of freezing solution (100 mM NaCl, 50 mM KH_2PO_4, 30% (w/v) glycerol, 5.5 mM NaOH, 3 mM $MgSO_4$), the worm

suspension was mixed well and aliquoted evenly between four cryovials (750 µl per tube). The cryovials were packed in a styrofoam box wrapped in tissue to achieve a slower freezing rate and put in a -80°C freezer. An aliquot was thawed the following day and plated to check there were surviving worms. Working populations of worms were refreshed from frozen stocks periodically to combat any genetic drift from normal strain maintenance. For recovery of a *C. elegans* stock, a frozen aliquot was thawed at room temperature and transferred onto a fresh NGM plate.

2.3.4 Administration of pharmacological compounds

All pharmacological compounds were obtained from Sigma-Aldrich. Concentrated solutions of each drug were prepared by dissolving compounds in 1 × phosphate-buffered saline (PBS; 2.7 mM KCl, 138 mM NaCl, 1.5 mM KH_2PO_4, 20.4 mM NaH_2PO_4 [pH 7.2]), dimethyl sulfoxide (DMSO) or ethanol at 50-100 mg/ml, and were added to molten NGM that had been autoclaved and cooled to 50-60°C. The mixture was agitated to ensure the compounds were dissolved and poured into 60-mm petri dishes. Vehicle control NGM plates containing equivalent amounts of PBS, DMSO or ethanol were also prepared. Freshly poured drug plates were stored in the dark at 4°C until 1-2 days before use and then moved to room temperature and seeded with *E. coli* OP50. Worms were grown for two generations on drug plates to ensure effective exposure (Figure 2.1). 10-20 gravid adults of test strains were cultured in the presence of the drug to lay eggs for 6 hours and then removed to set the eggs in synchrony. Plates were inverted and transferred to a container where descendants were then grown at 20°C for three days and selected for analysis at the L4 stage (defined as day 0).

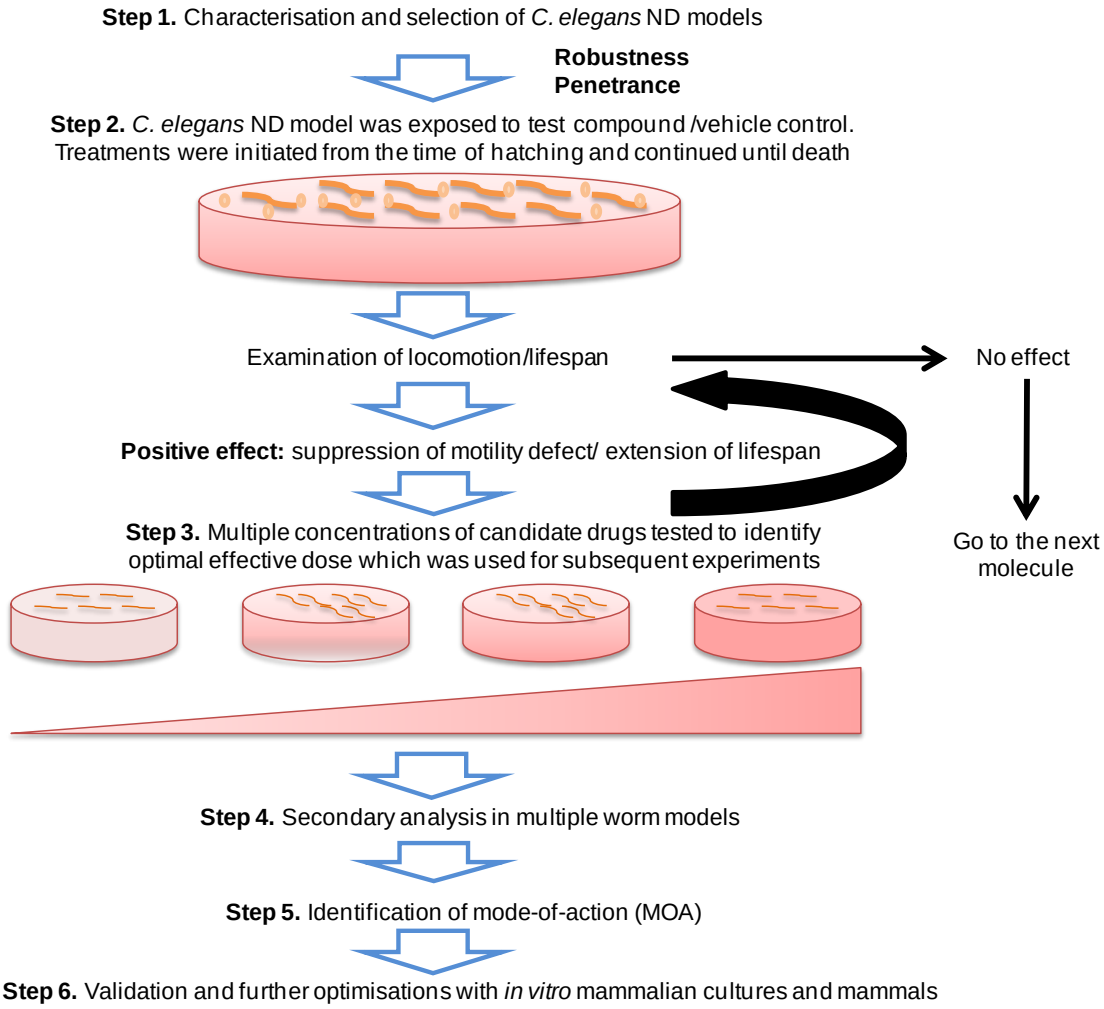

Figure 2.1: Experimental design for screening potential therapeutic compounds in neuorodegenerative disease (ND) models. Step 1. Selection of the *C. elegans* ND models for screening. Phenotypic criteria of chosen models were tested and ones with the most robust and reproducible behaviour phenotypes are well suited for assessing drug effects. Step 2. Selected ND models were grown for two generations on drug plates from conception to death to ensure effective exposure. Experiments involving pharmacological compounds were always done in parallel with a control group exposed to vehicle alone. Responses of worm ND model to drugs were assessed by comparing the locomotion and lifespan under various drug treatment concentrations which are parameters indicative of the worm physical healthiness. Compounds that cause significant rescue of locomotion impairment and increase in lifespan are considered good candidates for further testing. Drugs that failed to improve this measure of disease protein-related behavioural phenotypes at multiple concentrations of drug were not evaluated further. This testing was conducted in duplicate, and we found reproducible improvement of the pathological phenotypes for selected ND models. Step 3. The dose responses of promising compounds were profiled and effective doses were retested and serial dilutions were made to define the highest possible dose exempt of deleterious effect. Step 4. The efficacy of promising compounds was further evaluated in multiple NDs. Step 5. Explore the MOA of promising compounds i.e. test whether they alter biochemical endpoints such as levels of soluble and insoluble tau protein or reduce aggregation load. Step 6. These promising compounds may be further subjected to *in vitro* testing using human cells and *in vivo* testing in mammalian models of NDs.

2.3.5 Lifespan assay

For measurements of lifespan, parental worms were cultured and progeny were selected for analysis at the L4 stage (defined as day 0). In order to maintain statistical power, the starting number of worms was 10-20% higher than the intended final 50 hermaphrodites for each concentration. Approximately 25 hermaphrodites were cultured on each petri dish. Animals were scored every 1-2 days for survival by examining for touch provoked movement. Worms which did not display spontaneous movement or response to repeated touching were scored as dead. Worms found on contaminated plates, displayed internally hatched progeny, an extruded gonad, or desiccation caused by crawling off the agar were censored and excluded from the data. At least two trials were performed for all genotypes, and the data shown represent the average of replicates. Worms were transferred frequently during the first week of adulthood until the cessation of progeny production. Lifespan assays performed to test the effects of drug compounds or RNAi treatments on lifespan were always transferred onto fresh plates every 2-4 days to ensure the presence of active compound and to maximise RNAi efficacy.

2.3.6 Behavioural scoring

2.3.6.1 Thrashing assay

Thrashing assays quantify motor deficits in liquid medium and have been used extensively in studies of ND models as a measure of disease-associated cellular toxicity. Developmentally synchronised worms were transferred to 50 µl drops of Dent's Ringer solution (DRS; 10 mM HEPES, 140 mM NaCl, 6 mM KCl, 3 mM $CaCl_2$, 1 mM $MgCl_2$, pH 7.4) containing

0.1% (w/v) bovine serum albumin (BSA) to observe their thrashing movements. To assess their locomotory ability, the number of thrashes was counted for 1 minute after 10 minutes of equilibration. A thrash was counted when both the head and tail bent more than 45 degrees away from the anterior-posterior axis and back again. Animals with moving heads and stick-like bodies were scored as partially paralysed but were also analysed for head movements the left or right of the central body axis (lateral head movement) and for attempts at forward motion (forward advancement). Individuals were categorised as immobilised following 10 seconds of inactivity. 10-20 worms per strain were subjected to thrashing assays which were conducted at 20°C.

2.3.6.2 Nose touch avoidance assay

Nose touch avoidance was assayed by placing the blunt end of an eyelash hair, glued to a toothpick on an animal path while the animal was moving forward perpendicular to the direction of movement as previously described (Kaplan and Horvitz, 1993). These assays were conducted on NGM plates containing a thin layer of bacterial lawn. This was done by spreading 100 µl of an overnight culture of *E. coli* OP50 and allowing it to dry for a couple of hours. Animals were scored 10 times each for response to nose touch. Avoidance behaviour was quantified as the percentage of trials in which the animals responded to touch with an eyelash by stopping forward motion or initiating a reversal. This function is mainly carried out by ASH neurons. No more than 10 trials were conducted on a single worm at a time to avoid habituation and a minimum of 10 animals was tested for each genotype.

2.3.6.3 Self-brood size assay

When the synchronised population reached L4, individual hermaphrodites were picked onto 35-mm plates. Thereafter, the adult parents were transferred to new plates daily until the mother either failed to produce progeny for two consecutive days or died. Animals that crawled off of or burrowed into the NGM agar and did not return to the surface were not included in the data set. The progeny of the previous plate were counted the next day. The number of progeny from the various plates was added up and total number of progeny produced was counted once the offspring had matured to adulthood to give the final brood size.

2.3.7 RNA interference (RNAi) by feeding

RNAi experiments were conducted using feeding protocols according to standard procedures. RNAi in *C. elegans* was accomplished by feeding worms HT115 (DE3) bacteria expressing target-gene double-stranded RNA (dsRNA) from the pG-L4440 vector (Timmons *et al.*, 2001). *E. coli* strain HT115 lacks the dsRNA-specific RNase III but contains an isopropyl β-D-1-thiogalactopyranoside (IPTG)-inducible T7 RNA polymerase (Timmons *et al.*, 2003), carrying the pG-L4440 vector containing gene-specific RNAi trigger sequences. All RNAi feeding clones were obtained from the Vidal *C. elegans* Open Reading Frame (ORF) RNAi feeding library (Source Bioscience, Nottingham, UK) (Rual *et al.*, 2004).

90-mm plates of Luria-Bertani (LB) agar (1% tryptone, 0.5% yeast extract, 1% NaCl, 1.5% agar) with 100 µg/ml ampicillin were poured. Bacterial strains used for RNAi were streaked on separate plates grown from the frozen stock and incubated overnight at 37°C. Two discrete colonies from

each plate were each grown in 30 ml LB containing 100 µg/ml ampicillin overnight at 37°C, 220 rpm. The plasmid was then purified using the QIAprep Spin Miniprep Kit (Qiagen) and the correct insert verified by restriction endonuclease digest. Bacterial culture was also incubated with 1 mM IPTG at 37°C, 220 rpm for an additional 4 hours to allow the bacteria to produce dsRNA. 50 µl of the ten-fold concentrated cultures were spotted onto 1 mg/ml ethosuximide or vehicle control NGM plates supplemented with 100 µg/ml ampicillin and 2 mM IPTG media 4-7 days after pouring. RNAi-plates lose RNAi efficiency along with time course, so they were prepared newly in every experiment. RNAi plates were always kept in the dark, as IPTG is light sensitive.

RNAi treatments were performed as whole-life treatments and second generation RNAi feed worms were synchronised on fresh RNAi plates supplemented with test compound (ethosuximide) or vehicle (PBS). Feeding of HT115 carrying the pG-L4440 vector without an insert (L4440) served as the empty vector (no knock-down) negative control, whereas *hsp-1* was used as a positive control, as it gives a sterile phenotype (Simmer *et al.*, 2003).

2.3.8 Genomic DNA extraction and single worm PCR

To determine whether a worm is homozygous or heterozygous for a particular deletion allele, individual worms were picked into 10 µl of lysis buffer, consisting of diluted 5x Phusion® HF Buffer (NEB) and Proteinase K, and was frozen at −80°C. After one cycle of freeze-thawing, samples were incubated in a thermal cycler at 65°C for 90 minutes, followed by 95°C for 15 minutes. 2 µl of this lysate was typically used for genotyping PCR reactions using the primers listed in Table 2.2. PCR was performed in a final volume of

25 µl using 12.5 µl of OneTaq Quick-Load 2× Master Mix (NEB), 2 µl of template, forward and reverse primers (1 µl of 10 µM) and 9.5 µl of diethylpyrocarbonate-treated (DEPC) water. PCR amplifications rounds used 95°C for 2 minutes, followed by 30 cycles of 95°C for 30 seconds, 55°C for 30 seconds, 72°C for 30 seconds, with a final extension of 72°C for 5 minutes. Amplified products were then subjected to analysis on 2% agarose gels.

2.3.9 Total RNA preparation from *C. elegans*

Total RNA was isolated from 30 gravid adult hermaphrodite worms using the Absolutely RNA Microprep Kit (Stratagene) following the vendor's protocol with slight alterations. Briefly, the worms were transferred into 100 µl of Lysis Buffer- β-mercaptoethanol mixture and frozen at −80°C for 15 minutes. After three cycles of freeze-thawing, each sample was vortexed for 5 seconds with 100 µl of 70% ethanol and RNA was purified following the DNAse treatment step.

2.3.10 Reverse transcription and RT-PCR

For generation of cDNA, 10 µl of total RNA from previous step was reverse transcribed using the Tetro cDNA synthesis kit with random hexamer primers (Bioline) according to the manufacturer's protocol. Reverse-Transcriptase PCR (RT-PCR) analysis was performed in a final volume of 50 µl using 25 µl of 2 x MyTaq master mix (Bioline), 5 µl of cDNA, and forward and reverse primers (2 µl of 10 µM). PCR amplifications rounds used 95°C for 2 minutes, followed by 30 cycles of 95°C for 30 seconds, 55°C for 30 seconds, 72°C for 30 seconds, with a final extension of 72°C for 5 minutes. To control for equivalent levels of input RNA to verify homogeneous loading and cDNA

integrity, primers targeting the housekeeping gene β-actin were used as internal control. Amplified products were then subjected to analysis on 2% agarose gels.

2.3.11 Genetic crosses

2.3.11.1 Generation and maintenance of males

New strains are often generated by crossing two existing strains. Males were generated either by mating hermaphrodites with males from a wild-type male stock, or by heat-shocking hermaphrodites. Heat-shock increases the incidence of non-disjunction of the X-chromosome during meiosis and therefore leads to a higher incidence of males. Ten plates each containing 10 L4 hermaphrodites were exposed to 31°C for 6 hours and the progeny of these animals were then screened for males. Mating plates were typically maintained with nine males and three hermaphrodites on each plate, and worms were allowed to mate for 3 days to create a population rich in males (F1 progeny with approximately 50% males).

2.3.11.2 Crosses and selection of transgenic mutants

Genetic crosses of the stable integrated CK10 P_{aex-3}::*Tau V337M*; P_{myo-2}*::GFP* transgenic worms and *cca-1(ad1650)* deletion mutant worms in Chapter 4 were done by first crossing N2 males to CK10 P_{aex-3}::*Tau V337M*; P_{myo-2}*::*GFP hermaphrodites, to generate transgenic heterozygous males verified by pharyngeal GFP expression. This strategy allows unequivocal identification of progeny derived from mating, because fluorescent progeny (P_{myo-2}::GFP) must be heterozygous by definition. Transgenic male offspring were then back-crossed to isolate homozygous GFP (-Tau)-expressing

males. These were then mated with hermaphrodites of the same strain in order to create a population rich in males. Homozygosity was distinguished via uncoordination and coiler phenotypes as heterozygotes exhibited normal movement on plates. More robust GFP expression was also observed in the homozygous worms than the heterozygotes. GFP (-Tau)-expressing males were subsequently crossed twice with *cca-1(ad1650)* mutant hermaphrodites (generating cross progeny heterozygous for the Tau GFP transgene and the *cca-1* mutation in the 1st round). Parents were removed from the mating plate after overnight mating. Hermaphrodite progeny of the F1 generation, which are homozygous for the *cca-1(ad1650)* mutation but heterozygous for Tau GFP were isolated and allowed to self fertilise to give rise to an F2 generation, which includes worms homozygous for both transgene array and mutation. This enabled the differentiation between homozygous wildtype, as well as worms heterozygous or homozygous for the mutant *cca-1(ad1650)* allele. F2 progeny were then singled out and their progeny (the F3 generation) were screened to determine the genotype of the F2 parent. Homozygosity of the F2 generation hermaphrodites was determined by 100% propagation of the GFP expression signal in F3 progeny.

2.3.11.3 Crosses and selection of deletion mutants

In the case of the *dnj-14(ok237)* and *daf-16(mu86)* deletion mutant worms as well as *dnj-14(ok237)* and *daf-2(e1370)* deletion mutant worms depicted in Chapter 5, *dnj-14(ok237)* were first crossed with N2 males to obtain *dnj-14(ok237)* males, before *dnj-14(ok237)* males were mated to either *daf-16(mu86)* or *daf-2(e1370)* hermaphrodites. Twenty F1 cross progeny were singled onto individual plates and selfed at 20°C. PCR-based genotyping

(**2.3.8**) of the parental F1 animals confirmed the heterozygosity of the particular deletion alleles. Due to the slow growth phenotype of *dnj-14(ok237)*, slow growing F2 cross progeny of the *dnj-14(ok237)* and *daf-16(mu86)* cross were singled on NGM plates to lay eggs and both *dnj-14(ok237)* homozygosity and *daf-16(mu86)* deletion were analysed by single worm PCR. Because worms homozygous for the *daf-2(e1370)* allele at 25°C exhibit the constitutive dauer phenotype, F1 hermaphrodites (putative *daf-2(e1370)*/+; *dnj-14(ok237)*/+) were singled on NGM plates to lay eggs at 25°C. After 3-4 days, F2 animals which exhibit 100% constitutive dauer phenotype were selected and transferred to 15°C to recover and finish development before the *dnj-14(ok237)* deficiency was checked by PCR.

2.3.12 Microscopic analysis of *C. elegans*

2.3.12.1 Live imaging

Images were captured with a Nikon Eclipse Ti microscope driven by NIS-Elements 2.3 software (version 2.3; Nikon) using 300 ms exposure time at a magnification of 200x and 400x using a 20x and a 40x objective, respectively. Microscopy of living animals was performed by mounting the worms on cover glass (22 x 40 mm, VWR International, PA) in a 5 µl drop of polyethylene glycol (PEG)/glycerol. PEG/glycerol mounting medium is a blend of equal percentage (20:20) of PEG 20000 and glycerol in PBS which immobilises the nematode. Slides were rapidly sealed with a clean glass coverslip (13 mm, VWR International, PA). In all imaging experiments, between 5-10 *C. elegans* were mounted on a single slide and individual worms were randomly selected. Scoring was completed within 15-20 minutes of placing the coverslip, as the accuracy of this criterion for mortality is lost after the worms

are covered longer. GFP is subject to photobleaching, and the worms' condition deteriorates under a coverslip on the microscope. (Under ideal circumstances, scoring can be completed in 5-10 minutes). Scoring was therefore halted when fading or deterioration became apparent. Animals damaged in handling, or animals whose intestinal tracts appeared to be breaking down and were assumed to be dead, were excluded from scoring.

2.3.12.2 Quantification of axonal degeneration

Worms were synchronised and imaged under fluorescence microscopy as described above. They were scored for the number of gaps in the ventral and dorsal nerve cords. Although *C. elegans* has 19 GABAergic motor neurons, counts in control and experimental groups were slightly less than 19, presumably due to the occasional inability to distinguish individual cell bodies in closely opposed pairs of neurons.

2.3.12.3 6-hydroxydopamine cell death assay and quantitative analyses of neuronal degeneration

The 6-hydroxydopamine (6-OHDA) toxicity assay was performed as described previously (Nass *et al.*, 2001, McDonald *et al.*, 2007) with slight modifications. At 24 hours after synchronisation, L2/L3 BY250 worms were washed with sterile water from large 90-mm NGM plates at 20°C and transferred to glass conical tubes. An equal volume of 6-OHDA (Sigma-Aldrich) stock solution (100 mM 6-OHDA in 20 mM ascorbic acid (AA), the latter is required in order to stabilise 6-OHDA in solution) was added to the worm suspension to achieve the final concentrations of 50 mM 6-OHDA in 10 mM AA. Vehicle control animals were treated with 10 mM AA alone. Worms were then incubated in the dark for 1 hour at room temperature with gentle

agitation every 10 minutes. After treatment, the worms were washed with M9 buffer, the supernatant was discarded and the process was repeated. Worms were then placed on NGM plates seeded with OP50 bacteria and incubated at 20°C until analysis of P_{dat-1}::GFP expression at time points ranging from 2 to 72 hours after 6-OHDA exposure. For each time point, 20-40 worms per strain were immobilised with PEG/glycerol mounting medium as described above **(2.3.12.1)** and were analysed in at least three independent experiments, with a total of 71-120 animals scored in the same manner. In quantifying dopaminergic (DAergic) neurodegeneration, a worm was scored as 'wild type (WT)' when a full complement of all six anterior DAergic neurons is present with neuronal processes (the prominent dendrites in CEP neurons or axons in ADE neurons) were intact and fully extended to their target areas; neuron was scored as 'partially degenerating' when at least one degenerative change such as dendrite blebbing of any of the four neuronal dendrites or cell body rounding was observed; neuron was scored as 'completely degenerating', when loss of neuronal dendrites or cell bodies were evident. All six anterior DAergic neurons were scored in each animal. The percentage of nematodes in a population with intact anterior dopamine neurons was determined.

2.4 PROTEIN BIOCHEMICAL METHODS

2.4.1 Preparation of *C. elegans* protein extracts

Extracts were prepared following growth of worms to near-confluency on seven 90-mm diameter NGM plates. Worms were harvested in M9 buffer and

were frozen at -80°C overnight. The worm pellets were thawed on ice before use and homogenised using a Mikro-Dismembrator (Braun Biotech International, Melsungen, Germany) at 2000 rpm for 2 minutes in an equal volume of worm lysis buffer [140 mM KCl, 1 mM EDTA, 50 mM HEPES pH 7.4, 2% SDS and 1 tablet of protease inhibitor cocktail (Sigma)] with acid-washed glass beads (425-600 µm; Sigma) added to the level of the meniscus. Three holes were made in the base of each tube with a BD Microlance™ 3 25G hypodermic needle (Becton Dickinson & Co. Ltd, Ireland). The tube was placed in a 15 ml Falcon and crude protein extracts were centrifuged at 5000 rpm for 5 minutes at 4°C to obtain the lysates, followed by centrifugation at 13000 rpm at 4°C for 20 minutes to remove the worm debris and insoluble material. The supernatant was collected and aliquots were either used immediately or stored at -80°C.

Protein samples were also prepared by picking, freeze-thawing, and boiling 25-50 worms of selected strains in Laemmli buffer (4% (w/v) SDS, 20% (v/v) glycerol, 10% (v/v) 2-mercaptoethanol, 0.004% (w/v) bromphenol blue and 0.125 M Tris HCl, pH 6.8) at 95°C for 25 minutes.

2.4.2 Sequential extraction of Tau protein

Soluble and insoluble fractions were obtained using the methods previously employed to extract aggregation-prone proteins from mouse and worms (Ishihara *et al.*, 1999, Guthrie *et al.*, 2009, David *et al.*, 2010), with modifications (Figure 2.2). Extracts were prepared following growth of mixed stage populations of vehicle and ethosuximide treated Tau V337M worms to near-confluency on twenty 90-mm diameter NGM plates. Worms were washed off plates with M9 buffer and the collected worm pellets were then

stored at -80°C. After the freeze thaw cycle, frozen animals were directly homogenised using a Mikro-Dismembrator at 2000 rpm for 2 minutes in an equal volume of high-salt reassembly (RAB) buffer (100 mM MES, 1 mM EGTA, 0.5 mM $MgSO_4$, 20 mM NaF, 0.75 M NaCl, 0.5 mM PMSF, 0.1% protease inhibitor cocktail, pH 7.0) with acid-washed glass beads (425-600 µm; Sigma) added to the level of the meniscus. Crude protein extracts were centrifuged at 5000 rpm for 5 minutes at 4°C to obtain the lysates, followed by ultracentrifugation at 40000 rpm at 4°C for 40 minutes. The supernatant was subsequently boiled for 5 minutes, and the sample was centrifuged at 13000 rpm, 4°C for 15 minutes. The supernatant constitutes the RAB fraction. The resulting RAB-insoluble material was re-homogenised with radio-immunoprecipitation assay (RIPA) buffer (150 mM NaCl, 1% Nonidet P-40, 0.5% deoxycholate, 5 mM EDTA, 0.1% (w/v) SDS, 50 mM Tris, 0.5 mM PMSF, 0.1% protease inhibitor cocktail, pH 8.0) by sonication and ultra-centrifuged for 20 minutes at 40000 rpm to remove membrane proteins. The supernatant is the RIPA fraction yielding abnormal detergent soluble Tau. Finally, the RIPA-insoluble pellets were sonicated to resuspend, and were re-extracted with 70% formic acid (FA) to solubilise detergent-insoluble Tau, to remove worm cuticlar debris and recover most insoluble cytoskeletal aggregates. This was then centrifuged at 13000 rpm for 15 minutes. The FA

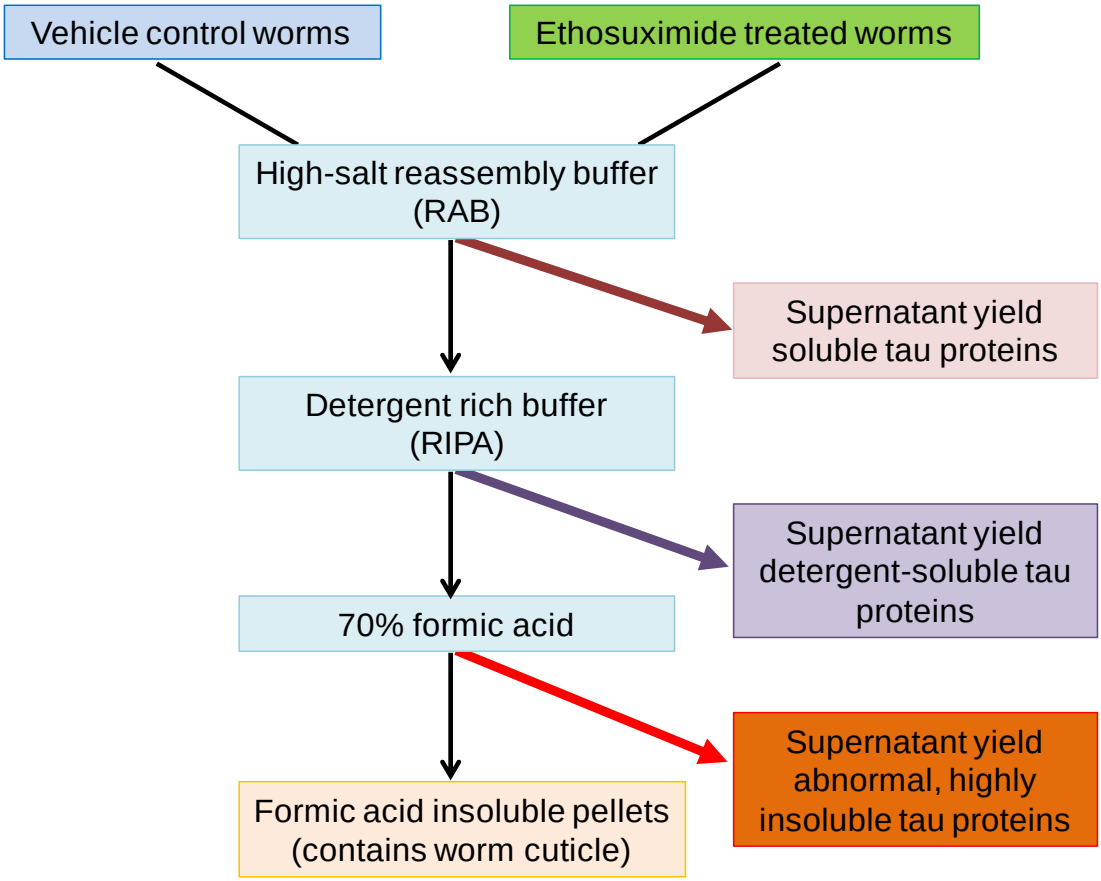

Figure 2.2: Flow chart of sequential extraction steps to isolate aggregation prone tau proteins (detailed in the Methods section). Equivalent masses of vehicle control and ethosuximide treated worms were homogenised in high-salt reassembly (RAB) buffer and blotted to estimate total tau protein. The supernatant following centrifugation constitutes the fraction of soluble Tau and the pellet is extracted with radio-immunoprecipitation assay (RIPA) buffer to extract detergent soluble material. The resultant RIPA insoluble material are finally extracted with 70% formic acid (FA) yielding the detergent insoluble fraction. Supernatants are blotted to estimate differing levels of Tau solubility with the RAB fraction representing the most soluble phase and the FA fraction representing the most insoluble phase.

fraction was then thoroughly dried using SpeedVac and resuspended by sonication in Laemlli buffer.

2.4.3 Protein electrophoresis

The supernatant from sequential fractions or protein extracts was mixed with equal volumes of Laemmli buffer and boiled at 95°C for 5 minutes. Samples were separated by electrophoresis through pre-cast NuPAGE® 12% Bis-Tris Gels and the corresponding MOPS buffer. Combs were removed from the gels and samples were loaded alongside 5 µl pre-stained protein ladder. Gels were run at 120 V until the dye reached the bottom of the gel.

2.4.4 Western blot analysis

The fractionated proteins were transferred to nitrocellulose membranes submerged in transfer buffer (0.025 M Tris, 0.192 M glycine, 20% methanol) in a BioRad Trans-blot Electrophoresis Transfer Cell, at 25 V overnight. Nitrocellulose was blocked for one hour in phosphate-buffered saline (PBS; 2.7 mM KCl, 138 mM NaCl, 1.5 mM KH_2PO_4, 20.4 mM NaH_2PO_4 [pH 7.2]) and 3% (w/v) dried skimmed milk with gentle rocking. The primary antibody was applied at an appropriate dilution in PBS supplemented with 3% (w/v) dried skimmed milk and incubated on a rocker at room temperature for 60 minutes. The nitrocellulose was washed three times in PBS with 0.1% Tween 20 (PBS-T) for five minutes before incubation with an appropriate horseradish peroxidase (HRP)-conjugated secondary antibody (Sigma) at 1:400 dilution for one hour on a rocker. The nitrocellulose was rinsed with PBS-T and immunoreactivity visualised using enhanced chemiluminescence (ECL) reagents A (2.5 mM luminol, 400 µM p-coumaric acid, 100 mM Tris.HCl pH 8.5) and B (0.018% H_2O_2, 100 mM Tris.HCl pH 8.5) mixed 1:1.

Images were captured using a ChemiDoc™ XRS gel imaging system running the Quantity One analysis software (Bio-Rad). The relative abundance of protein levels was quantified from the Western blots using the ImageJ 1.44p software. The intensity of protein was normalised against beta-actin.

Table 2.4: List of antibodies and their dilutions used for western blotting.

Antibodies	Manufacturer	Final Dilution
Anti-actin from mouse, monoclonal	Sigma-Aldrich, UK	1 in 1000
Anti-GFP from mouse IgG1κ (clones 7.1 and 13.1), monoclonal	Roche, Welwyn, UK	1 in 1000
Tau Monoclonal Antibody, Mouse (T46)	Invitrogen, Paisley, UK	1 in 1000
Anti-GFP, Rabbit IgG Fraction (Anti-GFP, IgG), polyclonal	Sigma-Aldrich, UK	1 in 400
Anti-Mouse IgG (whole molecule) - Peroxidase antibody produced in goat	Sigma-Aldrich, UK	1 in 400

2.5 MICROARRAY HYBRIDISATION AND ANALYSIS

2.5.1 *C. elegans* growth and collection

Maintenance of large synchronous cultures of old nematodes is challenging due to the offspring generated during the onset of reproductive output. Rather than using fluorodeoxyuridine to inhibit embryonic development, which has recently been shown to affect the worm (Aitlhadj and Stuerzenbaum, 2010, Davies *et al.*, 2012) and temperature sensitive strain GE24, *pha-1(e2123)*, in which reproduction resembles wild type at 15°C, but is 100% embryonic lethal at 25°C, we first treated gravid N2, *dnj-14(ok237)* and *dnj-14(tm3223)* adults with hypochlorite to release embryos. Synchronised embryos were then hatched on ethosuximide plates and grown at 20°C until day 2 of adulthood. 50 gravid hermaphrodites of each strain

were then picked to lay eggs on one drug dish for six hours at room temperature. Progeny were grown and 400 were selected at the L4 stage and transferred every 2 days until day 6 of adulthood was reached. 40 hermaphrodites were cultured on each Petri dish. When worms reached age day 6, they were washed off plates using 100 µl DNase/RNase-free distilled water (Invitrogen) and 400 µl of TRIzol® Reagent (Invitrogen) was added and the mixture was vortexed for 2 minutes. Worms were stored at -80°C until RNA isolation. Four individual replicates were reared and processed in tandem.

2.5.2 Total RNA extraction and purification

Total RNA was extracted using a combined TRIzol® Reagent (Invitrogen) and RNAeasy (Qiagen) column method. Following one freeze and thaw cycle, samples were disrupted and homogenised on a vortex shaker in a 4°C cold room for 40 minutes. A further 200 µl of TRIzol® was added and vortexed before the second freeze and thaw cycle. 140 µl of chloroform was added before centrifugation at 12000 x *g* for 15 minutes at 4°C. Following two separations of aqueous upper phase with chloroform, RNA was precipitated by adding dropwise to an equal volume of 70% ethanol made in RNase-free water. RNA was then treated with RNase-free DNase I (Qiagen) before purification and concentration using RNeasy Mini Kit (Qiagen) according to manufacturer's instructions. RNA concentration and purity were quantified spectroscopically using a NanoDrop 1000 spectrophotometer (Thermo Fisher Scientific, Waltham, MA, USA) with A_{280}/A_{260} and A_{260}/A_{230} ratios between 1.8-2.6 being considered acceptable RNA. 24 purified total RNA samples free from genomic DNA were then submitted to the Liverpool Genome

Facility Unit where they were fluorescently labelled with different fluorophores during reverse-transcription, combined and hybridised to Affymetrix *C. elegans* GeneChips (Affymetrix, High Wycombe, UK). Dr. Lucille Rainbow first performed RNA quality control in which the reliability of the RNA samples was ascertained using an Agilent 2100 Bioanalyser RNA 6000 Nano chips. An RNA integrity number (RIN) between 1 and 10 was then assigned, 1 = degraded and 10 = intact. In this study, RIN of greater than 7 out of 10 was accepted for further analysis by microarray and all RNA samples submitted showed no signs of degradation. The best three preparations per condition were used for subsequent RNA amplification, labelling and hybridisation to Affymetrix *C. elegans* GeneChips. The remaining preparations were used for qPCR validation of microarray results. 100 ng of total RNA was used as initial input, and the Affymetrix GeneChip 3'IVT Express Kit was used for target preparation for microarray expression analysis according to manufacturer's instructions. 15 µg of aRNA was fragmented, and 12.5 µg labelled fragmented aRNA was hybridised for 16 hours on *C. elegans* Genome arrays at 45°C in a GeneChip Hybridisation Oven 640. Following hybridisation the arrays were washed on a GeneChip® Fluidics Station 450 using the GeneChip Hybridisation, Wash and Stain kit and fluidics script FS450_0004 and scanned using the GeneChip® Scanner 3000 7G.

2.5.3 Data generation and diagnostic analysis

Initial diagnostic and differential expression (DE) analysis of the microarray data were performed by Dr. Yongxiang Fang from the Department of Functional and Comparative Genomics using the statistical analysis tools R packages Affy (version 2.15.2) which has been widely used in statistical

analysis of biological data and limma (version 3.14.4) that is specialised for Affymetrix data. Background correction and normalisation of raw Affymetrix array data were conducted using Robust Multi-array Average (RMA) function built in Affy package (Irizarry *et al.*, 2003). The data model is a linear model which has 6 parameters representing the $\log_2$ expression of 9 sample groups respectively. The 9 contrasts were evaluated based on the outcomes of model fitting. The interested contrasts were obtained by approach of making contrasts built in limma package. The significance test of the estimated logFC ($\log_2$ Fold Change) for each contrast was performed by empirical Bayes function packed in limma and *p*-values were adjusted using Benjamin and Hochberg False discovery rate (FDR) control approach to deal with the effect of multiple tests (Benjamini and Hochberg, 1995). DE genes with a FDR corrected *p*-value less or equal to than 0.01 and fold change greater than 2 were called significantly differentially expressed.

2.5.4 Bioinformatic analysis

To analyse and interpret gene expression data, differentially expressed genes (DEGs) which are consistently responsive to ethosuximide treatment in all conditions relative to untreated control were considered.

2.5.4.1 Gene Ontology analysis

The functional annotation and clustering of putative ethosuximide targets were assessed using both the Database for Annotation, Visualization and Integrated Discovery (DAVID) v6.7 (http://david.abcc.ncifcrf.gov/) software (Dennis *et al.*, 2003, Huang *et al.*, 2008) from the National Institutes of Health, and the mENCODE Modmine bioinformatic suite (http://intermine.modencode.org/) (Contrino *et al.*, 2012, Smith *et al.*, 2012b)

in order to identify trends in the biological processes and molecular functions of the identified DEGs. For gene enrichment analysis, Affymetrix *C. elegans* probe IDs of commonly regulated DEGs were first submitted to DAVID (http://david.abcc.ncifcrf.gov/) as a “Gene list” and following selection of *C. elegans* background, were converted to either Ensembl or Worm Base IDs using the Gene ID Conversion Tool (>90% converted). For GO Term analysis, the “Biological Process”, “Cellular Component” and “Molecular Function” categories were studied using the GO FAT default settings. Functional annotation clustering was performed with the default criteria and prevalence of annotation terms within the list of DE genes was compared to the prevalence in the whole *C. elegans* genome. Protein domains and pathway enrichment were also determined using DAVID by querying the Interpro and Kyoto Encyclopedia of Genes and Genomes (KEGG) databases, respectively. Enriched genes were obtained by performing Gene Functional Classification Clustering using threshold count 5, EASE 0.1 and medium stringency. GO terms and domains with less than 4 genes were discarded and an enrichment score over 1.3 represents a significant enrichment. Enrichment in GO categories, protein domains, pathways and publications were also assessed using modENCODE modMine. Human orthologues of the corresponding worm genes were derived from the OrthoList online tool (http://www.greenwaldlab.org/ortholist.). Within the search window, the list of enriched *C. elegans* DEGs was inputted as Ensembl gene IDs to retrieve the predicted human genes which were in the Ensembl ENSG ID format. All orthologous genes with a duplicate output in one of the species were counted only as one gene.

2.5.4.2 Motif analysis

Using complementary algorithms, we analysed within up to 200 bp of intergenic sequence upstream of common DEGs to identify shared DNA motifs. Regulatory Sequence Analysis Tools (RSAT; http://rsat.bigre.ulb.ac.be/rsat/) (Turatsinze *et al.*, 2008) was first used to retrieve the 200 bp upstream sequences of *C. elegans* genes, which were then submitted to RSAT oligo analysis (Thomas-Chollier *et al.*, 2008, Thomas-Chollier *et al.*, 2011) and peak-motifs analysis (Thomas-Chollier *et al.*, 2012a, Thomas-Chollier *et al.*, 2012b), multiple expectation maximisation for motif elicitation (MEME, http://meme.nbcr.net/meme/), BioProspector (http://seqmotifs.stanford.edu) and SCOPE motif finder (http://genie.dartmouth.edu/scope/), in each case specifying an oligonucleotide length of 6-8 bases while all the other parameters were set as default, to identify sequence elements that were statistically overrepresented. To display consensus motifs generated from BioProspector, retrieved motif matrices in TRANSFAC format were analysed by WebLogo (http://weblogo.berkeley.edu/logo.cgi).

2.5.4.3 Cross-database analyses

In order to increase the coverage of gene expression annotations and gain further insights into complex chemical-gene interaction networks, our microarray data was compared with 2 public high-content data repositories: Serial Pattern of Expression Levels Locator (SPELL Version 2.0.3, http://spell.caltech.edu:3000/) (Hibbs *et al.*, 2007) and Comparative Toxicogenomic Database (CTD, http://ctdbase.org/). Stringent subsets of commonly up- or down-regulated ethosuximide-responsive genes were

queried both combined as well separately in the SPELL search engine. Ethosuximide was directly searched within CTD for known therapeutic information, cross-species chemical-gene/protein interactions, and chemical- and gene-disease associations.

2.5.5 Real-time quantitative PCR

2.5.5.1 Primer design and analysis

qRT-PCR primers (Table 2.2) were designed using the DNA Dynamo Sequence Analysis Software (Blue Tractor Software, Llanfairfechan, UK) to the following criteria: gene specific primers were all between 20 and 25 bp long; the product of the PCR was between 280-330 bp in length; the product spanned an intron to give differentially sized genomic and cDNA products; the melting temperatures of the primer pairs were matched and were between 55 and 60°C. *act-1* and *pmp-3* which showed no significant changes in microarray analysis and has been extensively used as normalising genes in differential expression studies in *C. elegans* (Zhang *et al.*, 2012d) were chosen as reference genes. The compatibility and specificity of these primers were tested on samples from the microarray, and analysed by gel electrophoresis (**2.2.4**). Only primer sets showing single bands of the expected size were used for qPCR analysis. Melting curve analysis during qPCR was also performed with each primer pair to ensure that quantification is the result of only one product.

2.5.5.2 cDNA Synthesis and quantitative real-time RT-PCR

For each synthesis reaction, appropriate RNA sample volume was calculated with the results from the spectrophotometry and added to ensure the

presence of 200 ng of total RNA for each sample in the group, and 1 µl of random primers (250 ng/µl; Promega), 1 µl of dNTPs (10 mM; Invitrogen), and RNase-free water were added up to a volume of 12 µl. Samples were mixed, centrifuged briefly and incubated for 5 minutes at 70°C, and then immediately chilled on ice for 2 minutes. After this first incubation, 4 µl of 5X M-MuLV RNaseH- Reaction buffer for RT, 2 µl of 0.1 M DTT, 1 µl of RNaseOUT (40U/µl) and 1 µl of ProtoScript M-MuLV Reverse Transcriptase (NEB) were added to the 12 µl mix as a master mix. Contents were then incubated in a G-Storm GSX thermal cycler (GRI, Braintree, UK) first at 25°C for 5 minutes followed by 1 hour at 42°C before 2 minutes at 92°C to inactivate the RT enzyme. The cDNA was diluted (1:50) with DEPC treated water and stored at −80°C until required.

For gene expression analysis, master mixes for diluted cDNA samples mixed with DEPC water and selected qRT-CPR primers mixed with iTaq™ Universal SYBR® Green Supermix (BioRad) were made and added to 96-well plates sequentially to make a final reaction volume of 10 µl per well. A non-template control (sample was substituted by sterile water) was also included. Reactions were performed using an IQ5 real-time PCR detection system (Bio-Rad). The thermocycler was programmed to first heat to 95°C for 3 minutes, followed by 40 cycles of a 10 seconds denaturation step at 95ºC, a 30 seconds annealing step at 58°C, and a 30 seconds elongation step at 70ºC. The final cycle consisted of 30 seconds at 95ºC and after the thermocycling reaction, a 65-95°C melt curve with a gradient of 0.5°C was inserted, allowing detection of possible nonspecific products. All qRT-PCR reactions were carried out on 3 biological replicates with three technical

replications and transcript expression was analysed using Bio-Rad CFX Manager 3.0 software. The relative expression of each gene was calculated by normalising the Ct values for test genes to the two reference genes (*act-1*, and *pmp-3*).

2.6 MAMMALIAN CELL BASED METHODS

2.6.1 Cell culture

A mouse neuroblastoma cell line was used as the prototype neural progenitor cells in this study. Cells were passaged every 2-5 days. Adherent Neuro2A (N2A) cells were maintained as a monolayer culture in 75 cm^2 culture flasks in Dulbecco's Modified Eagle Medium (DMEM Gibco) supplemented with 10% foetal bovine serum (FBS), 1% penicillin/streptomycin and 1% non-essential amino acids (Gibco) and maintained in 75 cm^2 flasks at 37°C in a humidified atmosphere of 95%air/5% CO_2. Cells were subcultured at or near confluency by trypsinisation (0.25% trypsin; Mediatech Inc.) followed by dispersion of the cells into single cell suspension in new growth medium and plating onto new growing surfaces. Cell counts were assessed by applying an equal mixture of trypan blue dye and cell suspensions to the chambers of a haemocytometer.

Cells in the four corner squares were counted, excluding cells that touched the upper and left hand side edges of the squares. The mean number of cells per square was calculated, and this number was multiplied by $1.0x10^4$ to give the number of cells per ml. Depending on the analytical method, cells were diluted appropriately and seeded on different types of plates. For qRT-PCR

analysis, cells were grown on 6-well plates and seeded in duplicate for condition. For microscopy, cells were seeded on glass-bottom 35 mm dishes (10 mm glass surface diameter, MatTek Corporation, Ashland, MA, USA).

2.6.2 Transfection

Cells were taken at 60-80% confluence and plated out in 35-mm glass bottom dishes (MatTek, Ashland, MA). To stimulate differentiation prior to transient transfection and to limit the loss of compound activity as a result of protein binding in the serum-cultured cell lines, N2A cell media was exchanged for DMEM supplemented with 2% FBS, 1% penicillin-streptomycin, 20 µM retinoic acid and 0.56 mg/ml ethosuximide. In all the experiments, cells in medium with equal volumes of PBS served as the controls. Cells were then transiently transfected with 3 µg of polyQ97-eGFP-pcDNA3.1(+) Myc His plasmid constructs (a generous gift from Professor Stephen High, University of Manchester, originally made by Professor Ron Kopito's lab in Stanford) or polyQ25-eGFP-pcDNA3.1(+) Myc His control plasmid construct using PromoFectin transfection reagent (PromoKine) according to the manufacturer's protocol. The transfection reaction mixture was incubated at room temperature for 30 minutes to allow the lipid and DNA complexes to associate then added dropwise to the cells. Cells were then maintained at 37°C before being used in experiments.

2.6.3 Ethosuximide treatment and RNA extraction

To analyse the effect of ethosuximide on the expression of FOXO targeted genes, qRT-PCR was used. Cells were plated subconfluently at a density of 1.5×10^6 cells per well in flat bottom 6-well microtiter plates in a total volume of 3 ml growth medium supplemented with 10% regular FBS. After overnight

incubation to allow cells to adhere to wells, media was exchanged for DMEM containing 2% FBS, 1% penicillin/streptomycin and 20 μM retinoic acid to induce N2A cell differentiation. After 24 hours, N2A cells were treated with vehicle control (PBS) or increasing concentration of ethosuximide (100 μg/ml, 0.56 mg/ml and 1 mg/ml, covering the clinically relevant concentrations) for 5 hours. A stock solution of ethosuximide was prepared in PBS at a concentration of 100 mg/ml. Following treatment, the full content of a 6-well culture plate was pooled for each experimental condition. Total RNA was then isolated from 3 independent treatments of N2A cells by first homogenising cells directly in RLT buffer (Qiagen) containing β-mercaptoethanol and guanidine and subsequently using RNeasy Mini Kit (Qiagen) following manufacturer's instructions. To avoid DNA contamination, the samples were exposed to an on-column treatment with RNase-Free DNase 1 (Qiagen). The isolated total RNA were quantified by use of OD measurement at 260 and 280 nm using a spectrophotometer (Thermo Fisher Scientific, Madison, WI, USA) (all RNA samples had an A_{280}/A_{260} ratio >1.8).

2.6.4 cDNA synthesis and real-time RT-PCR quantification of mRNA expression of FOXO target genes

1 μg of DNase-treated total RNA was reverse transcribed to cDNA and qRT-PCR was run as described in **2.5.5.2**. Mouse gene-specific primer sequences obtained from PrimerBank (http://pga.mgh.harvard.edu/primerbank/) were validated by RT-PCR and gel electrophoresis. For each sample, the Ct values for test genes were normalised to that for the reference genes glyceraldehyde-3-phosphate dehydrogenase (GAPDH) and β-actin (ACTB), and a sample without cDNA was used as no template control. Transcript

expression analysis was performed with Bio-Rad CFX Manager 3.0 software (Biorad), which automatically set the baseline and the threshold.

2.6.5 Confocal laser scanning microscopy and image analysis

Live transfected cells were imaged using a a Leica AOBS SP2 microscope (Leica Microsystems, Heidelberg, Germany) with an optimal pin hole of 1 airy unit and using both a 20x dry objective with a 0.5 numerical aperture and a 63x water-immersion objective with a 1.2 numerical aperture. The percentages of aggregates and rate of cell death were determined at 24, 48 and 72 hours post-transfection. To monitor neuronal viability, media was aspirated before cells were incubated for 20 minutes in 2 ml of Krebs-Ringer buffer [20 mM Hepes (pH 7.4), 145 mM NaCl, 10 mM glucose, 5 mM KCl, 3 mM $CaCl_2$, 1.3 mM $MgCl_2$ and 1.2 mM NaH_2PO_4] containing 0.5 µM SYTOX Orange® nucleic acid dye (Invitrogen) at 37°C and 5% CO_2. For dual imaging of EGFP-tagged polyQ proteins and dying/non-viable cells labelled with SYTOX Orange®, cells were excited with 488 nm and 453 nm lasers and light was collected at 465-500 nm (Alexa 488) and 615-690 nm (Alexa 594), respectively. The channels of the images were taken sequentially with a frame average of 1. Five to ten low- and high-magnification fields were randomly taken for each condition. EGFP and SYTOX Orange® fluorescence and phase images were exported as Tiff files and were superimposed by using the Leica LAS AF Lite imaging software. A minimum of 50 cells per condition were counted either manually or by using the ImageJ Java-based imaging software (NIH, USA) in which GFP channel images were measured with the '*Analyze particles*' command with a threshold of 180-255. Average

percentage of transfected cells with aggregates was calculated from three independent experiments.

2.7 STATISTICAL ANALYSIS

If two data sets were being directly compared, Student's *t*-test was used. For comparison of multiple data sets i.e. age-dependent thrashing in one analysis, a one-way analysis of variance (ANOVA) was used. These tests were performed in Microsoft Office® Excel® 2007.

Lifespan analyses were performed using the Online Application for the Survival Analysis of Lifespan Assays (OASIS; http://sbi.postech.ac.kr/oasis/introduction/) (Yang *et al.*, 2011). Mean lifespans were compared using the log-rank (Mantel-Cox) test, and mortality at more specific time points was compared using Fisher's exact test.

CHAPTER 3: PHENOTYPIC CHARACTERISATION AND SELECTION OF *C. ELEGANS* NEUORODEGENERATIVE DISEASES MODELS

3.1 INTRODUCTION

In order to delineate the complex patho-mechanisms of human neurodegenerative disorders (NDs), a large number of animal models have been generated and have facilitated the testing of potential therapeutic strategies and investigation of disease progression in a manner not possible in humans. Modeling of NDs has been primarily conducted in mouse and invertebrate models which reproduce cellular and behaviour phenotypes akin to the broader clinical manifestations. The employment of a plethora of powerful model organisms with shorter generation times such as *C. elegans, S. cerevisiae* and *D. melanogaster*, has expedited the initial screening of genetic and pharmacological modifiers and target characterisation which in turn can not only illuminate a prospective cellular cause of protein-misfolding diseases like HD, PD, ALS and AD, but also the neuroprotective mechanisms against underlying functional aspects of neurodegeneration (Brignull *et al.*, 2007, Kearney, 2011)

In particular, the use of the nematode *C. elegans* as a primary platform to probe the poorly defined disease mechanisms of NDs and a more rapid and cost-effective means towards novel gene and drug discovery has escalated over the last decade. As described in Chapter 1, the *C. elegans* nervous system functionally recapitulates many of the characteristics of the vertebrate brain. This along with other major advantages offered by *C. elegans* i.e. its amenability to high-throughput genetic, genomic, proteomic, and drug screening approaches have facilitated the evaluation of the pathological similarities between targeted *C. elegans* neurons and human

disease neurons to provide new insights into different aspects of the human neurodegenerative maladies.

Indeed, a diverse set of informative, tissue-specific *C. elegans* ND models have been developed by molecular, genetic and chemical manipulations (Appendix Table A1), i.e. using mutagenesis (deletion libraries, transposon based insertion), RNA interference (RNAi)-mediated knockdown, transgenic overexpression of exogenous neurodegeneration-associated, aggregative proteins in specific tissues, or acute and chronic exposure to neurotoxins (Johnson *et al.*, 2010). The most widely studied are the tissue-specific transgenic models which manifest abnormal behavioural or pathological phenotypes that faithfully recapitulate the salient cellular, molecular and pathological aspects of several distinct human NDs processes. These models have been based on muscular or neuronal expression of aggregation-prone proteins such as mutant Tau, SOD1 and α-synuclein proteins, polyQ constructs, Huntingtin fragments and toxic $A\beta_{1-42}$, with features that are reflective of the human NDs including accumulation of disease proteins in abnormal aggregates and toxic disease protein-induced neuronal loss and dysfunction. Most of these models were subjected to medium- or high-throughput genome-wide forward and reverse genetic screens to identify genetic regulators and cellular processes of α-synuclein inclusion formation (van Ham *et al.*, 2008), polyQ (Nollen *et al.*, 2004) and mutant SOD1 aggregation (Wang *et al.*, 2009b), α-synuclein and polyQ-induced toxicity (Parker *et al.*, 2007), presenilin function (Link, 1995) and Tau-induced pathology (Kraemer *et al.*, 2006), as well as chemical screens that directly explore effective pharmacological compounds that prevent or

improve loss of neuronal function in ND states prior to testing in higher organisms (Braungart *et al.*, 2004, Voisine *et al.*, 2007, Sleigh *et al.*, 2011, McCormick *et al.*, 2013). A handful of lead molecules originating from worm-based screening assays such as insulin sensitisers for the treatment of type 2 diabetes or insulin resistance, and voltage gated ion channel modulators to treat arrhythmia are already in advanced stages of drug discovery (Artal-Sanz *et al.*, 2006). Numerous novel compounds and known human drugs were efficacious in worm ND models and, more importantly, shown to be transferrable to mammals (Parker *et al.*, 2005, Cherny *et al.*, 2012, Vaccaro *et al.*, 2012, Matlack *et al.*, 2014).

To date, diverse genetic modifier screens in multiple ND model systems have identified a plethora of genes and pathways that can be modulated to delay and even prevent disease states. Most of these genetic modulators and underlying cellular mechanisms affected appear to be disease specific despite the shared feature of protein misfolding/aggregation. Unlike most identified genetic modifiers, chemical modifiers are not disease-specific and have therapeutic potential for multiple NDs (Chen and Burgoyne, 2012). It was reported that generally neuroprotective interventions can be identified by searching for compounds that are able to compensate for the loss of an endogenous physiological neuroprotective factor (Sleigh *et al.*, 2011). Work from our lab has shown that *dnj-14*, the worm orthologue of the human *DNAJC5* gene mutated in Adult-onset Neuronal Ceroid Lipofuscinosis (ANCL), is an evolutionarily conserved neuroprotective protein and can be found in all neurons. Thus drugs that can bypass its function may be generally neuroprotective, and would require further assessment using

different worm models. Indeed, the *C. elegans* null mutant model of ANCL containing loss of function mutations in *dnj-14* has already demonstrated its potential for chemical genetic screening, by identifying a *sir-2.1*-independent neuroprotective effect of resveratrol (Kashyap *et al.*, 2014).

Each model system has unique experimental advantages and the integration of different analyses across a range of different disease models offers exceptional promise for multi-model target discovery, an in depth understanding of ND pathology, and guiding the development of therapeutic interventions by identifying new pharmacological and genetic modifiers of ND pathology.

In this perspective, we take a combinatorial approach by integrating multiple well-defined disease-specific *C. elegans* models for pathogenesis of the different ND-associated proteins to test therapeutic interventions that target shared pathogenic pathways. In this chapter, nine models of various different NDs were selected and characterised. Several assays were performed to measure different outcomes of toxicity exhibited by distinct models. Yet the heterogeneity, incomplete manifestations and lack of reproducibility displayed by most ND models tested are likely to obscure their ability to reliably detect modifiers and yield information that parallels human NDs and these models were therefore dismissed. Three distinct worm ND models: ANCL, FTDP-17 and ALS models which involve deletion of an endogenous neuroprotective gene (*dnj-14*) and pan-neuronal expression of disease-associated mutant Tau and SOD1 proteins, exhibited robust and reproducible phenotypes, and are therefore ideal for the modifier screening depicted in Chapter 4.

3.2 RESULTS

3.2.1 Selection of *C. elegans* neurodegenerative disease models for phenotypic characterisation

To establish tractable models for efficient probing of the age-dependent human NDs, our first step, as shown in Appendix Table A1, was to gather information from literature on all existing *C. elegans* NDs models. Many studies have relied heavily on transgenic models with muscle-specific expression of misfolded proteins for reasons of experimental convenience: muscle-specific promoters are strong and well-characterised; muscle cells are significantly larger than neurons to provide an easy means to study transgene expression, product localisation, protein-induced toxicity and protein aggregation; facilitating work under comparatively low magnification; muscle cells are also more amenable to RNAi, in comparison to neurons (Lehmann *et al.*, 2012).

Given that pathologies of human NDs usually manifest primarily in neurons and processes, the threshold for pathology relevant to neurons is likely very different to muscle cells. Models with transgene expression in neuronal tissues may therefore more accurately represent the disease protein-induced toxicity seen in ND. Expression in muscle does not directly capture the neurodegeneration seen in ND and could lead to identification of muscle-specific regulators not expressed in neurons. Also certain neuronal tissue-specific genes that affect neurodegeneration and the actual site where the misfolded proteins in question cause disease, are likely to be missed (van Ham *et al.*, 2009). Thus, all the muscle expression models were excluded from our initial list. The remaining neuronal models were prioritised by

assessing the robustness, reproducibility and reliability of their reported neurodegenerative phenotypes, availability of the models and ease of scoring.

An important prerequisite for effective high-throughput genetic or pharmacological screening, is the availability of a robust disease model that reliably exhibits the critical manifestations of the corresponding NDs. *C. elegans* models with weak or non-existent phenotypes are less likely to be informative and were thus excluded. It is essential for the selected disease models to generate phenotypes that are pathologically relevant to human disease states and can be scored quickly and easily for improvement to accommodate extensive screening paradigms. Readily assayed neurodegenerative phenotypes i.e. motility defects of a number of the models would provide a particularly suitable, direct and sensitive read-out for high-throughput screening of large numbers of drug candidates or molecular targets of protein-evoked neurotoxicity. Disease-related phenotypes should not only be robust and easily discernible, so that the models would be informative without having to look at subtle behavioural differences, but also quantitative to facilitate the detection of not just the strong modifiers, but also weak modifiers that may still significantly modify the phenotype. Low phenotypic variability would also be favoured in order to gain power in the statistical identification of positive hits (Garcia-Alcover *et al.*, 2013).

In this regard, nine distinct *C. elegans* neuronal models of various forms of human NDs (Table 3.1) that developed robust neurodegenerative phenotypes were chosen, obtained and analysed based on their well characterised pathology. To further control for phenotypic variability, almost

all of our selected transgenic models are outcrossed stable integrants, as this ensures all worms have the same transgene expression levels within the isogenic population and the removal of background and unwanted mutations from the integration process. This in turn can help to reduce clonal heterogeneity.

Although *C. elegans* ND models are increasingly used for genetic and chemical screening, their relatively rapid disease-onset seems simplistic and questionable in the context of complex, chronic NDs (Weinberg and Wood, 2009). Not all worm ND models generated can be used for subsequent screens. Some are of limited suitability to investigate particular mechanisms in detail depending on the intention of the experiment. It is therefore necessary to address the appropriateness of the selected ND models before considering their use as model system for screening. Phenotypic characterisation of the selected disease models was our next step in establishing informative models for which neuron-specific, novel modifiers of disease protein-mediated pathogenesis can be identified.

Type of disease model	NDs	Genotype	Phenotypic Analysis	Reported Phenotype
Mutant	**ANCL**	***dnj-14*** $^{-/-}$	Locomotion, pharyngeal pumping, **lifespan**, food-race, aldicarb, chemotaxis, mechanosensation, and fluorescence microscopy	**Short lifespan; age-dependent progressive impairment in locomotion; chemosensory defects; neurodegeneration**
Mutant	**SMA**	***smn-1*** $^{-/-}$	**Locomotion,** pharyngeal pumping, lifespan	**Thrashing rate progressively declined and almost completely ceased after 5 days post-L1. Pharyngeal pumping rates showed a rapid and progressive decline. Mean lifespan is 6.0 days Vs 17.7 days for N2**
Transgenic overexpression	**FTDP-17**	**TauV337M**	**Locomotion**, aldicarb, **fluorescence microscopy**	**Strongly defective locomotion; accumulation of insoluble tau; neurodegeneration; impaired presynaptic cholinergic transmission; reduced lifespan**
Transgenic overexpression	**ALS**	**G85R SOD1-YFP**	**Locomotion**, aldicarb and **fluorescence microscopy**	**Severely reduced forward crawling, thrashings and were strongly resistant to aldicarb**
Transgenic overexpression	**AD**	**$A\beta_{1-42}$**	**Locomotion,** chemotaxis, 5-hydroxytryptamine sensitivity, lifespan, food-sensing assay, egg laying	**Defective in chemotaxis toward benzaldehyde, associative learning, and thrashing; hypersensitive to serotonin; forms amyloid deposits; partial sterility due to germline proliferation defects and embryonic lethality**
Transgenic overexpression	**HD**	**Htt-Q150**	**Dye filling, nose-touch**	**Accelerated polyQ mediated neurodegeneration. Vast majority (>90%) of ASH neurons undergo cell death in less than three days; severe defect in the nose touch response**
Transgenic overexpression	**PD**	**α-syn WT**	**Food-sensing assay**, dopamine level measurement, fluorescence microscopy, toxicant exposures, oxygen consumption and mitochondrial membrane potential analysis	**Failure in modulation of locomotory rate in response to food**
Transgenic overexpression	**PD**	**CAT-2**	Fluorescence microscopy, **food-sensing assay**	
Chemical treatment	**PD**	**GFP WT subjected to 6-OHDA + ascorbic acid**	**Fluorescence microscopy**	**Neuronal process blebbing, cell body rounding with process loss, and cell body loss reproducibly appear in this order within a few hours.**

Table 3.1: Selected *C. elegans* neuronal models of human neurodegenerative diseases (NDs) for phenotypic characterisation. Transgene expressions of many *C. elegans* ND models are limited to muscle cells. In our study, neuronal-relevant models were favoured as they provide better relevance to NDs than muscle expression models. Neuronal models were subsequently prioritised on the basis of information presented in the literature. In each case we independently confirmed the pattern of expression of the promoters and validated the reliability of the chosen models by analysing their neurodegenerative phenotypes. A combination of imaging and behavioural analyses that were applied in our study to verify previous observations are highlighted in bold. We assessed the robustness, reliability and reproducibility of selected ND models to determine whether they are suitable for future modifier screening: NDs: FTDP-17, Frontotemporal dementia with parkinsonism-17; ALS, Amyotrophic lateral sclerosis; AD, Alzheimer's disease; HD, Huntington's disease; PD, Parkinson's disease, SMA, Spinal muscular atrophy.

3.2.2 Neuropathological characterisation of established *C. elegans* neuronal models of human NDs

3.2.2.1 Characterisation of *C. elegans* Adult-onset Neuronal Ceroid Lipofuscinosis (ANCL)

As mentioned in Chapter 1, both *in vitro* and *in vivo* studies have demonstrated a potential generally neuroprotective role of the presynaptic chaperone cysteine string protein (CSP), which is supported by recent findings that mutations in the human CSPα gene *DNAJC5* result in ANCL, a rare hereditary neurodegenerative disorder clinically characterised by progressive deterioration of cognitive and motor skills, generalised seizures and premature death (Noskova *et al.*, 2011). DNJ-14 is the worm orthologue of the *DNAJC5* gene mutated in ANCL and loss of function mutations in *C. elegans dnj-14* have been the main focus of our lab. In-depth characterisation of a neuronal worm ANCL model and demonstration of its potential for chemical screening were pursued by another PhD student before the initiation of this study (Kashyap *et al.*, 2014). It was reported that *dnj-14* is a key neuroprotective gene like its mammalian homologue, CSP, since two mutant alleles of *dnj-14, ok237* and *tm3223,* recapitulated important features of ANCL and neurodegeneration by exhibiting age-dependent aggravation of motor dysfunction, a reduction of neurotransmitter release and severe progressive chemosensory defects which precede neurodegeneration of sensory neurons (Kashyap *et al.*, 2014). As shown in Figure 3.1, *dnj-14* mutants also exhibited a significant higher mortality compared to the wild-type (WT) N2 [Mean lifespan in days of adulthood with SEM: N2=19.11 ± 0.62; *dnj-14*(*ok237)*=15.79 ± 0.44], with a 17% reduction (p<0.0001) in the

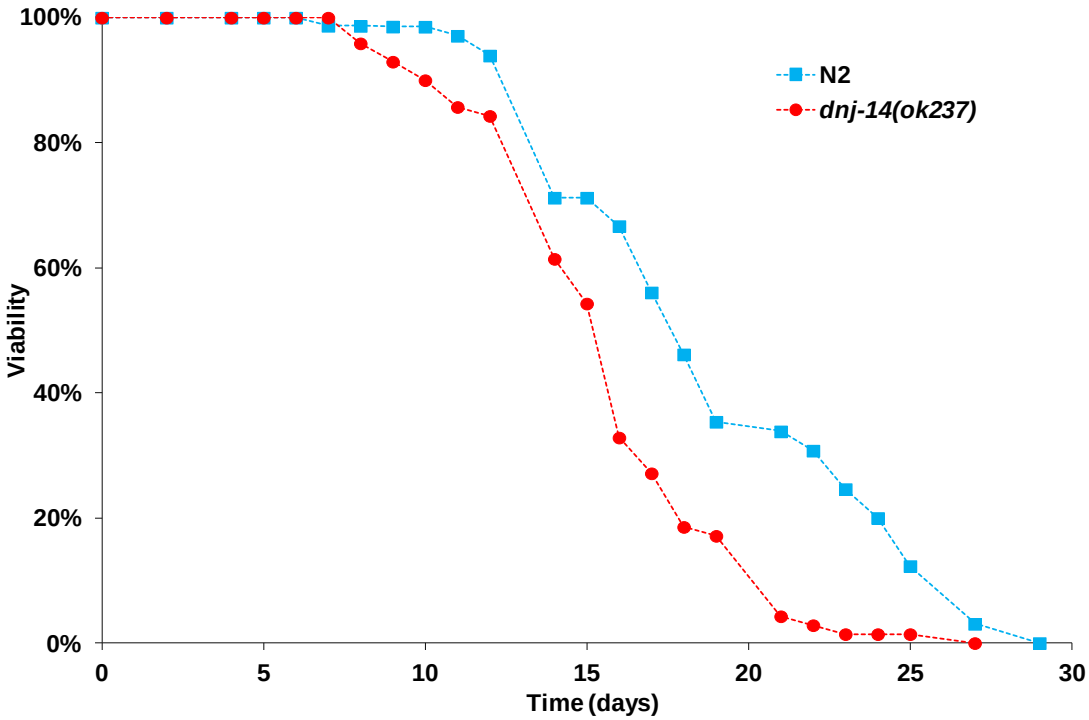

Figure 3.1: *C. elegans* ANCL model has a short lifespan. Kaplan-Meier survival curves of synchronously ageing ANCL model *dnj-14(ok237)* and wild-type (WT) N2 DRH hermaphrodites cultured at 20 °C. Worms were age-synchronised by timed-egg lay and once the progeny reached L4 stage, 25 worms were transferred onto individual seeded plates, and monitored for survival every alternate day and transferred to fresh plates to prevent progeny formation. Day 0 corresponds to L4 stage. The lifespan of populations of synchronised *dnj-14(ok237)* worms was observed and compared with the WT N2 strain. Statistical analysis was performed using Online Application for the Survival Analysis of Lifespan Assays (OASIS; http://sbi.postech.ac.kr/oasis/introduction/) (Yang *et al.*, 2011). Log-rank (Mantel-Cox) test was used to calculate significance. The lifespan of *dnj-14(ok237)* mutants is significantly lower (***p<0.0001) than the WT N2. Above represented are pooled data from two independent biological replicate studies. Mean lifespan in days of adulthood: N2=19.11 ± 0.62 (n=105); *dnj-14(ok237)*=15.79 ± 0.44 (n=108).

mean lifespan. Utilisation of the *dnj-14(ok237)* mutants and their lifespan as phenotypic readout in a previous focused drug screen identified a *sir-2.1*-independent neuroprotective effect of resveratrol (Kashyap *et al.*, 2014), thus confirming the suitability of this model for neuroprotective drug screening.

3.2.2.2 Establishment of physiological defects in a *C. elegans* model for Alzheimer's disease (AD)

To consolidate the previous observations of $A\beta_{1-42}$ induced toxicity in *C. elegans*, we selected and obtained the strain CL2355 [*smg-1(cc546ts)*; *snb-1*::*Aβ*$_{1-42}$::long 3′-UTR] which was engineered to inducibly express the signal peptide::$A\beta_{1-42}$ pan-neuronally upon temperature upshift (Dosanjh *et al.*, 2010, Lublin and Link, 2013). It also harbours strong intestinal GFP courtesy of the co-injected P_{mtl-2}::GFP construct (Figure 3.2A). Strain CL2122 is the empty vector control with no $A\beta_{1-42}$ that also controls for intestinal GFP expression, while strain PD8120 was used as a control for the hypomorphic *smg-1(cc546ts)* mutation in the background of CL2355. To assess neurotoxicity-associated phenotypes arising from transgenic expression of diseased proteins in *C. elegans* neurons, we examined behavioural phenotypes regulated by the nervous system and associated neuronal dysfunction. A simple, yet effective, method to assay neuronal function in *C. elegans* is by assessing thrashing behaviour. When placed in liquid, WT animals thrash actively by repeatedly moving the head and tail to the same side of body, the rate of which can be determined by counting the frequency of the elicited continual body bends per minute. We assayed and compared the motor activity of young and aged adult $A\beta_{1-42}$ expressing CL2355 and control worms reared at the permissive (17°C) and restrictive temperature

(25°C) conditions. The motility of CL2355 worms grown at both 17°C and 25°C was similar to that of CL2122 control animals of the same age at early adulthood, with only minor motor disturbance but no obvious abnormality (Figure 3.2B). Additional ageing caused motility defects such that, by day five, aged CL2355 had > 65% reduction in motility relative to that of CL2122 (Figure 3.2C) and *smg-1(cc546ts)* (Figure 3.2D) grown at 25°C. This decrease in motility was only greatly enhanced by the seventh day of adulthood, as the thrashing rate by the 7-day-old CL2355 animals was < 35% that of CL2122 and *smg-1(cc546ts)* at 25°C (Figures 3.2 A-D). This effect is therefore $A\beta_{1-42}$-expression-dependent since aged control animals CL2122 and *smg-1(cc546ts)* only showed minor degrees of age-related decline. However, the thrashing defect of this neuronal AD model is only semi-penetrant, due to a high degree of worm-to-worm variability. By visual inspection, the behavioural phenotype of individual CL2355 animals varied greatly from being WT to having severely impaired locomotion.

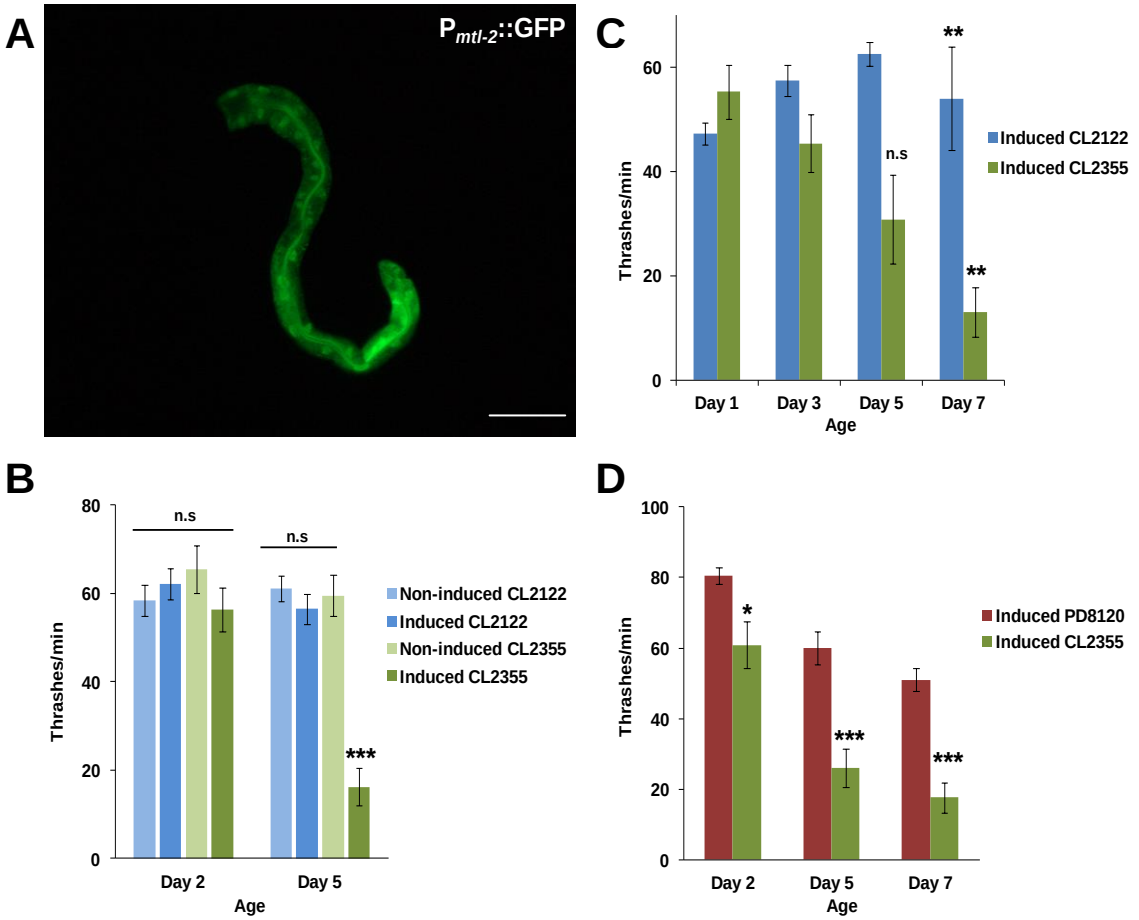

Figure 3.2: Movement defects of temperature-inducible Aβ$_{1-42}$-neuronal expression *C. elegans* strain CL2355. A) Fluorescence microscopy of a non-induced worm with basal expression of *mtl-2::*GFP. *mtl-2* metallothionein gene is expressed exclusively in the intestine; the intensity of *mtl-2::*GFP expression varies in a temperature-dependent manner. Head of worm is to left. Scale bar represents 200 µm. B-D) Quantification of movement defects following temperature-dependent induction of Aβ$_{1-42}$ in transgenic CL2355 animals. A thrashing assay was used to determine whether the neuronal expression of Aβ$_{1-42}$ would affect the behavioural phenotypes of the AD model. Aβ$_{1-42}$ transgenics and controls were assayed for motility in liquid medium at different ages. Synchronised worms of strain CL2122 (empty vector control with no Aβ$_{1-42}$), temperature-inducible Aβ$_{1-42}$-neuronal expression strain CL2355 and strain PD8120 *smg-1(cc546ts)* mutant were maintained at 17°C, and the temperature was then up-shifted to 25°C at 36-48 hrs after hatching to induce the expression of Aβ$_{1-42}$. Rate of body thrashing in liquid for CL2355 raised at 25°C on agar media plates is significantly different from that of CL2122 and PD8120 as locomotion was greatly diminished in the aged neuronal Aβ$_{1-42}$ strain but not in both control strains. The error bars denote standard error of the mean (SEM) from three repetitions of the experiment, and differences were considered non-significant (n.s. $p>0.05$) or significant (*$p<0.05$, **$p<0.01$, ***$p<0.0001$). Statistical analysis: *t*-test to compare control worms with CL2355 neuronal Aβ$_{1-42}$ expressing worms before temperature induction, and after temperature induction.

3.2.2.3 Characterisation of frontotemporal dementia with parkinsonism-17 (FTDP-17) models

The two *C*. *elegans* FTDP-17 models studied here are transgenic for the human Tau protein with the V337M FTDP-17 mutation (Kraemer *et al.*, 2003). The integrated transgene array is expressed in all neurons. While CK10 worms carry both the mutant Tau transgene and the P_{myo-2}::GFP reporter marker for pharyngeal expression (Figure 3.3B), CK49 are triple transgenic worms generated by crossing CK10 with a CZ1200 strain expressing P_{unc-25}::GFP GABAergic marker transgene only (Figure 3.3A) and therefore contain the P_{aex-3}:: *Tau V337M*, P_{myo-2}::GFP and P_{unc-25}::GFP reporter marker transgenes (Figure 3.3C). Using a synchronised population of worms, locomotion at several time points throughout adulthood were quantified with the thrashing assay (Figure 3.3D), as motor deficits have been shown to be a reliable indicator of Tau pathology in *C. elegans*. CK10 and CK49 lines were dumpy and small, and exhibited significantly greater impairment of movement than N2 WT and CZ1200 which serve as non-transgenic (non-Tg) and GFP transgenic control worms, respectively. CK10 worms were partially paralysed and displayed a distinctive dorsal coiler phenotype that is typically associated with mutations causing motorneuron dysfunction. They were also unable to move co-ordinately as a result of the severe neurotoxicity of this mutant protein, but are capable of intermittent short bursts of very fast head thrashes. CK49 were severely uncoordinated (Unc), dumpy, unresponsive and they barely bend in liquid with little or no displacement from the starting position. Each mutant Tau-expressing line never displayed fast body movement even as young adults as their strikingly

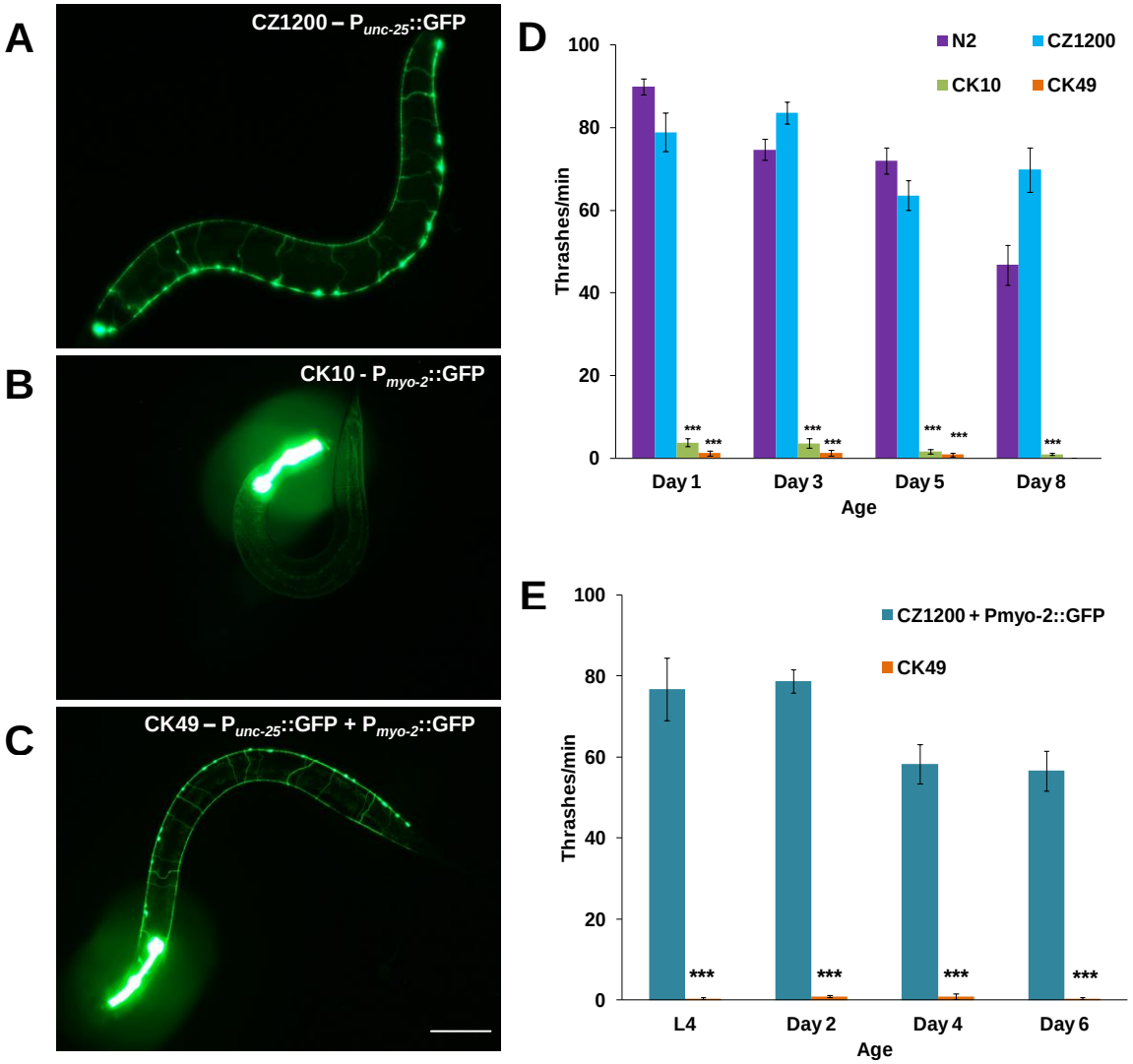

Figure 3.3: Pan-neuronal expression of mutant human Tau transgenes resulted in severe locomotion defects. A-C) Visualisation of GFP-labelled strains used. A) Strain CZ1200 expressing only an integrated P_{unc-25}::GFP transgene in GABAergic neurons was included as a control. Scale bar represents 200 µm. B) CK10 animals have strong signal in the pharynx that derives from the integrated P_{myo-2}::GFP reporter. C) Strain CK10 was crossed with CZ1200 to generate a triple transgenic line that is homozygous for three integrated transgenes - mutant Tau transgene, the P_{unc-25}::GFP GABAergic and P_{myo-2}::GFP pharyngeal marker transgenes. All worms depicted are young adults and are oriented with anterior end left, posterior end right and ventral side down. D, E) Quantification of movement defects induced by the expression of mutant Tau. Time points for locomotion assessments were chosen to span the majority of normal worm life span. D) Transgenic CK10 and CK49 worms displayed significantly reduced body thrashes in liquid compared with N2 and CZ1200 which serve as non-transgenic (non-Tg) and GFP transgenic control worms, respectively. CK10 worms are severely uncoordinated and displayed partial paralysis and dorsal coiling phenotypes, but are capable of intermittent short bursts of very fast head thrashes; CK49 demonstrated an additional decrease in movement beyond the severe impairment present at day 1 of adulthood as worms aged, approaching complete paralysis by day 8. N2 WT and CZ1200 worms moved normally and exhibited minor movement decline as worms age until day 8 of adulthood. E) Double transgenic control worms expressing both P_{myo-2}::GFP and P_{unc-25}::GFP marker transgenes displayed WT body thrash rates. Results shown represent the average data from two independent experiments. For each assay, at least ten animals were used for each genotype and their average values are shown. The error bars denote SEM from three repetitions of the experiment. Statistical significance ***p<0.0001 in all cases, compared with the non-transgenic worms (N2) was determined using paired Student's *t*-test.

severe locomotion phenotype manifested during larval stages and persisted throughout the development and aging, culminating in nearly complete paralysis by day 8 of adulthood. These are therefore distinguished from normal worm aging-related declines in motility. N2 WT and CZ1200 show decreased motility as worms age, with significant N2 movement decline demonstrated by day 8 of adulthood; they do not become paralysed except at extremely advanced ages, typically ~18-20 days.

Once the decline in behavioural response was established, it was important to confirm if the loss of behaviour is caused by loss of neuronal function associated with pan-neuronal expression of Tau V337M protein. Neuronal structural defects, notably, neurodegeneration in the VD- and DD-type classes of GABAergic motor neurons have been demonstrated in neurodegenerative *C. elegans* models (Kraemer *et al.*, 2003, Fatouros *et al.*, 2012). *unc-25* encodes the GABA biosynthetic enzyme glutamic acid decarboxylase (Jin *et al.*, 1999) and hence the addition of the P_{unc-25}::GFP marker in CK49 worms allowed the structural and morphological integrity of the GABAergic neuronal network to be inspected in more detail for possible motorneuron abnormalities associated with transgene expression that may account for the motility defect. In strain CZ1200 carrying the GFP reporter alone, both the dorsal and ventral nerve cords are continuous and contain the normal complement of 19 inhibitory motor neurons (Figure 3.4A; C-F, left panels). The uncoordinated behaviour of CK10 and CK49 was already apparent at day 1 of adulthood, indicating that the simple expression of mutant human Tau was sufficient to cause constant neuronal dysfunction. Indeed, CK49 exhibited profound degeneration of the GABAergic motor

neuron network whereby persistent discontinuities and exaggerated varicosities appeared in the axonal bundles of the dorsal and ventral nerve cords (Figures 3.4 A and B; C-F, right panels) that were also already visible at day 1 of adulthood. Though the number of axonal gaps in CK49 did not rise with age, an extension of gaps was observed in neurites of both the ventral and dorsal nerve cords (Figure 3.4E and F, right panels). 10-day-old worms from the mutant lines showed degenerating axons throughout the ventral and dorsal nerve cords. These neuronal structural defects are therefore consistent with the severe motor defects exhibited by CK49.

A general caveat of using transgenic markers in *C. elegans* is that they can produce various levels of cytotoxicity and are likely to be of no interest in the context of normal cellular physiology. We therefore performed additional control experiments to ensure that the robust phenotypic traits observed stem from Tau V337M induced- neurotoxicity, not as a result of an overabundance of the reporter proteins or transgene insertion. A double transgenic negative control with expression of both P_{myo-2}::GFP and P_{unc-25}::GFP was generated. As shown in Figures 3.3E and 3.4B, introduction of two GFP reporter constructs did not produce any significant defects, as double transgenic control worms showed no locomotion impairments or axonal degeneration with very few, if any, gaps compared with CK49 worms. In contrast, the CK49 phenotype is more severe than both CK10 and CK10; P_{myo-2}::GFP, thus suggesting that driving GFP transgene expression in GABA neurons might have exacerbated the effect of Tau expression.

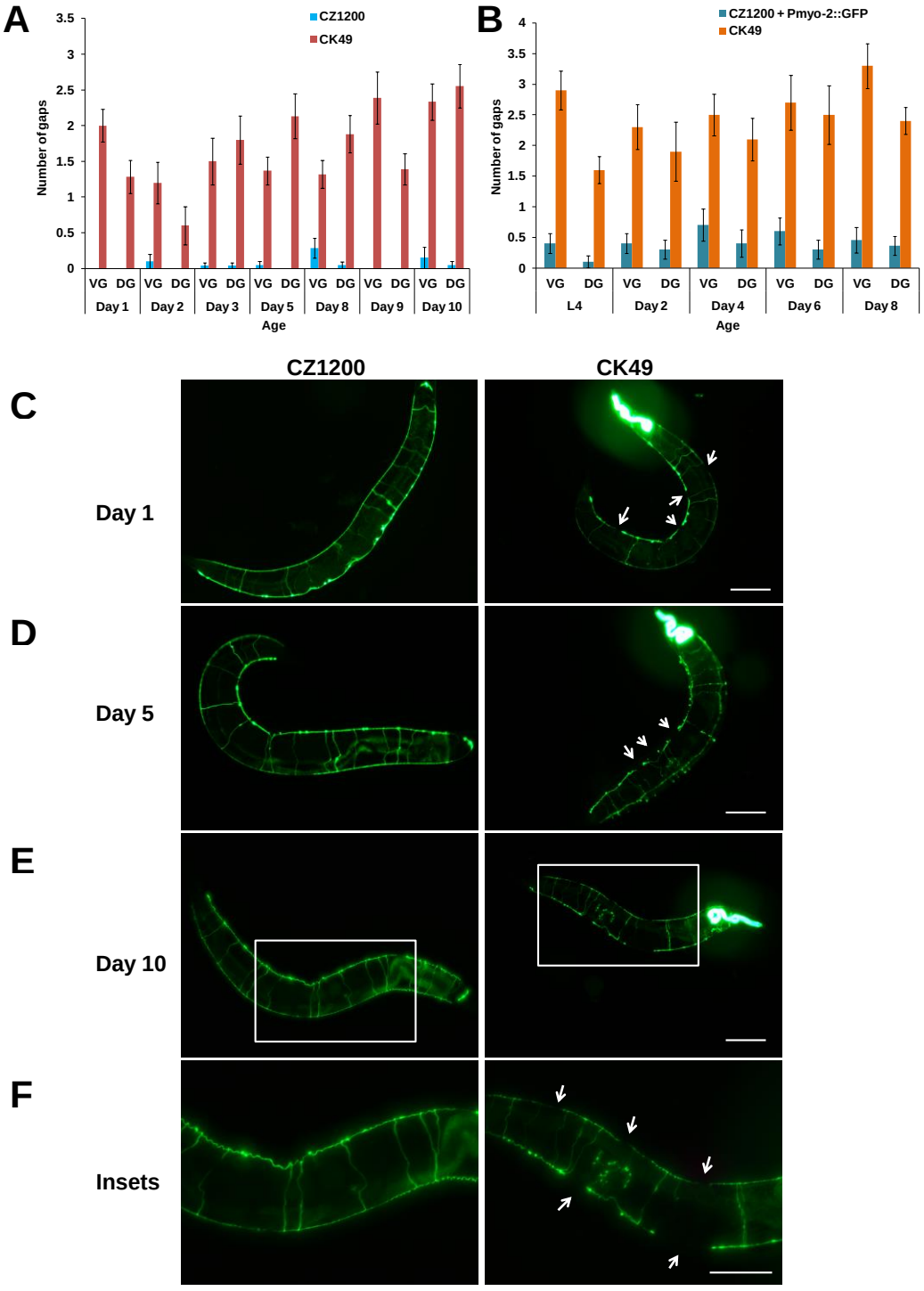

Figure 3.4: Assessment of neurodegenerative changes in GABAergic motor neurons by visual scoring of GFP reporter. Triple transgenic CK49 worms expressing the $P_{aex\text{-}3}$::V337M Tau, $P_{myo\text{-}2}$::GFP, and a $P_{unc\text{-}25}$::GFP reporter transgene marking the cell bodies and processes of all *C. elegans* GABAergic neurons was compared with CZ1200 single transgenic for $P_{unc\text{-}25}$::GFP and double transgenic control expressing both $P_{myo\text{-}2}$::GFP and $P_{unc\text{-}25}$::GFP markers to score for neurodegenerative neuronal loss. A, B) Graph plotting the average number of ventral (VG) and dorsal (DG) cord gaps at different ages of adulthood. C-F) All panels are micrographs of representative whole worms. CZ1200 (left panels) and CK49 (right panel) were examined at age 1 day (C), 5 days (D), and 10 days (E). In CZ1200, intact ventral and dorsal cords were observed. In contrast, CK49 mutant Tau transgenic GABAergic reporter strain exhibited severe degeneration of neuronal processes. VC and DC gaps (arrows) are disruptions in the continuity of the ventral and dorsal nerve cords, respectively. The error bars denote SEM from two repetitions of the experiment. At least 10 worms were scored per strain and per time point. Scale bar represents 200 µm for all panels except for the last two panels (F) which are high magnification of boxed areas of Figure 3.4 E.

`During the routine maintenance of the CK49 stocks, several independent WT revertants arose spontaneously and displayed a complete behavioural and morphological reversion to the WT phenotype. Isolation of revertants from Unc worms gave rise to a mixed population of phenotypically WT and Unc worms. It is possible that the presence of the toxic transgenes in the CK49 strain has increased its tendency to modify (suppress) phenotypes similar to what was observed with an ALS and polyQ model (Gidalevitz *et al.*, 2006, Gidalevitz *et al.*, 2009). Its low progeny number further renders this strain particularly unstable, resulting in segregation of lines revertant from toxic to WT phenotype during selection.

A series of experiments was performed to examine the nature of the incorporated Tau transgene in the revertants. The presence of Tau transgene was first confirmed using the single-worm PCR for a fragment of human *MAPT* cDNA, and strong signals for the expected 425 bp band was detected in the all mutant-Tau expressing lines including the revertants, but not in the CZ1200 GFP reporter line (Figure 3.5A). Therefore, reversion is not due to loss of the Tau transgene.

We then asked if the expression of the Tau transgene was inhibited at the level of mRNA. In order to compare the Tau transcript levels, RT-PCR analysis was carried out which revealed that there was no transcriptional silencing of the integrated array as the expression levels of Tau mRNA were detectable in both paralysed and revertants (Figure 3.5B). No obvious changes were observed apart from insignificant dampening of the Tau expression.

To examine whether the revertant phenotypes observed result from changes in the level of Tau V337M protein, the overall Tau protein level was studied by western blotting using anti-Tau antibody and demonstrated that human Tau protein expression was barely detectable in the revertants, whereas Tau proteins were expressed at similar levels with an expected Mw of about 64 kDa in both CK10 and CK49 Unc lines (Figure 3.5C). The observation of slight reduction in GFP expression but near absence of Tau expression in CK49 revertants reflects minimal Tau V337M proteotoxicity and suggests that the phenotypic reversion was likely due to inefficient translation of the transgene-derived mRNA or increased protein degradation or turnover due to unknown changes in these revertant worms. As a result, the expressed level of Tau was insufficient to exert its deleterious effect on the worms.

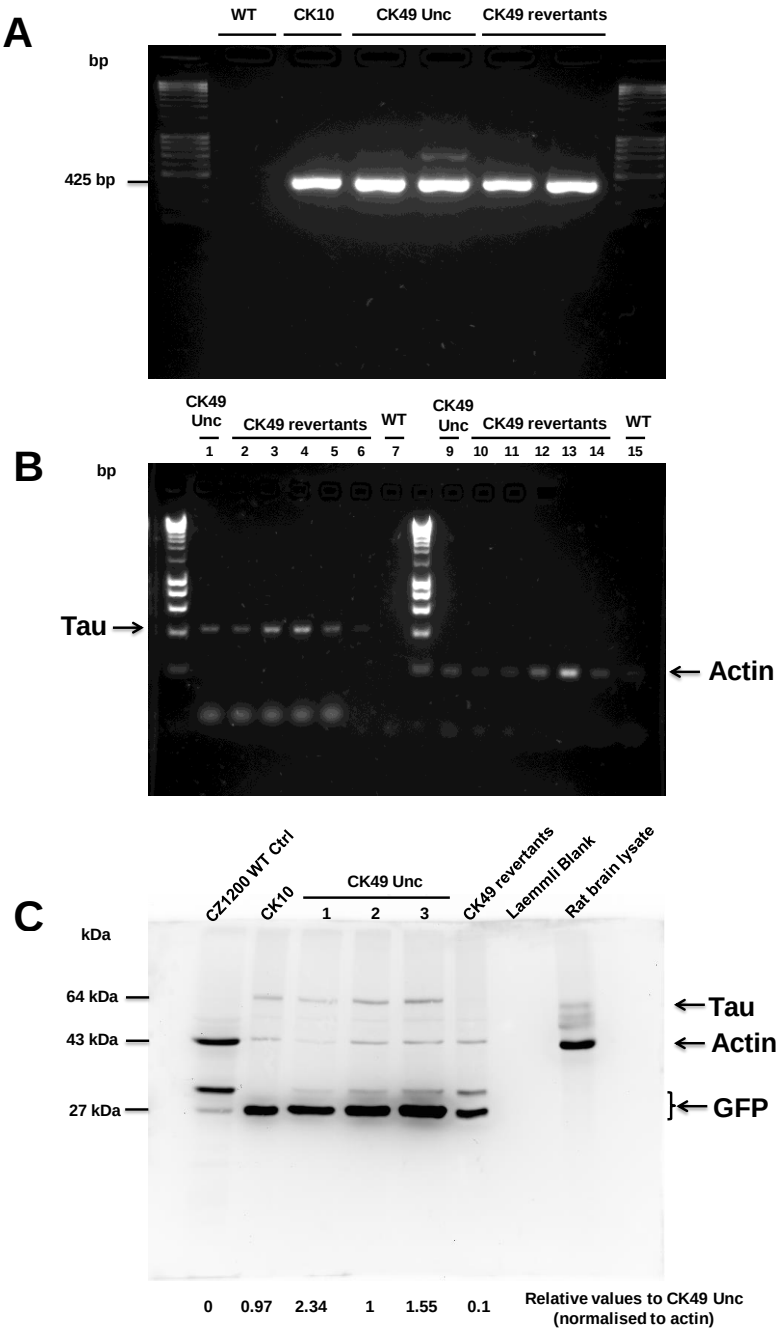

Figure 3.5: Analysis of spontaneous phenotypic reversion. A) The upper panel shows the detection of Tau transgene. Single-worm PCR for a 425 bp fragment of Tau cDNA, which was detected in the CK10, CK49 Unc and CK49 revertant lines, but not in the GFP reporter line, CZ1200 WT control. DNA size marker in bp. B) RT-PCR expression analysis of Tau transcript in WT, CK49 Unc and CK49 revertant lines. The picture shows amplification bands of fourteen PCR reactions (including the parallel internal control) starting with seven different amounts of template cDNAs. No detectable Tau expression differences were observed among all CK49 transgenic lines. The endogenous *C. elegans* gene actin served as an internal control. Both PCR and RT-PCR analysis were repeated three times with identical results. C) Biochemical confirmation of protein over-expression. Representative western blot of total protein levels from independently integrated V337M Tau-strains, as indicated. The blots were probed with a T46 Tau antibody, which recognises the C-terminal region of both non-phosphorylated and phosphorylated Tau and thus detect total Tau levels; anti-actin antibody was used as loading control and anti-GFP. CK49 revertants and CZ1200 worms showed no reactivity to the T46 Tau antibody, while CK10 Tau proteins are expressed at similar levels to those of CK49 Unc. The major full-length isoform of Tau at 64 kDa in size is indicated. Multiple bands present in rat brain lysate indicate Tau truncation products, alternate start sites, or cleavage products of full-length Tau. The doublet GFP bands evident in all CK49 lines are due to the presence of two GFP markers. The numbers below the gel represent the quantification of Tau signals using ImageJ software which were normalised against actin. The values are relative to CK49 Unc levels.

3.2.2.4 Pan-neuronal expression of an ALS-associated mutant version of human SOD1 in *C. elegans* produces severe locomotor defects

To explore the potential use of a worm ALS model of SOD1 toxicity, we obtained and studied two distinct models engineered to express human WT SOD1 and mutant SOD1 exclusively in neurons (P_{snb-1}::WT SOD1-YFP and P_{snb-1}::G85R SOD1-YFP (Figure 3.6A), which will hereafter be referred as WT SOD1-YFP and G85R SOD1-YFP worms, respectively. While WT SOD1 proteins can bind to copper and zinc, the catalytically inactive mutant G85R is deficient in copper and zinc binding and significantly destabilised (Wang *et al.*, 2009b). Previous literature has shown that the WT and the G85R mutant SOD1 were significantly different in their neurotoxic properties. In our study, both the WT SOD1-YFP and G85R SOD1-YFP worms developed profound locomotor defects compared to N2 worms at all stages of adulthood, as measured by their thrashing rate in liquid medium (Figure 3.6B). WT SOD1-YFP worms exhibited a mild worsening effect with an average of ~54% decrease in locomotor activity compared to N2 WT. As anticipated, G85R SOD1-YFP mutant exhibited particularly strong motility defects that were consistently more severe than those of the WT SOD1-YFP such that their thrashing was reduced by > 85% relative to WT SOD1-YFP counterparts at all time points (p<0.0001). On average, G85R SOD1-YFP worms exhibited minimal movement in isotonic liquid. Given that ALS may involve the deposition of non-mutant SOD, the observation that WT SOD1-YFP is mildly toxic in this model suggests that this model might also have relevance to ALS.

Because the motor dysfunction phenotypically resembles that of the FTDP-17 models, the basis for the defective locomotion of the SOD1 transgenic *C. elegans* could therefore also result from the abnormalities of motor neurons that innervate the body wall muscles. Using fluorescence microscopy, we looked for similar neuronal structural defects associated with mutant Tau expression that may account for the severe motility defect in the ALS models. However, we could not detect any age-dependent gross abnormalities in nervous system morphology of either WT SOD1-YFP or G85R SOD1-YFP worms (Figures 3.6 C and D), and no differences in YFP intensity were evident by eye when observing the two worm strains. This, however, does not preclude subtle neuronal defects. Previous studies have noted differing characteristics of fluorescence of neuronal cell bodies along the ventral nerve cord that are suggestive of aggregate formation (Wang *et al.*, 2009b), but were unable to identify a direct correlation between motor neuron loss/gross defects in nervous system and locomotory activity (Lakso *et al.*, 2003, Boccitto *et al.*, 2012).

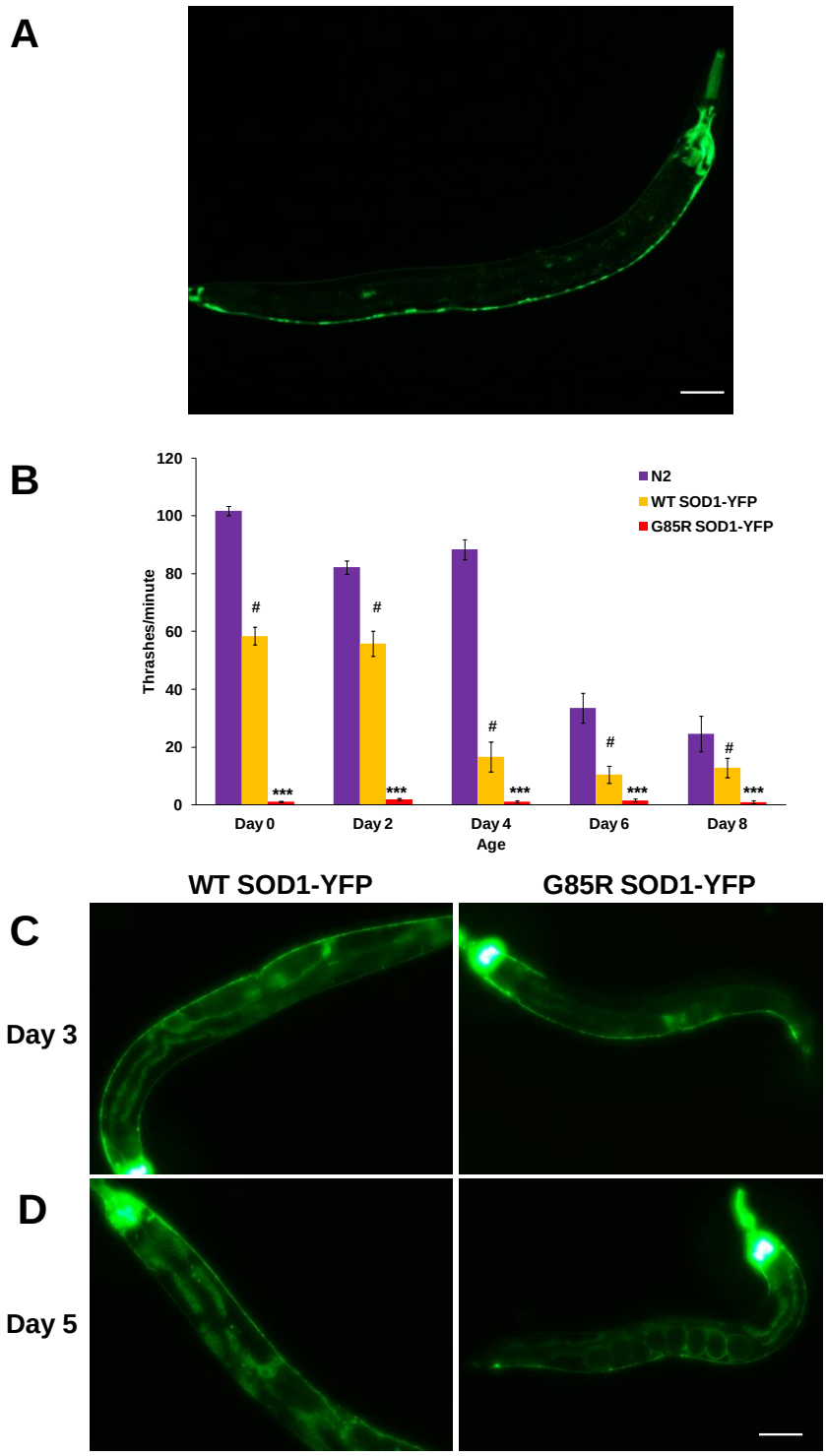

Figure 3.6: Transgenic *C. elegans* expressing neuronal SOD-1 develops pronounced movement defects. A) Expression pattern of YFP-tagged human SOD1 (hSOD1) driven by the pan-neuronal *snb-1* promoter was assessed by fluorescence microscopy. Lateral view of stably-transformed WTSOD1-YFP transgenic L4 animal showing expression of fluorescent protein in nerve ring region, in ventral nerve cord, in dorsal nerve cord, as well as in commissural and lateral neuronal cell bodies, and in tail region. The large motor neurons in the ventral cord and lateral wall neuron are easily detectable. Head of worm is to right. B) Motor activity, as measured by thrashing scores for 0-day-old (L4) to 8-day-old animals, shows age-related reductions in motor activity in all strains used. The G85R hSOD1-YFP strains had significantly impaired locomotion than the WT hSOD1-YFP strain (***p<0.0001). Asterisks indicate the significance between G85R hSOD1-YFP and WT hSOD1-YFP controls, whereas hash marks indicate the significance between WT hSOD1-YFP and N2 WT. Error bars represent the standard error of means (SEM). The figure is representative of two independent experiments. C, D) Despite evident motor dysfunction, only subtle differences in the fluorescent pattern of neuronal cell bodies along the ventral nerve cord were detected in G85R hSOD1 worms, even during later adult life. Scale bar represents 200 µm.

3.2.2.5 Reproducible neurodegeneration in the dopaminergic neurons of 6-OHDA-induced PD model

Previous studies have established that WT *C. elegans* dopaminergic (DAergic) neurons are highly sensitive to treatment with neurotoxins. Exposure to an appropriate concentration of neurotoxins have led to loss of the fluorescent DA neuronal marker due to degeneration of DA neurons, and generated ideal pharmacological models for identification of neuroprotective compounds or potential functional partners of PD-related genes. We chose to use the dopamine-selective neurotoxin, 6-hydroxydopamine (6-OHDA), for its experimental convenience. To determine whether *C. elegans* DAergic neurons are sensitive to the 6-OHDA *in vivo* as previously reported, the integrated $P_{dat\text{-}1}$*::*GFP reporter strain BY250, which expresses strong and specific green fluorescence in all eight DAergic neurons (Figure 3.7A) was utilised in our experiment, and degeneration of the six anterior DAergic neurons in response to either 10 mM ascorbic acid (AA) alone (vehicle control) or both 50 mM 6-OHDA and 10 mM AA were analysed. Addition of AA helps to stabilise 6-OHDA in solution. GFP-labeled DAergic neurons were examined for the presence of all six anterior DAergic neurons at time points 2, 24 and 48 hours after 6-OHDA treatment and were scored for evidence of DAergic neuron survival. The amount of nematodes exhibiting WT anterior DAergic neurons, partial or complete DAergic neurodegeneration was determined in the whole population. Consistent with published reports, the characteristic degenerative changes of GFP fluorescence in DAergic neurons were detected in 6-OHDA-treated worms as their DAergic neurons undergo a

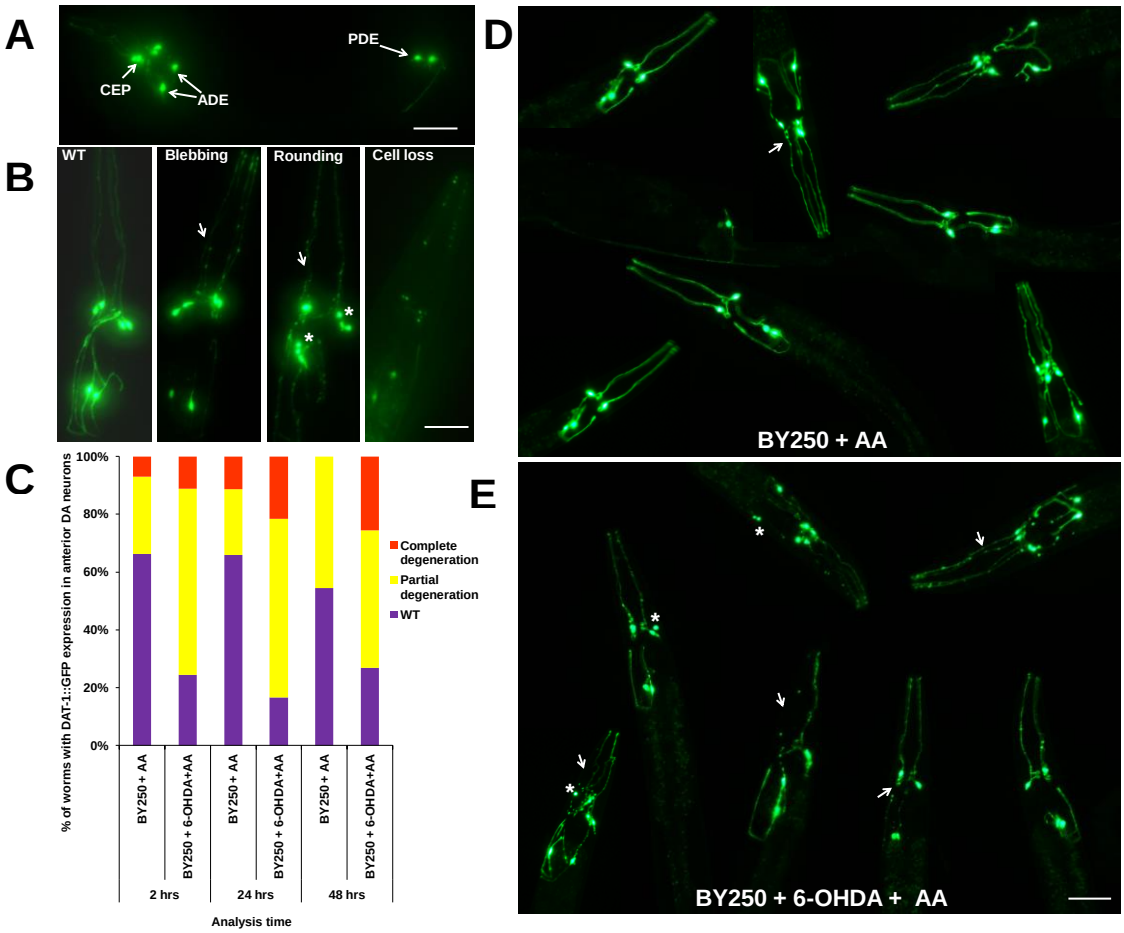

Figure 3.7: Characterising the 6-OHDA-induced responses in *C. elegans* A) DA neurons cell bodies and neurites in BY250 worms were visualised using an integrated $P_{dat\text{-}1}$::GFP DA transporter marker. *C. elegans* has eight DA neurons: six are located in the anterior region, which can be subclassified in pairs as two anterior deirid neurons (ADE), two dorsal cephalic neurons (CEP) which are postsynaptic to the ADE neurons and two ventral CEPs that are not postsynaptic to the ADEs; two posterior deirid neurons (PDE) located posteriorly are also shown. Arrows depict the four CEP neuron processes and indicate the ADE and PDE cell bodies in a young worm. Anterior is to the left. B) Representative examples of worms scored which display the three characteristic stages of DA neurodegeneration in response to 6-OHDA. Magnification of anterior region of *C. elegans* shows only the anterior-most DA neurons. WT: In this example, all six anterior DA neurons of this worm appear robust and the dendrites are intact and fully extended. Neuronal process blebbing; cell body rounding: this worm exhibited prominent cell body rounding (asterisk) and dendrite blebbing (arrows); cell body loss: this worm exhibited a complete loss of GFP in most DA neurons as CEP and ADE neurons have all degenerated and are no longer visible in any focal plane, only retention of GFP expression in the remnants of neuron cell bodies and broken neuritis. All scale bars represent 20 µm. C) Percentage of worms exhibiting WT, partially or completely degenerating ADEs and CEPs neurons/dendrites after 6-OHDA treatment at different time points is presented. The six anterior DA neurons were examined for each worm (at least 30 worms/condition) following exposure to either 10 mM AA alone as vehicle control or both 50 mM 6-OHDA and 10 mM AA, and the GFP expression pattern in the respective cells was examined 2, 24 and 48 hours post-exposure (see *Materials and Methods*). Data are depicted as means from six independent experiments. D) Representative worms from the analysis charted in Figure 3.7C performed 24 hours post-6-OHDA-exposure are presented. BY250 worms treated with AA alone expressed intact and strong GFP in all six DA neurons and dendrites in the heads. Meanwhile, majority of BY250 incubated with 50 mM 6-OHDA showed a marked GFP expression reduction in the dendrites of ADEs and CEPs, many of the cell somas became round (asterisk) and blebs appeared along the dendrites of CEPs (arrows).

reproducible death from exposure to 50 mM 6-OHDA that begins within ~2 hours of treatment. These acute, reproducible changes include readily observable CEP dendrite blebbing and cell body rounding (Figure 3.7B). A complete loss of GFP expression was also observed in DAergic neurons and dendrites at later time points i.e. 48 hour post-exposure (Figures 3.7 B and C).

As shown in Figures 3.7 D and E, which are representative fluorescence images of GFP expression in multiple BY250 worms at 24 hours post-6-OHDA-exposure, 6-OHDA triggered differing degrees of DAergic neurodegeneration in each worm. Most of the cell somas became round and blebs appeared along the dendrites (Figure 3.7E). Quantitatively, 70% of AA alone–treated vehicle controls displayed intact and strong GFP in all six DAergic neurons. However, 70-80% of worms exhibited degenerating neurons and processes after treatment with both 50 mM 6-OHDA and 10 mM AA (Figures 3.7 C-E).

3.2.2.6 Homozygous deletion of *C. elegans smn-1* results in a rapid decline in neuromuscular function

The first *C. elegans* model developed for human spinal muscular atrophy (SMA) was a *smn-1(ok355)* null mutant in which a large deletion in the gene homologous to SMN, *smn-1*, caused a complete loss of *smn-1* function which in turn causes lethality (Briese *et al.*, 2009). A balanced strain LM99 was obtained to facilitate identification of heterozygous and homozygous animals which were subsequently assayed for thrashing. Heterozygous animals are overtly normal and are distinguishable by pharyngeal GFP, while homozygous progeny have no GFP expression. We will hereafter refer to

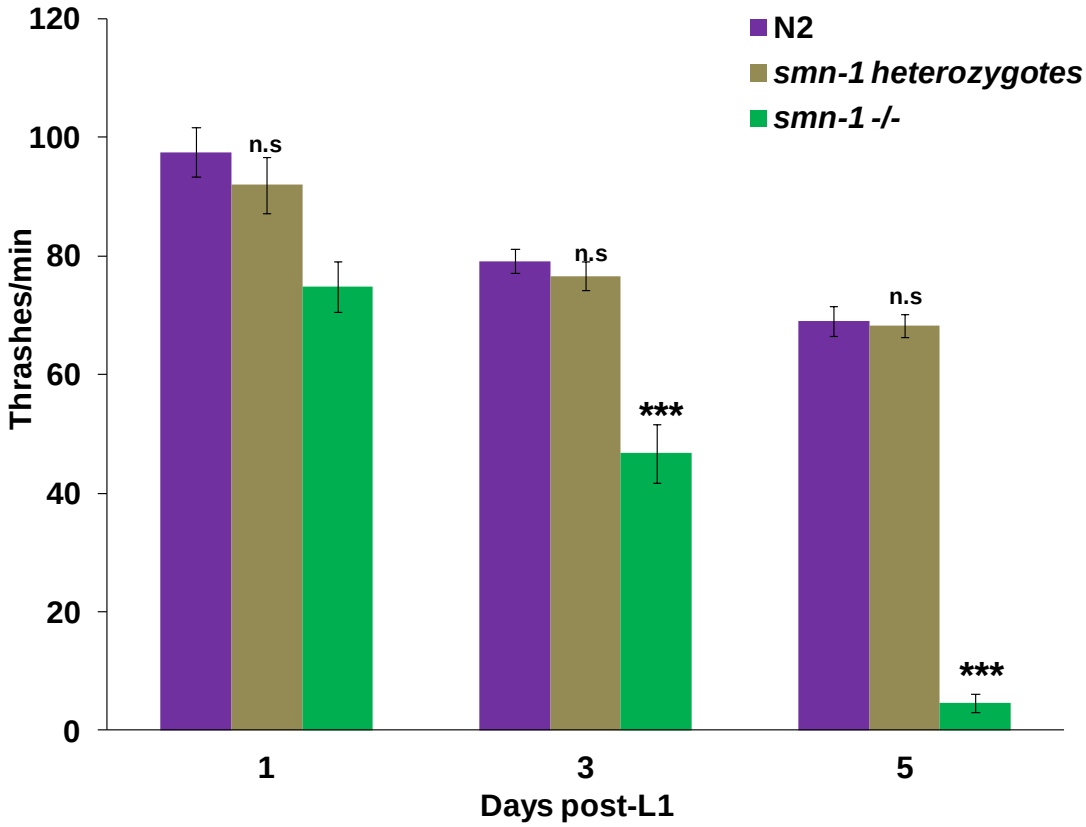

Figure 3.8: Motor activity of SMA mutant model as measured by the trashing assay. Thrashing rates of N2 WT and *smn-1(ok355)* heterozygotes and homozygotes after 10 minutes in Dent's solution were counted manually. Age-related reductions in motor activity were observed in all strains. *smn-1(ok355)* heterozygotes showed slightly lower score than non-transgenic N2 animals, whereas *smn-1(ok355)*$^{-/-}$ consistently thrashed at a slower rate than its age-synchronised counterparts. Thrashing of *smn-1(ok355)*$^{-/-}$ animals progressively declined and almost completely ceased after 5 days post-L1 stage. The error bars denote SEM from two independent experiments, and differences were considered non-significant (n.s. $p > 0.05$) or significant (***$p < 0.0001$).

smn-1$^{-/-}$ and *smn-1(ok355)/*hT2[*qIs48*] animals as homozygotes and heterozygotes, respectively. Animals that are homozygous for *smn-1*$^{-/-}$ can survive for several days due to partial maternal rescue. It has been suggested that heterozygotes load sufficient SMN-1 maternal protein and/or mRNA into oocytes to support development through embryogenesis and early larval stages (Dimitriadi and Hart, 2010). As previously observed, during early development, the thrashing rate of homozygous *smn-1*$^{-/-}$ larvae did initially resemble the heterozygotes and N2 WT animals. Eventually maternally-loaded *smn-1* product is lost and homozygotes undergo larval arrest. Not only did their thrashing progressively decline and almost completely cease after 5 days post-L1 (Figure 3.8), homozygotes grew slower than their heterozygote siblings, were shorter, sterile, and most died before reaching adulthood. In contrast, there were no statistically significant differences between heterozygotes and N2 WT in locomotor activity at any time point throughout the assay.

3.2.2.7 *C. elegans* polyQ models exhibit perturbed neuronal dysfunction without neuronal cell death

The two HD models chosen for characterisations were, firstly, strain HA659 which co-expresses GFP with an N-terminal human huntingtin fragment containing a polyQ tract of 150 residues (Htt-Q150) strongly in non-essential ASH neurons and more weakly in other neurons (Figure 3.9A). Secondly, strain HA759 in which the Htt-Q150 is expressed in ASH sensory neurons of polyglutamine enhancer-1 (*pqe-1*) mutant sensitised background that was previously suggested to specifically accelerate expanded polyQ-induced toxicity and causes age-dependent ASH neuronal death within 3 days. First,

we addressed the ASH functionality of both HA659 and HA59 in a nose-touch assay (Figure 3.9B). On day 3 of adulthood, N2 WT animals stopped forward motion and reversed in response to nose touch in 70-80% of nose touch trials. Htt-Q150 and OSM-10::GFP co-expression in young HA659 and HA759 animals produced mild nose touch abnormalities when challenged with a mechanosensory stimulus, as worms responded in only 58% of nose touch trials. However, aged HA659 and HA759 worms on day 8 of adulthood were strongly defective for ASH-mediated nose touch avoidance response. A modest but significant defect was observed for HA659 (51%) and a pronounced defect was observed for HA759 in which Htt-Q150 caused a marked decrease in this response to 14% (Figure 3.9B).

To verify ASH apoptotic cell death, we used fluorescence microscopy to assess ASH neuron viability in young 3-day-old and aged 8-day old HA659 and HA759 adults by monitoring the presence or absence of GFP expression. Previous studies have indicated that in *pqe-1(rt13)* mutant animals expressing Htt-Q150, the vast majority (>90%) of HA759 ASH neurons became absent in less than three days predominantly during larval stages, indicative of rapid neurodegeneration and neuronal cell death. Apart from occasional dendritic breaks, we failed to observe the highly penetrant ASH cell death in any young (day 3) or old (day 8) HA759 worms. As shown in Figures 3.9 C and D, expression of the Htt-Q150 transgene in sensitised background did not significantly increase the percentage of dead ASH neurons scored as the vast majority of ASH neurons remained morphologically intact. There was a minimum of ASH neuronal death, with 11% dead cells observed at 3 days, increasing at 8 days to just 20%.

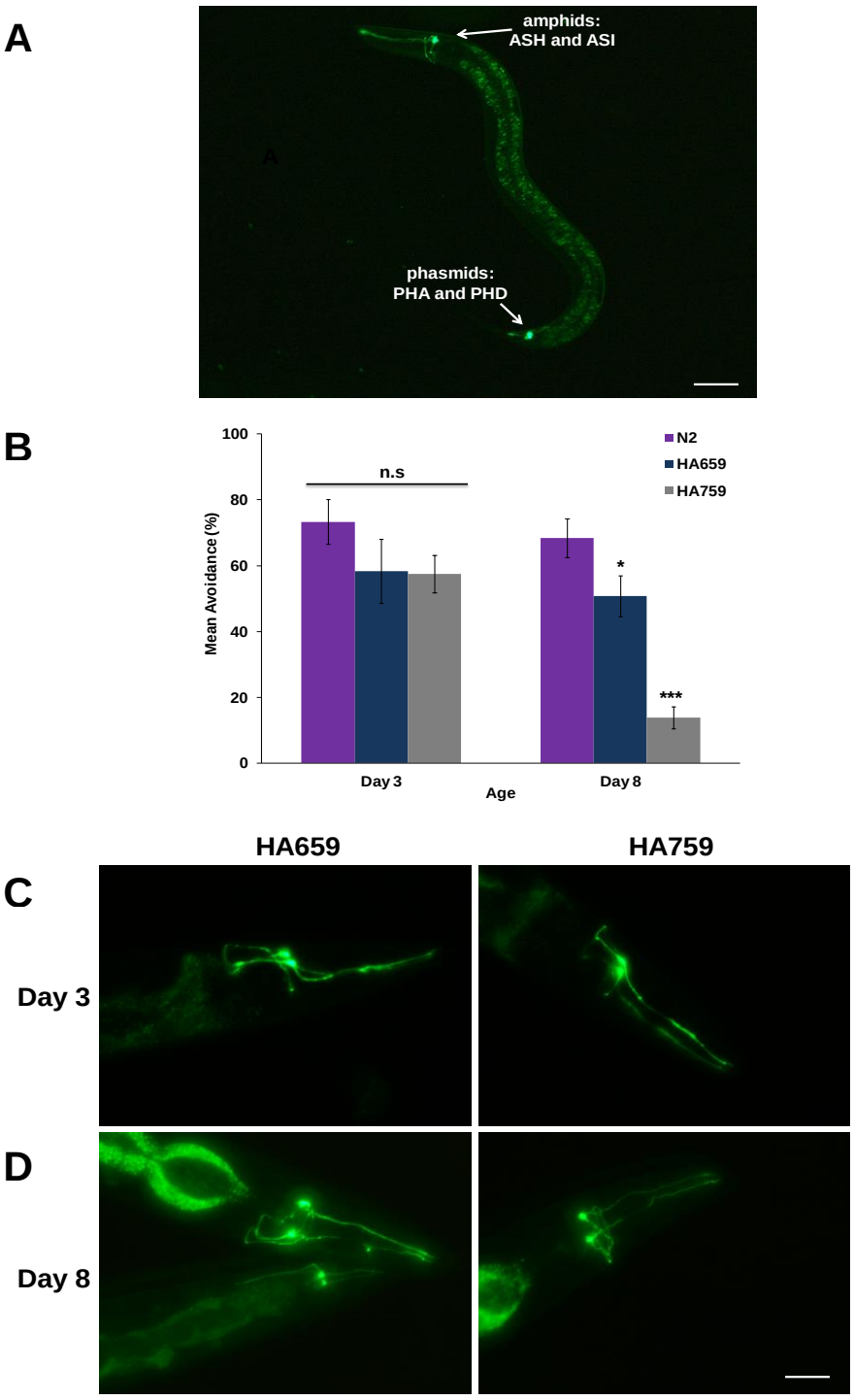

Figure 3.9: PolyQ expansion perturbs ASH function in aged animals. A) Expression pattern of $P_{osm\text{-}10}$::GFP in *C. elegans* assessed by fluorescence imaging. *osm-10* is expressed in a bilateral pair of chemosensory neurons in all larval and adult animals known as amphid (ASH, ASI) in the head and phasmid (PHA, and PHB) in the tail. Its function is required in the main avoidance/osmotic avoidance neuron ASH. B) Nose touch response depends directly on ASH sensory neurons' function. To test nose-touch response, an eyelash was placed in front of a forward moving worm's nose and avoidance behaviour was quantified as mean % of trials in which the transgenic or control animals responded to nose touch responded by stopping forward motion or immediately recoiled. Worms were scored 10 times each for response to nose touch. Results here show that young worms all have normal nose touch response. However, on day 8, HA659 had significantly impaired response to nose touch as compared to wild type. Htt-Q150 expression in sensitised ASH neurons leads to a severe defect in the nose touch response of HA759 model. Error bars indicate SEM. C, D) Assessment of ASH survival. Live neurons express GFP, and neuronal death is evaluated by a loss of GFP fluorescence in bilateral ASH neurons. ASH neuronal viability was assayed in live animals at the times indicated. However, the highly penetrant ASH apoptotic cell death was not evident in any young (day 3) or old (day 8) HA759 worms. n ≥ 10 animals per strain were imaged. Scale bars, 20 µm

3.3. DISCUSSION

The study of behavioural and neuropathological phenotypes of the ND models has been plagued by inconsistent results across laboratories. This stems from the technical differences (i.e. transgenic constructs, modes of gene targeting, transgene expression levels and scoring criteria for various phenotypes) and the intrinsic differences between the models (i.e. the manner by which specific *C. elegans* tissues respond to misfolded proteins). In this study, we selected and characterised well-defined neuronal *C. elegans* models of various forms of human ND that were shown previously to develop profound neuronal dysfunctions associated with protein misfolding and aggregation to identify lines with the most robust phenotypic differences, best suited for genetic and preclinical therapeutic efficacy studies. We focused on behavioural phenotypes of the chosen ND models, particularly behaviours that have been established as neuronally controlled. Among the behavioural assays that have been well established in *C. elegans* to assess neuronal toxicity-evoked phenotypic abnormalities include thrashing, body bend, paralysis, chemotaxis, pharyngeal pumping, food-sensing and egg-laying (Leung *et al.*, 2008). The thrashing assay was applied in our study, since the most striking behavioural phenotype of our selected models was the loss of coordinated movement leading to nearly complete paralysis and this has been used as the read-out for many previous genetic and pharmacological screens (Alavez *et al.*, 2011, Tauffenberger *et al.*, 2012, Liachko *et al.*, 2013, McCormick *et al.*, 2013, Munoz-Lobato *et al.*, 2013). More than 60 neurons in the *C. elegans* nervous system innervate muscle cells to evoke the wave of muscle contraction-relaxation leading to locomotion; it is therefore not

surprising that dysfunction or loss of these neurons results in lack of coordination and paralysis, and contribute to the neurodegenerative demise.

Accumulating evidence indicates that proteostasis (protein homeostasis) is a critical component of longevity and several studies using transgenic *C. elegans* models of protein-misfolding disorders have led to the discovery that genes (Morley *et al.*, 2002, Hsu *et al.*, 2003, Morley and Morimoto, 2004, Cohen *et al.*, 2006) and compounds (Calamini *et al.*, 2011, Fatouros *et al.*, 2012, Lublin and Link) which prolong lifespan also restore proteostasis. The short *C. elegans* lifespan is therefore associated with the age-dependent onset of NDs and has also been monitored as a read-out in multiple screens (Nussbaum-Krammer and Morimoto, 2014). However, whether *C. elegans* lifespan is a robust neurodegenerative biomarker is debatable as recent work suggested that lifespan extension is not a straight prediction for neuroprotective properties (Tauffenberger *et al.*, 2013). Nevertheless, numerous compounds such as EGb761 (Wu *et al.*, 2002) reserpine (Srivareerat *et al.*, 2009, Saharia *et al.*, 2012), trehalose (Honda *et al.*, 2010), metformin (Onken and Driscoll, 2010), celecoxib (Ching *et al.*, 2011), ferulsinaic acid (Sayed, 2011), NG-094 (Haldimann *et al.*, 2011), astragalan (Zhang *et al.*, 2012a), salidroside (Xiao *et al.*, 2014), thioflavin T, curcumin and rifampicin (Alavez *et al.*, 2011) were shown to enhance lifespan and ameliorate proteotoxicity of Aβ and/or polyQ protein aggregation models.

In line with these studies, deletion of an endogenous neuroprotective gene *dnj-14*, the sole *C. elegans* orthologue of the CSP-encoding *DNAJC5* gene that is mutated in ANCL resulted in a reproducible and significant lifespan reduction, which parallels with the increased mortality associated

with mutations in *DNAJC5* homologues in humans (Benitez *et al.*, 2011, Noskova *et al.*, 2011, Velinov *et al.*, 2012, Cadieux-Dion *et al.*, 2013), mice (Fernandez-Chacon *et al.*, 2004) and flies (Zinsmaier *et al.*, 1994). The biochemical and genetic analysis of CSP function in various systems produced compelling evidence that CSP could be a key player in neuroprotection against several if not one ND. Such an involvement was hinted at by the discovery that impaired/toxic proteins typically found in NDs may interfere with CSPα, SNARE complex assembly, dynamin1 assembly and ion channel complexes, and in part, contribute to neurodegeneration (Donnelier and Braun, 2014). The recent identification of CSPα as a human ND gene and the implication of CSP in AD (Dolzhanskaya *et al.*, 2014), ANCL (Noskova *et al.*, 2011), HD (Miller *et al.*, 2003) and PD (Chandra *et al.*, 2005) strongly suggest that this presynaptic co-chaperone could be generally neuroprotective in multiple NDs. CSP was shown to functionally overlap *in vivo* with the PD protein, α-synuclein, for preventing neurodegeneration. The profound neurodegeneration and lethality in CSP mutant mice can be ameliorated by transgenic overexpression of normal α-synuclein and exacerbated in α-synuclein knock-out mice (Fernandez-Chacon *et al.*, 2004, Chandra *et al.*, 2005). Similarly, it was also suggested that CSP binds to mutant Htt, but not to normal Htt. The sequestration and subsequent depletion of CSP by expanded polyQ stretches eliminates the robust inhibition of N-type Ca^{2+} channels promoted by CSP (Miller *et al.*, 2003). Studies by multiple independent labs have consistently shown that the cellular CSP-neuroprotective pathways are also compromised in ANCL (Benitez *et al.*, 2011, Noskova *et al.*, 2011, Velinov *et al.*, 2012, Cadieux-Dion

et al., 2013) which further strengthen the claim that CSPα could be generally neuroprotective in multiple NDs. Moreover, very recent work has implicated CSPα in AD, as unusually severe disease course and lysosomal lipofuscin inclusions, previously believed to be exclusive to NCLs were found to be present in very early onset (age 30) and rapidly progressing AD caused by a novel presenilin1 mutation (Dolzhanskaya *et al.*, 2014). A pronounced decrement of CSPα was observed in postmortem AD frontal cortex (Zhang *et al.*, 2012c) and the SNARE complex assembly was also impaired in human brain tissue from patients with AD (Sharma *et al.*, 2012). An alternative approach to identify generally neuroprotective interventions is to search for compounds that are able to compensate for the loss of an endogenous physiological neuroprotective factor such as CSPα (Sleigh *et al.*, 2011). As explained before, the extreme severity of fly *csp* mutants coupled with the unfeasibility of performing high throughput screens in mice suggests that the worm *dnj-14* model may be a more efficient platform for screening neuroprotective factors. Indeed, prior to my studies, a focused drug screen which had been performed in the lab on the *dnj-14(ok237)* mutants to identify compounds that compensate the loss of *dnj-14* demonstrated the pro-longevity properties of resveratrol on the *C. elegans* ANCL model, and was subsequently shown to act via a PDE-inhibition-dependent and *sir-2.1*-independent manner (Kashyap *et al.*, 2014). *dnj-14* mutant is therefore an efficient model that could contribute significantly to the study of the molecular basis of age-related NDs and the identification of potential therapeutic targets.

It has been suggested that a phenotype with a complete penetrance of 100% is most suitable for pharmacological or genetic screening purposes (Garcia-Alcover *et al.*, 2013). The pronounced motor dysfunction of both the FTDP-17 and ALS models is a reproducible phenotype shown by many researchers and our observations (severe locomotion impairments, profound degeneration of the GABAergic motor neuron network) are consistent with previous findings that aberrations in these disease proteins result in aggressive neuropathologies resembling those found in transgenic fly/mouse models and human patients. The robust early-onset phenotype decouples the Tau aggregation-mediated toxicity from age-related alterations of proteostasis; its rapid occurrence is also within a timeframe that allows for efficient testing, and therefore, would be a particularly suitable read-out for time- and cost-effective pharmacological or genetic screens to uncover specific modulators of Tau and SOD pathologies (Boccitto *et al.*, 2012, Fatouros *et al.*, 2012). However, one must be cautious in comparing the effects of treating animals with a pharmacological agent altering the timing /course of neuronal degeneration, and the consequences of toxic mutant transgenes that have a chronic loss of activity (Wang *et al.*, 2012). Our observation of a complete phenotypic reversion in CK49 FTDP-17 model corresponds to what were previously observed with transgenic ALS and polyQ models. The utility of the CK49 strain for future screening is therefore restricted, since it is likely that any physiological effects seen upon relatively acute pharmacological treatments would be masked by the occurrence of or the selection for adaptive changes in protein homeostasis and gene expression (Wang *et al.*, 2012). Performing assays on freshly

thawed/crossed worms or periodically re-building the strain can circumvent the generation of revertants, but would not be an effective long term solution. The alternative CK10 Tau model which displays less severe, yet still robust phenotypic defects may better inform on drug testing. CK10 does not revert and has already facilitated the identification of dopamine D2 receptor antagonist as a potential neuroprotective strategy for targeting Tau aggregation and neurotoxicity in a primary drug screen (McCormick *et al.*, 2013).

We also observed progressive and robust locomotion deficits in the SMA model which are in accordance with previous studies. However, a caveat of using the *smn-1(ok355)* null mutant for screens is the severity of the mutation which compromises the viability of the worm and therefore making identification of modifiers of the phenotype very demanding (Edens *et al.*, 2014). Indeed, the sudden manifestation and rapid progression of the neuromuscular defects, in concert with the technical difficulties associated with partition of *smn-1* homozygotes make screening of the locomotor phenotype particularly challenging (Sleigh and Sattelle, 2010) and to date no drug screening has been performed in this null-mutant SMA model. However, recent technical improvements in *C. elegans* handling most prominently the development of the Complex Object Parametric Analyzer and Sorter (the COPAS BioSorter) and microfluidic worm manipulation have now overcome many of the practical limitations in using this *C. elegans* model for HTS (Pulak, 2006). The COPAS BioSorter has been successfully used to ascertain data on the length and genotype of *smn-1(ok355)* to separate the null mutant worms, based on their small size and lack of GFP fluorescence,

and in a subsequent genome-wide RNAi screen uncovered multiple genetic modifiers of the SMA model (Dimitriadi and Hart, 2010). In a similar manner, this approach could be adapted to screen compound libraries for drugs that ameliorate *smn-1* loss-of-function defects. Indeed, this method has already been successfully used in high-throughput neurotoxin screening (Boyd *et al.*, 2010), thus indicating the potential of this instrument for large-scale phenotyping and screening for neuroprotective compounds in various other NDs. Genetic screens for modifiers of the deleterious phenotypes of *smn-1(ok355)* identified the small conductance Ca^{2+}-activated K^{+} (SK) channels as a cross-species invertebrate SMN modifier which was further manipulated pharmacologically (Dimitriadi and Hart, 2010, Dimitriadi *et al.*, 2013). Activating the SK channel by an SK channel activator riluzole was shown to improve the neuromuscular function of the *smn-1(ok355)* null mutant by significantly increasing both its motility and pharyngeal pumping rates during feeding, as well as preventing axonal defects in Smn-deficient rat hippocampal neurons. An E3 ubiquitin ligase, mind bomb 1 (*Mib1*) was also identified as a cross-species modifier as depletion of Mibl increased the SMN protein levels in cultured cells and significantly ameliorated the *smn-1(ok355)* pharyngeal pumping defects (Kwon *et al.*, 2013). To overcome the drawback of *smn-1(ok355)* null mutant and aid the development of drug screening, Sleigh and colleagues identified a less severe *smn-1(cb131)* mutant allele that causes weak motor defects and a slightly reduced lifespan, and more closely resembles the severity of SMA (Sleigh *et al.*, 2011). Using this mutant, they screened a library of chemicals for potential drugs and identified six chemicals that could ameliorate the mild defects of the worms. The most

effective ones include two FDA-approved drugs, 4-AP (a potassium channel blocker) and gaboxadol hydrochloride (a GABAA receptor agonist), and one novel compound Neu5Ac (a monosaccharide).

We found that some phenotypes, i.e. defective food sensing behaviours or cilia dye-filling, while quantifiable, are not robust and sensitive enough to be rapidly used and would be technically difficult to assay on a large-scale (data not shown). The food sensing assay has been used to assess the effect of overexpression on the function of DA neurons and has in numerous studies demonstrated the defective, dopamine–mediated basal slowing response behaviour of neuronal α-synuclein PD models (Kuwahara *et al.*, 2006) and the impaired, serotonin-controlled, enhanced slowing response behaviour of neuronal $A\beta_{1-42}$ model (Dosanjh *et al.*, 2010). It yielded equivocal results in our study (data not shown), since the inability to control for behaviour during a given observation window has made speed measurements variable. The age-dependent alterations in basal slowing response, though observed, were inconsistent in our selected PD models with α-synuclein or CAT-2 overexpression (data not shown). Similarly, though the pan-neuronal expression of the $A\beta_{1-42}$ induced age-dependent motility impairments in our chosen CL2355 AD model, the defect was only semi-penetrant due to high individual phenotypic variability, thereby rendering this model inappropriate for high-throughput screening purposes. However, most recent work has demonstrated that the technical difficulties and highly variable behavioural parameters of this neuronal AD model can be circumvented by utilising motion tracking analysis which accurately and efficiently assesses the locomotion speed of multiple worms for a longer

duration (Machino *et al.*, 2014). This approach further revealed that Aβ toxicity affects the embryonic stage as well as the adult phases.

Despite cumulative results which have consistently suggested that chemical manipulation is a very potent method for quantitative evaluation of anti-PD drugs (Schober, 2004, Betarbet *et al.*, 2006) and small-scale screens have used them to identify compounds neuroprotective against 6-OHDA (Marvanova and Nichols, 2007) and MPP^+ toxicity (Braungart *et al.*, 2004, Mocko *et al.*, 2010, De Jesus-Cortes *et al.*, 2012), pharmacological models may not be ideal for extensive use in our future screens. One issue that arises was the marked variability in the effects of 6-OHDA treatment and in the time to degeneration among different studies (Wolozin *et al.*, 2011), with some groups observing severe DA neuronal loss with dosages as low as 5 mM two hours after exposure and other groups observing survival up to 72 hours after exposure (Kuwahara *et al.*, 2006, Hamamichi *et al.*, 2008). While 6-OHDA was effective in lesioning DAergic neurons in our 6-OHDA model which exhibited full sensitivity to its toxicity, 30-40% of our vehicle control population treated with ascorbic acid alone also displayed mild degenerative changes which have not been reported before. Overall, a major limitation of pharmacological models has been the tenuous relationship between the experimental manipulations used to induce the loss of DAergic neurons and the pathophysiological mechanisms leading to PD in humans (Chesselet *et al.*, 2008). Since the basis for this model derives from sensitivity to an exogenous agent which induces rapid and acute DAergic neurodegeneration, the effect may be too strong to accurately represent the progressive nature of PD pathology (Betarbet *et al.*, 2006), thus limiting the utility of the 6-OHDA

model for evaluating the neuroprotective influence of promising hits. In addition, behavioural assessment of most toxin-induced models has been minimal (Chesselet *et al.*, 2008), and discrepancies often result due to the various methodologies that have been used for analysing DAergic degeneration and fluorescence intensity levels.

While behavioural impairment of the FTDP-17 model manifested itself through neuronal morphological abnormalities, it is noticeable that despite measurable neuronal dysfunctions in both ALS and HD models studied here, there were no observable cell deaths, even during later adult life. This resembles the observation in an earlier report of Parker *et al.* (Parker *et al.*, 2001) where polyQ expansion in *C. elegans* PLM neurons abolished touch sensitivity function but did not induce cell death. This lack of cell death suggests physiological relevance to both SOD1 and polyQ toxicities in mammalian neurons which are likely to be functionally affected for a period of time before being subjected to cell death (Wang *et al.*, 2009b).

The deficits seen for the HD models in the present set of experiments were much less pronounced than those in other publications. Previous studies have consistently illustrated that enhanced mutant huntingtin toxicity in HA759 animals severely impairs both ASH survival and function. Though a strong, late-onset defect in nose touch response was observed for both HA659 and HA759 worms in our study, analysis of ASH neuronal integrity in these Htt-Q150 expressing animals failed to detect any highly penetrant ASH cell death in young or even old adult HA759 worms. Apart from this lack of phenotypic robustness and reproducibility, our chosen models for polyQ toxicity have other limitations. Since the huntingtin fragments are expressed

in only four cells, not only can cellular specificity of degeneration not be addressed, but biochemical and microarray assays would also be difficult. In addition, not all of the genes that have been implicated in HD are expressed in the ASH neurons, the selective neuronal susceptibility of these models to polyQ-mediated degeneration could therefore hinder the throughput efficiency.

Though neuroprotective activities of several compounds have previously been confirmed in our selected HD and 6-OHDA-inducd PD models (Marvanova and Nichols, 2007, Voisine *et al.*, 2007), thus validating the utilisation of these models as a chemical screen platform for drugs that slow down polyQ toxicity- and neurotoxin-mediated degeneration, we have to consider that evaluating different levels of damage would not be a useful measure for high-throughput screening, given the quantity of worms on a slide and the short time available for viewing. Attempting to assess the extent of damage can also lead to ambiguity and inaccuracy in scoring. Fine details are likely lost due to dopaminergic and chemosensory neurons entering and exiting different focal plane and glare from brighter neuronal bodies can overwhelm any degenerative differences that might exist in surrounding neuronal structures.

In summary, from the lines compared in this work, our data support the utility of the ANCL, FTDP-17 and ALS models for future screening. The results from the AD and HD models phenotyping were not robust enough to justify using these lines for testing potential chemical and genetic modifiers. The results from the neurotoxin-induced PD and SMA models phenotyping

were encouraging, but their utilities for screening are limited by technical difficulties.

CHAPTER 4: ETHOSUXIMIDE IS NEUROPROTECTIVE IN MULTIPLE *C. ELEGANS* NEURODEGENERATIVE DISEASE MODELS

4.1 INTRODUCTION

A major challenge in current neurodegeneration research is the identification of effective disease-modifying therapies which arises from an insufficient knowledge about the contribution of multiple pathways to disease pathogenesis. Over the past decades, *C. elegans* has increasingly been used as a model system to study the underlying molecular mechanisms that give rise to neurodegeneration because of its well defined genetic characteristics, abundance, short lifespan and tractability to genetic manipulation. Indeed various laboratories have developed and characterised a diverse set of *C. elegans* models of various human neurodegenerative diseases (NDs), including Alzheimer's (Link, 1995), Parkinson's (Nass *et al.*, 2001) and polyglutamine expansion diseases (Satyal *et al.*, 2000). Genetic screens performed in these models have identified a variety of genes that can suppress or increase disease progression and are thus potential therapeutic drug targets. However, relatively few of these genetic modifiers are common to more than one disease model, despite the shared feature of protein misfolding/aggregation (van Ham *et al.*, 2009, Chen and Burgoyne, 2012).

Complementary to its utility for screening for genetic contributors to NDs, *C. elegans* is a useful pharmacological model for testing potential neuroprotective compounds. Numerous well-characterised ND models have been readily exploited for triaging compounds from large libraries consisting of novel and pre-approved drugs, and for testing the effects of individual drugs, prior to validation in vertebrate models. Attention has mainly focused on screening existing FDA-approved medications rather than novel

compounds, as repurposing of drugs pre-approved for other indications obviates the need for early toxicity trials and thus expedites translation to clinical testing (Corbett *et al.*, 2012, Zhang *et al.*, 2014). For example, *C. elegans* AD models expressing human $A\beta_{1-42}$ have identified neuroprotective effects of several approved compounds, including antibiotics bacitracin, rifampicin (Lublin *et al.*, 2011) and tetracycline (Diomede *et al.*, 2010), the antidepressant fluoxetine (Keowkase *et al.*, 2010b), and the psychopharmalogical and antihypertensive drug reserpine (Arya *et al.*, 2009) in Aβ toxicity. Similarly, dopamine D2 receptor antagonists, in particular azaperone, have been shown to effectively ameliorate mutant Tau-induced functional defects and reduce aggregation in a frontotemporal dementia with parkinsonism-17 (FTDP-17) Tauopathy model (McCormick *et al.*, 2013). A wide variety of other neuroprotective compounds have also been identified in chemical screens using worm neurodegeneration models including spinal muscular atrophy (Sleigh *et al.*, 2011), Parkinson's (Wolozin *et al.*, 2011) and Huntington's diseases (Voisine *et al.*, 2007). Voisine *et al.* (Voisine *et al.*, 2007) demonstrated that FDA-approved drugs including lithium chloride, widely used to treat psychiatric conditions like bipolar disorder, the antitumor antibiotic mithramycin and trichostatin A, a class I and class II HDAC inhibitor, independently and in combination suppressed polyQ-induced neurotoxicity. Treatment of a *C. elegans* model of MJD with valproic acid, another HDAC inhibitor, also led to improved locomotor activity accompanied by a decrease in mutant ataxin-3 (ATXN3) aggregation (Teixeira-Castro *et al.*, 2011). Multiple PD models, notably the toxin-induced models have aided in the discovery and validation of bromocriptine (dopamine receptor agonist),

rottlerin (protein kinase C inhibitor and regulator of autophagy), selegiline (FDA-approved for treating major depressive disorder), amantadine (anti-viral), acetaminophen (widely prescribed for treatment of mild pain and fever) and sorafenibfor (treatment of renal cell carcinoma) as potential pharmacological interventions for PD (Wolozin *et al.*, 2011). A mutant SMA model facilitated the screening of the NINDS collection of 1040 chemical compounds and two FDA-approved drugs, 4-aminopyridine (potassium channel-blocking agent that reduces symptoms of multiple sclerosis) and gaboxadol hydrochloride (selective GABAA receptor agonist developed for treatment of chronic pain and insomnia), were shown to rescue phenotypic dysfunction (Sleigh *et al.*, 2011) with potential for further study in vertebrate models for the treatment of SMA. Treatment with methylene blue, a tricyclic phenothiazine drug (Wainwright and Amaral, 2005) which has been in use as a medical drug as well as a staining reagent (Schirmer *et al.*, 2011), was shown recently not only to rescue toxic phenotypes (including neuronal dysfunction and oxidative stress) associated with mutant TDP-43 and FUS in *C. elegans* and zebrafish ALS models (Vaccaro *et al.*, 2012), but also ameliorated Tau mediated toxicity in a newly established Tau pro-aggregant strain (Fatouros *et al.*, 2012).

There is growing evidence for a protective role of antiepileptic drugs against a range of neurodegenerative conditions. The traditional first-line antiepileptic drug, valproic acid has been shown to significantly inhibit production of Aβ and phosphorylated Tau and improve cognitive performance in AD mouse models (Qing *et al.*, 2008). The therapeutic effects of valproic acid have been ascribed to inhibition of GABA transmission,

voltage gated sodium channels, T-type calcium channels and HDACs. Treatment of nematodes with moderate concentrations of valproic acid extended lifespan and delayed age-related degenerative changes in body movement (Evason *et al.*, 2008). Furthermore, valproic acid reduced the mutant ATXN3 aggregation and motor dysfunction of a *C. elegans* model of MJD which was dependent upon DAF-16/FOXO and the insulin/IGF-1 signalling (IIS) pathway (Teixeira-Castro *et al.*, 2011). Valproic acid was also shown to have no effect on TDP-43 toxicity (Tauffenberger *et al.*, 2013), but significantly protected *C. elegans* dopaminergic neurons against α-synuclein toxicity via an ERK-MAPK-dependent mechanism (Kautu *et al.*, 2013). Other established antiepileptic drugs such as clonazepam, phenytoin, phenobarbital and carbamazepine, have shown mild neuroprotective activity in ischemic models of neuronal injury. Newer anticonvulsants such as felbamate, lamotrigine, levetiracetam, topiramate, vigabatrin and zonisamide, which have fewer drug interactions and simpler pharmacokinetics may yield new efficient treatment strategies due to their antiepileptogenic and neuroprotective properties in various animal models (Pitkanen, 2002, Willmore, 2005). Topiramate and levetiracetam (Sanchez *et al.*, 2012) were recently shown to have neuroprotective effects against the neuropathology and behavioural impairment in an AD mouse model engineered to overexpress human amyloid precursor protein (APP) and Aβ in the brain. They increased Aβ clearance and the activation of AMPK/Akt, up-regulated Aβ transport and autophagic degradation, and inhibited GSK-3β activation, HDAC activity and amyloidogenic APP processing at the γ-secretase site. A multicenter, randomised, double-blind, placebo-controlled study (Murata *et*

al., 2007) in Japan provided data suggesting that zonisamide, has efficacy in treating motor symptoms in patients with PD.

Most compounds identified in *C. elegans* chemical screens to date are effective in only a single neurodegenerative model, suggesting that translational potential may be disease-specific. However, some compounds, such as resveratrol, have been shown to be protective in a range of worm models and also in mammalian systems (Parker *et al.*, 2005, Karuppagounder *et al.*, 2009, Bizat *et al.*, 2010, Tauffenberger *et al.*, 2013, Kashyap *et al.*, 2014). Resveratrol, a polyphenolic compound naturally occurring in plants and found in dietary products was shown to ameliorate neurotoxicity induced by expanded huntingtin, mutant TDP-43 and prion proteins in transgenic HD (Parker *et al.*, 2005), ALS (Tauffenberger *et al.*, 2013) and Creutzfeldt-Jakob disease (Bizat *et al.*, 2010) worm models, or as a result of loss of an endogenous neuroprotective gene *dnj-14* in a new adult-onset neuronal ceroid lipofuscinosis (ANCL) model (Kashyap *et al.*, 2014). This demonstrates that it is possible to identify generally neuroprotective compounds that alleviate the functional consequences of protein misfolding common to neurodegeneration. In this chapter, we demonstrate that the antiepileptic drug ethosuximide could be a promising general modifier of early-onset proteotoxicity since it was efficacious in multiple worm ND models, reducing proteotoxicity and enhancing lifespan not only in a *C. elegans* null mutant model of ANCL, but also in a distinct worm frontotemporal dementia model and polyglutamine expansion diseases model based on transgenic expression of mutant human Tau and polyQ expansions. Ethosuximide is an FDA approved succinimide most widely

prescribed for the treatment of petit mal epileptic absence seizures in humans and has recently been explored for its potential as a therapeutic for age-related diseases since it was shown to delay degenerative changes and extend the lifespan of *C. elegans* (Evason *et al.*, 2005). But in the context of neurodegeneration ethosuximide has been less well documented. In the second part of this chapter, the possible mechanisms of action of ethosuximide were investigated. While the primary target of ethosuximide in clinical uses is low voltage gated T-type calcium channel, our results suggested that ethosuximide exerts protective effects via a mechanism that is independent of T-type calcium channel. Furthermore, our data revealed an imperfect correlation between the ability of ethosuximide to alter biochemical endpoints such as levels of soluble and insoluble Tau protein and polyQ aggregation and suppress proteotoxicity. We have also excluded the possibility that the protective effects of ethosuximide are due to changes in the *E. coli* food source.

4.2 RESULTS

4.2.1 Ethosuximide efficiently attenuated pathological phenotypes manifested by different ND models

4.2.1.1 Ethosuximide consistently improved the survival of an ANCL model

Multiple independent studies have recently demonstrated that the rare hereditary human ND adult-onset neuronal ceroid lipofuscinosis (ANCL) is caused by mutations in the *DNAJC5* gene which encodes a neuronal chaperone of the DnaJ/Hsp40 family of molecular chaperones known as cysteine string protein (CSP), which prevents the misfolding of presynaptic proteins (Zinsmaier *et al.*, 1994, Chamberlain and Burgoyne, 2000, Sharma *et al.*, 2011, Greaves *et al.*, 2012, Sharma *et al.*, 2012, Kyle *et al.*, 2013). CSP knockout mice have early mortality and exhibit age-related neurotransmission defects, sensorimotor dysfunction and presynaptic neurodegeneration. The *C. elegans* model of ANCL established by our laboratory for age-dependent neurodegeneration has a mutation in the *dnj-14* gene. DNJ-14 is the worm homologue of CSP and *dnj-14* null mutants are characterised by reduced lifespan and age-dependent sensorimotor defects and neurodegeneration, similar to CSP knockout mice (Fernandez-Chacon *et al.*, 2004, Kashyap *et al.*, 2014).

Aiming to see whether we can use the ANCL model to identify compounds with therapeutic potential for ANCL and possibly other neurodegenerative diseases, this lab has previously undertaken a focused screen of ten chemical compounds with either known lifespan extending or

neuroprotective properties on various different ND models or on lifespan in wild type (WT) worms. These include lithium chloride (Carmichael *et al.*, 2002, Berger *et al.*, 2005, Voisine *et al.*, 2007, McColl *et al.*, 2008), C2-8 (Zhang *et al.*, 2005, Chopra *et al.*, 2007), ethosuximide (Evason *et al.*, 2005), mianserin (Petrascheck *et al.*, 2007), mithramycin (Ferrante *et al.*, 2004, Voisine *et al.*, 2007) and resveratrol (Wood *et al.*, 2004, Karuppagounder *et al.*, 2009), and it was investigated whether they could ameliorate the defects caused by loss of *dnj-14*. The anti-epileptic drug, ethosuximide along with resveratrol were observed to produce a robust and reproducible lifespan extension in *dnj-14(ok237)* worms. While work on resveratrol was carried over by another PhD student (Kashyap *et al.*, 2014), preliminary findings for ethosuximide were further expanded upon in this study.

To evaluate the potential of ethosuximide and to ascertain the optimal concentration for improving the survival of the ANCL model, we examined how the *dnj-14(ok237)* animals responded to different concentrations of ethosuximide. We generated a dose response curve by exposing the worms to ten concentrations of ethosuximide in plates varying from 0 mg/ml to 4 mg/ml (Figure 4.1A). It was observed that this effect was concentration-dependent, with 1 mg/ml ethosuximide offering the most significant lifespan increase, raising the mean lifespan of *dnj-14(ok237)* worms by over 40% (Figure 4.1A; Appendix Table A2) compared to the mean lifespan under the vehicle PBS. At higher doses (4 mg/ml) ethosuximide was observed to shorten lifespan. Notably, none of the concentrations used had any significant effect on the lifespan of WT N2 *C. elegans* (Figure 4.1B). To test if ethosuximide was also able to rescue the sensory defect in *dnj-14* mutants,

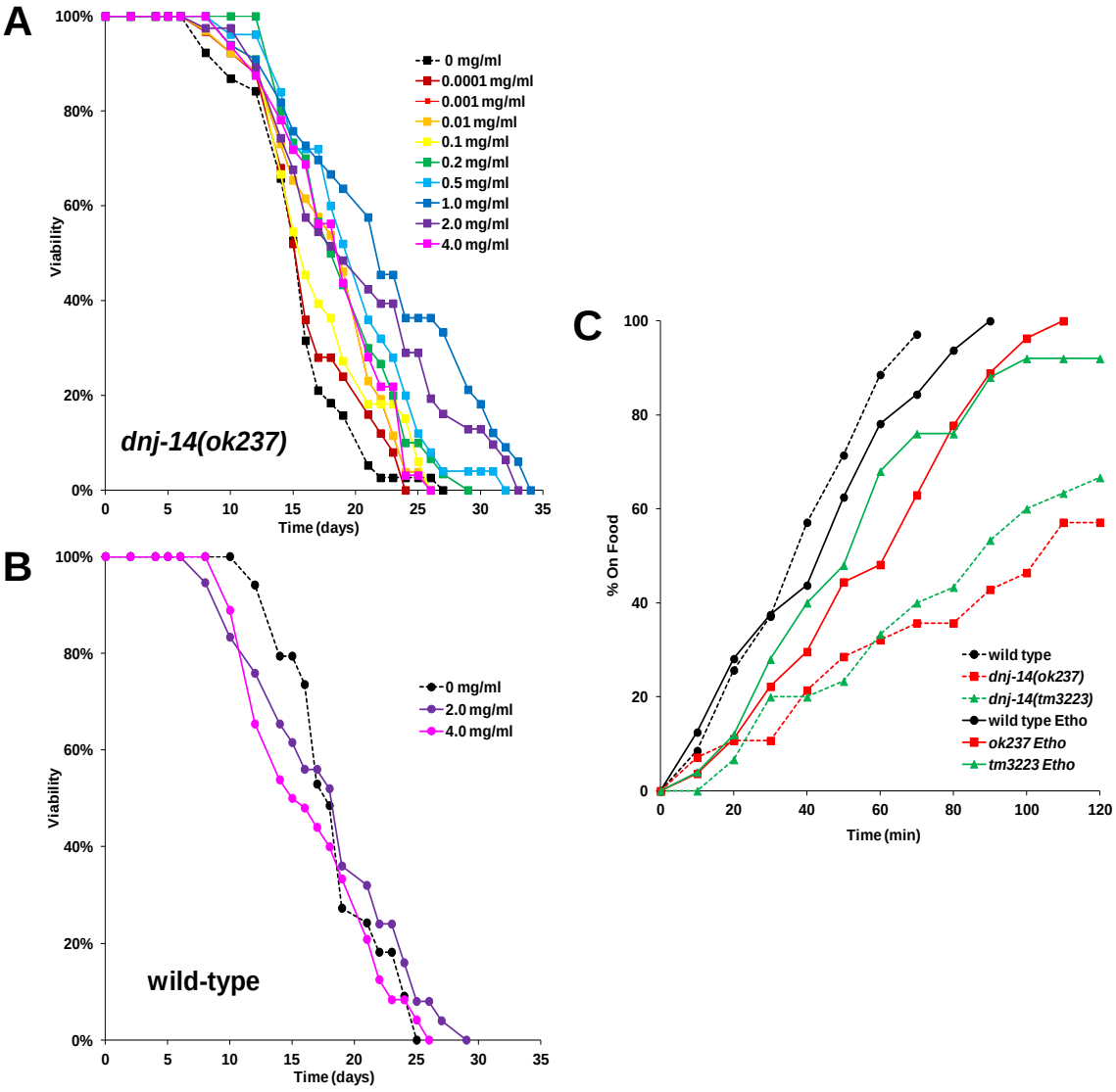

Figure 4.1 Ethosuximide increases lifespan and sensory function in a *C. elegans* ANCL model. Dose–response Kaplan–Meier survival curves of synchronously ageing A) RM2754 *dnj-14(ok237)*; B) WT N2 hermaphrodites cultured at 20 °C with vehicle alone (0 mg/ml) or with ethosuximide dissolved in PBS at the indicated concentrations (0.0001-4 mg/ml), from conception until death. Worms were age-synchronised by timed-egg lay and once the progeny reached L4 stage, 25 worms were transferred onto individual seeded drug/vehicle control plates, and monitored for survival every alternate day and transferred to fresh plates to prevent progeny formation. Day 0 corresponds to L4 stage. The lifespan of populations of synchronised *dnj-14(ok237)* worms was observed and compared with the WT N2 strain. Statistical analysis was performed using Online Application for the Survival Analysis of Lifespan Assays (OASIS; http://sbi.postech.ac.kr/oasis/introduction/) (Yang *et al.*, 2011). Log-rank (Mantel-Cox) test *w*as used to calculate significance and 0.001 mg/ml and 0.2-4 mg/ml were found to be significant compared to vehicle control treated *dnj-14 (ok237).* Treatment with 1 mg/ml ethosuximide extended the mean lifespan of *dnj-14(ok237)* most significantly (****p*<0.0001). Ethosuximide did not significantly increase lifespan in N2 control worms, suggesting a specific rescue of the defects caused by loss of DNJ-14. Most animals cultured in the presence of 4 mg/ml ethosuximide died or arrested development before reaching the fourth larval stage, and the adult lifespan of the rare animals that survived to adulthood were analysed. Data shown are derived from a single lifespan assay using 50-55 worms for each drug concentration and are displayed as raw survival curves. Statistical detail and combined data for repetitions of the experiments are presented in Table A2 of the appendix. C) Ethosuximide rescue of the *dnj-14* food sensing defect. The time taken to move to a bacterial food source was measured in 6-day-old wild type N2, *dnj-14(ok237)* and *dnj-14(tm3223)* strains in the presence or absence of 2 mg/ml ethosuximide. Data shown are from a single assay conducted by Dr. Sudhanva Kashyap using 25-35 worms of each strain per condition.

Dr. Sudhanva Kashyap performed a food race assay, which measures the time taken for animals to move a defined distance to a bacterial food source. As previously observed (Kashyap *et al.*, 2014), *dnj-14* mutants were severely impaired in this assay, with similar results seen using two different *dnj-14* alleles *(ok237* and *tm3223)*. Ethosuximide rescued food sensing activity of both mutants, but had no stimulatory activity in WT N2 worms (Figure 4.1C). Taken together, these data suggest that ethosuximide is able to ameliorate the neurotoxicity induced by the loss of the DNJ-14 synaptic chaperone protein.

4.2.1.2 Ethosuximide alleviated Tau pathology

To determine if ethosuximide had general neuroprotective activity, we evaluated its effects on a *C. elegans* FTDP-17 Tauopathy model (Kraemer *et al.*, 2003). FTDP-17 is one of many human Tauopathies in which characteristic neurofibrillary tangles are formed from hyperphosphorylated Tau. As shown in Chapter 3, overexpression of human mutant Tau V337M throughout the *C. elegans* nervous system causes severe motility defects, neurodegeneration, short lifespan and accumulation of insoluble Tau. The highly penetrant and easily observable motility phenotype of this model is well suited for assessing drug effects (McCormick *et al.*, 2013). We observed that ethosuximide significantly improved the severely impaired motility phenotype of Tau V337M transgenic worms. To ensure that suppression of locomotion impairment was not a general effect of compounds on *C. elegans* movement or an artifact of the thrashing assay employed, we also treated the Tau V337M transgenic worms with two other compounds which affected the locomotion, lifespan and neurodegeneration phenotypes of the *dnj-14(ok237)*

mutants in a positive way: resveratrol and its analogue p-propenylanisole (resveratrol 1) along with ethosuximide. Their abilities to suppress the severe, Tau-induced, motor dysfunction were analysed by exposing Tau V337M worms to each drug chronically throughout their life. Quantification of the proportion of paralysed versus moving worms revealed an increased percentage of motile Tau V337M worms upon ethosuximide treatment, with no effect on movement of the WT transgenic control strain (Figure 4.2). Resveratrol and its analogue resveratrol 1 resulted in a partial but insignificant rescue of locomotion impairment. Resveratrol may have the potential to protect against Tau-induced toxicity as it ameliorated the behavioural phenotype but this effect was not as strong as the effect of ethosuximide. However, ethosuximide's therapeutic activity was reduced with ageing, as the extent of motility amelioration at day 5 and onwards was less than that observed at day 1 and 3 with increasing percentage of aged transgenic Tau V337M worms displaying impaired mobility. It is likely that when the peak of neuronal dysfunction and degeneration occurs, the expression level of Tau in aged Tau V337M line might be above the threshold for which the drugs can be efficacious against the overt proteotoxicity to allow restored locomotion.

To ascertain the optimal concentration for improving Tau-induced behavioural defects, we next examined how the animals responded to different concentrations of ethosuximide. We generated a dose response curve by exposing Tau worms to increasing concentrations of ethosuximide in plates, and the animals were assessed visually for any effects on the phenotype. As shown in Figure 4.3A, the vehicle-treated Tau V337M worms

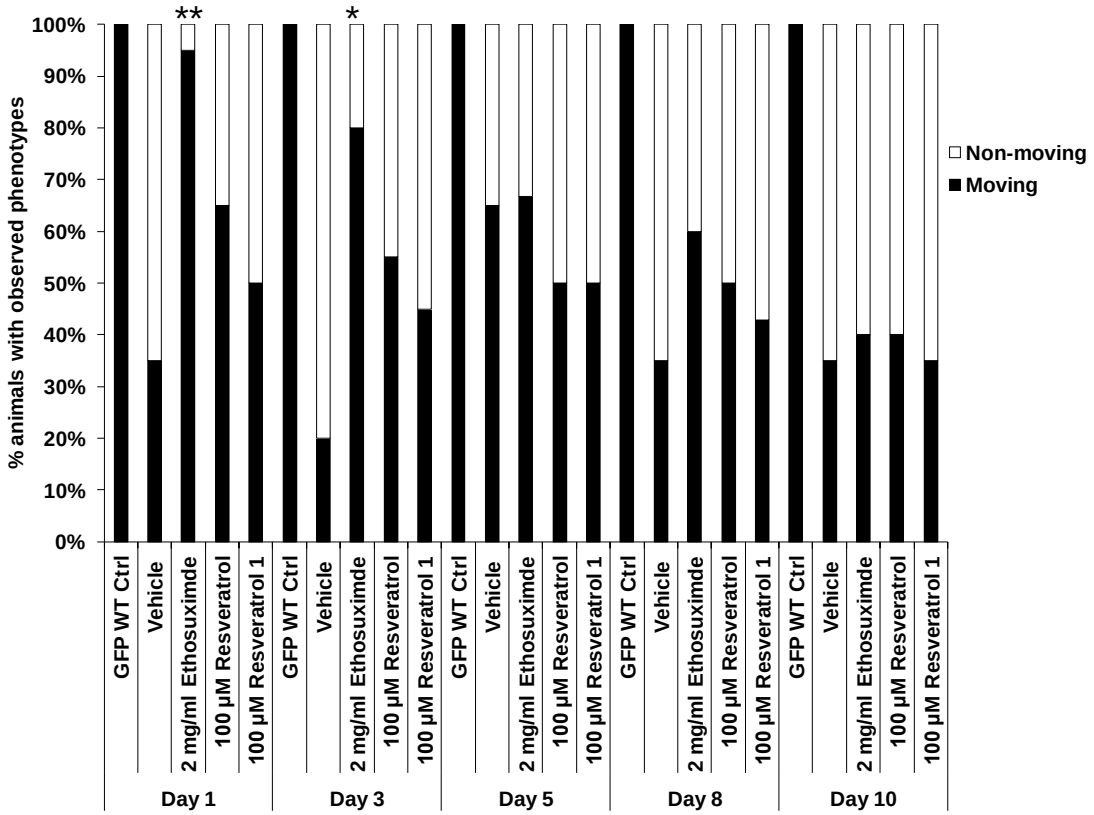

Figure 4.2 Treatment of Tau V337M transgenic animals with chemical compounds. To further corroborate the protective effect of ethosuximide, we tested its efficacy in ameliorating motor dysfunction associated with mutant Tau expression by treating at birth and measuring responses throughout adulthood. Synchronised Tau V337M transgenic worms were hatched and fed on compound-containing NGM medium for three days at 20°C. The 3 compounds examined were ethosuximide, resveratrol, and its analogue resveratrol 1. 2 mg/ml ethosuximide treatment caused a significant increase in the proportion of motile Tau V337M worms compared to the vehicle control treated worms at day 1 and day 3 (*p<0.05, **p<0.001), while not affecting the transgenic WT GFP N2 line. Resveratrol and resveratrol 1 showed no significant rescue of motor dysfunction. However, ethosuximide exhibited reduced potency in rescuing the behavioural phenotype induced by aged Tau mutants after day 5 of adulthood during which severe behavioural phenotype already has manifested. Data shown are pooled from two independent experiments, each with 10-30 worms per data point.

were severely impaired in their ability to swim. However, treatment with ethosuximide improved the motility in a dose-dependent manner. These effects appear to be Tau-specific, because the WT transgenic control worms expressing the GFP marker in GABAergic neurons showed normal behaviour that was unaltered by the ethosuximide treatment (Figure 4.3B).

Tau V337M transgenic worms also exhibited a short lifespan phenotype (Kraemer *et al.*, 2003). To investigate the effects of ethosuximide supplementation on longevity, lifespan assays were performed on ethosuximide treated Tau V337M and WT transgenic worms and compared with vehicle-treated controls. Ethosuximide significantly enhanced the mean lifespan of Tau V337M worms in a concentration-dependent manner as compared to the vehicle treated Tau V337M worms (Figure 4.3C; Appendix Table A2), but had no effect on transgenic WT control worms (Figure 4.3D). Comparable to the dose-dependent longevity effect of ethosuximide seen with *dnj-14(ok237)* mutants, maximal lifespan extension of Tau V337M worms was observed at 2 mg/ml, which conferred a 42% lifespan increase, while lower dosages caused smaller but significant extensions (Figure 4.4; Appendix Table A2).

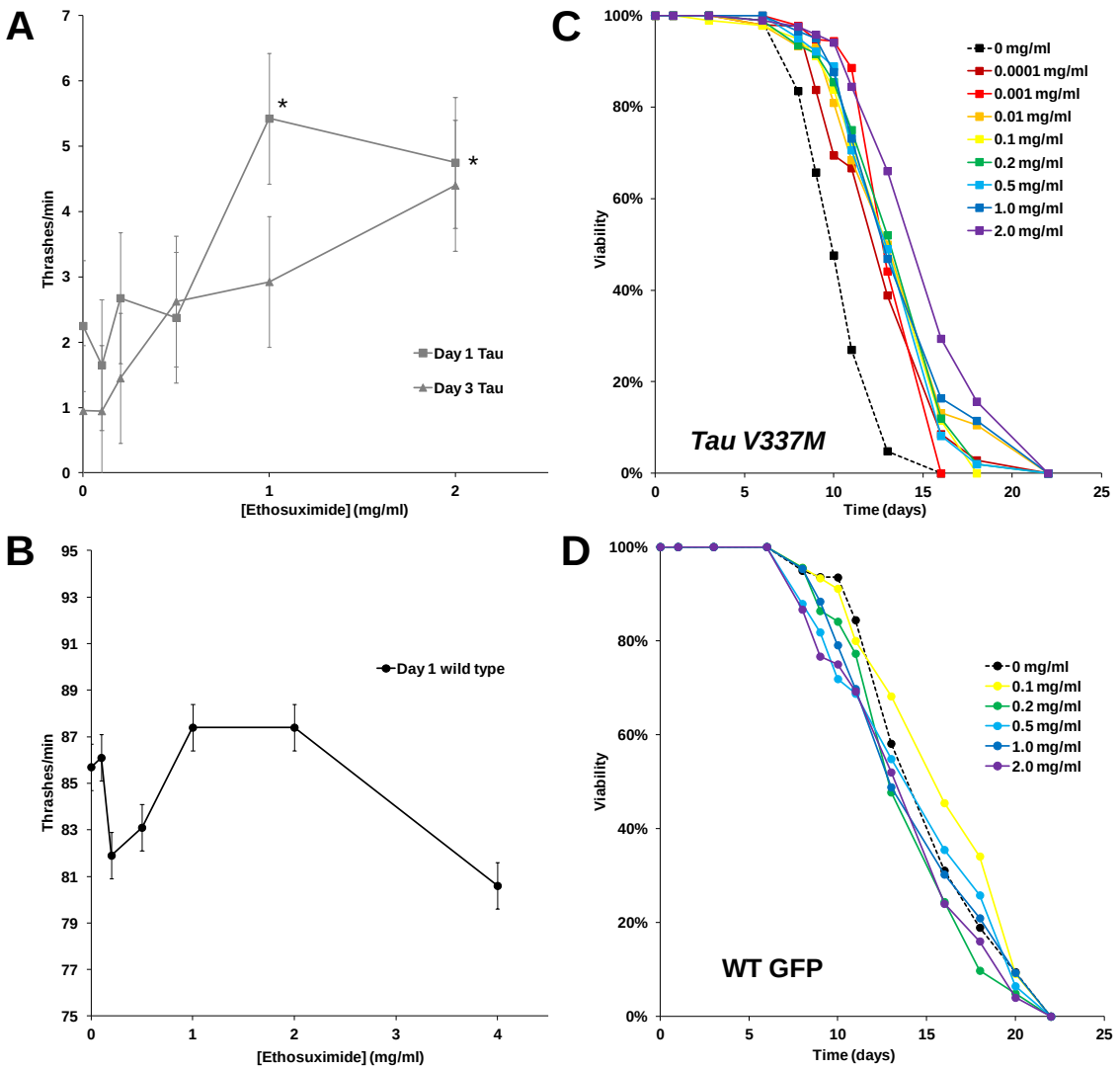

Figure 4.3 Ethosuximide leads to partial amelioration of Tauopathy-induced behavioural deficits along with lifespan extension. A-B) Dose–response curves for ethosuximide in mitigating the severe behavioural impairment of Tau V337M transgenic lines which manifested since L4. WT control worms expressing the GFP marker in GABAnergic neurons showed normal behaviour that was unaltered by the ethosuximide treatment compared with vehicle control treated animals. Behavioural results data are pooled from two independent experiments, each with 10-15 worms per genotype per concentration and are shown as mean ± SEM. Significant (*p<0.05) increases were seen at 1 mg/ml and 2 mg/ml ethosuximide in Tau V337M worms. Dose–response Kaplan–Meier survival curves of synchronously ageing C) Tau V337M transgenic; D) WT N2 hermaphrodites cultured at 20 °C with vehicle alone (0 mg/ml) or with ethosuximide dissolved in PBS at the indicated concentrations (0.0001-2 mg/ml). Ethosuximide exerted strong protection against mutant Tau–mediated toxicity, but had no measurable effect on the behaviour or lifespan of WT transgenic control worms. Ethosuximide treatment for both motility and lifespan assays was initiated from the time of hatching and continued until death. Worms were age-synchronised by timed-egg lay, survival and body movement were monitored beginning at the L4 stage and day 1 of adulthood, respectively. For lifespan analysis, 25 worms were transferred onto individual seeded drug/vehicle control plates, and viability was scored at the timepoints indicated and transferred to fresh plates to prevent progeny formation. Statistical analysis was performed using Online Application for the Survival Analysis of Lifespan Assays (OASIS; http://sbi.postech.ac.kr/oasis/introduction/) (Yang *et al.*, 2011). Log-rank (Mantel-Cox) test was used to calculate significance and all tested concentration were found to be significant compared to those treated under vehicle PBS. Data shown are pooled from two independent lifespan assays using 50-102 worms for each drug concentration. Statistical details of this experiment are summarised in Table A2 of the appendix.

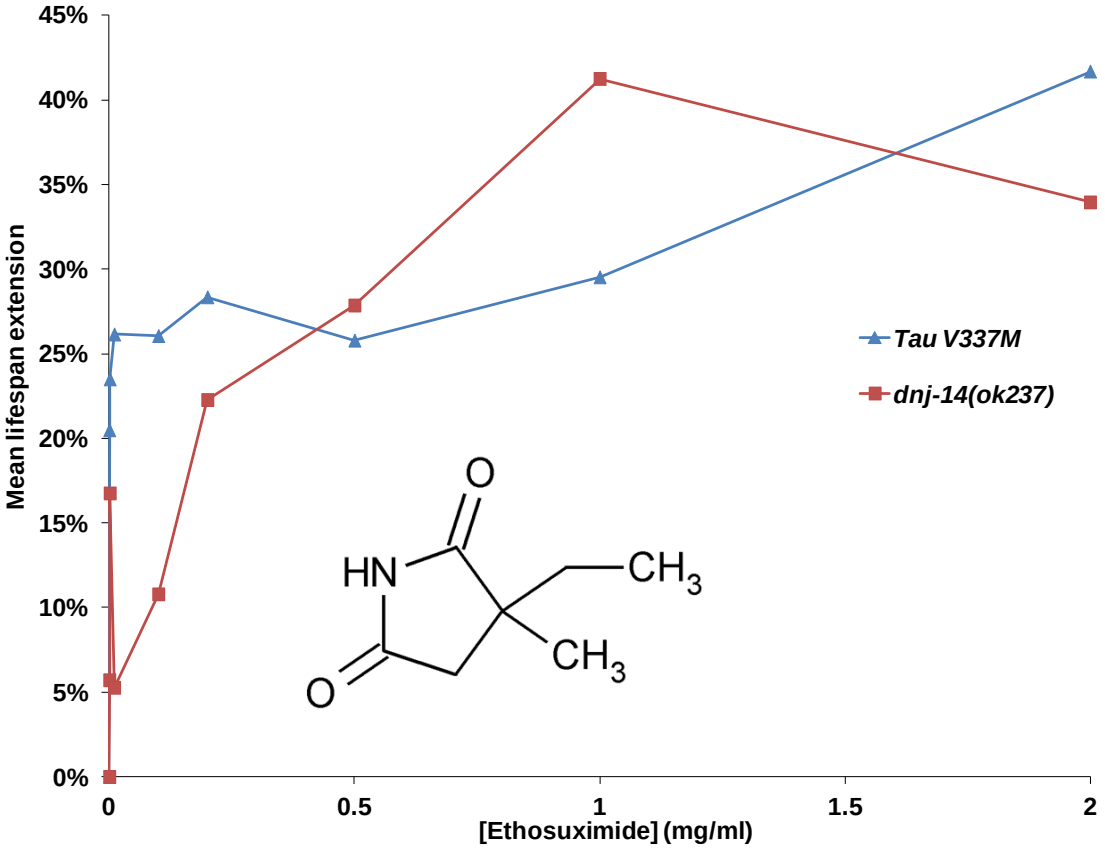

Figure 4.4 Comparison of concentration-dependence of mean lifespan extension in ethosuximide treated ANCL model and FTDP-17 model. The average percentage change in mean lifespan of *dnj-14(ok237)* mutants and Tau V337M transgenic worms treated with PBS vehicle control or 0.0001, 0.001, 0.01, 0.1, 0.5, 1, 2 and 4 mg/ml ethosuximide was plotted as a function of dosage. The chemical structure of ethosuximide, which is chemically designated as α-ethyl-α-methyl-succinimide (3-ethyl-3-methyl-pyrrolidine-2,5-dione) is shown. At lower dosages, ethosuximide significantly enhanced the mean lifespan of both ND models, though this effect was not as strong as higher dosages (1-2 mg/ml) which conferred the largest increase of lifespan versus the vehicle control in lifespan extensions, extending mean lifespan of both models by more than 40%. Statistical details of this experiment are summarised in Appendix Table A2

4.2.2 Mechanism of action of ethosuximide

4.2.2.1 Ethosuximide treatment decreases neuronal deposition of abnormal Tau but not polyQ aggregation

Our subsequent work focused on the mechanisms by which ethosuximide ameliorates motor dysfunction and extends lifespan. In view of the known association of protein misfolding/aggregation with both neurodegeneration and ageing, it was reasoned that ethosuximide's general protective effect, as demonstrated above, may be linked to modulation of protein aggregation. Detergent insolubility is one of the biochemical markers of pathological Tau protein in AD and other Tauopathies. Similarly, it has been shown that in a *C. elegans* Tauopathy model, mutant Tau protein accumulates in detergent insoluble aggregates. To clarify whether ethosuximide could influence the equilibrium between soluble and insoluble aggregated Tau forms, we subjected both vehicle- and ethosuximide-treated Tau V33M transgenic worms to a regimen of sequential extractions with buffers of increasing solubilising strengths, as previously described (Kraemer *et al.*, 2003). We then examined the solubility/aggregation profile of Tau in transgenic Tau V337M worms by using monoclonal mouse anti-Tau antibodies in western blotting. We observed no major differences in total Tau levels in ethosuximide treated Tau transgenic worms as compared to vehicle controls (Figures 4.5 A and B). The rescuing effect of ethosuximide is therefore not due to transgene suppression or reduced expression of toxic mutant Tau protein. The protein levels of mutant Tau V337M were not distributed equally between different fractions as only a small fraction of the total Tau protein available was abnormal in ethosuximide treated worms while the majority

was RAB soluble. Ethosuximide treatment did appear to alter Tau solubility as quantification of the RAB high salt soluble and RIPA detergent soluble Tau levels relative to total levels of Tau revealed a shift in the equilibrium towards more soluble Tau as indicated by the slightly increased RAB Tau levels and a significant reduction in detergent-soluble Tau in ethosuximide-treated compared with untreated worms (Figure 4.5B). However, we struggled to detect the most detergent insoluble formic acid (FA) fraction.

To directly visualise effects of ethosuximide on aggregation of toxic proteins, we utilised previously established *C. elegans* muscle models of CAG-repeat disorders expressing YFP alone (Q0), a non-pathogenic Q-stretch (Q24) or expanded polyQ proteins (Q35 and Q40) (referred to as Q0, Q24, Q35 and Q40 worms hereafter). The formation of intracellular polyQ deposits in muscle cells can be easily monitored since the expression of yellow fluorescent protein (YFP) fused to glutamine expansions greater than 35-40 residues in worm body wall muscle cells induces polyQ-dependent aggregation and toxicity (Satyal *et al.*, 2000, Morley *et al.*, 2002), which mimics the polyQ length dependence observed for HD. Q0 and Q24 worms which control for phenotypic changes exhibited diffuse soluble fluorescence, whereas Q35 and Q40 lines exhibited age-dependent aggregation, consistent with previous studies (Nollen *et al.*, 2004). PolyQ stretches in Q35::YFP animals caused an intermediate aggregation phenotype with the appearance of punctate fluorescence in Q35 worms at day 3 of adulthood, while polyQ stretches in Q40::YFP worms produced a more striking aggregation phenotype with the premature appearance of polyQ foci in Q40

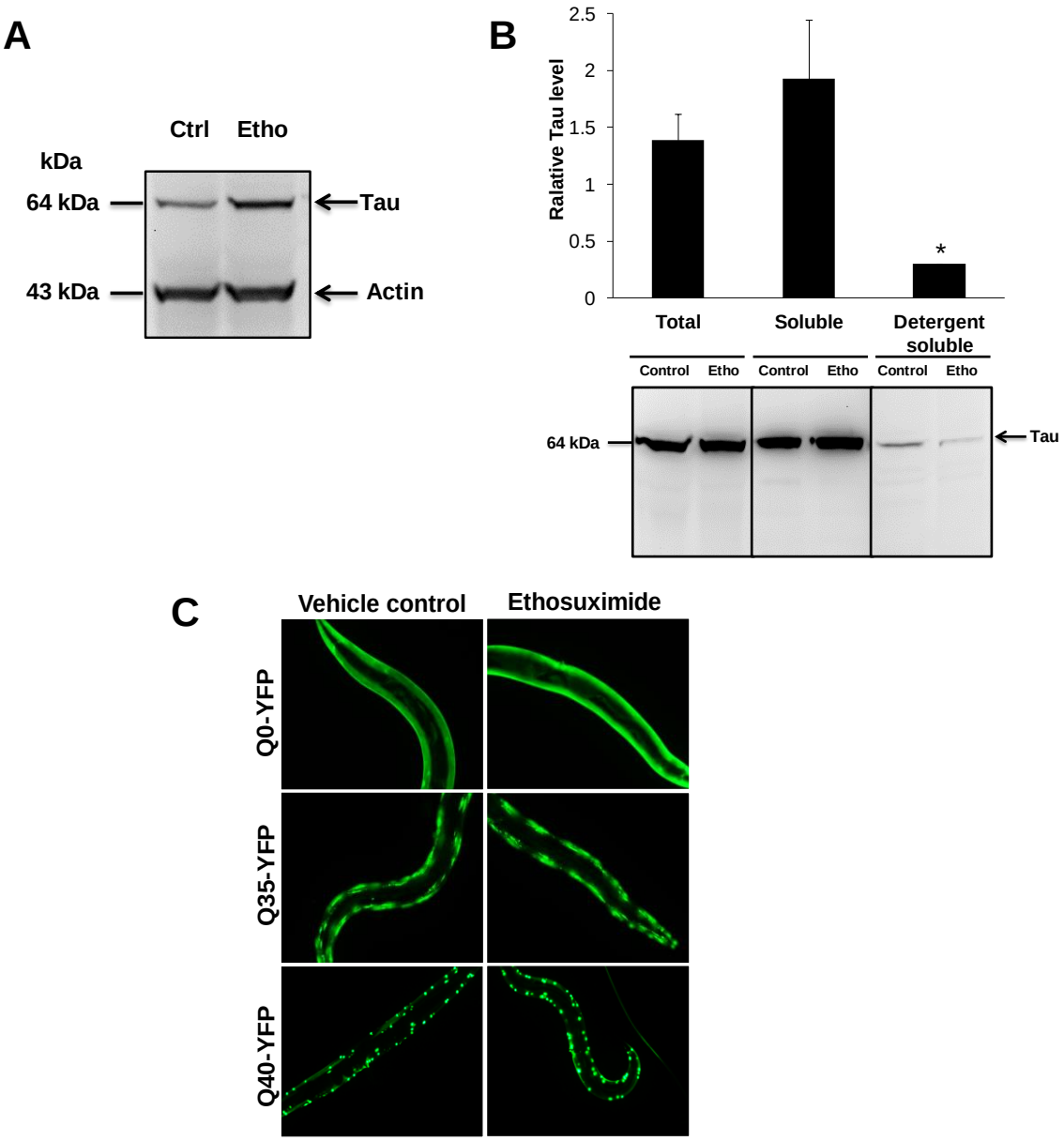

Figure 4.5 Ethosuximide reduces accumulation of detergent-soluble, abnormal Tau but does not affect muscle polyglutamine aggregations. A, B) Western blot analysis of Tau protein solubility from transgenic strains expressing human mutant Tau V337M treated with or without ethosuximide. Sequential extraction of Tau from mixed populations of synchronised Tau V337M transgenic worms after treatment with vehicle or 2 mg/ml ethosuximide with buffers of increasing solubilising strength was performed as described in the *Materials and Methods*. Supernatants of each fraction were blotted with pan Tau antibody to estimate differing levels of Tau solubility. Representative immunoblot from three experiments and quantification of the total, soluble and detergent soluble Tau after ethosuximide treatment are shown. No noticeable difference of total Tau expression by ethosuximide treatment was observed. Tau was demonstrated prominently in RAB soluble fraction. Ethosuximide treatment led to a small and variable increase in RAB soluble Tau accumulation, but considerable decrease in the abnormal Tau species extracted with RIPA. Signal intensities were measured by densitometry and normalised against the untreated samples (n=3 biological replicates). C) Ethosuximide does not prevent polyglutamine aggregation. Fluorescence microscopy was used in order to evaluate if the aggregation state of polyQ expressed in the muscle cells could be altered by ethosuximide. Representative live fluorescence images of two independent experiments depicting polyQ aggregation of Q0, Q35 and Q40 transgenic strains treated with either PBS control (left panel) or ethosuximide at 1 mg/ml (right panel) from conception at 20°C are shown. Q35 and Q40 body sections showed distinct morphology of aggregates in 6 day old worms with or without ethosuximide treatment. Vehicle and ethosuximide treated 6-day-old Q0::YFP adults (top) show diffuse GFP distribution, whilst 6-day-old Q35::YFP (middle) and Q40::YFP (bottom) treated with and without 1 mg/ml ethosuximide showed minimum *in vivo* aggregation suppression. 10 animals of each strain were scored in two independent trials. Scale bar, 100 µm.

worms as young as L4 stage. Ethosuximide, however, did not affect the diffuse fluorescence distribution exhibited by Q0 animals (Figure 4.5C, top right panel). Neither was the widespread punctate fluorescence distribution displayed by Q35 and Q40 animals at adult day 6 affected by the drug (Figure 4.5C, middle and bottom right panels).

4.2.2.2 Ethosuximide induced protection is further extended to polyQ expansion-associated cellular toxicity

A direct link between the ameliorated locomotion and the reduced level of aggregation of toxic proteins or improved body-wall muscle histology has been well established. To determine if ethosuximide leads to functional improvement of treated polyQ transgenic worms despite a lack of reduction of polyQ aggregates within muscle cells, we studied the effect of ethosuximide on the mobility and lifespan of these worms. 1 mg/ml was chosen for further experiments because the animals responded to ethosuximide in the most consistent manner at this concentration. In line with previous studies, we found that the phenotypes observed in worms expressing expanded polyQ tracts aggravated as the animals aged, similar to the progressive exacerbation of the human polyQ-associated disease symptoms with age (Figure 4.6A). Vehicle treated Q35 and Q40 worms exhibited significantly enhanced motor neuron dysfunction and hence overt neuronal toxicity when compared with Q0 and Q24 worms. At day 0 of adulthood, vehicle treated Q35 and Q40 animals showed an unimpaired motility similar to that observed in Q0 and Q24, but by adult day 6 they exhibited a striking loss of motility. Relative to control WT animals, Q35 and Q40 animals exhibited muscle dysfunction resulting in a 97% and 65% loss

of motility at 6 days of age, respectively. Relative to Q35 animals that exhibited a rapid decline in motility, Q40 animals exhibited an intermediate but variable motility defect, while both Q0 and Q24 animals exhibited a gradual mild decline in locomotion. Exposure to 1 mg/ml ethosuximide improved the motility of aged Q35 and Q40 animals considerably by >50% relative to their untreated counterparts, but had no significant effect on Q0 and Q24 strains (Figure 4.6A).

We also observed that Q35 and Q40 worms aged more rapidly, their mean lifespan being 12.2 days and 14.1 days, respectively; compared to 18.6 days for Q0 and 17.1 days for Q24 worms (Figure 4.6B; Appendix Table A2). Ethosuximide prolonged the mean lifespan for both Q35 (to 14.8 days) and Q40 (to 15.9 days) by 21% and 13%, respectively compared with their untreated counterparts. Ethosuximide had no significant effect on the lifespan of Q0 worms, whereas drug treated Q24 animals exhibited a 20% increase in mean lifespan (to 20.6 days) compared with their untreated counterparts (17.1 days).

Collectively, these results show that while muscle function is preserved upon ethosuximide treatment, this is not due to gross alterations in polyglutamine protein aggregation. Ethosuximide is likely to act non-cell autonomously as demonstrated by its differential protective effects on *C. elegans* aggregation models and on the basis that damage of diverse cell types collectively contribute to the loss of selective neurons which leads to functional defects. However, cell-autonomous effects cannot be ruled out as ethosuximide could specifically target a ubiquitous protein expressed in both neurons and muscle, and impact upon the disease progression.

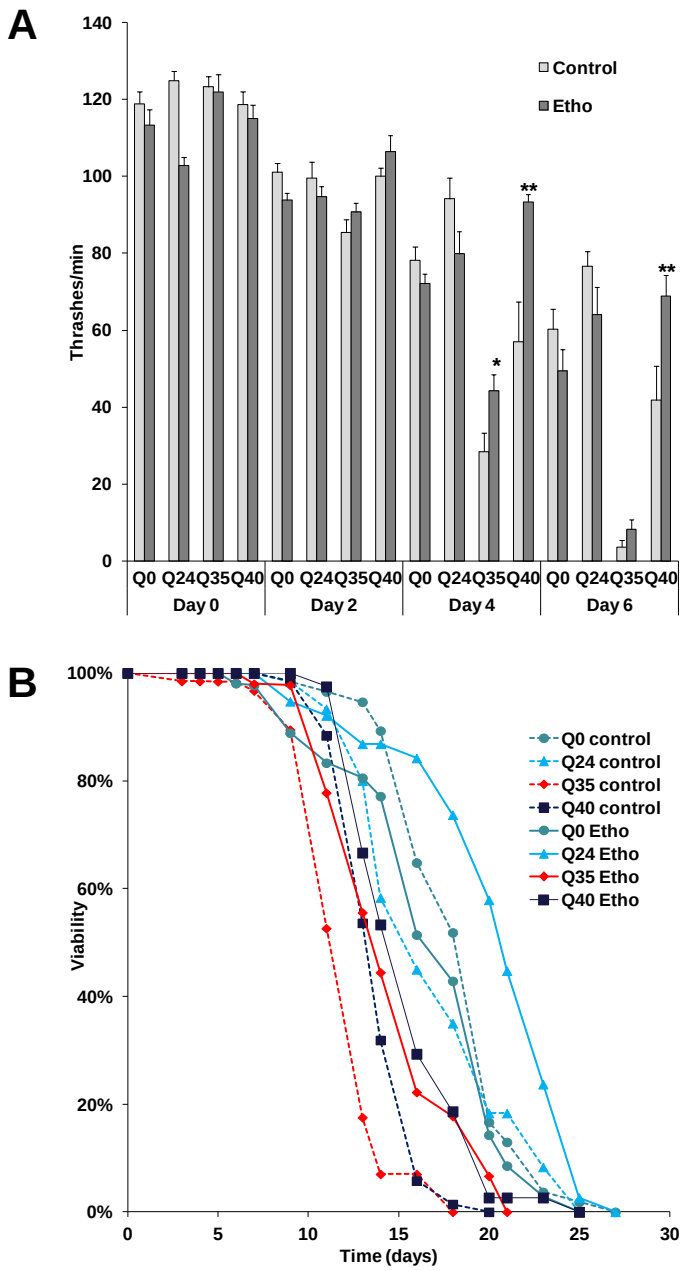

Figure 4.6 Reduction of polyQ expansion-associated cellular toxicity by ethosuximide A) Effect of ethosuximide treatment on age-dependent changes in the locomotion of *C. elegans* expressing polyQ-YFP fusion proteins with 0 (Q0), 24 (Q24), 35 (Q35) or 40 (Q40) glutamine residues in body wall muscle cells. Q30 and Q40 worms show progressive muscle degeneration, loss of motility and premature death. Rescue of polyQ expansions-associated cellular toxicity was determined by comparing the motility of Q35 and Q40 animals treated with either PBS alone or ethosuximide to that of Q0 and Q24 animals Ethosuximide specifically alleviates impaired mobility of Q35 and Q40::YFP worms relative to vehicle control animals which showed no ethosuximide protection. The graph represents the means ± S.E.M (error bars) from two independent experiments (n= 20-40 worms per strain per condition; *p<0.05, **p<0.001). B) Effect of ethosuximide on lifespan of *C. elegans* model of poly-Q overexpression. Kaplan-Meier survival survival plot of age-synchronised polyQ worms cultured at 20 °C and treated with PBS vehicle control (dashed lines) or 1 mg/ml ethosuximide (solid lines). 1 mg/ml ethosuximide treatement showed a significant increase in lifespan of Q35 and Q40 worms, and Q24 after day 14, while no increase in lifespan was observed in polyQ0. Statistical analysis was performed using Online Application for the Survival Analysis of Lifespan Assays (OASIS; http://sbi.postech.ac.kr/oasis/introduction/) (Yang *et al.*, 2011). Data shown are derived from a single lifespan assay using 50-90 worms for each drug concentration and are displayed as raw survival curves. PolyQ transgenics were synchronised and treated with 1 mg/ml ethosuximide at birth and harvested at L4 stage to monitor body movement and survival changes. Statistical details of this experiment are summarised in Appendix Table A2.

4.2.2.3 Ethosuximide action is independent of T-type calcium channels

Different *C. elegans* mutants can be utilised to identify the pathways modulated by various drugs. Previous studies using vertebrate cultured cells have led to the proposal that the efficacy of ethosuximide in generalised absence epilepsy is mediated by blockade of the low voltage activated (LVA) T-type calcium channel in the soma and dendrites of thalamic relay and reticular neurones (Coulter *et al.*, 1990, Gomora *et al.*, 2001, Crunelli and Leresche, 2002). The primary sequence and the electrophysiological parameters demonstrated that *C*. *elegans* CCA-1 is most similar to vertebrate T-type calcium channel α_{1I} subunit (42% identity), with typical T-type kinetics, voltage dependence and pharmacology (Steger *et al.*, 2005). Based on prior studies showing that ethosuximide can increase the lifespan of worms mutated for *cca-1*, which indicates that LVG T-type calcium channel is not required for ethosuximide to influence longevity of WT worms (Collins *et al.*, 2008), we therefore constructed a double mutant Tau V337M; *cca-1(ad1650)* strain (Figure 4.7A) to determine if ethosuximide's therapeutic action in the FTDP-17 model was mediated via inhibition of CCA-1. Double *cca-1(ad1650)*; *dnj-14(ok237)* homozygotes cannot be easily generated with both mutations on the X-chromosome.

If ethosuximide functions in a pathway that is dependent on the calcium channel, then we would expect the Tau V337M; *cca-1(ad1650*) cross-progeny to be mobile and long-lived and their phenotypic improvements abrogated upon ethosuximide exposure. As seen in Figure 4.7B, loss of *cca-1* had minimum effect on toxicity, as a similar large percentage of both Tau V337M; *cca-1(ad1650)* homozygotes (58%) and Tau

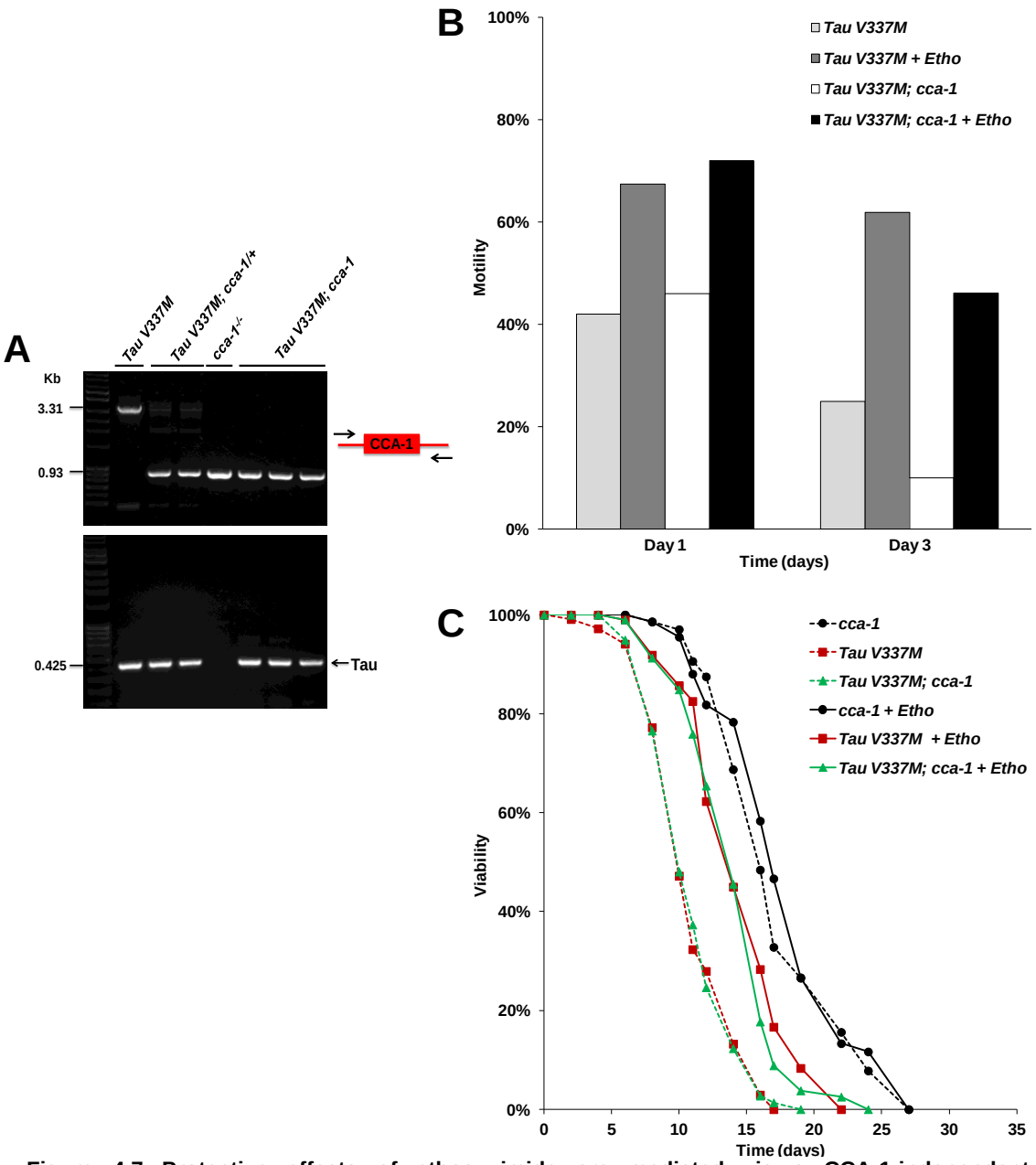

Figure 4.7 Protective effects of ethosuximide are mediated via a CCA-1-independent mechanism. To test the involvement of CCA-1 in ethosuximide activity, we crossed Tau V337M transgenic animals with loss-of-function mutations for *cca-1(ad1650)* to generate a homozygous cross progeny and tested if ethosuximide maintained neuroprotective activity. A) PCR confirmation of Tau V337M; *cca-1(ad1650)* double mutant lines. F2 progeny was segregated and were genotyped for *cca-1(ad1650)* homozygosity by PCR using primers that flanked the *ad1650* deletion. PCR analysis identified individual worms homozygous or heterozygous for the *ad1650* allele. Tau V337M worms WT for *cca-1*(*ad1650)* display one PCR product of 3.3 kb, whereas *ad1650* heterozygotes detected two bands. *cca-1*(*ad1650)* homozygotes displayed only the expected 930 bp band. The homozygosity of Tau in *cca-1(ad1650)* was verified by both GFP and PCR. B) CCA-1 repression is not required for ethosuximide protection against Tau V337M-induced paralysis. Ethosuximide supplementation ameliorated the impaired motility of the Tau V337M transgenic strain and the double mutant Tau V337M; *cca-1(ad1650)* strains to similar extents. C) Ethosuximide extends lifespan in Tau V337M mutants in the absence of CCA-1. Kaplan-Meier survival curves illustrate that lifespan of ethosuximide treated Tau V337M transgenic worms homozygous for the *cca-1(ad1650)* allele was strongly protected. Lifespan assays were performed on single mutant *cca-1(ad1650)*, transgenic (Tau V337M) and double mutant Tau V337M; *cca-1(ad1650)* strains grown at 20°C in the presence (solid lines) or absence (dashed lines) of 1 mg/ml ethosuximide. The lifespan of Tau V337M; *cca-1(ad1650)* double mutant under the vehicle control is similar to Tau V337M single mutant, but is significantly rescued upon treatment with ethosuximide. Data shown are pooled from two independent experiments using over 100 worms in total per strain/condition.

V337M transgenic worms (54%) without ethosuximide treatment exhibited severely impaired motility phenotype. Ageing exacerbated the motility defects, increasing the percentage of Tau V337M worms and Tau V337M; *cca-1(ad1650)* with impaired mobility by 17% and 36%, respectively. Ethosuximide treatment, however, mitigated the impaired motility of Tau V337M transgenic worms and double mutant harboring a loss-of-function mutation of CCA-1 to a similar extent, both at day 1 and day 3 (Figure 4.7B). The increase in motility produced by ethosuximide is therefore independent of the worm T-type channel.

This was further corroborated in the subsequent lifespan assay in which Tau V337M; *cca-1(ad1650)* homozygotes and Tau V337M transgenic worms displayed a mean adult lifespan 11.3 and 11.5 days, respectively. Following ethosuximide supplementation, there was negligible change in lifespan of *cca-1(ad1650)* single mutant control worms. However, the ability of ethosuximide to increase longevity in the single Tau V337M transgenic strain was fully maintained in the Tau V337M; *cca-1(ad1650)* homozygotes, significantly extending the mean lifespan by 29% and 27%, respectively (Figure 4.7C; Appendix Table A2). Taken together, these results indicate that the mechanism of ethosuximide action does not does not involve inhibition of CCA-1.

4.2.2.4 Protective effects of ethosuximide are not due to changes in the *E. coli* food source

One contributor to late-age mortality in *C. elegans* is the detrimental effect of their *E. coli* food source, and drugs that decrease bacterial pathogenicity have been repeatedly shown to extend worm lifespan (Gems and Riddle,

2000, Garigan *et al.*, 2002). This therefore raised the possibility that ethosuximide was acting as an antibiotic on the OP50 *E. coli* and thereby indirectly affecting worm lifespan. In addition, it has recently been shown that some drugs, for example metformin, increase *C. elegans* lifespan via changes to *E. coli* metabolism (Cabreiro *et al.*, 2013). To determine if such bacterial effects contribute to the mechanism of action of ethosuximide in lifespan extension, we used the antibiotic kanamycin to kill the OP50 food source and thus prevent both bacterial metabolism and pathogenicity. In single treatments, 10 mM kanamycin and 1 mg/ml ethosuximide supplementation increased the mean lifespan of Tau V337M worms by 37% and 48%, respectively (Figure 4.8). A combined treatment of kanamycin and ethosuximide caused a significant and approximately additive 72% extension in mean lifespan. As kanamycin clearly did not affect the ability of ethosuximide to increase lifespan (Figure 4.8; Appendix Table A2), this suggests that ethosuximide's protective effects are independent of bacterial metabolism and pathogenicity.

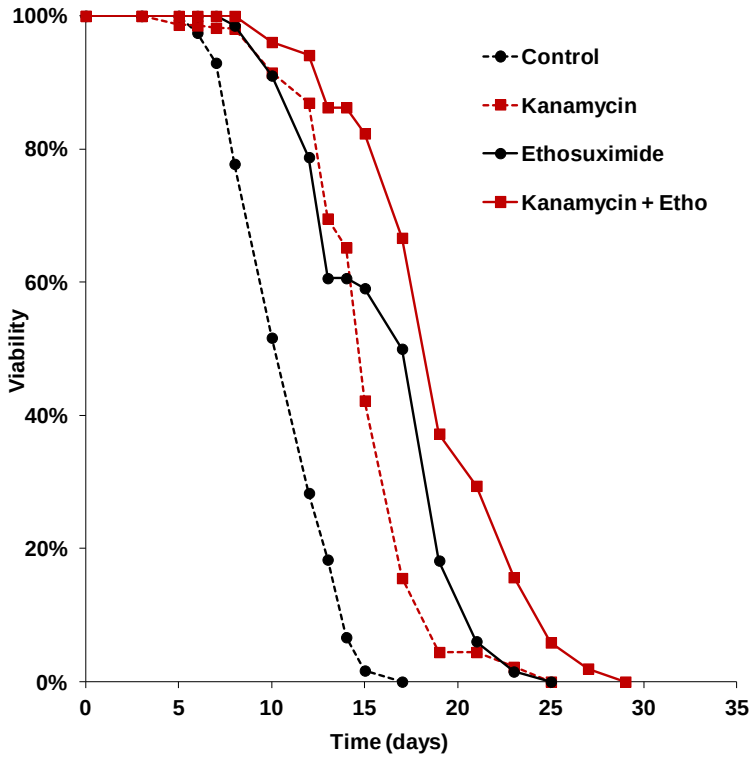

Figure 4.8 Ethosuximide extends lifespan through a mechanism distinct from that of antibiotic kanamycin. Ethosuximide extends lifespan using an inviable bacterial food source. Lifespan assays were performed on Tau V337M worms grown at 20°C in the presence (solid lines) or absence (dashed lines) of 1 mg/ml ethosuximide. Tau V337M transgenic worms were cultured with vehicle PBS, 1 mg/ml ethosuximide alone, 10 mM kanamycin alone or with both kanamycin and ethosuximide from conception until death. Both 1 mg/ml ethosuximide and 10 mM kanamycin significantly extended lifespan when applied to worms independently, but their combined treatment produced an additive effect. Data shown are from a single lifespan assays using over 80 worms in total per condition.

4.3 DISCUSSION

There is considerable current interest in the idea of repurposing existing medicines for the treatment of neurodegenerative diseases (Corbett *et al.*, 2012). FDA-approved bioactive compounds, therapeutic agents, and natural products with well established safety and bioavailability profile, would require far fewer resources to bring to market as repurposed therapeutics for neurodegeneration than completely novel drugs needing to go through extensive toxicology testing and early-phase clinical trials demonstrating safety, disease-specificity, tolerability and effective cerebrospinal fluid (CSF) penetration (Ekins and Williams, 2011, Zhang *et al.*, 2013a). The data presented here suggest that ethosuximide may be a candidate for such an approach. Ethosuximide, a small heterocyclic ring compound of the succinimide class, has been widely prescribed for several decades to treat generalised absence seizures in children and has a number of potential molecular targets. It is cheap to manufacture, well tolerated at high doses and has a good safety record (Goren and Onat, 2007). Ethosuximide also has >95% bioavailability and freely crosses the blood-brain barrier, with levels of the drug in CSF and multiple brain regions being similar to those found in plasma (Goren and Onat, 2007). Perhaps the most intriguing therapeutic value for ethosuximide is its potential to reduce the risk and delay the onset of age-associated NDs. In this chapter, we expand upon previous findings to demonstrate the remarkable versatility of ethosuximide, in ameliorating the pathological phenotypes manifested by three distinct worm ND models: ANCL, frontotemporal dementia and polyglutamine expansion diseases. These models involve deletion of an endogenous neuroprotective

gene (*dnj-14*), pan-neuronal expression of a disease-associated mutant Tau protein, and muscle-specific expression of aggregation-prone polyglutamine stretches, respectively. Nevertheless, these contrasting models share the property of altered proteostasis, suggesting that ethosuximide may act to counteract the proteotoxicity common to many NDs. The rescue of impaired motor activity and short lifespan, two consistent physiological biomarkers of *C. elegans* ageing and neurodegeneration, was specific to the neurodegenerative models used, as ethosuximide had no significant effect on the respective WT controls.

Furthermore, while our work was nearing completion, an independent study reported a neuroprotective effect of ethosuximide against human mutant mTDP-43-mediated proteotoxicity in a transgenic *C. elegans* model of ALS, and this protection was shown to be *daf-16* dependent, but *hsf-1*, *sir-2.1* and *skn-1* independent (Tauffenberger *et al.*, 2013). The ability of ethosuximide to ameliorate the phenotypes of so many different worm ND models suggests that it merits consideration for therapeutic applications in patients.

Although several reports exist on the therapeutic and experimental uses of ethosuximide, data on the mechanism by which ethosuximide exerts its anti-epileptic action is scarce and unclear. Varying methods (whole-cell patch-clamp, voltage-clamp, ruptured-patch method), cell types (HEK-293-cells, thalamic neurons, thalamic-cortical cells) and concentrations (0.7 mM to 3.05 mM) were employed in previous *in vitro* electrophysiological studies and demonstrated ethosuximide's antagonistic action towards membrane currents. Ethosuximide has long been thought to act by partial blockade of T-

type calcium channels in thalamocortical reticular nucleus neurons, thus preventing oscillatory firing characteristic of absence seizures (Coulter *et al.*, 1989b, Coulter *et al.*, 1989a, Kostyuk *et al.*, 1992, Huguenard, 1999, Gomora *et al.*, 2001). However, there is still controversy over whether this blockade is the whole story (Crunelli and Leresche, 2002, Manning *et al.*, 2003), as further work has suggested that actions on other voltage-sensitive ion channels, such as sodium and potassium channels, contribute to the overall therapeutic effect of ethosuximide (Leresche *et al.*, 1998, Crunelli and Leresche, 2002, Kobayashi *et al.*, 2009). Ethosuximide was found to decrease persistent sodium current (Leresche *et al.*, 1998) and inhibit G protein-activated inwardly rectifying potassium channels (Kobayashi *et al.*, 2009). Farber *et al.* (Farber *et al.*, 2002) also demonstrated that ethosuximide inhibited sodium channels to prevent NMDA receptor hypofunction (NRHypo) neurotoxicity that contributes to NDs like AD. Two recent studies further implicated ethosuximide in neuronal differentiation and neurogenesis as rat muscle-derived stem cells were shown to differentiate primarily into neural-like cells in the presence of basic fibroblast growth factor and 4 mM ethosuximide (Kang *et al.*, 2013), while 1 μM ethosuximide induced increasing number of GABAergic neurons generated from cortical stem cells (Sondossi *et al.*, 2014). The neurogenic effect of other antiepileptic drugs such as valproate (Laeng *et al.*, 2004), lamotrigine, topiramate (Chen *et al.*, 2010), lithium chloride, and carbamazepine (Higashi *et al.*, 2008) has also previously been demonstrated.

Our finding that the beneficial effects of ethosuximide on motility and longevity in a frontotemporal dementia model persist in strains harbouring a

null mutation in the *C. elegans* T-type calcium channel, *cca-1*, suggests that ethosuximide's neuroprotective activity is not mediated by inhibition of T-type channels, nor was it a result of the inhibition of a negative effect of the bacterial food source. This conclusion is supported by previous work in *C. elegans* showing that lifespan extension by ethosuximide is unaffected by a different mutant allele of *cca-1* (Collins *et al.*, 2008). Given that the *C. elegans* genome does not encode voltage-sensitive sodium channels (Bargmann, 1998), it seems likely that ethosuximide ameliorates neurodegeneration via a novel ion-channel-independent mechanism.

Using a variety of pharmacological and genetic experiments, previous studies of the effects of ethosuximide in *C. elegans* have suggested several potential mechanisms of action. The Kornfeld group first explored ethosuximide and several derivatives as lifespan extending compounds in *C. elegans* and showed that ethosuximide supplementation not only promoted the longevity but also prevented age-related physiological and reproductive decline of WT *C. elegans* (Evason *et al.*, 2005, Collins *et al.*, 2008). It was suggested that the potent pro-longevity effects of ethosuximide are likely due to modulation of neuronal signalling specifically by perturbing WT *C. elegans* chemosensory neuron function, which prevents worms from sensing food, resulting in a perceived state of dietary restriction and hence lifespan increase (Collins *et al.*, 2008). However, it has recently been shown that ethosuximide's ability to extend lifespan persists even under maximal dietary restriction conditions (Choi *et al.*, 2013), thus arguing against this mechanism. Furthermore, the *dnj-14* worm model of ANCL used in this study is short-lived and exhibits profound chemosensory impairment, ethosuximide

supplementation not only prolonged the survival of *dnj-14* null mutant worms but also ameliorated their impaired chemotaxis, thus it is difficult to reconcile this proposed mechanism with these observations. None of the WT controls utilised for all three ND models was affected by ethosuximide both in terms of behaviour and lifespan regardless of the concentration used, and we observed an actual decrease in lifespan of ethosuximde treated controls. This therefore is also inconsistent with the results reported in earlier studies wherein a significant increase in lifespan of the WT worms was seen. During the course of the present study, another group reported the neuroprotective effect of ethosuximide and demonstrated that its ability to ameliorate human mutant TDP-43-induced proteotoxicity and protein aggregation in a transgenic *C. elegans* ALS model requires DAF-16, a FOXO transcription factor known to regulate development and longevity, but is independent of other key regulators of aging and stress signalling such as *hsf-1, sir-2.1* and *skn-1* (Tauffenberger *et al.*, 2013). In contrast, earlier work demonstrated that ethosuximide's protective activity might be mediated through IIS-DAF-16 pathway-independent mechanisms as lifespan increase in response to ethosuximide was still maintained in *daf-16* mutants (Evason *et al.*, 2005).

Manifestations of pathological phenotypes in many *C. elegans* ND models have been linked to the muscular or neuronal aggregation of toxic $A\beta_{1-42}$, α-synuclein proteins, mutant Tau, SOD1 or polyQ peptides (Morley *et al.*, 2002, Kraemer *et al.*, 2003, Link *et al.*, 2003, Kuwahara *et al.*, 2006, Wang *et al.*, 2009b). The protective role of genetic and pharmacological modifiers in functional analyses appears to correlate well with the level of aggregation of the specific toxic peptide in most cases. However, in the

present study, ethosuximide triggered more significant protection on aggregation-associated toxicity as compared with aggregation itself. The drug appears to have differential effects on aggregation and the associated toxicity depending on the affected cellular function, as we observed a mild (although statistically significant) increase in mobility (hence decrease in toxicity) of treated Tau and polyQ models was observed, yet ethosuximide exposure only slightly reduced the accumulation of abnormal neuronal Tau, and did not result in any observable amelioration of the muscle polyQ aggregations. Similarly, coffee extract (Dostal *et al.*, 2010), PBT2 (McColl *et al.*, 2012) and salidroside (Xiao *et al.*, 2014) have been shown to provide protection to pathological protein-induced behavioural dysfunction of *C. elegans* protein aggregation models with no evident effect on aggregating proteins. This lack of correlation between toxicity and aggregation has been reported by several studies (Kirkitadze *et al.*, 2002, Arrasate *et al.*, 2004, Ross and Poirier, 2005, Treusch *et al.*, 2009, Silva *et al.*, 2011b, Voßfeldt *et al.*, 2012, Gidalevitz *et al.*, 2013). Using various disease models, they have demonstrated that there is genetic uncoupling between suppression of aggregation process and interference with the associated toxicity, and total insoluble protein abundance does not dictate toxicity which is the outcome of a complex series of misfolding events, involving multiple species and aberrant interactions within the cell (Silva *et al.*, 2011b). This is also likely due to the disparity between muscle and neuronal models which have different capabilities in responding to protein misfolding and chemical and genetic manipulations (Tauffenberger *et al.*, 2013). Compounds like thioflavin have been shown to reduce Aβ and polyQ toxicity in muscle cells (Alavez *et*

al., 2011), but exhibited no activity in neuronal TDP-43 model. It has been suggested that an upper/lower aggregation threshold must be reached to induce the cellular and behavioural symptoms, yet surpassing the toxic threshold is likely to limit the protective efficacy of drugs. Furthermore, aggregates and inclusions have been linked both to toxicity and protection (Treusch *et al.*, 2009). It was suggested that ethosuximide reduced neurotoxicity and mTDP-43 insolubility in treated TDP-43 animals by acting through the IIS pathway to increase the cellular capacity to prevent toxic insoluble protein accumulation (Tauffenberger *et al.*, 2013). Indeed, drugs that interfere with protein aggregation protect protein homeostasis, and can influence disease pathology. Ethosuximide activation may have therefore upregulated expression of proteasomal subunits and proteasome activity (Arlt *et al.*, 2009, Kapeta *et al.*, 2010) to increase the degradation of Tau which has previously been directly implicated in protection against Aβ toxicity in cell culture models (Park *et al.*, 2009a).

Interestingly, ethosuximide has also been assessed as a potential HDAC inhibitor in cultured cells (Eyal *et al.*, 2004). Moreover, the magnitude of ethosuximide-induced protection was strictly dependent on the age of the models as ethosuximide treatments were highly effective in early prevention of behavioural impairments caused by transgenic Tau and polyQ expressions, but were not nearly as effective in older worms. Previous studies have also reported that the positive effects of ethosuximide supplementation were temperature dependent, observed at 15˚C and 20˚C, but not at 25˚C, and results varied in relation to the food substrate on which worms were fed (Collins *et al.*, 2008). More recent work has shown that UV-

exposure converts ethosuximide into a toxic compound that dramatically shortens life span. This demonstration of a strict timing requirement in addition to culture conditions for the activity suggests a complexity in the MOA of this drug.

It is noteworthy that the selected worm models of NDs may have different sensitivities to ethosuximide in rescue of pathological phenotypes. Ethosuximide dosage required for optimal functional improvement in the most recent study by Tauffenberger *et al.* (4 mg/ml) is much higher than the ED_{50} of ethosuximide presented in this study and by Evason *et al.* The externally applied concentration of 1-2 mg/ml described here equates to a measured internal concentration within the worm of 15-30 µg/ml (Evason *et al.*, 2005) which is close to the therapeutic dose range of ethosuximide for epilepsy in humans (40 to 100 µg/ml) (Goren and Onat, 2007), suggesting that neuroprotective doses could be achieved in patients. Prohibitively high doses of most exogenously applied pharmacologicals are required to induce robust phenotypes in *C. elegans* due to its extensive physical and enzymatic xenobiotic defenses, which could limit the availability of the compound to its targets as the drug is unlikely to accumulate to effective concentrations within worm tissues and therefore results in considerably reduced potency (Rand and Johnson, 1995, Evason *et al.*, 2005, Burns *et al.*, 2010). Indeed, Evason *et al*. reported a 66-fold difference of ethosuximide concentration between the external environment and uptake in *C. elegans* required for a phenotypic response. Previous study has also shown that though ethosuximide was effective in preventing NRHypo neurotoxicity, its ED_{50} of 336 mg/kg was 10-fold greater than that reported to be needed to treat pentylenetetrazol-

induced seizures and was inactive in a mouse maximal electroshock seizure (MES) seizure model (Farber *et al.*, 2002).

Evidently, considerable further work is needed to uncover the exact mechanism(s) of action of ethosuximide. We have yet to establish whether ethosuximide would maintain its potency when ND models are treated during pre- and post-symptomatic periods i.e. from L4 (adult day 0) to adult day 2 when the initial behavioural symptoms began to develop or later in life, once a significant number of aggregates have been formed. A direct link between the ameliorated locomotion and the amelioration in body-wall muscle histology i.e. preservation of body wall muscle nuclei and sarcomere integrity has been documented (Munoz-Lobato *et al.*, 2013). This therefore raises the possibility that ethosuximide might be affecting muscle development and maintenance. To rule out this possibility, myofibrillar structural changes upon ethosuximide treatment could be observed via phalloidin staining.

Ethosuximide could be influencing the toxicity of aggregation-prone proteins by other ways. For instance, mitochondrial deficits are key events in most ND (Wang *et al.*, 2012) and have also been related to pathological phenotypes in *C. elegans* models of ND. Indeed, increased mitochondrial fragmentation has been reported in Aβ and α-syn worm models (Kamp *et al.*, 2010, Fonte *et al.*, 2011). Hence modulating the mitochondrial network integrity could be a possible mechanism for the protective function. Moreover, exposure to low doses of thermal and oxidative stressors such as juglone, paraquat and plumbagin which are deleterious to worms at high concentrations have been shown to result in pro-longevity through stress hormesis mechanisms linked to the antioxidant response (Hunt *et al.*, 2011).

Future studies should therefore involve testing these compounds to determine if ethosuximide exerts protective effects and minimises toxicity in ND models by acting as a hormetic chemical.

Taken together, ethosuximide is clearly a potential candidate for repurposing as a treatment for NDs. Not only does this pre-approved drug have a great economic advantage because of its low cost and high tolerability, ethosuximide is also capable of delaying pathology in multiple worm models of NDs. Based on our observations, we anticipate more detailed examinations of the influence of ethosuximide on the progression of a broader spectrum of diseases associated with proteotoxic stress in mammalian systems. Pharmacogenetic approaches are ongoing in our study to unravel the potential multitarget mechanism that mediates neuroprotective effect of ethosuximide and to elucidate all the spectra of genes affected by ethosuximide exposure. This in turn should encourage further screening and characterisation of other neuroprotective compounds, and ultimately may assist in accelerating the clinical evaluation and development of drugs to combat protein conformational disorders in general.

CHAPTER 5: *C. ELEGANS* TRANSCRIPTOMIC RESPONSE TO ETHOSUXIMIDE

5.1 INTRODUCTION

The anticonvulsant drug ethosuximide (2-ethyl-2-methylsuccinimide) is widely prescribed for the past decade as a frontline treatment for absence seizures in children. In addition to this established therapeutic area, increasing support is being given towards its potential neuroprotective and general health-promoting properties. Indeed, as discussed in Chapter 4, the use of antiepileptic drugs (AEDs) as a possible neuroprotective strategy is receiving increasing attention due to their potential beneficial effects in reducing neuropathologies resulted from brain ischemia, Alzheimer's disease (AD), Parkinson's disease (PD), amyotrophic lateral sclerosis (ALS) and Machado-Joseph disease (MJD) in both invertebrates and vertebrates. We have further demonstrated in our analyses the general neuroprotective activity of ethosuximide since it was able to ameliorate the phenotypes of three contrasting worm neurodegenerative disease (ND) models.

However, exploitation of ethosuximide's therapeutic applications is likely to have been impeded by a lack of molecular understanding of its mode of action. Although several reports exist on its therapeutic and experimental uses, many questions regarding the pharmacological action of ethosuximide remain to be answered and have been a subject of much debate. In humans and mammals, ethosuximide is generally believed to act through the blockade of low voltage gated T-type currents in a state-dependent manner, with potential antagonistic action towards sodium or potassium channels to counteract abnormal brain excitability by either decreasing excitatory transmissions or enhancing synaptic inhibition in the cortex. Recent studies have proposed mechanisms centered around differentiation of different types

of stem cells, as ethosuximide was shown to stimulate neuronal differentiation of rat skeletal muscle-derived stem cells (Kang *et al.*, 2013) as well as promoting neurogenesis of rat GABAergic neurons from cortical stem cells (Sondossi *et al.*, 2014). Several studies including our own have demonstrated that ethosuximide action in *C. elegans* is independent of T-type calcium channels (Collins *et al.*, 2008). It was also suggested that ethosuximide elicits its beneficial effects by inhibiting chemosensory function and acts in either a *daf-16*-dependent or -independent pathway (Collins *et al.*, 2008, Tauffenberger *et al.*, 2013). DAF-16 is an evolutionarily conserved FOXO family transcriptional factor (TF) at the intersection of regulations of metabolism, ageing, innate immunity, and stress responses. Its associations with ethosuximide-mediated neuroprotection and lifespan extension, however, have been under much debate. Elucidating the mechanistic action of ethosuximide will therefore vastly increase its application range and will contribute to neuroprotection and healthy ageing.

Gene-expression microarray technology and associated bioinformatic data mining tools are well-proven approaches that are increasingly employed in neuroscience to provide a better understanding of disease pathology and development of more specific and effective drugs. By utilising vertebrate and invertebrate tissues and cultured cell lines, these techniques have helped to identify the simultaneous transcriptional regulation of thousands of targets associated with complex disease mechanisms and therapeutic effects. Indeed, via a genome wide approach, tremendous progress in understanding the mechanics of ageing, neuropsychiatric and neurodegenerative disorders (Loring *et al.*, 2001, Chan *et al.*, 2002, Colangelo *et al.*, 2002, Napolitano *et*

al., 2002, Mandel *et al.*, 2003, Bonin *et al.*, 2004, Dangond *et al.*, 2004, Grünblatt *et al.*, 2004, Miller *et al.*, 2004, Ricciarelli *et al.*, 2004, Bassilana *et al.*, 2005, Borovecki *et al.*, 2005, Strand *et al.*, 2005, Duke *et al.*, 2006, Weinreb *et al.*, 2007) as well as the pharmacological responses to chronic drug exposure (Altar *et al.*, 2008, Zhou *et al.*, 2008) *in vitro* and *in vivo* has already been achieved.

Due to the innate complexity of human nervous tissue i.e. diverse neuronal cell types in the brain, variable and low magnitude differences in gene expression, and the need to use post-mortem material, relatively few microarray studies on NDs have been conducted (Mandel *et al.*, 2003). In the past decade, microarray-based transcriptional profiling has been effectively applied to *C. elegans* to investigate changes in tissue-specific gene expression associated with larval development (Hill *et al.*, 2000, Jiang *et al.*, 2001), ageing (Lund *et al.*, 2002, Murphy *et al.*, 2003, Golden and Melov, 2004, McElwee *et al.*, 2004, Rodriguez *et al.*, 2014), dietary restriction (Palgunow *et al.*, 2012), sex differences (Jiang *et al.*, 2001), neuronal signalling (Colosimo *et al.*, 2004, Portman and Emmons, 2004, Cinar *et al.*, 2005, Fox *et al.*, 2005, Kunitomo *et al.*, 2005, Rodriguez *et al.*, 2014), organogenesis (Gaudet and Mango, 2002), dauer formation (Shaw *et al.*, 2007, Than *et al.*, 2013) and developmental defects (Reinke *et al.*, 2000). Transcriptional responses of *C. elegans* to acute environmental stressors such as heat (GuhaThakurta *et al.*, 2002), heavy metals (Jeong *et al.*, 2011, Caito *et al.*, 2012), environmental xenobiotics (Reichert and Menzel, 2005, Jones *et al.*, 2013) or toxins (Cui *et al.*, 2007, Menzel *et al.*, 2009, Kao *et al.*, 2011, Lewis *et al.*, 2013, Boehler *et al.*, 2014), pathogens (Kim, 2008) and

polyphenolic compounds (Viswanathan *et al.*, 2005, Pietsch *et al.*, 2012) have also been extensively explored.

Here, to help better understand the underlying mechanisms of the therapeutic effects of ethosuximide exposure, we conducted global gene expression analyses using the Affymetrix *C. elegans* whole genome microarray platform and compared the transcriptome of ethosuximide-treated adult-onset neuronal ceroid lipofuscinosis (ANCL) models and wild-type (WT) worms to that of unexposed controls, and used the results as a framework for follow-up experiments.

We first defined a subset of differentially expressed genes (DEGs) that were shared between all ethosuximide-treated strains. Following validation of the microarray data by quantitative real-time polymerase chain reaction (qRT-PCR) analysis, various downstream bioinformatic investigations including Gene Ontology (GO) analyses, regulatory motif discovery, publication enrichment analysis, comparative analyses with curated data sources and literature were performed which revealed a wide range of DAF-16-dependent transcriptional alterations. Enrichment analyses of the common DEGs resulted in the detection of several overrepresented functional categories, of which metabolic, longevity/ageing, chromatin remodelling and protein ubiquitination related pathways were most markedly enriched. Many DEGs also contained DAF-16 regulatory elements within their promoter regions and were known to be among the top most responsive DAF-16 TF targets. Moreover, ethosuximide induced transcriptomic alteration in all treated strains has shown consistency with ageing-related expression profiles from previous genome-wide studies. The importance of DAF-16 TF in

ethosuximide-mediated protection was further substantiated by RNA interference (RNAi) and cell culture experiments. Ethosuximide was shown to consistently induce the transcriptional activity of several mammalian FOXO target genes and conferred protection against expanded polyglutamine peptides-induced aggregation, and is likely to have differential regulatory effects under different cellular contexts.

5.2 RESULTS

5.2.1 Exposure to 1 mg/ml ethosuximide results in significant changes in gene expression

To gain further insight into the molecular basis of ethosuximide-induced protection, whole genome *C. elegans* DNA microarray was utilised to monitor and compare the global gene expression profiles of aged *dnj-14(ok237* and *tm3223)* mutant worms of ANCL and WT worms treated with or without ethosuximide (Figure 5.1). 1 mg/ml was chosen for further experiments because the worms have responded to ethosuximide in the most consistent manner at this concentration. Cultivations for RNA samples were conducted in conjunction with postdoctoral fellow Dr. Hannah McCue. We extracted and purified the total RNA from three separate biological replicates of 400 synchronised ANCL mutants and WT worms exposed to ethosuximide or left untreated until day 6 of adult stage. Spectrophotometric quantifications of isolated RNA quality and quantity are provided in Table S5.1 in the appendices. Subsequent microarray experimentation and initial diagnostic and differential expression (DE) analyses of the raw microarray data were carried out by Dr. Lucille Rainbow and Dr. Yongxiang Fang from the Department of Functional and Comparative Genomics, respectively. The correctness of the WT control strain was however in doubt since a reporter line with P_{unc-25}::GFP and *lin-15* rescuing plasmid co-injected into a temperature-sensitive *lin-15(n765)* mutant background (henceforth referred to as P_{unc-25}::GFP) was thought to have been used instead of the canonical WT strain N2. As a result, additional samples were prepared and a second run of the array experiment measuring triplicate untreated and

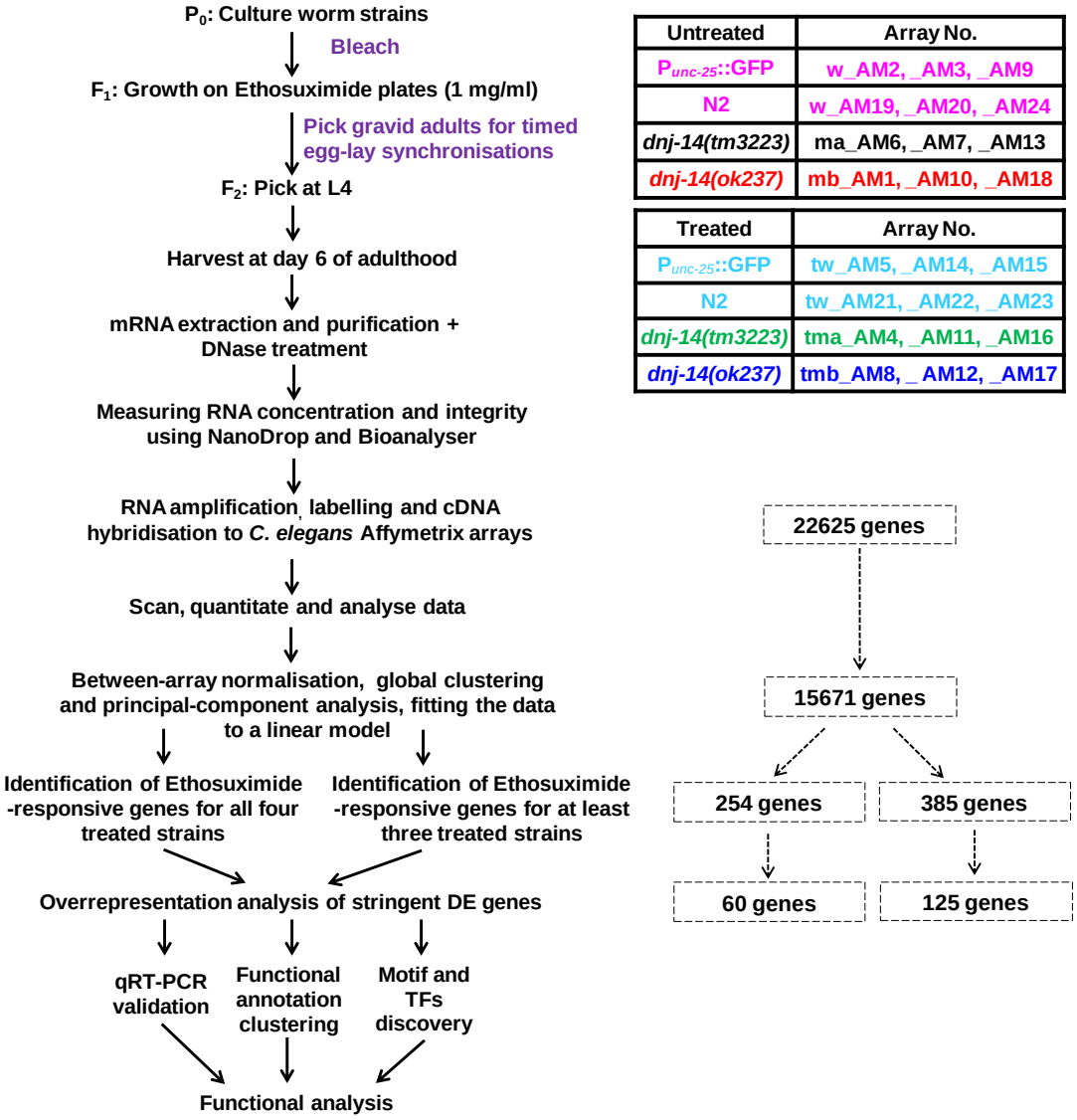

Untreated	Array No.
P_{unc-25}::GFP	w_AM2, _AM3, _AM9
N2	w_AM19, _AM20, _AM24
dnj-14(tm3223)	ma_AM6, _AM7, _AM13
dnj-14(ok237)	mb_AM1, _AM10, _AM18

Treated	Array No.
P_{unc-25}::GFP	tw_AM5, _AM14, _AM15
N2	tw_AM21, _AM22, _AM23
dnj-14(tm3223)	tma_AM4, _AM11, _AM16
dnj-14(ok237)	tmb_AM8, _ AM12, _AM17

Figure 5.1: Steps for identification of ethosuximide-responsive genes using the microarray. A schematic approach to the data analysis. With 22625 probe sets, only 3-13% of all transcripts showed medium or high levels of differential expression in response to ethosuximide as compared to the untreated. To narrow the scope of our analysis and reduce the number of false-positive DEGs among probe sets, we controlled for the FDR at the level of 0.01. Following filtering and removal of duplicate identifications, the final analysis resulted in a list of common overlapping set of transcripts with 125 and 60 stringent ethosuximide-responsive genes identified across either at least three or all four treated strains.

ethosuximide treated samples drawn from the correct WT strain was conducted and analysed. Nevertheless, gene expression profile of P_{unc-25}::GFP was included in all our downstream data analyses.

C. elegans full genome microarrays contain 22625 probes transcripts for 20149 *C. elegans* genes. Comparison of the transcriptomes of ethosuximide treated strains with those of untreated using first a relaxed criterion with a false discovery rate (FDR) of ≤ 0.05, revealed 385 common genes (genes overlapping between expression profiles) differentially expressed in treated *dnj-14(ok237)*, *dnj-14(tm3223)* and WT N2 strains relative to untreated control group. Of these 385, 134 genes were increased in expression and 251 were decreased in expression. Examination of gene lists derived for all four ethosuximide treated strains revealed 254 common DEGs consisting of 97 up-regulated and 157 down-regulated genes. Multiple uncharacterised genes were increased in expression in both *dnj-14* mutants and/or P_{unc-25}::GFP worms but decreased in expression in WT worms and vice versa, In order to narrow the scope of our analysis and reduce the number of false-positive DEGs among probe sets, we considered all genes extracted from a more stringent FDR cut-off of ≤ 0.01 (Table S5.2i in the appendices) that would increase probability of finding genes regulated by ethosuximide and focused on the intra-specific responses of all 4 strains after exposure to ethosuximide. This reduced our list to 125 triply regulated genes consisting of 61 up-regulated and 64 down-regulated genes (Figure 5.1; also, see Table S5.2ii in the appendices), and 60 DEGs containing 40 up-regulated and 20 down-regulated genes being common across all four profiles upon exposure to ethosuximide (Figure 5.1; Table S5.2iii). A small

number of overlapping genes between multiple profiles is a signature for highly specific ethosuximide responses.

A correlation heatmap (Figure 5.2A) illustrates the genomic similarities and divergences between untreated and ethosuximide treated replicate samples. In general, most of the replicates demonstrated a high reproducibility. All ethosuximide treated samples are distinctly different from their untreated counterparts (as indicated by lower correlation coefficients). Transcriptomic responses of ANCL models and P_{unc-25}::GFP worms to ethosuximide are more similar to each other than either are to the N2. Untreated P_{unc-25}::GFP and N2 samples are distinctly different, though less differences can be observed between these two samples after ethosuximide treatment. Principal components analysis (PCA) on the entire dataset showed relatively tight grouping of individual biological samples, therefore confirming that the quality of the microarray data was consistent across biological replicates for all eight conditions (Figure 5.2B). The expression profiles of untreated samples appear to be in close proximity with each other and cluster separately from ethosuximide-treated samples. Additional exploratory plots for quality assessment and differential gene expression analyses can be found in Figures S5.1 A-F. The Venn diagrams in Figures 5.2 C and D present an overview of the number of stringent DEGs that was responsive to ethosuximide and the respective concordance between the strains. The complete data including expression values, statistics, and gene annotations can be viewed in Tables S5.2 in the appendices.

Array No.	Sample Type
w_AM2, _AM3, _AM9	Untreated P_{unc-25}::GFP
w_AM19, _AM20, _AM24	Untreated N2
tw_AM5, _AM14, _AM15	Ethosuximide treated P_{unc-25}::GFP
tw_AM21, _AM22, _AM23	Ethosuximide treated N2
ma_AM6, _AM7, _AM13	Untreated *dnj-14(tm3223)*
tma_AM4, _AM11, _AM16	Ethosuximide treated *dnj-14(tm3223)*
mb_AM1, _AM10, _AM18	Untreated *dnj-14(ok237)*
tmb_AM8, _ AM12, _AM17	Ethosuximide treated *dnj-14(ok237)*

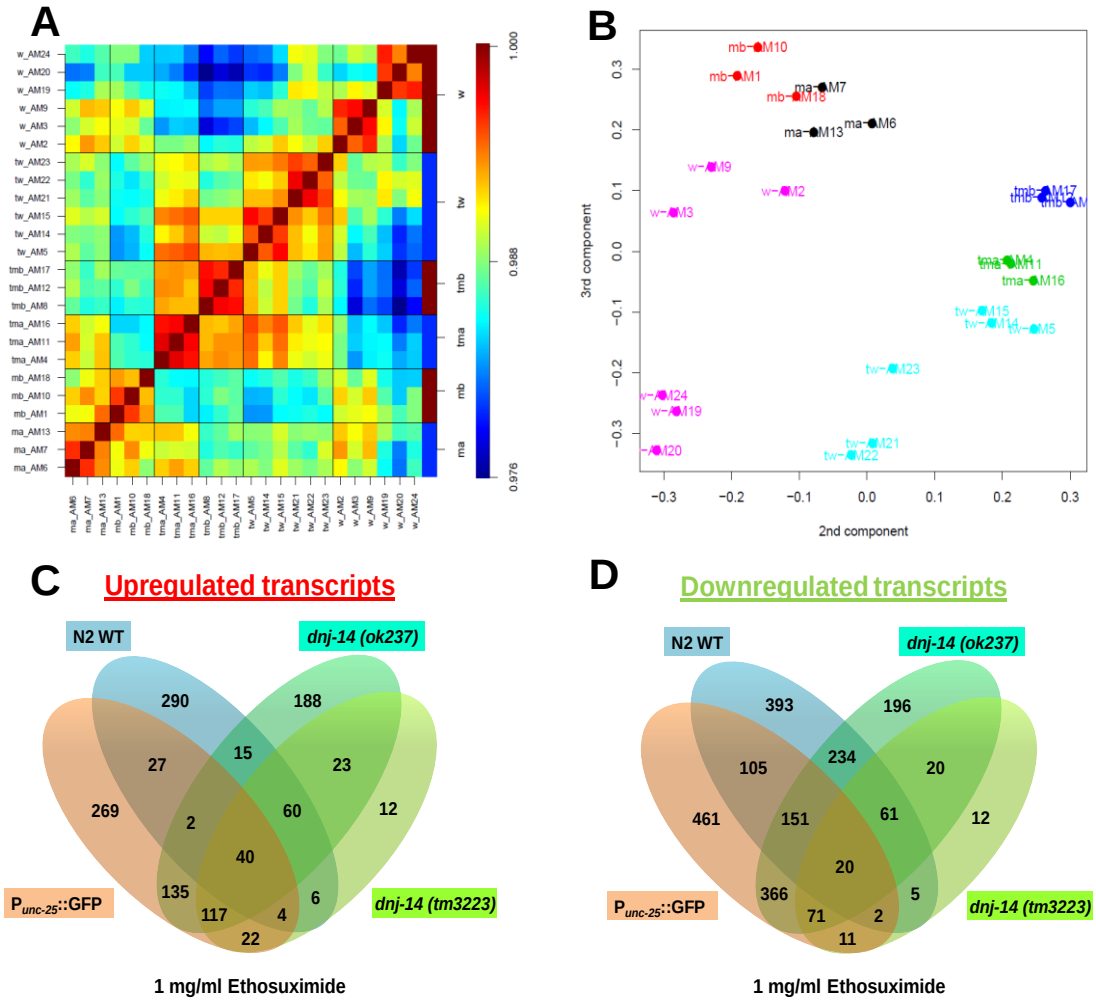

Figure 5.2: Whole-genome expression profiling of *dnj-14(ok237)* and *dnj-14(tm3223)* mutants, P_{unc-25}::GFP and WT N2 treated with ethosuximide: A) Pearson correlation coefficient-based heatmap of expression similarity and divergences among eight conditions (4 untreated and 4 ethosuximide treated) based on genes that showed significant correlations. All three replicates are shown independently for each condition. In total, there are 24 different arrays, and the array number for each biological replicate and the corresponding sample type are summarised. Samples are clustered along both axes based on their correlation value and the diagonal of the heatmap indicates the amount of the Pearson correlation between corresponding sample types. High covariance is indicated in dark red, low covariance is indicated in dark blue. Yellow and green regions indicate weak correlations/uncorrelated assets (see colour bar). B) Comparative analyses of transcription profiles in ethosuximide treated strains. The distance between respective worms denoting the similarities or dissimilarities between untreated and ethosuximide treated strains is shown using PCA plot. All three biological replicates in each condition show a high reproducibility. C-D) Venn diagrams summarising the level of overlap of significantly up (left)- or down (right)-regulated genes grown under ethosuximide relative to untreated control group. Numbers of regulated genes uniquely expressed in either one of the treated strains or commonly expressed in all profiles within each subset are listed. Intersections represent shared regulated genes. Only a small portion of DEGs are common among the four ethosuximide-treated samples. Selected criteria for inclusion in these subsets were a FDR corrected p-value less than 0.01 and no FC restrictions.

Commonly regulated DEGs that showed at least a 2-fold change (FC, up or down) were considered as significant ethosuximide-responsive genes and are listed in Table 5.1. Genes whose expression was most significantly up-regulated include an hypothetical NADH oxidase (T10B5.8), five cytochrome P450 genes (*cyp-14A3, cyp-35B1/dod-13, cyp-35C1, cyp-34A2, cyp-34A9/dod-16*), two short chain dehydrogenase (*dhs-26, dhs-2*) and six UDP-glucoronosyl transferases (*ugt-25, ugt-8, ugt-14, ugt-63, ugt-41*) belonging to Phase I and Phase II cellular metabolism. Several individual genes that were up-regulated are also worthy of note. For example, there was a 5.3-fold increase in transcript levels of *asm-3*, one of three *C. elegans* acid sphingomyelinase, homologous to mammalian ASM and is a critical and positive regulator of the DAF-2/IIS pathway. *ttr-44* of the TransThyretin-Related (TTR) family which previously exhibited significant induction in long lived *daf-2* mutants was up-regulated by 3.1-fold. The human TTR gene was also recently suggested to have a neuroprotective function in AD by inhibiting Aβ aggregation and detoxifying cell damaging conformers (Li and Buxbaum, 2011). Expression of asparagine synthase (*asns-2*) which has been predicted to function in amino acid metabolism was also up-regulated by 2.5-fold. This gene was previously up-regulated under stringent and moderate developmental-dietary restriction (Palgunow *et al.*, 2012). The most significantly down-regulated common genes contain a high proportion of uncharacterised genes and individual genes belonging to the galectin gene class (*lec-2*) that regulates diverse biological phenomena, Toll-interleukin 1 receptor domain protein (*tir-1*) that functions as an upstream regulator of a conserved mitogen-activated protein kinase (MAPK) signaling pathway in the

Ensembl ID	Gene title	Gene symbol	FC	FDR	Human orthologue
T10B5.8	hypothetical NADH oxidase	T10B5.8	8.0	9.73E-03	
C10H11.3	UDP-GlucuronosylTransferase	*ugt-25*	7.2	2.47E-03	UGT3A2, UGT3A1
ZK816.5	Short chain DeHydrogenases	*dhs-26*	6.6	1.73E-03	DHRS1
K09A11.4	CYtochrome P450 family	*cyp-14A3*	5.6	2.67E-03	CYP2J2
W03G1.7	Acid SphingoMyelinase	*asm-3*	5.3	1.01E-03	SMPD1
C23G10.6	hypothetical UDP-glucosyltransferase	*UDP-glucosyltransferase*	5.1	3.60E-03	UGT3A2, UGT3A1
H23N18.3	UDP-GlucuronosylTransferase	*ugt-8*	4.7	2.33E-03	
C30G12.2	hypothetical Alcohol dehydrogenase	*C30G12.2*	4.2	3.58E-03	
F25D1.5	hypothetical protein dehydrogenase	*dehydrogenase*	3.9	1.43E-03	CTC-490E21.13
H23N18.2	UDP-GlucuronosylTransferase	*ugt-14*	3.9	3.15E-03	UGT3A2, UGT3A1
C04F5.7	UDP-GlucuronosylTransferase	*ugt-63*	3.7	3.46E-03	
C06B3.3	CYtochrome P450 family	*cyp-35C1*	3.6	2.81E-03	ACPP
K07C6.4	CYtochrome P450 family	*cyp-35B1/dod-13*	3.2	7.76E-04	CYP2A7P1
C56A3.2	TransThyretin-Related family domain	*ttr-44*	3.1	1.52E-03	
C05C10.4	hypothetical protein intestinal acid PHOsphatase	*pho-11*	3.1	3.46E-03	ACP2
T20G5.7	Downstream Of DAF-16 (regulated by DAF-16)	*dod-6*	3.0	1.92E-03	
F10D2.11	UDP-GlucuronosylTransferase	*ugt-41*	3.0	1.39E-03	UGT3A2, UGT3A1
F55A12.4	Short chain DeHydrogenases	*dhs-2*	3.0	2.99E-03	HSD17B6
T10H4.11	CYtochrome P450 family	*cyp-34A2*	2.7	3.52E-03	CYP2A7P1
B0213.15	CYtochrome P450 family	*cyp-34A9/dod-16*	2.5	3.84E-03	
M02D8.4	ASparagiNe Synthetase	*asns-2*	2.5	2.63E-03	ASNS
F28D1.5	THaumatiN family	*thn-2*	2.3	2.30E-03	
T08B1.3	ALdehyde deHydrogenase	*alh-5*	2.2	2.45E-03	ALDH3A2
C32H11.1	hypothetical protein with a CUB domain	C32H11.1	2.2	2.18E-03	
T04A11.4	hypothetical protein	T04A11.4	2.1	2.01E-03	CTC-490E21.13
C24B9.9	Downstream Of DAF-16 (regulated by DAF-16)	*dod-3*	2.1	2.03E-03	
T09F5.12	---	---	-2.0	9.51E-04	
K05F1.10	putative secreted TIL-domain protease inhibitor	K05F1.10	-2.0	4.89E-03	
C35E7.5	hypothetical protein	C35E7.5	-2.1	5.96E-04	
T28A11.19	hypothetical protein	T28A11.19	-2.1	1.38E-03	
F22F1.1	HIstone H1 Like	*hil-3*	-2.2	5.16E-04	HIST1H1A
T28A11.16	hypothetical protein	T28A11.16	-2.3	3.60E-03	
ZC247.1	hypothetical protein	ZC247.1	-2.4	1.74E-03	
Y40B1B.3	F-box B protein	*fbxb-66*	-2.4	1.63E-03	
F13B10.1	TIR (Toll and Interleukin 1 Receptor) domain protein	*tir-1*	-2.4	3.69E-03	SARM1
F52H3.7	gaLECtin	*lec-2*	-2.5	2.65E-04	LGALSL

Table 5.1: 36 significant DEGs which are consistently responsive to ethosuximide treatment in all microarray experiments. Selected criteria for inclusion in this gene subset were a FDR corrected *p*-value less than 0.01 and a calculated mean FC in expression greater than 2 or less than -2. Each entry in the table represents a common significant ethosuximide-responsive gene which was differentially expressed by at least two-fold. Red shading indicates up-regulated genes; green shading indicates down-regulated genes.

innate immunity and F-box proteins (*fbxb-66*), which ubiquitinylate misfolded proteins to target them for degradation.

5.2.2 Validation of microarray data by real-time QPCR (qRT-PCR)

Following optimisations of the compatibility and specificity of designed qPCR primers (Figure 5.3A), the reliability of the expression level obtained from the microarray analysis was validated. 7 significant DEGs which showed the greatest fold up-regulation following ethosuximide exposure in the microarray experiments were assessed and independently verified using qRT-PCR. The directionality and amplitude of the expression FC determined by qRT-PCR for all 7 candidate genes were concordant with those obtained by microarrays (Figure 5.3B). The magnitude of the FC, however, was much higher using qRT-PCR than that suggested by microarray analysis. The great quantitative-fold differences between these 2 methods have been attributed to the use of random hexamer primers in the reverse transcriptase step (Laing *et al.*, 2012) and underestimation of expression FCs by microarray analysis (Yuen *et al.*, 2002), indicating the higher sensitivity of qRT-PCR assay as microarray studies assess thousands of genes simultaneously. Despite such exaggerated expression differences, it is important to note that there was no change in the expression of level of *pph-6* in our microarray experiments, which was included in the qRT-PCR analysis as a negative control, in addition to the two normalising genes *pmp-3* and *act-1*.

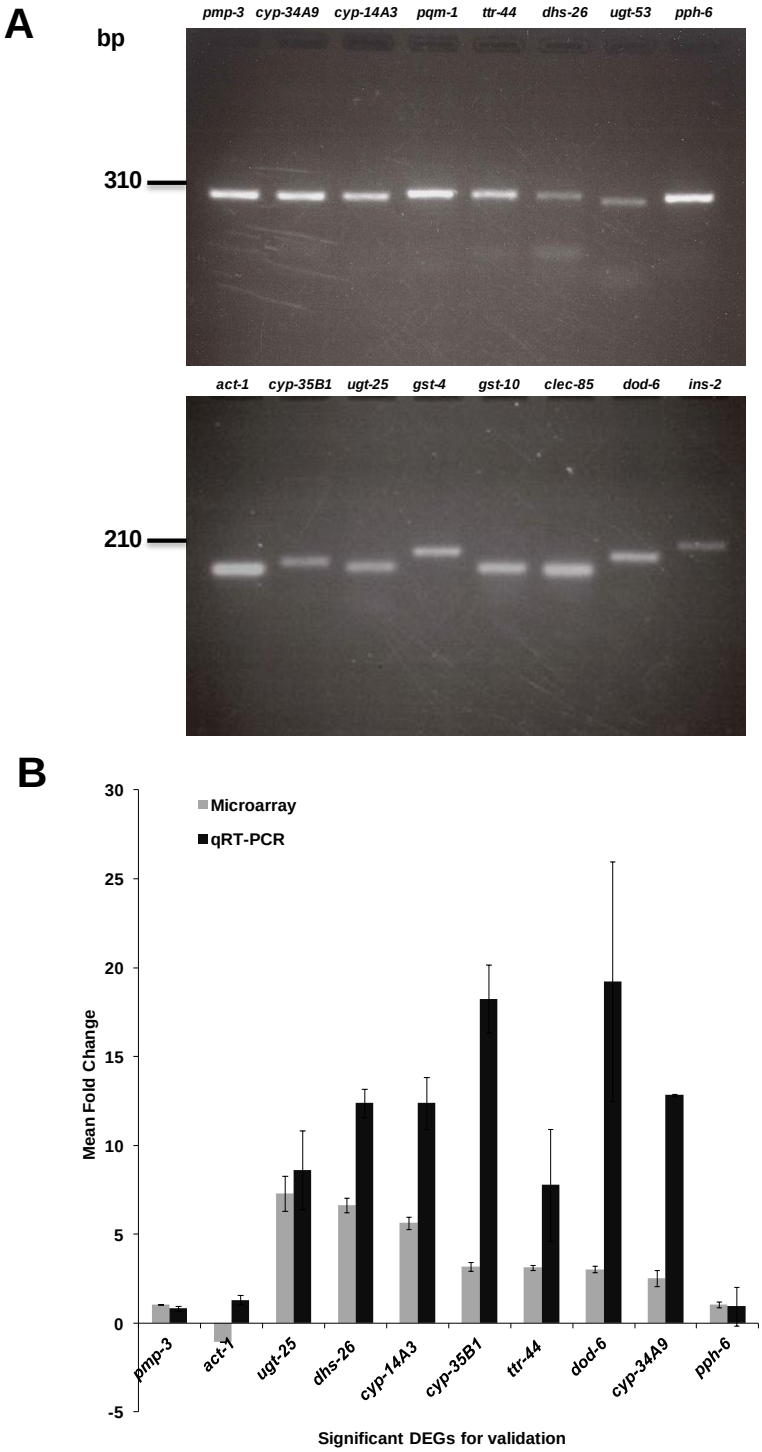

Figure 5.3: qRT-PCR confirms up-regulation of selected top ranking-genes in response to ethosuximide: A) qRT-PCR primers (Table 2.2) were designed to the following criteria: gene specific primers were all between 20 and 25 bp long; the product of the PCR was between 280-330 bp in length; the product spanned an intron to give differentially sized genomic and cDNA products; the melting temperatures of the primer pairs were matched and were between 55 and 60°C. B) Validation of gene expression pattern using qRT-PCR. All of the genes examined (*ugt-25, dhs-26, cyp-14A3, cyp-35B1, ttr-44, dod-6* and *cyp-34A9*) were proposed to be significantly up-regulated by ethosuximide in the current microarray experiment (Table 5.1) and their high level of induction was confirmed by qRT-PCR. *act-1* and *pmp-3* showed no significant changes in microarray analysis and was used as normalising genes. There was also no change in the expression level of *pph-6* in the microarray experiments which was included in the qRT-PCR analysis as a negative control. Results are expressed as mean FC relative to the unexposed control. Three biological and technical replicates were carried out and the error bars represent the standard error of mean.

5.2.3 Evaluation of transcript profiles based on annotation enrichment analyses

In all downstream analyses, we concentrated on DEGs that showed consistent response to ethosuximide and were shared by at least 3 treated strains. In this way, we assume to emphasise those cellular functions specific to ethosuximide response. Their transcriptional profiles were subjected to detailed analyses to obtain further functional insights into ethosuximide-induced gene expression responses and to identify pathways linked to its mode of actions. The principal approach applied was a functional annotation enrichment analysis of common DEG sets, to subdivide the up-and down-regulated transcripts into meaningful functional groups based on their GO identifiers (Table 5.2i). To increase the coverage of annotation, conserved protein domains and KEGG (Kyoto Encyclopedia of Genes and Genomes) pathways were also assessed. Refinement of transcriptome analysis was undertaken using the freely available DAVID software from the National Institute of Allergy and Infectious Disease (NIAID) and mENCODE Modmine bioinformatic suite which integrate resources from several gene identifier databases (Huang *et al.*, 2008) or collections of extensive experimental metadata (Smith *et al.*, 2012b), to assign annotation terms to DEGs and interpret the functional relevance of identified DEG lists to pharmacological mechanism. Both perform statistical analyses to identify significant over-representation of functional gene classifications within uploaded gene lists which is indicative of a significant impact on the biological functions associated with the GO identifiers. Fold enrichment (Table 5.2ii) was calculated in DAVID after the prevalence of particular gene categories within

the up-loaded gene list was compared to the prevalence of those categories in the *C. elegans* genome as a whole and DEGs within the list were clustered based on similar functional annotation terms.

Functional clustering of commonly regulated DEGs with a stringent FDR cut-off of less than 1% revealed a multitude of significantly enriched terms by ethosuximide exposure (Tables 5.2i and ii; Figure 5.4; Table S5.3). Many were however redundant categories represented by the same genes across and within the three GO domains (biological process, cellular component, and molecular function). Both DAVID and modMine GO analyses agreed that there was a significant enrichment for GO terms related to “lipid glycosylation”, “lipid modification”, “oxidation reduction”, “determination of adult lifespan” and “chromatin assembly”.

Common DEGs up-regulated in response to ethosuximide exposure clustered into five groups. Table 5.2i depicts the top four clusters all of which had significant enrichment scores of greater than 1.3. The most significantly enriched group (Cluster 1, enrichment score 5.45) contains eight cytochrome P450 (CYPS) genes belonging to the CYP2 families (*cyp-14A3, cyp-34A2, cyp-34A9/dod-16, cyp-35B1/dod-13, cyp-35C1, cyp-33A1, cyp-35A2, cyp-35A3*), three short chain dehydrogenase genes (*dhs-23, dhs-26, dhs-2*) and an aldehyde dehydrogenase (*alh-5*). These enriched genes (Table S5.3) share annotation terms relating to oxidoreductase activity, ion binding and multicellular organismal ageing. Cluster 2 and 3, with an enrichment score of 4.23 and 4.1 respectively, are essentially overlapping and contains the same group of 6 putative UDP-glucuronosyl/glucosyl transferases (UGTs) involved in regulation of lipid metabolism (F08A8.2, *ugt-51, ugt-8, ugt-41, ugt-14, ugt-*

25). These are also important phase II metabolism enzymes, functioning by conjugating glucuronosyl/glucosyl groups to endogenous and exogenous compounds to aid in their excretion from the organism. Enriched genes (Table S5.3) comprised of *cyp-34A9, cyp-35B1, dod-6, dod-3, ftn-1* which are amongst the most responsive downstream targets of DAF-16/FOXO, and *thn-1, spp-1* are associated with the term ageing and lifespan determination (cluster 4; enrichment score 3.13). *ftn-1*, encodes the *C. elegans* orthologue of the iron-storage protein ferritin heavy chain which is known to play an important role in iron homeostasis (Ackerman and Gems, 2012, Leibold and Anderson, 2014). As demonstrated by previous genetic and genomic studies, there is a close interconnection between the insulin/IGF (insulin-like growth factor)-like signaling (IIS) pathway-mediated lifespan extension and redox homeostasis in *C. elegans*. This is reflected in our GO analysis since ontology terms related to oxidation reduction is essentially overlapping and represents the same genes in the ageing cluster (Table S5.3).

Common DEGs down-regulated in response to ethosuximide exposure showed a significant enrichment to chromatin remodelling (Cluster 1; enrichment score 4.29) related functional categories encompassing ‘‘cellular macromolecular complex assembly, chromatin assembly or disassembly, DNA packaging, nucleosome assembly and chromatin organisation’’ (Table 5.2i, Table S5.3i). Enriched genes (Table 5.3) consist of a H2B histone (*his-8*) and H1 linker histone variants (*his-24, hil-2, hil-3, hil-7*) which are important chromatin factors with roles in heterochromatin packaging and gene regulation, a pro-apoptotic gene (*dct-1*) with similarity to the mammalian BNIP3 proteins and was previously found to be up-regulated

i

Functional clustering of up-regulated proteins

Cluster	Enrichment score
Oxidation reduction	5.45
Lipid metabolism	4.23
NAD binding and reduction	4.10
Longevity/ageing	3.13

Functional clustering of down-regulated proteins

Cluster	Enrichment score
Chromatin remodeling	4.29
Cyclin-like F-box	1.90

ii

	Gene Ontology Term	Fold enrichment for common DEGs
Biological Process	GO:0055114~oxidation reduction	8.3
	GO:0030258~lipid modification	21.2
	GO:0030259~lipid glycosylation	24.1
	GO:0008340~determination of adult life span	6.1
	GO:0006333~chromatin assembly or disassembly	41.5
	GO:0006334~nucleosome assembly	58.3
	GO:0065004~protein-DNA complex assembly	50.4
	GO:0006323~DNA packaging	44.4
	GO:0051276~chromosome organisation	15.9
	GO:0043933~macromolecular complex subunit organisation	15.4
Cellular Component	GO:0000785~chromatin	39.2
	GO:0032993~protein-DNA complex	54.5
	GO:0005694~chromosome	19.3
	GO:0043232~intracellular non-membrane-bounded organelle	4.0
Molecular Function	GO:0009055~electron carrier activity	10.5
	GO:0046906~tetrapyrrole binding	11.7
	GO:0005506~iron ion binding	7.4
	GO:0030246~carbohydrate binding	7.3
	GO:0003677~DNA binding	3.5
Protein Domain	IPR017973:cytochrome P450, C-terminal region	28.3
	IPR002213:UDP-glucuronosyl/UDP-glucosyltransferase	22.4
	IPR002347:glucose/ribitol dehydrogenase	26.7
	IPR002198:short-chain dehydrogenase/reductase SDR	20.2
	IPR016040:NAD(P)-binding domain	12.2
	IPR001810:cyclin-like F-box	5.0

iii

Publication Enrichment	*p*-Value
Genes that act downstream of DAF-16 to influence the lifespan of *Caenorhabditis elegans*.	9.96E-05
CYP35: xenobiotically induced gene expression in the nematode *Caenorhabditis elegans*.	0.00168

Table 5.2: Functional enrichment analysis of common DEGs. i) Functional clustering of DEGs that are commonly regulated after ethosuximide treatment. The reported enrichment score was calculated by DAVID according to the Fisher exact score of each clustered term. The higher the value, the more enriched the cluster. Only clusters that consisted of 4 or more genes with an enrichment score higher than 1.3 were considered as significant and included in the final list of overrepresented GO categories. Complete information can be found in Table S5.3i. ii) Shown is the fold enrichment for common DEGs in relation to the overall count in significantly enriched GO terms. iii) modMine publication analysis revealed an enrichment in DAF-16/FOXO regulated genes. Red shading stands for up-, green shading for down-regulated genes; respective pale colouring corresponds to $p \leq 0.05$, deep colours to $p \leq 0.001$. Full list of GO terms can be found in Table S5.3ii.

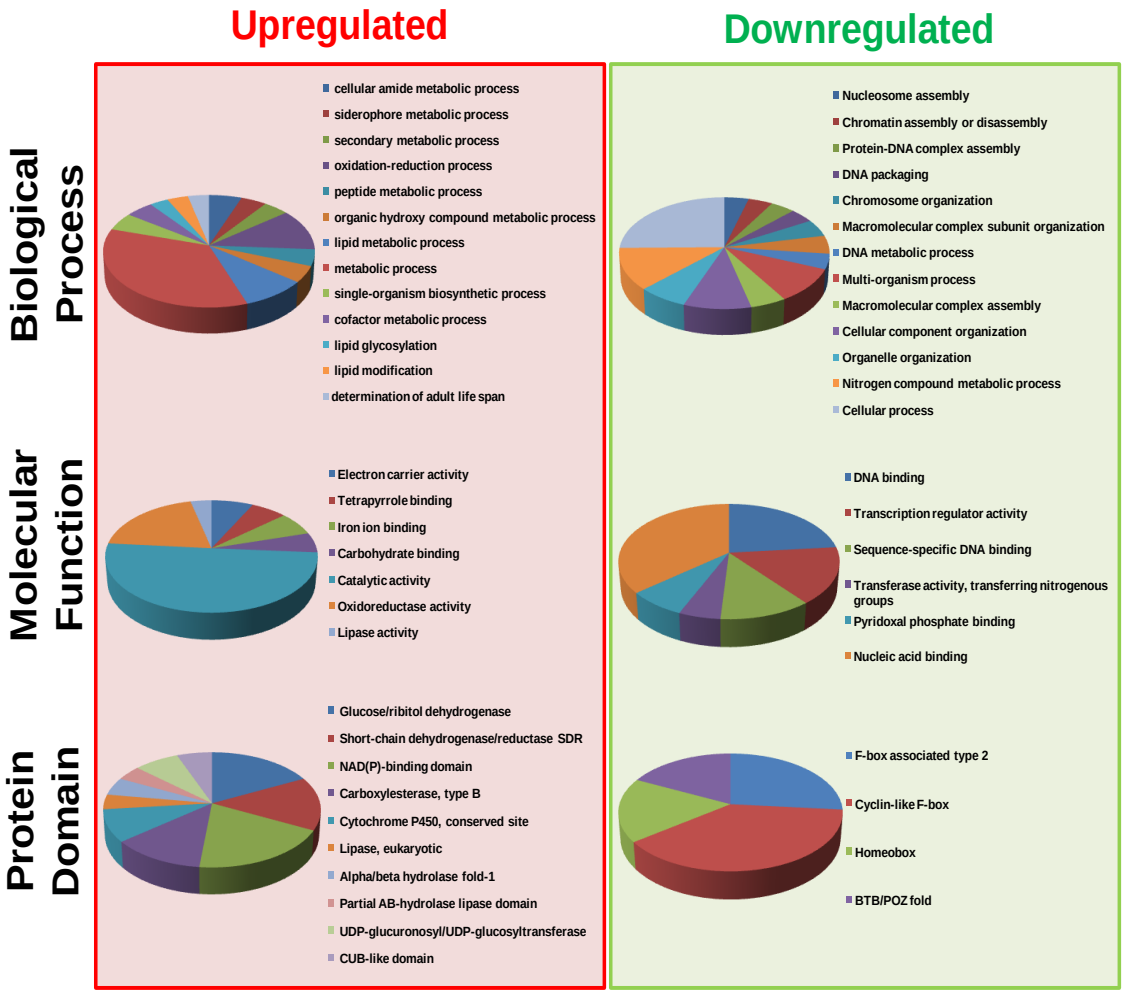

Figure 5.4: Transcriptional effects of ethosuximide in *C. elegans*. The pie charts depict the most frequent GO identifiers found within the stringent common DEGs subsets and represent the actual number of enriched DEGs associated with each of the GO-terms. Significantly enriched GO terms taken from DAVID and modMine analyses were assigned to stringent up- and down-regulated DEGs and revealed that the over-representated and overlapping functional gene classes were related to lipid metabolism, biotransformation and cellular macromolecular complex assembly in ethosuximide derived transcript profiles.

in a SKN-1-independent manner under tert-butyl hydroperoxide-(t-BOOH) induced stress (Oliveira *et al.*, 2009), and an unknown gene (Y55B1BR.3). The second most enriched cluster (enrichment score: 1.9) for down-regulated DEGs included genes associated with F-box B proteins (*fbxb-11, fbxb-41, fbxb-63* and *fbxb-66*) and 2 unknown (C33E10.1, C39B5.2) genes. F-box proteins are components of Skp1-Cullin-F-box (SCF) E3 ubiquitin ligase complex that targets proteins for ubiquitination and eventual degradation. A total of 39 enriched DEGs derived from significantly over-represented GO terms and their corresponding human orthologues are listed in Table 5.3. Detailed information for each functional cluster, including subterms and enriched genes within each group are provided in Tables S5.3.

Moreover, the domain enrichment analysis identified DEGs that were significantly enriched for CYP, UDP, SDR, and cyclin F-Box domains (Table 5.2ii) which are associated with cellular redox balance, metabolism and ubiquitin proteosome system. However, both DAVID and modMine analyses did not reveal any significant pathway enrichment. DAVID enrichment analysis of common DEGs of medium stringeny (FDR ≤ 0.05) did result in the detection of glycolysis pathway, which is involved in general energy metabolism, in up-regulated genes and Wnt signaling and TGF-β signaling pathways in down-regulated genes (data not shown).

modMine publication enrichment analysis (Table 5.2iii) further revealed an enrichment for DAF-16 target genes. These observations motivated us to consider the possibility that our microarray might reveal DAF-16/FOXO-dependent transcriptional responses to ethosuximide.

Sequence	Gene	Gene name	Human orthologue
T08B1.3	*alh-5*	ALdehyde deHydrogenase	**ALDH3A2**
C30G12.2	*C30G12.2*	C30G12.2	
K09A11.4	*cyp-14A3*	CYtochrome P450 family	**CYP2A7P1, CYP2J2**
T10H4.11	*cyp-34A2*		**CYP2A7P1**
B0213.15	*cyp-34A9/dod-16*		**CYP2A7P2**
K07C6.4	*cyp-35B1/dod-13*		**CYP2A7P3**
C06B3.3	*cyp-35C1*		**CYP2A7P4**
C12D5.7	*cyp-33A1*		**CYP2J2**
C03G6.15	*cyp-35A2*		**CYP2A7P1**
K09D9.2	*cyp-35A3*		
F55A12.4	*dhs-2*	DeHydrogenases, Short chain	**HSD17B6**
R08H2.1	*dhs-23*		**HSD17B14**
ZK816.5	*dhs-26*		**DHRS1**
F25D1.5	*F25D1.5*		
F08A8.2	*F08A8.2*	F08A8.2	**ACOX1**
C24B9.9	*dod-3*	Downstream Of DAF-16 (regulated by DAF-16)	
T20G5.7	*dod-6*		
H23N18.2	*ugt-14*	UDP-GlucuronosylTransferase	**UGT3A2, UGT3A1**
C10H11.3	*ugt-25*		
F10D2.11	*ugt-41*		
H23N18.3	*ugt-8*		
C03A7.11	*ugt-51*		
C23G10.6	*C23G10.6*		
C54F6.14	*ftn-1*	FerriTiN	**FTH1**
F28D1.3	*thn-1*	THaumatiN family	
T07C4.4	*spp-1*	SaPosin-like Protein family	
Y55B1BR.3	*Y55B1BR.3*	Y55B1BR.3	
C33E10.1	C33E10.1	C33E10.1	
C39B5.2	C39B5.2	C39B5.2	
F45C12.5	*fbxb-11*	F-box B protein	
M01D1.8	*fbxb-41*		
F55C9.13	*fbxb-63*		
Y40B1B.3	*fbxb-66*		
Y73B6BL.9	*hil-2*	HIstone H1 Like	**HIST1H1A**
F22F1.1	*hil-3*		
C01B10.5	*hil-7*		
M163.3	*his-24*	HIStone	
F45F2.12	*his-8*		**HIST1H2BL**
C14F5.1	*dct-1*	DAF-16/FOXO Controlled, germline Tumor affecting	**BNIP3**

Table 5.3: DEGs derived from highly enriched functional clusters Red shading denotes increased expression, and green shading denotes decreased expression relative to untreated group.

5.2.4 Regulatory motif analysis: Ethosuximide responsive genes are enriched in DAF-16-associated element (DAE)

To investigate further how the ethosuximide target genes might be regulated, we analysed the promoter sequences of common DEGs to identify any over-represented transcription factor binding sites (TFBS) and regulatory elements and ultimately TFs responsible for ethosuximide-induced transcriptional changes. Since it was demonstrated that highly occupied regions of TF binding are located close to the transcription start sites (TSSs) of genes (Van Nostrand and Kim, 2013) and the most effective upstream promoter region sizes in which responsiveness to certain DNA motifs is largest within a 200 bp window of TSS (Tepper *et al.*, 2013), 200 bp upstream regions for each of promoter sequences of common ethosuximide-responsive genes were mined for overrepresented motifs. Regulatory Sequence Analysis Tools (RSAT) oligo (Table S5.4) and peak-motifs analyses revealed that the most significantly enriched among any of the overlapping datasets was the motif CTTATCA (Table 5.4), which is the concensus sequence for the DAF-16-associated element (DAE). This motif was first identified as an overrepresented sequence in the promoters of DAF-16-regulated target genes in the IIS pathway (Murphy *et al.*, 2003) and was subsequently identified as a predicted erythroid-like TF family (ELT) TF binding site (Budovskaya *et al.*, 2008). RSAT peak-motif analysis which integrates a combination of tried and tested algorithms and uses systematic analysis of regulatory networks ChIP-Seq (Chromatin Immunoprecipitation coupled with Next Generation Sequencing) data to find motifs. It further compares the over-represented motifs with existing databases that contain collections of

experimentally proven binding sites for vertebrate and invertebrate TFs. As shown in Table 5.4, ~25% of ethosuximide responsive genes have at least one DAE or its variants located 200 bp upstream of the TSS. Multiple copies of these motifs were present but the consensus sites were mostly juxtaposed in the upstream promoter regions of selected candidates (Figure 5.5). While the DAE was the main motif extracted, RSAT peak-motif analysis also discovered accessory motifs that co-occurred with DAE and appear to be commonly observed core promoter sequence elements in *C. elegans*. These include a TATATAAA motif that co-occurred at more than 20% of the binding sites and matches annotation for vertebrate TF TATA-binding protein (TBP), forkhead box L1 (FOXL1), myocyte specific enhancer factor (MEF2A) and AT rich interactive domain 3A (ARID3A); and a GC-rich motif that matches annotation for various subclasses of zinc finger TFs including the Kruppel-like factor (KLF4, KLF5) and beta-beta-alpha (EGR1, SP1, and SP2), which participate in the cell cycle regulation, transformation of neuroendocrine cells, inflammation, immunity, differentiation, cell growth, tumorigenesis, and apoptosis. ~15% of DEGs commonly regulated in all four ethosuximide treated strains has a ACTACAA High Mobility Group box (HMG) motif known to be bound by SOX10. However, no clear match to any known nematode TF consensus sequences can be found for these over-represented motifs in any databases.

Since it was suggested that using a combination of different motif finding tools maximises the chance of obtaining significant motifs (Tran and Huang, 2014), I repeated the motif analysis by querying 3 other motif analysing web tools: MEME-DREME, SCOPE motif finder and

BioProspector, and observed a reassuring enrichments (Table 5.4) for the DAE motif and their variants. MEME and SCOPE detected several similar motifs with RSAT analyses that either corresponded to or resembled the GATA binding sites. BioProspector also identified the DAE motif and its variants but returned the same sequences multiple times and did not uncover any other binding motifs.

While the enrichment of the DAE could be explained by the presence of the IIS genes, DAE consensus (TGATAAG/CTTATCA) has more similarity to a GATA motif than to the forkhead consensus (TGTTTAC/GTAAACA) and it was suggested that DAE was unlikely to be bound by DAF-16 itself, but rather should be bound by a separate factor. However, DAE was recently shown to be directly bound by DAF-16 in *in vitro* gel shift assays (Zhang *et al.*, 2013b). DAF-16-binding element (DBE) has been considered as the true forkhead consensus (TGTTTAC/GTAAACA) that directly binds with DAF-16 TF and is regulated specifically by the IIS pathway. DBE, however, was not among the most over-represented motifs in any of our motif analyses.

Motif	Logo		Occurrences		Other algorithms that identified the regulatory element			Transcription factor	
	Consensus	Reverse consensus	Three treated strains	All four treated strains	MEME-DREME	BioProspector	SCOPE	Vertebrate	Nematode
DAF-16 Associated Element (DAE) CTTATCA			19%	24%	✓	✓	✓	GATA2, Gata1, TAL1::GATA1	PQM-1, NHR-28, UNC-62, GMEB-1, NHR-77, ELT-3, PHA-4, FOS-1, DAF-16, W03F9-2, BLMP-1, MDL-1, ALR-1
		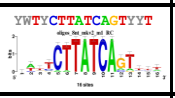	25%	25%	✓	✓	✓		
			15%	-	X	✓	X		
TATA box GTATA(T/A)(T/A)AG			22%	12%	✓	X	✓	TBP, MEF2A, ARID3A, FOXL1	?
			12%	-	X	X	X		
?	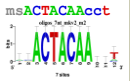		-	15%	X	X	X	SOX10	?
Sp1 like site CNCCGCCC	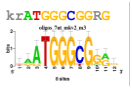	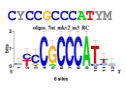	-	24%	✓	X	X	Klf4, KLF5, SP1, SP2 ZNF263, ZNF354C, EGR1	?

Table 5.4: Ethosuximide-responsive genes are enriched for a DAF-16 Associated Element (DAE) motif. To identify candidate regulatory sequence motifs for ethosuximide-responsive genes, 200 bp upstream regions for each of promoter sequences of common DEGs were mined for overrepresented motifs (see 5.2.2.4.2 in Materials and Methods) using the 'oligo-analysis' and 'peak-motifs analysis' option of RSAT web server. Repeat analyses were also performed using multiple motif analysing softwares. Table of overrepresented consensus motifs found by RSAT peak-motifs analysis containing graphic representation of motifs identified and their reverse complements, agreement with BioProspector, MEME and SCOPE, occurrences and corresponding vertebrate and nematode transcription factors.

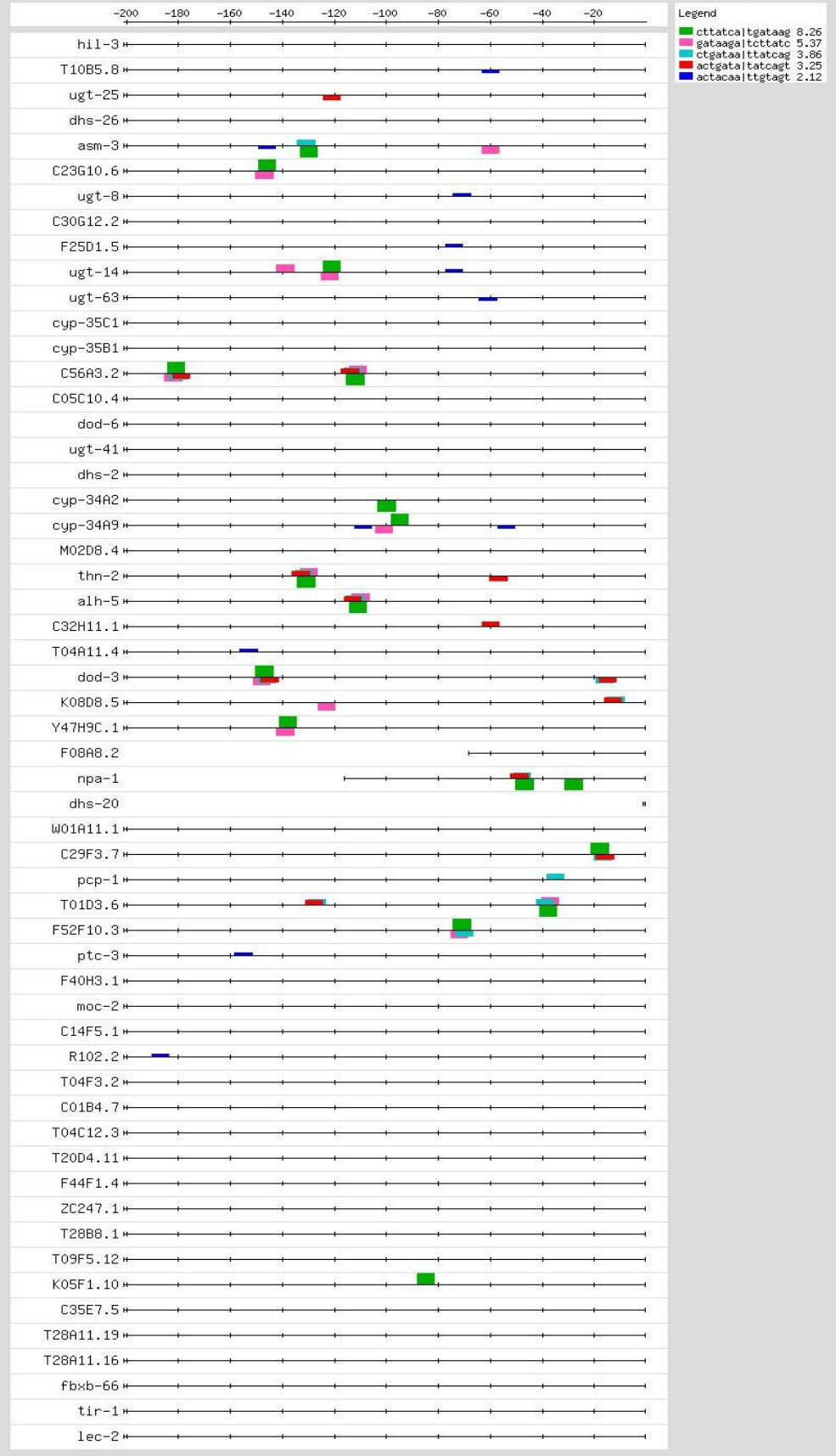

Figure 5.5: Location of putative motifs. 200 bp region upstream of selected common ethosuximide-responsive genes containing over-represented motifs. Small boxes indicate the location of the motif. Bars shown underneath the lines represent elements running in the opposite direction.

5.2.5 Comparison of transcript profiles with curated data sources and selected microarray datasets from literature

To determine if similar gene expression profiles had been observed and reported by others in the research community and to study transcriptional co-regulation of ethosuximide responsive genes, stringent subsets of commonly up or down-regulated ethosuximide-responsive genes were queried using the web based application Serial Pattern of Expression Levels Locator (SPELL Version 2.0.3, http://spell.caltech.edu:3000/). SPELL is a transcriptome data repository search engine that integrates all previously published *C. elegans* microarray data collected under a variety of experimental conditions (189 expression datasets to date) (Hibbs *et al.*, 2007) to yield not only an ordered graphical representation of significant data sets containing similar spatial and temporal expression patterns with the candidate genes, but also predict additional genes with a high degree of similarity with respect to expression profiles. The degree of expression data similarity represented by weight scores and data set classifiers are summarised in Table 5.5i and Table S5.5i

While ethosuximide-responsive DEGs exhibited most consistent concordance with an ageing/longevity expression profile (Golden *et al.*, 2008) in all queries performed, the degree of similarity with respect to expression profiles was low (1.1%-3.8%). By querying common DEGs separately rather than combined, the smaller subset of genes yielded a slightly higher expression data similarity (3.1%-8%, data not shown). Despite overlapping expression data set associations between the queried DEGs lists, no definitive commonalities are implicated within the evaluated dataset due to inconsistent and the generally vague overall nature of the data set classifiers.

i

Triply regulated				Quadruply regulated		
Rank	**Weight**	**PubMedID**	**Tag(s)**	**Weight**	**PubMedID**	**Tag(s)**
1	3.60%	18778409	Ageing	3.20%	18778409	Ageing
2	1.60%	21589891	Germline	3.00%	21931806	Chemical stimulus
3	1.60%	23352664	Lifespan	2.40%	23300685	Oxidative stress, lifespan
4	1.60%	21931806	Chemical stimulus	1.90%	20798549	Metabolism
5	1.50%	20798549	Metabolism	1.70%	22560298	Gene expression
6	1.50%	19745112	Gene expression	1.70%	20816092	Insulin-like signaling, stress
7	1.40%	15772128	Development	1.60%	19379696	Germline immortality
8	1.40%	21765926	Stress hormesis	1.60%	22083954	Innate immunity
9	1.30%	21363964	Dosage compensation	1.50%	21363964	Dosage compensation
10	1.20%	23300685	Oxidative stress, lifespan	1.10%	21723504	Lifespan, stress response

ii

Gene Array		Triply regulated		Quadruply regulated	
		Up	**Down**	**Up**	**Down**
Longevity mutants and dauers	*daf-2* pathway targets	**14%**		**8%**	
	daf-16 pathway targets	**6%**	**4%**	**5%**	**2%**
	Age-regulated genes	**3%**		**2%**	
	Shared dauer and insulin pathway targets	**1%**	**0%**	**1%**	**0%**
	Most responsive *daf-16* regulated genes	**16%**	**6%**	**14%**	**2%**
Food deprivation	Genes in response to fasting	**0%**	**11%**	**0%**	**11%**
	Starvation (dietary restriction)	**4%**		**3%**	
Stress	*skn-1* pathway targets	**0%**		**0%**	
	Hyperbaric oxygen stress (oxidative stress)	**1%**	**0%**	**1%**	**0%**
	Commonly regulated in oxidative stress and aging	**4%**	**0%**	**4%**	**0%**
	Commonly regulated in oxidative stress and *daf-16*	**8%**	**0%**	**7%**	**0%**
	Commonly regulated in stress, aging, and *daf-16*	**4%**	**0%**	**10%**	**0%**
Polyphenolic action	1 mM Resveratrol regulated genes	**1%**		**1%**	
	200 µM Quercetin regulated genes	**2%**		**1%**	
	300 µM Tannic acid regulated genes	**0%**		**0%**	
Immune response	Immune effector genes	**15%**		**4%**	
	daf-2 pathway and *Pseudomonas aeruginosa* infection	**2%**		**2%**	
Toxin	Genes in response to cadmium toxicity	**6%**	**6%**	**5%**	**4%**

iii

Enzyme	Total # in Genome	Abbr.	N2 WT	P_{unc-25}::GFP	*dnj-14(ok237)*	*dnj-14(tm3223)*
Cytochrome P450	75	cyp	8	12	17	12
UDP-glucuronosyl/glucosyl transferase	72	ugt	7	8	15	12
Glutathione peroxidase	8	gpx	0	0	0	0
Glutathione S-transferase	57	gst	1	5	5	3
Superoxide dismutase	5	sod	0	0	1	0
Thioredoxin	5	trx	1	1	1	0
Thioredoxin reductase	2	trxr	0	0	0	0
Catalase	3	ctl	0	0	0	0
Peroxiredoxin	3	prdx	0	0	0	0
Sestrin	1	sesn	0	0	0	0
Isocitrate dehydrogenase	2	idh	0	0	0	0
Glutaredoxin	5	glrx	0	0	0	0
Ferritin	2	ftn	1	1	1	1

Table 5.5: Data set associations. i) Top ten data set associations for stringent common DEGs datasets queried using the SPELL search engine. The highest-scoring (greatest weight) data set is an expression profile of ageing (Golden *et al.*, 2008). Gene expression data sets and their associated PubMed ID, tags and weight are indicated. ii) Manual comparisons of gene expression patterns of relevant gene clusters or transcriptional profiles in the literature to findings in this study. Only a small proportion of common DEGs showed an overlap with expression profiles on other various stress conditions. iii) Lack of enrichment of known detoxification enzymes in response to ethosuximide treatment. Full analyses of database and literature comparisons can be found in Tables S5.5ii and iii.

Furthermore, the mRNA levels of ethosuximide-responsive genes also co-regulated with ageing/longevity, development and metabolic process associated genes when queried over all available data sets. Top 100 hits are shown in Table S5.5i.

A search within the Comparative Toxicogenomic Database (CTD, http://ctdbase.org/) which integrates and compares data resources related to chemical-gene/protein interactions and chemical- and gene-disease associations in both vertebrates and invertebrates revealed 12 top ethosuximide interacting genes collated from previous analyses of ethosuximide-treated insect microsomes, xenopus oocyte and fly epileptic model. These included 5 cytochromes (CYP19A1, CYP2E1, CYP313A1, CYP3A, CYP6A8), 1 GST (GSTE9), 3 potassium inwardly-rectifying channel (KCNJ3, KCNJ5, KCNJ6), 1 heat shock protein HSP83, 1 calcium-binding protein REGUCALCIN and a fly specific gene GXIVSPLA2. In addition, the database also offered possible modes of action and gene-affected cellular functions in which GO terms related to transmembrane transport, more specifically, voltage-gated potassium channel activity and oxidoreductase activity were significantly enriched among genes that interacted with ethosuximide.

To investigate further if ethosuximide-responsive transcripts share an interplay of conserved genetic pathways, I compared our stringent datasets with selected gene clusters and published transcriptional profiles generated from large-scale genomic studies of longevity mutants, dauer larvae (McElwee *et al.*, 2004), worms treated with lifespan-extending polyphenols (Viswanathan *et al.*, 2005, Pietsch *et al.*, 2012) and worms exposed to

ageing (Budovskaya *et al.*, 2008), food deprivation (Van Gilst *et al.*, 2005, Palgunow *et al.*, 2012), stress (Park *et al.*, 2009b) and immunity challenging conditions (Table 5.5ii). A meta-analysis dataset (Evans *et al.*, 2008) of different *daf-2* alleles (Murphy *et al.*, 2003, McElwee *et al.*, 2004) and immune-challenged nematodes (Troemel *et al.*, 2006, Shapira and Tan, 2008) was also utilised. The analyses yielded some agreement with previously characterised *daf-16* targets and immune effectors, but the overall overlap between commonly regulated ethosuximide-responsive transcripts and transcriptional fingerprints of the conditions assessed was not pronounced.

5.2.6 Ethosuximide does not induce a stress response

Considerable evidence has shown that *C. elegans* subjected to mild degrees of stresses such as growth factor withdrawal, starvation, exogenous oxidative or thermal stress, often enhance stress resistance and increase longevity, through a process termed stress-induced hormesis. Therefore, it needs to be tested whether ethosuximide is capable of inducing stress and its protective effects are merely as a result of an initiated compensatory defensive mechanism. From the assessment of microarray data, confirmatory qRT-PCR (Figure. 5.6A) and literature comparison (Tables 5.5i-iii), it is evident that the transcriptomic response to ethosuximide exposure was inconsistent with a general stress response. Not only were general stress associated heat shock proteins and glutathione-s-transferases (*hsp-17, hsp-16.1*, *hsp-16.49, gst-5, gst-1, gst-38, sip-1, hsp-70,* s*od-4 and hsf-1*) absent or minimally induced in our microarray experiments, others such as oxidative stress-related genes (*gst-4 and gst-10*) which were differentially expressed showed

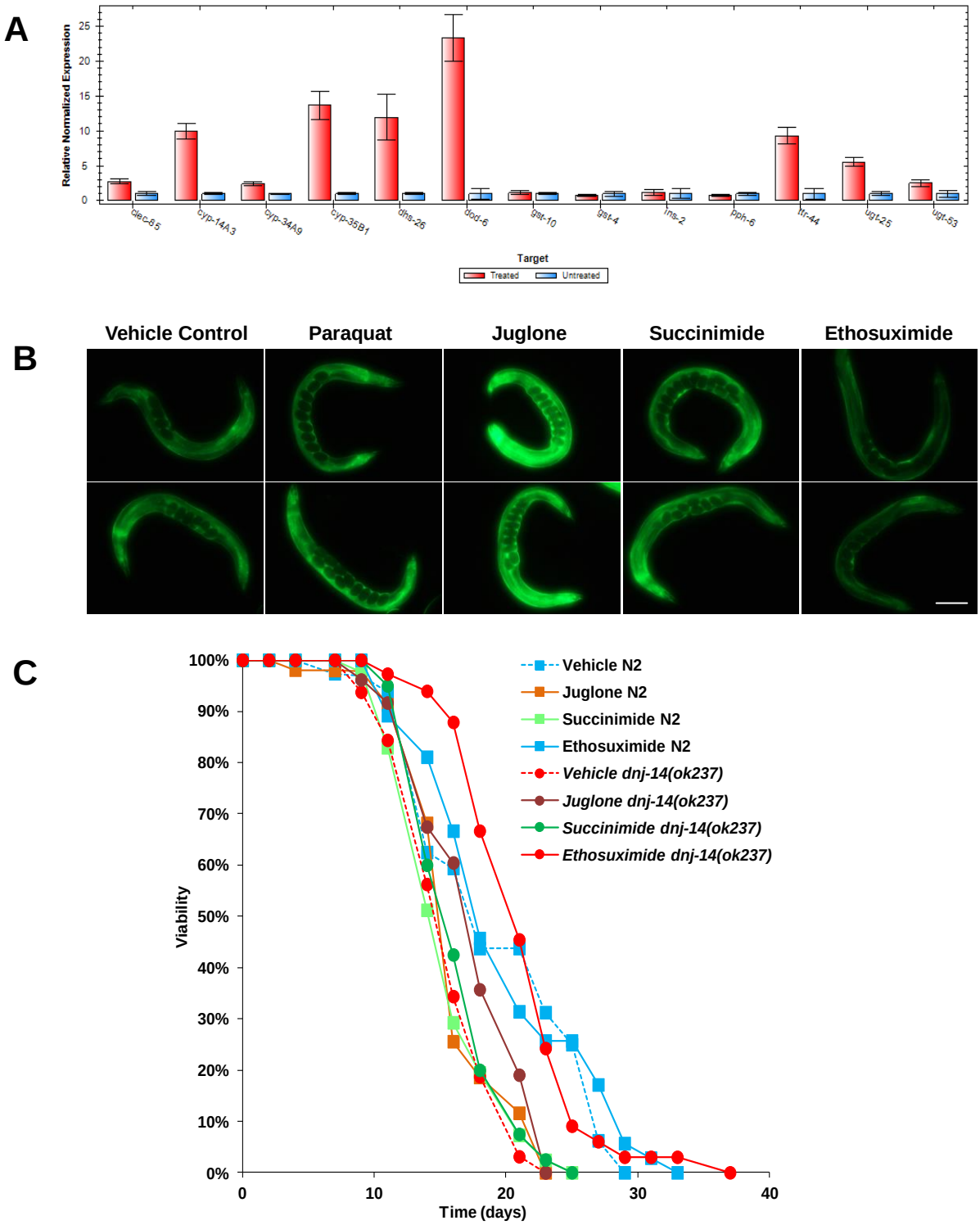

Figure 5.6: Lack of a generalised stress response and hormesis. A) *gst-4* and *gst-10* are genes that have been associated with oxidative stress responses, and they showed no evidence of induction in qRT-PCR analysis. B) Ethosuximide does not promote activation of oxidative stress-responsive gene reporter. WT N2 young adult worms carrying a P_{gst-4}::GFP stress reporter transgene were exposed to various treatments and observed for transgene expression by fluorescence microscopy as described in 5.2.1.8 of Materials and Methods. Note lack of P_{gst-4}::GFP induction following ethosuximide exposure in comparison with same worms treated with oxidative stressor juglone and paraquat (positive transgene induction controls). All images were taken at 20x magnification using fluorescence microscopy within an exposure time of 300 ms. Scale bar represents 200 µm for all panels. C) Longevity by ethosuximide is not mediate by hormesis. This experiment was done once. Numerical values and statistical analyses for the lifespan experiments presented in this figure are included in Table A2 of the appendix.

no significant change in expression (Figure 5.6A; Tables S5.2). Commonly regulated DEGs were also not significantly enriched in ROS-detoxifying activities or ROS-damage repair activities (Table 5.5iii, Table S5.5iii).

SKN-1, the sole orthologue of NF-E2-related (Nrf) TF in *C. elegans* is a major mediator of detoxification and longevity, and the transcriptional induction of SKN-1 target genes often reflects oxidative stress. The activity of SKN-1 *in vivo* can be indirectly measured by monitoring the fluorescence of a GFP reporter driven by the promoter of a well-established glutathione S-transferase (GST) gene target regulated by SKN-1, *gst-4* (P_{gst-4}::GFP). GSTs are a large class of detoxification enzymes that catalyse the conjugation of glutathione to electrophiles and play central roles in phase II detoxification (Pickett and Lu, 1989, Rushmore and Pickett, 1993). In *C. elegans*, expression of *gst-4* and Phase II detoxification genes are strongly activated by hormetic compounds, redox cycling compounds, electrophiles, and heavy metals in a SKN-1 dependent manner (Hasegawa *et al.*, 2008, Kahn *et al.*, 2008, Leung *et al.*, 2011, Leung *et al.*, 2013). We therefore utilised the transgenic worm strain CL2166 expressing the *gst-4*::GFP translational reporter as a biosensor of stress hormesis to monitor if ethosuximide activates SKN-1. In parallel, we also subjected *dnj-14(ok237)* and N2 WT control worms to 100 µM paraquat and 40 µM juglone (dosages that have previously been shown to result in hormesis-induced lifespan extension) and compared their lifespan to those treated with vehicle control, 1 mg/ml succinimide and ethosuximide. As shown in Figure 5.6B, 40 µM juglone which causes rising intracellular ROS level induced strong P_{gst-4}::GFP expression with increased magnitude of whole worm fluorescence,

particularly in hypodermis and intestine. The increase in fluorescence was also evident with 100 µM paraquat exposure, Paraquat caused embryonic lethality when worms were treated from birth, so images analysis was subsequently performed on worms that were treated with paraquat post-L4 stage. In contrast, the beneficial dose of 1 mg/ml ethosuximide was not associated with any changes in P_{gst-4}::GFP fluorescence, with weak expression in the head and body muscles comparable those treated with vehicle control. Exposure to succinimide which is similar in chemical structure but lacking anticonvulsant activity in vertebrates appeared to slightly increase the P_{gst-4}::GFP fluorescence (Figure 5.6).

Lifespan analysis (Figure 5.6C) further demonstrated that while ethosuximide considerably extended the lifespan of *dnj-14(ok237)* worms but not N2 worms, juglone at hormetic dosage resulted in only minor lifespan extension in *dnj-14(ok237)* mutant while significantly shortened the lifespan of N2 WT control. In contrast, succinimide and vehicle control did not enhance lifespan in either N2 WT or *dnj-14(ok237)* worms. Together, these data strongly suggest that the ethosuximide-mediated longevity was not the result of an over-compensatory increase in oxidative defenses in response to increased levels of ROS.

5.2.7 Role of *daf-16*-dependent IIS pathway in ethosuximide-mediated protection

5.2.7.1 Ethosuximide did not affect translocation of DAF-16

Analysis of microarray data strongly suggested that the candidate effector for ethosuximide's benefits is DAF-16/FOXO, the pro-longevity TF that plays a central role in IIS pathway. We therefore focused our attention on DAF-

16/FOXO because of its well-characterised function in *C. elegans* and previous associations with ethosuximide. Considerable evidence has shown that the downstream signalling output of DAF-2//IIS pathway can be assayed by using a GFP reporter strain (TJ356) (Henderson and Johnson, 2001). In presence of ample food and favourable conditions, DAF-16/FOXO is sequestered by 14-3-3 proteins in the cytoplasm following AKT-1/AKT-2 kinase-mediated phosphorylation and remains cytosolic and transcriptionally inactive. The DAF-16::GFP fusion protein therefore appears to be evenly distributed in the cytoplasm and nucleus of cells throughout the body of the worm. Conversely, upon various forms of environmental stressors and some mutations causing reduced signalling in the DAF-2//IIS pathway, sequestration is alleviated allowing translocation of DAF-16::GFP into the nucleus, where it engages in transcriptional regulation of DAF-16 downstream target genes (Gami and Wolkow, 2006). To explore whether ethosuximide modulates the molecular signalling cascade of DAF-2 to DAF-16 and promotes the transcriptional activities of DAF-16/FOXO and ultimately influences longevity, I compared the DAF-16::GFP patterns of ethosuximide treated worms to those subjected to stressors. Figures 5.7 A-E show representative fluorescent images of DAF-16::GFP-expressing worms following different durations of exposure to thermal stress (heat-shocking for 1.5 hour at 34°C), oxidative stress (exposure to 40 µM juglone), starvation (incubation without food), and 1 mg/ml and 4 mg/ml ethosuximide. As expected, rapid translocation of the reporter was evident after acute heat-shocking (Figure 5.7 panel A) and starvation (Figure 5.7 panel C) as DAF-16::GFP fusion protein was dramatically enriched in the nucleus of cells.

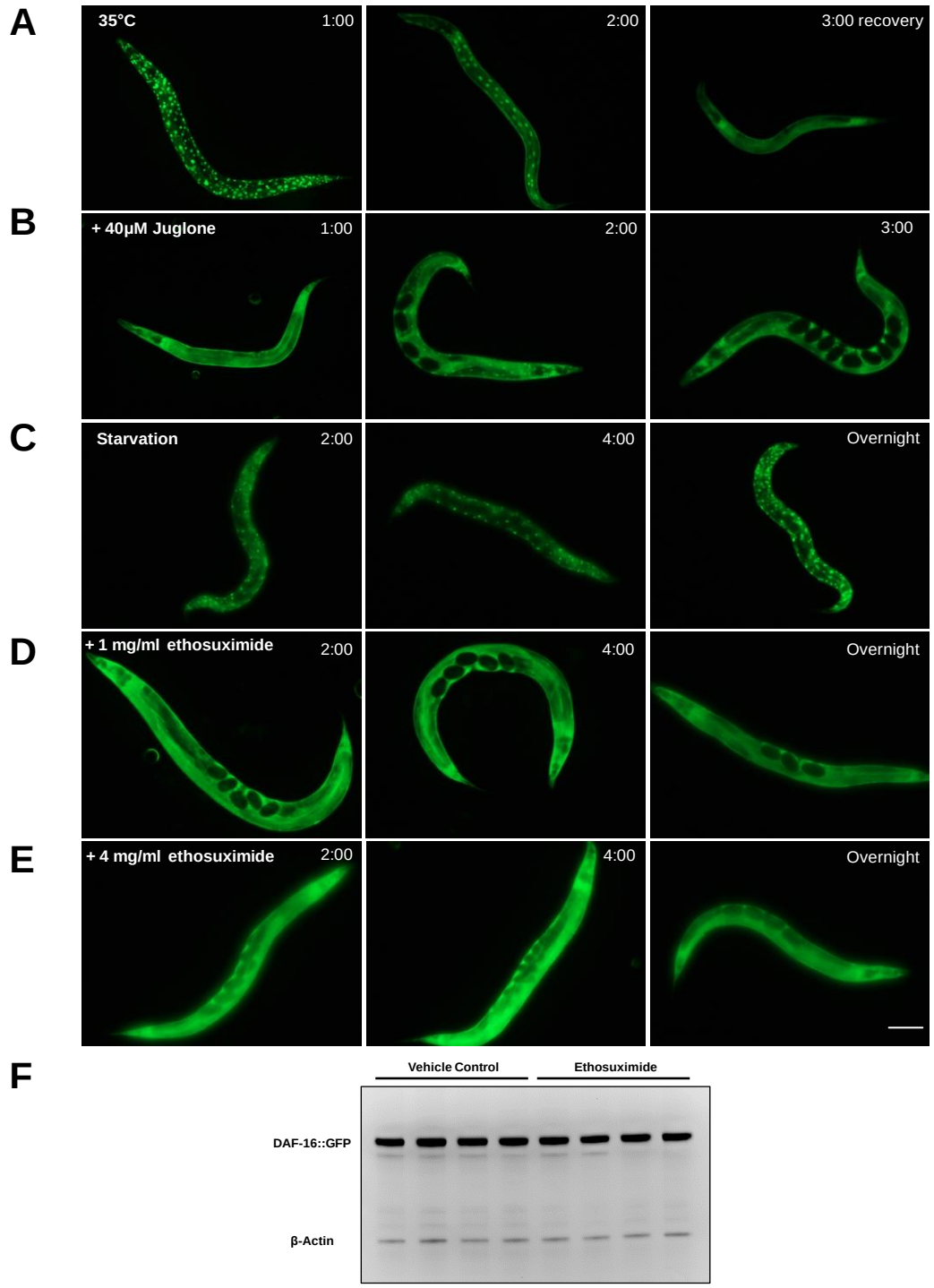

Figure 5.7: Ethosuximide does not cause obvious nuclear translocation of DAF-16. The fluorescence pattern and protein levels of DAF-16::GFP were monitored. A) Fluorescent micrographs of *daf-16* translational GFP reporter expression pattern in young TJ356 adults that were subjected to different durations of heat-stress (A), oxidative-stress (B), starvation (C) and ethosuximide (D, E) exposure. As expected, heat-shocking and overnight starvation gave rise to a dramatic nuclear accumulation of DAF-16::GFP (A, C). Upon recovery post-heat shocking, DAF-16::GFP exhibited a largely uniform cytosolic distribution pattern (A, upper right panel). Exposure of worms to 40 µM juglone (B) resulted in subtle DAF-16 nuclear localisation, but not to the same extent as that found in heat-shocked or starved worms as cytoplasmic DAF-16::GFP staining remained detectable with some punctate pattern observed in the anterior region. In contrast, no nuclear accumulation of DAF-16::GFP were observed in the presence of either 1 or 4 mg/ml ethosuximide. This effect was seen uniformly in all the animals on the plate (D, E). All images were taken at 20x magnification using fluorescence microscopy within an exposure time of 300 ms. Scale bar represents 200 µm for all panels. Time after exposure is listed as hours:minutes. n ≥ 25 worms imaged in three independent experiments. F) DAF-16::GFP protein level was also assessed following ethosuximide exposure by probing western blot with anti-GFP and anti-actin antibodies.

Upon recovery post-heat shocking, constitutively nuclear DAF-16::GFP was lost as nuclear DAF-16::GFP translocated back into the cytosol with essentially the same kinetics (Henderson and Johnson, 2001). Interestingly, the juglone treated animals showed an intermediate pattern of DAF-16::GFP, with evidence of clear enrichment in many nuclei, but not to the same extent as that found in heat-shocked and completely starved animals (Figure 5.7 panel B). In contrast, exposure to 1 mg/ml and 4 mg/ml ethosuximide did not alter the localisation pattern of DAF-16::GFP (Figure 5.7 panels D, E).

Many ethosuximide treated worms appeared to have brighter GFP florescence relative to their untreated counterparts, indicating that it is possible ethosuximide may have increased DAF-16 protein abundance. To address this, western blot analysis was performed on TJ356 worms to compare levels of DAF-16::GFP protein to see if there is an increase in total protein levels upon ethosuximide treatment (Figure 5.7F). Using an anti-GFP antibody, extracts from the DAF-16::GFP showed a high running band that corresponded to the DAF-16::GFP fusion protein which are equally highly expressed in both vehicle control and ethosuximide treated transgenic strain, thereby indicating that ethosuximide does not increase DAF-16::GFP total protein levels.

5.2.7.2 *daf-16* and *daf-2* show synthetic lethality with *dnj-14*

To test the functional significance of DAF-16/FOXO TF in ethosuximide-mediated protection, double mutants homozygous for *dnj-14(ok237)* and *daf-16(mu86)* were constructed and examined. However, in the presence of homozygous *daf-16(mu86)*, most *dnj-14(ok237)* homozygotes exhibited significantly slower growth rate and low brood size and were too sick to grow

to adulthood. This synthetically deleterious interaction was also observed with loss of function of another IIS pathway regulator *daf-2(e1370)*.

Following genetic crosses, *dnj-14(ok237)* homozygosity was confirmed by the presence of a smaller band using primers flanking the *dnj-14* deletion region combined with the absence of a band amplified with a primer internal to the deletion (Figure 5.8A). *dnj-14(ok237)* homozygotes were also identifiable by their slower growth rates and low brood size. *daf-16(mu86)* is an 11 kb genomic deletion that removes nearly all of the winged-helix domain and ~1 kb upstream of the 5′ UTR (Lin *et al.*, 2001). A predicted PCR product of 13038 bp by external primers flanking the deletion region is theoretically possible, but it does not amplify under conditions used for cycling. Thus internal primers were used to amplify a smaller WT *daf-16* product while external primers amplified an even smaller deletion-sized band (Figure 5.8A). However, genotyping of *daf-16(mu86)* allele in F3 cross progeny was inconclusive as it yielded a WT band with an internal primer (data not shown). We, therefore, did not characterise this allele further.

daf-2(e1370) homozygosity was selected for by the exhibition of constitutive dauer phenotype at 25°C and *dnj-14(ok237)* homozygosity was scored by PCR as described above. However, all of the F3 adult worms genotyped were either heterozygotes or WT and none were homozygous for the *dnj-14(ok237)* allele (Figure 5.8B).

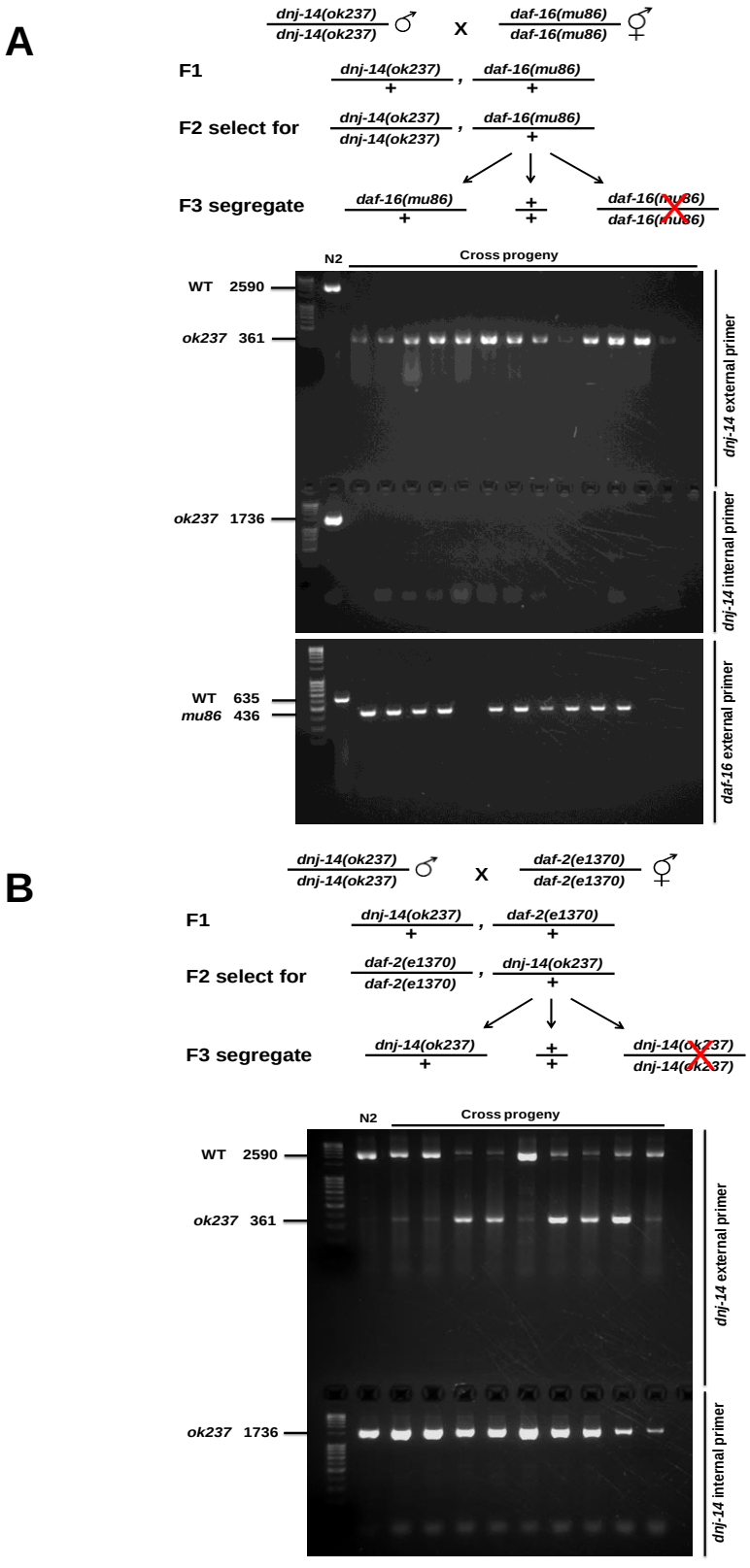

Figure 5.8: *dnj-14(ok237)* shows synthetic deleterious interactions with the IIS pathway regulator *daf-16(mu86)* and *daf-2(e1370).* Confirmation of synthetic lethality by double mutant analysis. *dnj-14*$^{-/-}$;*daf-16*$^{-/+}$ and *daf-2*$^{-/-}$;*dnj-14*$^{-/+}$ F2 lines were selected by PCR, and F3 progeny were then scored for the A) *mu86* and/or B) *ok237* allele. Homozygosity was verified in putative double mutants by two parallel reactions, one with the external primers which flank the deletion regions and another with internal primers inside the deletion regions. A) Homozygosity of *dnj-14(ok237)* was verified by the presence of a smaller sized band combined with absence of the mutant band. However, PCR from gDNA with the *daf-16* primer pair yielded a product with *daf-16(+)* but not *mu86.* B) Homozygosity of *daf-2(e1370)* was confirmed, but none of the F3 cross progeny were homozygous for the *dnj-14(ok237)* allele.

The penetrance and severity of phenotypes observed in the putative double mutants appear to be variable ranging from severe developmental delay, low brood phenotype, embryonic and early larval arrest. The overt differences in growth rates and brood size were assessed by singling individual hermaphrodite larvae from each one of the above genotypes onto single 35-mm worm plates. The animals were allowed to self for 15 days, and then the central two-thirds of each plate were imaged.

As shown in Figure 5.8C, *daf-16(mu86)* single mutants and N2 WT worms produced fast growing F1 and F2 progeny that quickly exhausted the bacterial food supply (Figure 5.8C, left panels). Plates harbouring cross progeny that were homozygous for the *dnj-14(ok237)* allele, grew slower than both *daf-16(mu86)* and N2 WT worms, and contained only F1 animals existing as mature adults that had not yet produced F2 progeny (Figure 5.8C, upper right panel). In contrast, plates containing the *dnj-14*$^{-/-}$*;daf-16*$^{-/?}$ animals grew the slowest as a thick OP50 bacterial lawn was still evident after 15 days of incubation (Figure 5.8C, bottom right panels). Putative double homozygous progeny were selectively propagated and most were too sick to develop into adults as 43% of the cross progeny plates did not result in any progeny. Further assays confirmed that *dnj-14*$^{-/-}$*;daf-16*$^{-/?}$ worms have an extremely low brood size, producing on the order of > 10-fold fewer progeny than the corresponding single mutant strains and N2 WT worms (Figure 5.8D). *dnj-14(ok237)* single mutants also showed a considerably lower brood size. These results therefore suggest that loss of *daf-16(mu86)* in *dnj-14(ok237)* mutants further reduced the ability of worms to grow and reproduce efficiently.

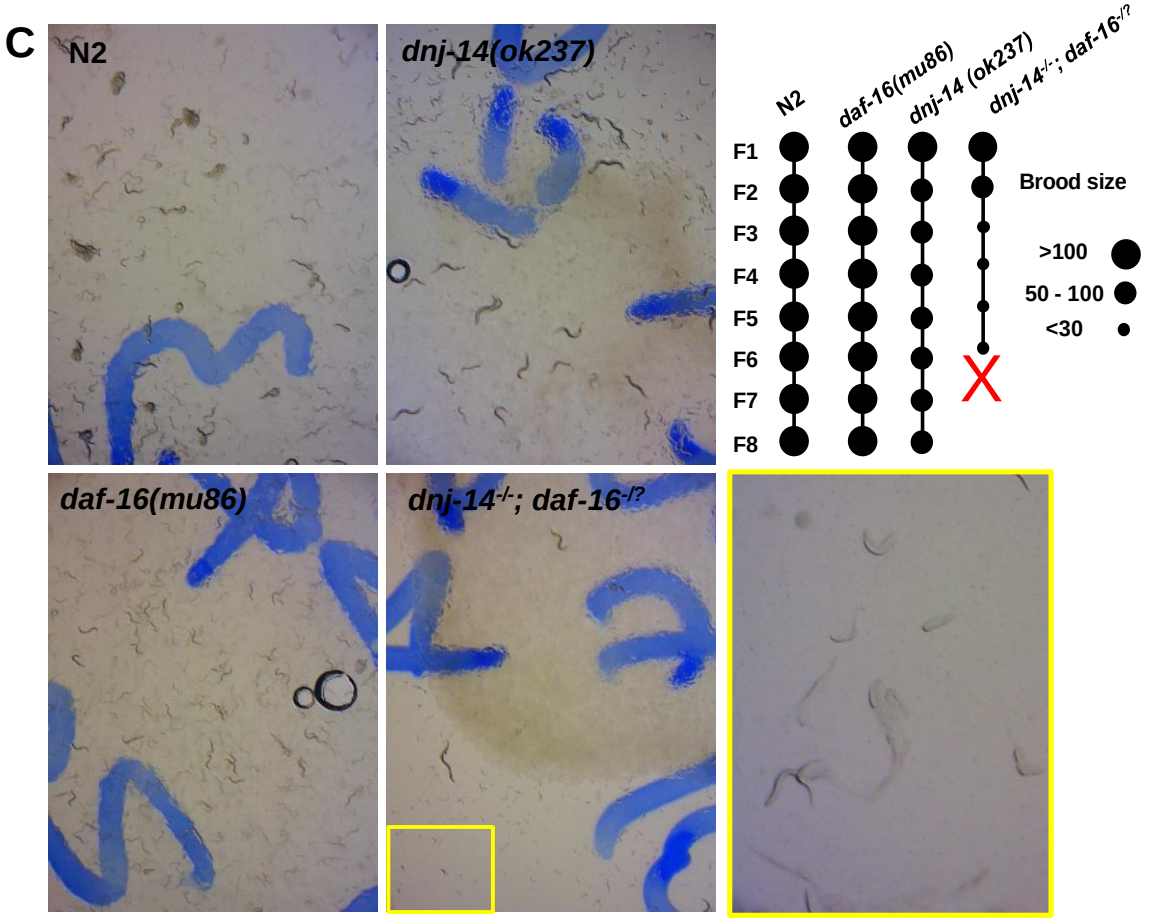

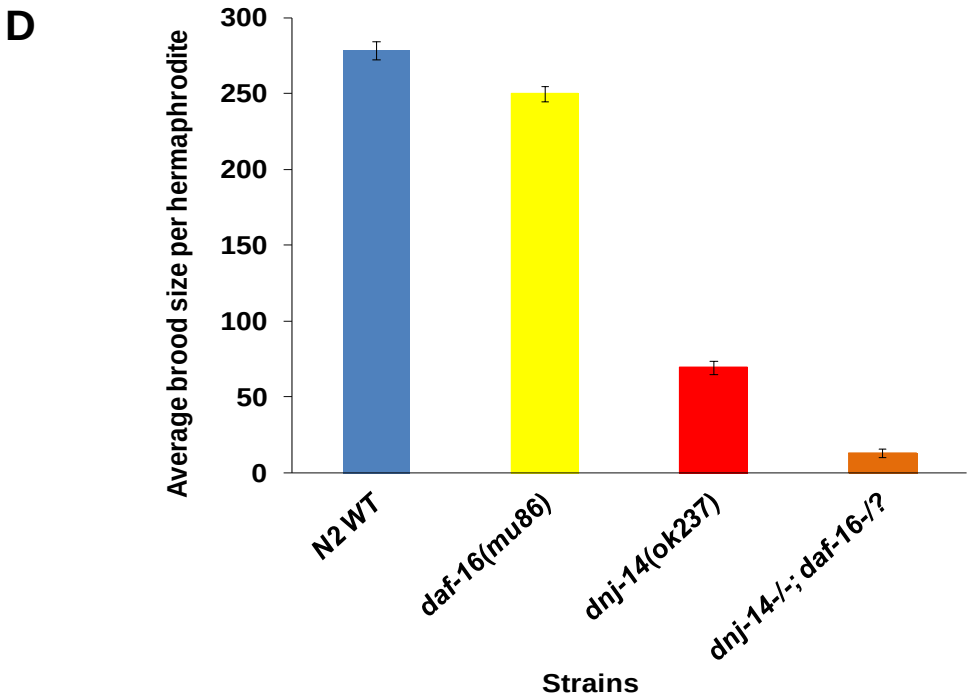

B) Macroscopic view of the population growth rate of cross-progeny relative to N2 WT worms and single mutants is shown. Single plates initiated with 1 L3-L4 larvae and grown for 15 days before imaging the central two-thirds of each plate at equivalent magnification. On the WT and single mutants' plates, the food supply was exhausted rapidly by the fast growing worms; no bacteria remained whereas the OP50 lawn remained the same on putative double mutant plate. Worm lines were propagated over 7 generations as described. C) Brood sizes were measured by single plating L4 hermaphrodites from each strain and transferring each adult to a fresh plate daily. Progeny were counted immediately after each transfer.

5.2.7.3 Ethosuximide-mediated lifespan extensions were dependent on *daf-16*

Since *daf-16(mu86);dnj-14(ok237)* and *daf-2(e1370);dnj-14(ok237)* double combinations were not viable, DAF-16 depletion was subsequently derived from RNAi mediated inactivation of the *daf-16* gene in order to evaluate the contribution of DAF-16 to the longevity conferred by ethosuximide. RNAi knock-down of DAF-16 expression and lifespan measurement were performed in both the *dnj-14(ok237)* mutant model of ANCL and N2 WT worms in the presence or absence of exogenous ethosuximide by feeding them bacteria producing DAF-16 dsRNA sequences. *C. elegans* has eight putative *daf-16* isoforms with different expression patterns (Bansal *et al.*, 2014). Our laboratory has the Vidal *C. elegans* ORF RNAi Library of bacterial RNAi feeding strains (Rual *et al.*, 2004) and a search in the database revealed the presence of multiple *daf-16* clones. Restriction analysis identified one of the clones as *daf-16* isoform a (*daf-16a*) which has been implicated in *C. elegans* lifespan regulation (Figure S5.2A in the appendices). The Vidal RNAi constructs targeting the coding sequences of *daf-16* are however not specific and will therefore knockdown all the isoforms, whereas RNAi constructs targeting the 3′UTR sequence are gene-specific. Ethosuximide treatment of *dnj-14(ok237)* worms on control RNAi bacteria caused a robust 27% extension in mean lifespan (Figures 5.9 B and D; Table A2 and Figure S5.2B in the appendices) as previously observed. No significant difference (p=0.9164) was observed when equivalent ethosuximide treatment was applied in control RNAi bacteria fed N2 WT worms (Figures 5.9 A and D; Appendix Table A2). Significant longevity

difference between *hsp-1* (Figure 5.9E) and *daf-16* (Figure 5.9F) RNAi in all backgrounds were consistently observed compare to L4440 negative control RNAi (Figure 5.9D). In particular, RNAi of *hsp-1* resulted in sick and short-lived worms in the absence of ethosuximide, but allowed for significant (p<0.0001) lifespan extension by ethosuximide in all backgrounds (Figure 5.9E) indicating that *hsp-1* is not required for the protective effect of ethosuximide. In contrast, while diminishing the function of DAF-16 in the absence of ethosuximide substantially reduced the lifespan of all strains used, non-specific *daf-16* RNAi completely abrogated the longevity effect of ethosuximide in *dnj-14(ok237*).

Furthermore, loss of *daf-16* also markedly reduced the lifespan of the sensory mutant strain *osm-3(p802)* but did not eliminate the lifespan extension by ethosuximide (Figures 5.9 C and F) as the drug was able to significantly enhance the mean lifespan of all RNAi bacteria fed *osm-3(p802)* (Appendix Table A2). This therefore is not in accordance with previous findings that *osm-3* mutants were resistant to the lifespan extension effect of ethosuximide, and that ethosuximide acts by inhibiting chemosensation in a DAF-16-independent pathway. Together, these data confirmed that DAF-16 is indeed required for the ethosuximide-mediated protection.

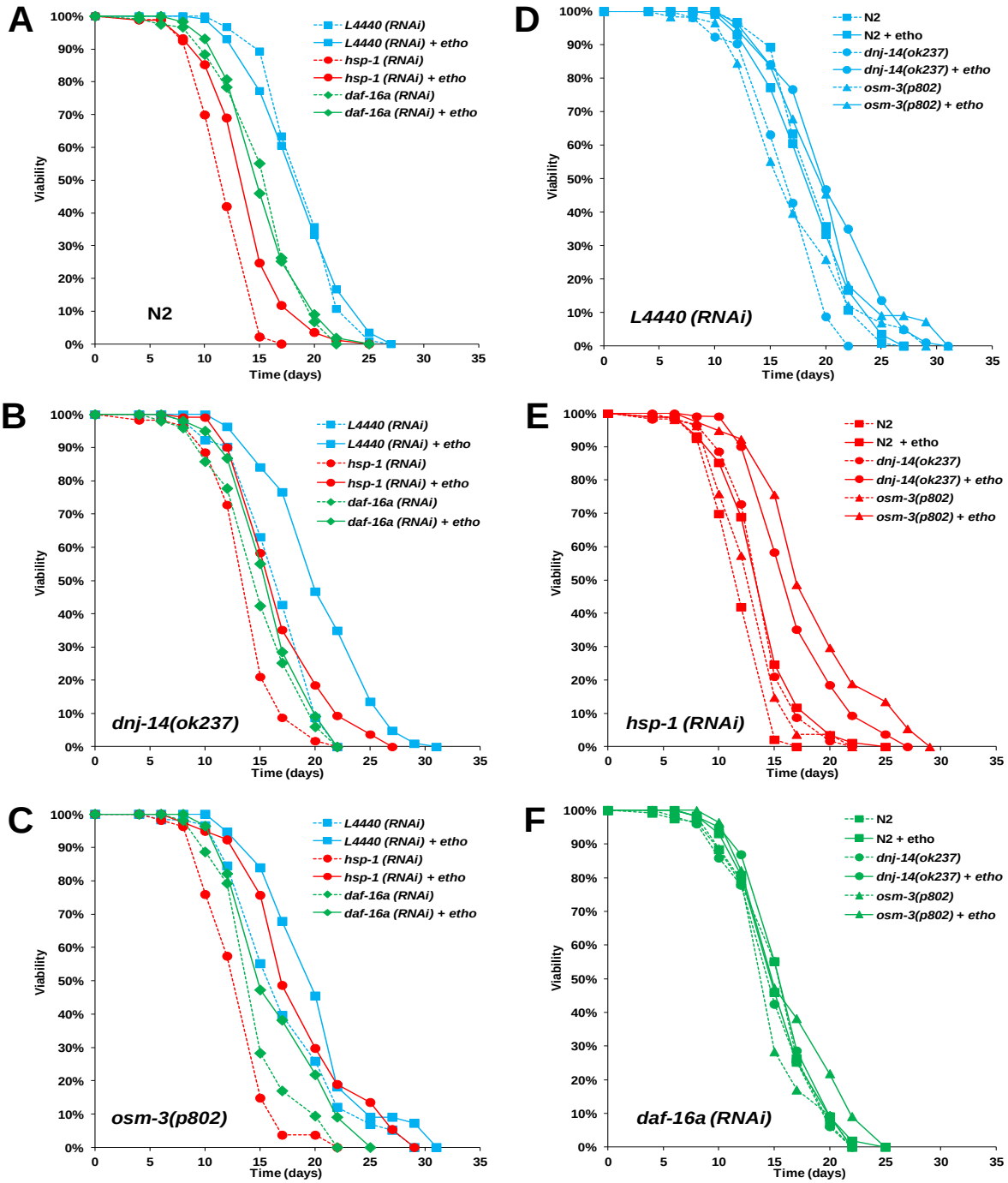

Figure 5.9: Ethosuiximide increases lifespan in a *daf-16* mediated pathway and may function independently of *hsp-1*. Survival curves of A) N2 WT, B) *dnj-14(ok237)* and C) *osm-3(p802)* worms on *E. coli* containing D) empty vector L4440 (negative control), E) *hsp-1* (positive control) or F) *daf-16* dsRNA-producing vector. All three sets of lifespans were done simultaneously on NGM + Ampicillin + IPTG plates in the presence of either vehicle control (dashed line) or 1 mg/ml ethosuximide (solid line)**.** Ethosuximide treatment significantly increased the lifespan of *dnj-14(ok237)* (p<0.0001) and *osm-3(p802)* (p<0.005) fed with empty vector control RNAi when compared with N2; L4440 (RNAi). *hsp-1* (E) and *daf-16* (F) RNAi knockdown always induced larger lifespan reduction in all genetic backgrounds assessed for. While ethosuximide significantly delayed mortality rates of all *hsp-1* RNAi fed worm strains, RNAi targeting *daf-16* completely suppressed the lifespan extension effect of ethosuximide in N2 and *dnj-14(ok237)* worms, but allowed for significant lifespan extension in *osm-3(p802)*. RNAi bacteria were obtained from the Vidal library. Lifespan analysis was performed on RNAi plates as described in Materials and Methods. Worms were grown on RNAi bacteria for 2 generations before proceeding with the experiment. A,B) Data is representative of the average of at least two independent experiments that were pooled and analysed using Online Application for the Survival Analysis of Lifespan Assays (OASIS; http://sbi.postech.ac.kr/oasis/introduction/). (C) Lifespans represent one experiment. Numerical values and statistical analyses for all lifespan experiments presented in this figure are included in Table A2 of the appendix.

5.2.8 Dose-dependent effects of ethosuximide on mammalian FOXO target genes

Given that DAF-16/FOXO is highly conserved between *C. elegans* and mammals, I further tested whether ethosuximide could affect the transcriptional activity of DAF-16 homologues FOXO1, FOXO3, and FOXO4-regulated target genes in the context of a higher eukaryotic system in order to definitively validate the activity of DAF-16/FOXO in the enduring effects of ethosuximide. FOXOs have been shown to modulate cell cycle arrest, apoptosis, autophagy, angiogenesis, differentiation, stress resistance, insulin signalling, stem cell maintenance and metabolism (Salih and Brunet, 2008). Nine mammalian FOXO target genes involved in cell cycle regulation (*Ccng2, Cdkn1a, Cdkn1b, Rbl2*), DNA repair (*Gadd45a*), apoptosis (*Bim*), stress response (*Cat, Sod2*) and insulin signalling (*Eif4ebp1*) were selected and their mRNA expression levels in a mouse neuroblastoma cell line (N2A) following ethosuximide exposure were then examined using qRT-PCR. Analysis was initially performed on undifferentiated N2A cells treated with increasing ethosuximide concentrations at different time points which resulted in either no change in gene expression or great experimental and gene expression pattern variations (data not shown). N2A cells were then differentiated following plating with retinoic acid (RA) for 24 hours before exposure to either ethosuximide or the vehicle control for 5 hours. As a result, the mRNA expression of several FOXO target genes increased following ethosuximide treatment in a dose-dependent manner. Ethosuximide therefore appears to play a more substantial role in regulating FOXO target genes in differentiated N2A cells relative to undifferentiated. As depicted in

Figure 5.10, there was a lack of significant change in gene expression at the pharmacological dose of 100 µg/ml. At 0.56 mg/ml, the optimal concentration which stimulated neuronal differentiation in muscle-derived stem cells (Kang *et al.*, 2013), and 1 mg/ml, which was the physiologically significant concentration in worm ND models, ethosuximide significantly up-regulated the mRNA expression of FOXO target genes involved in cell cycle regulation (*Ccng2, Cdkn1b, Rbl2*) and DNA damage repair (*Gadd45a*). The ability of ethosuximide to induce the transcriptional activity of FOXOs in N2A cells therefore further substantiated our *C. elegans* data, namely that the downstream signalling of the IIS pathway was triggered by ethosuximide.

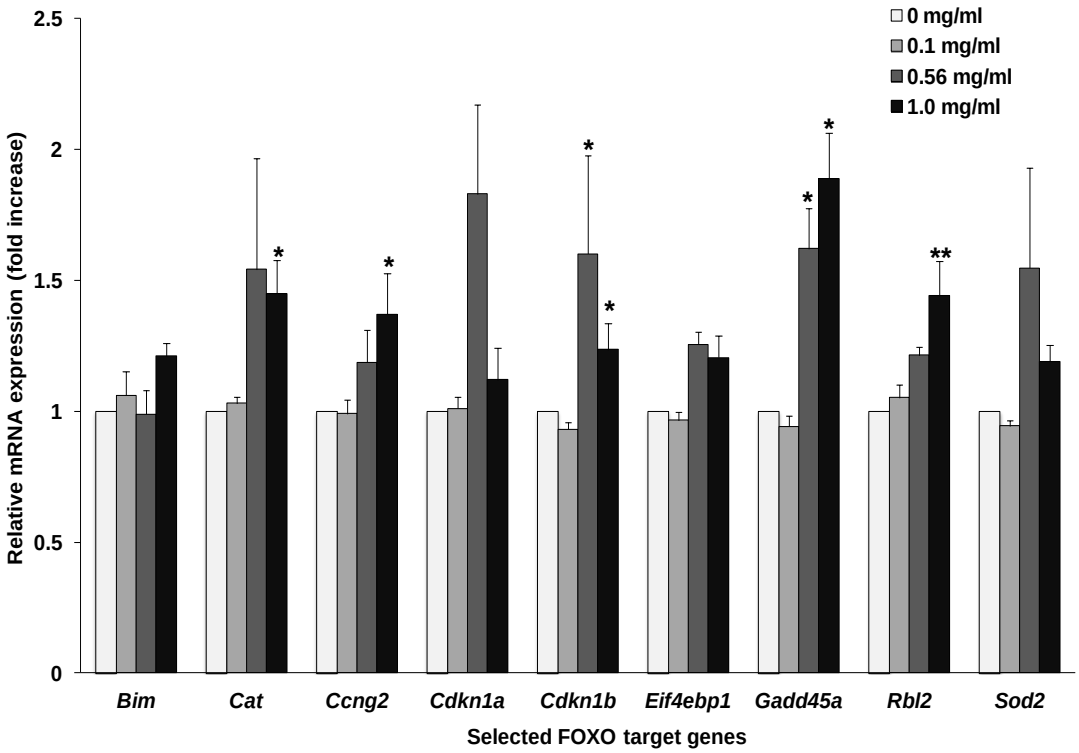

Figure 5.10: Dose-dependent effects of ethosuximide on mammalian FOXO target genes mRNA expression levels. Expression levels of several FOXO target genes, which include *p27* (*Cdkn1b)*, *p130 (Rbl2)*, *Ccng2*, and *Gadd45a* were induced in presence of ethosuximide. Mouse qPCR primers were checked for compatibility and specificity (Figure S5.3). All experiments were performed in biological and technical triplicates. Data represented are a compilation of the 3 independent experiments and are represented as mean ± SEM. * denotes a *p*-value ≤ 0.05, **denotes a *p*-value ≤ 0.01.

5.2.9 Ability of ethosuximide to suppress neuronal aggregation formation in mammalian cells

To gain further insight into the protective mechanism of ethosuximide against the pathological protein-induced toxicity within neuronal cells, we assessed the effect of ethosuximide on a previously described cell polyQ model which transiently expresses a strongly aggregating polyQ97 construct (Park *et al.*, 2013). The aggregation of polyQ in cells was visualised by the fluorescence of EGFP. N2A cells which were transiently transfected with either non-pathological polyQ25 stretches or pathological polyQ97 proteins fused to EGFP were subjected to confocal microscopy analyses at 24, 48 and 72 hours post-transfection (Figures 5.11 A and B). As expected, there was barely any aggregation of polyQ25 either in the presence or absence of ethosuximide, since transfected polyQ25 proteins were evenly distributed throughout the cytosol. In contrast, there was a marked increase in the number of cells with polyQ97 aggregates. As shown in Figure 5.11B, while the polyQ25 expressing cells looked healthy, several distributions of intracellular polyQ aggregates were observed in the cytoplasm of most polyQ97 transfected N2A cells (arrows). Some appeared in the forms of isolated and prominent aggresomes, while others were small and scattered throughout the cytosol. When aggregates appeared, many cells rounded up, which is indicative of toxicity. Moreover, because the remaining EGFP-fluorescence in the cytosol was low, the field of view were dominated by only bright aggregates. The amount of total condensed aggregates increased over incubation time up to 72 hours (Figure 5.11A). After that period, it was difficult to discriminate aggregates since most of the polyQ97-expressing cells were

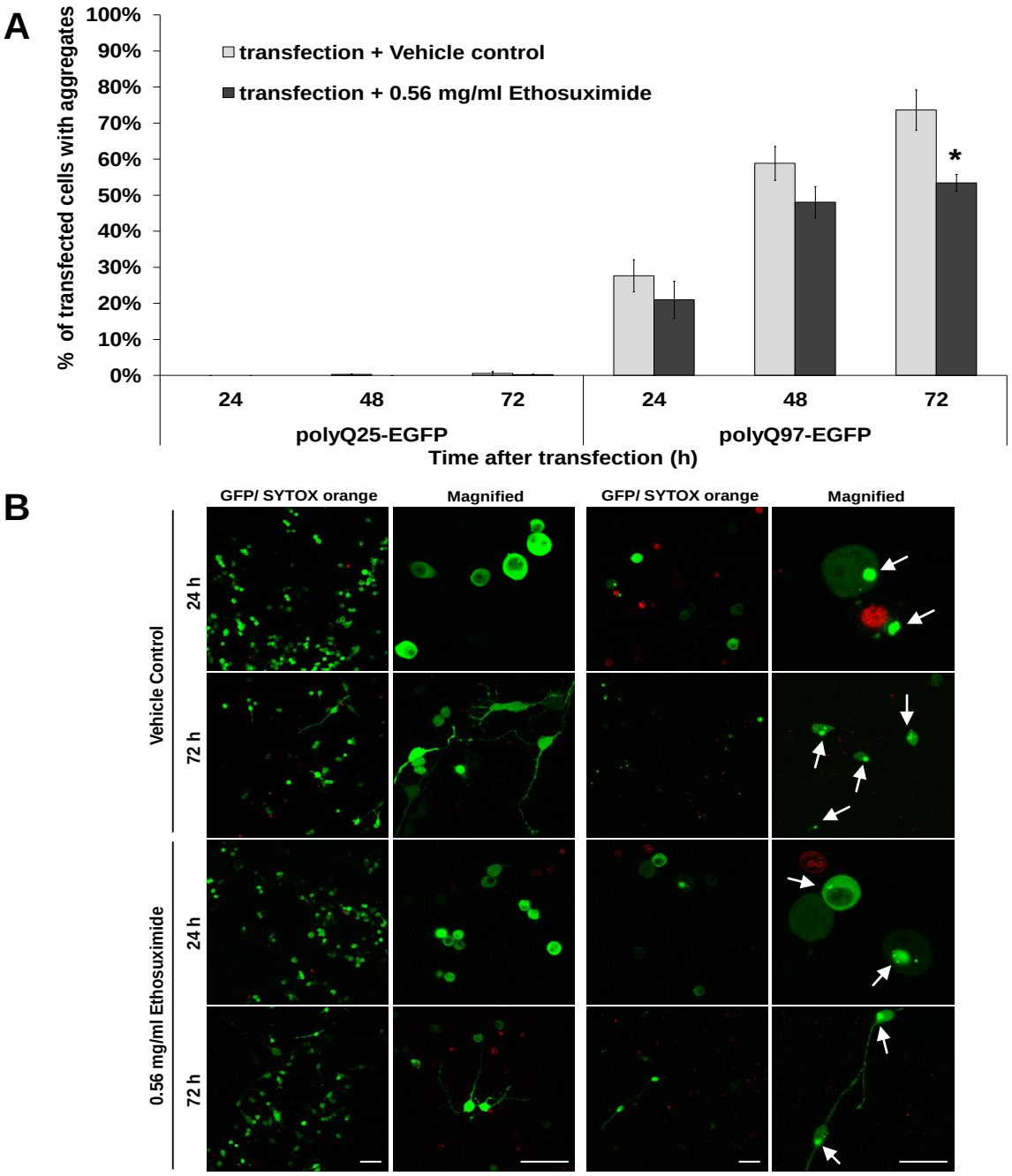

Figure 5.11: Effect of ethosuximide on intracellular aggregate formation of polyQ linked pathological stretches and cell death induction in neuro2a (N2A) cells. Expression of the non-pathological stretches (polyQ25) and pathological stretches (polyQ97) fused to EGFP in N2A cells at 24, 48 and 72 hours after transfection. Ethosuximide treatment ameliorated polyQ97 peptides-induced toxicity. A) The number of polyQ-EGFP transfected N2A cells bearing fluorescent aggregates versus total transfected green cells were quantified at indicated post-transfection times both manually and by ImageJ thresholding analysis (data are mean ± SEM of 3 independent experiments; $*p < 0.05$). Transfection efficiencies were however much lower for expanded polyQ97 peptide constructs compare to the control polyQ25 peptide. B) Overlay of EGFP (green) and SYTOX orange staining (red) confocal images which illustrated that the presence of aggregated proteins was only observed in polyQ97-expressing cells. Aggregates appeared relatively sparse in the cytoplasm at 24h, but the amount of polyQ97-EGFP aggregates increased in time. Cell death was also simultaneously monitored by staining the live cultures with the SYTOX orange dye which specifically stains dying or dead cells. However, barely any double positive cells were detected. Confocal images were produced using identical scan-settings. Scale bar: left panels of either polyQ25- or polyQ97-EGFP, 100 µm; right panels (magnified views), 5 µm. The arrows indicate condensed aggregates. Approximately 100 cells were counted from randomly selected fields in each experiment.

too shrunken. An additional complication was that the transfection efficiency was much lower for N2A cells expressing polyQ97 peptide constructs compared to those bearing control polyQ25 peptide in either absence or presence of ethosuximide. Following manual and thresholding analyses of total number of transfected cells, the presence of aggregates was confirmed by eye in each field. Individual polyQ-EGFP aggregates were counted and the percentage of polyQ-EGFP transfected N2A cells bearing fluorescent aggregates was determined. Ethosuximide treatment was able to significantly reduce the fraction of transfected cells bearing aggregates by 20% (p<0.036) as compared with the vehicle control (Figure 5.11A).

To determine whether ethosuximide could influence polyQ peptides-induced toxicity and cell death, the viability of transfected N2A cells was simultaneously monitored by staining the live cultures with SYTOX orange dye that specifically labels the nuclei of dying or dead cells with compromised membranes but not living cells. Expression of expanded polyQ peptides should result in increased numbers of SYTOX Orange-positive cells. Interestingly, the rate of cell death could not be quantified since majority of the transfected polyQ97 cells retained the viability of the cells despite abundant aggregations. Cell crenulations and cell shrinkage were occasionally observed but hardly any SYTOX Orange and GFP double-positive cells indicative of cell death were detected in Q97-EGFP transfected N2A cells. It is likely that cell death correlated with a concomitant loss of EGFP and gain of the SYTOX Orange dye, but the uptake of SYTOX Orange dye into polyQ peptide expressing cells could have been preceded by the

rapid loss of GFP fluorescence, thus a much more sensitive method of detection such as flow cytometry analysis would be needed.

5.3 DISCUSSION

Since many gaps remain in our knowledge of the molecular mechanisms underlying ethosuximide-induced protection, we sought to, in this chapter, delineate the whole picture of transcriptional changes in response to ethosuximide by using full-genome DNA microarrays. A recent study assessing the transcriptomic changes induced by various AEDs in a *Drosophila* epilepsy model (Singh *et al.*, 2011) revealed that, while DEGs showed enrichment of processes related to metabolism in flies treated with gabapentin and levetiracetam, ethosuximide treated flies lacked DEGs and enriched GO categories. Their results further suggested that AEDs' transcriptomic effect is mediated by neutralisation of up-regulated genes related to cell communication pathways i.e. inositol phosphate metabolism, phosphatidylinositol signaling, endocytosis, and hedgehog signalling, as well as the gene expression pathways encompassing spliceosome, RNA degradation, and ribosome. To the best of our knowledge, transcriptomic response of nematodes to ethosuximide exposure has not previously been described and it would therefore give us a unique starting point in understanding the beneficial effects and mode of action of ethosuximide.

Based on our annotation analyses, ethosuximide treatment positively-regulated transcripts highly enriched in processes related to lipid metabolism, redox regulation and longevity/ageing, while down-regulating transcripts strongly enriched in functions related to chromatin remodelling and UPS activity.

The concerted action of detoxification enzymes cytochrome P450 (CYP), short-chain dehydrogenase (SDR), UDP-glucuronosil/transferase

(UGT) and glutathione-S-transferase (GST) in the three successive phases of evolutionarily conserved endobiotic or xenobiotic metabolism has been well characterised in different organisms (Timchalk *et al.*, 2002, Viñuela *et al.*, 2010)**.** Their inductions in long-lived *daf-2* mutants and dauer larvae have further led to the proposal of their potential roles in longevity assurance (McElwee *et al.*, 2004). Both CYPs and SDRs including alcohol dehydrogenases catalyse oxidation, hydroxylation, and dealkylation reactions in phase I drug metabolism to modify substrates and result in chemically reactive functional groups. These groups are required for entry into Phase II metabolism, which represent the actual detoxification reactions as major effectors GSTs, UGTs, sulfotransferases, and acetyltransferases catalyse the conjugation of drugs to sulphate, glutathione, or carbohydrates to enhance solubility, which in turn greatly facilitates their clearances from the cell during Phase III metabolism (Omiecinski *et al.*, 2011).

While the transcriptomic response to ethosuximide might appear at first glance to be dominated by induction of genes required to maintain proper redox homeostasis, which point towards detoxification and stress responses, care needs to be taken when interpreting the complex transcriptional responses to drug exposure and drawing links between gene expression profiles and physiological effects (Gerhold *et al.*, 2001, Gerhold *et al.*, 2002, Laing *et al.*, 2012). It has been reported that short drug exposure provides a measure of transcriptome changes that are likely to be affected directly by the action of the drugs (i.e. primary targets), whereas prolonged exposure provides a measure of transcriptome changes caused by both direct and indirect effects. Thus it is essential to resolve genes whose

transcript levels are changed by direct ethosuximide effects from unintended gene expression induced by secondary effects (Chengalvala *et al.*, 2007, Plant *et al.*, 2009). Secondary drug targets indirectly affected through gene regulatory networks were also found to mainly function in stress response (Eckdahl *et al.*, 2008). In addition, the substrates specificity for drug-conjugating and drug transporter proteins are either poorly understand or in the case of CYPs, broad with overlapping roles in many constitutive biological processes i.e. biosynthesis of steroids, fatty acids, prostaglandins, and vitamin D in addition to drug metabolism (Danielson, 2002). Indeed, several of the induced xenobiotic enzymes in our GO annotation analysis overlapped into other functional categories and are therefore more likely to implicate them in ageing and endogenous lipid metabolism rather than xenobiotic metabolism.

Moreover, ethosuximide significantly induced the expression of CYPs, SDRs, and UGTs without any GST inductions. There were other indications of a lack of generalised stress response, ROS-detoxifying or ROS-damage repair activities upon ethosuximide treatment, since heat shock proteins (HSPs) and many of the genes implicated in the oxidative stress response, including, catalases (*ctl-2* and *ctl-1/3*), superoxide dismutase (*sod-4*), peroxiredoxin (*prdx-3*), glutaredoxin (*glrx-10*), glutathione peroxidase (*gpx-2*), and glutathione S-transferase (*gst-4*) were either absent or showed no evidence of induction in both the microarray and qRT-PCR analyses. Limited overlap was also observed in genes regulated by *skn-1* in response to toxins, pathogens or oxidative stress and those that were induced by ethosuximide. The lack of detectable induction of GST-4::GFP, DAF-16::GFP nuclear

enrichment and hormetic prolongevity activity further suggest that the protective effects of ethosuximide were not as a result of an over-compensatory increase in response to increased levels of various stresses.

Our transcriptomic results were based on the analyses of only a subset of the total genes represented on the microarray (3%), since our criteria for identifying ethosuximide-responsive genes was very focused and thus resulted in the loss of a large number of genes during stringent downstream filtering of the data. This was therefore likely to have excluded many genes that are in fact affected by ethosuximide but are uncharacterised. Low stringency criteria are expected to detect more genes associated with ethosuximide at the expense of increasing the number of false-positives to be validated by other bioinformatic and experimental means. Several individual DEGs which were significantly induced but have not been ascribed a functional annotation were also excluded from the GO-clusters. An example of this is *ttr-44* of Transthyretin-like genes (TTRs) which is a well known transport protein that binds and carries steroid hormone. Transthyretin was previously shown to be significantly induced in long lived *daf-2* mutants and/or dauer larvae (McElwee *et al.*, 2004), and has in recent years been acknowledged as a neuroprotective component in NDs, such as AD and PD (Fleming *et al.*, 2009). While increased production of TTR following activation of HSF-1 *in vitro* potently inhibited both Aβ aggregation and toxicity (Wang *et al.*, 2014), expression of human WT or Ala60-mutated TTR was also shown to protect against the amyloid beta (Aβ)-induced proteotoxicity in a worm AD model (Diomede *et al.*, 2012). Interestingly, another significant DEG that was absent in the enriched GO clusters, *asm-3*,

one of the 3 worm orthologues of mammalian acid sphingomyelinases which was previously uncovered as an ageing gene in *C.elegans* genome-wide RNAi screen (Kim and Sun, 2007) and was subsequently shown by the same group as a positive regulator of DAF-2/IIS signalling and a potential anti-ageing target (Kim and Sun, 2012), was in fact up-regulated in our study. Multiple biochemical, molecular, cellular and clinical evidence have suggested that activation of lysosomal ASM and the resultant generation of ceramide play a central role in several common disease pathologies (Smith and Schuchman, 2008). More recent work demonstrated that elevated ASM activity plays a negative role in ageing (Kim and Sun, 2012) as well as AD pathogenesis (Lee *et al.*, 2014), and proposed restoration of ASM activity to the normal range as a potential therapeutic strategy for aging and AD pathology, since pharmacological inhibition of ASM resulted in significant lifespan extension in *C. elegans* as well as increased autophagic degradation and improvement of pathological and clinical findings in validated mouse model of AD. While *asm-3* was shown to regulate *C. elegans* lifespan by modulating the *daf-2*/IIS pathway (Kim and Sun, 2012), ASM was directly linked to autophagy–lysosome pathway function (Lee *et al.*, 2014). ASM was also suggested as a key target of antidepressant drugs in the hippocampus which in turn mediates neurogenesis and neuronal networks that determine behaviour (Gulbins *et al.*, 2013). Thus our finding that ethosuximide significantly induced *asm-3* expression is difficult to interpret and will require additional study.

It is also noteworthy that a sharp decline in the expression and activity of transcriptional targets with advancing age has been reported as

transcriptome to compounds such as leonardite humic acid HuminFeed® (Menzel *et al.*, 2012) and oxidative stressor juglone (Przybysz *et al.*, 2009) were shown to be more responsive in young larvae and/or adults than old adults. DEGs that were dramatically regulated in young larvae had no significant changes in older animals due to a marked reduction in their ability to mount an adaptive response to drug treatment (Zhao and Wang, 2012). Our microarray was performed on aged day 6 worms since *dnj-14* mutant models of ANCL exhibit age-dependent phenotypes that culminate at day 6 of adulthood. This could have therefore excluded many additional ethosuximide genes that are differentially regulated and, in turn, enriched in additional processes and pathways in young adults but weren't detected in aged animals.

Furthermore, it has been shown that not all cellular processes are controlled at the level of gene expression. Some processes, such as protein synthesis and modification, occur post-transcriptionally or post-translationally. An example of this is chronically administered mood-stabilising agents lithium and valproic acid which were proposed to modulate signaling pathways through a post-transcriptional or post-translational mechanism (Plant *et al.*, 2009) .

As discussed in Chapter 4, the regulatory role of DAF-16/FOXO TF in ethosuximide-mediated protection is the subject of much active debate and research. *C. elegans* DAF-16 is homologous to the mammalian FOXO3a, one of the four members of the evolutionarily conserved FOXO TFs that function as sensors of the insulin signaling pathway and is implicated in the regulation of a wide range of physiological processes which are important to

longevity, development, stem cell maintenance, innate immunity, metabolic responses, tumour suppression, energy generation and cellular stress responses (Antebi, 2007). Much of our current understanding of the complex and multifaceted FOXO regulatory network and several of its converging signalling pathways comes from experimental and bioinformatic studies done on the *C. elegans* DAF-16. Here, we provided several lines of evidence suggesting that DAF-16/FOXO TF does indeed play a prominent role in ethosuximide's mode of action.

modMine publication enrichment analysis first revealed a significant overrepresentation of genes known to be transcriptionally regulated by DAF-16/FOXO. Comparisons of stringent ethosuximide-responsive genes with expression data from various literatures also revealed a degree of overlap with characterised DAF-16 targets. Major differences in the experimental techniques and data analysis methods employed in previous studies, such as different experimental platforms, statistical cut-offs and downstream data processing may partially explain the lack of agreement between the published results.

Next, our consensus motif analyses revealed a high representation of genes whose upstream binding regions included a motif matching the DAE in the regulation of ethosuximide. According to the previous studies, both DAE and DBE were found to be the most enriched in the promoters of DAF-16 targets. While presence of DBEs (a longevity-associated promoter element) suggests direct DAF-16 regulation in response to reduced IIS signal or DAF-16 nuclear localisation, the GATA-containing motif DAE was considered not a true forkhead consensus and lacked a definitive binding trans-factor.

Kenyon's lab, however, demonstrated that DAF-16 can directly bind the DAE both *in vitro* and *in vivo*, though with a much lower affinity compared to the canonical DBE (Zhang *et al.*, 2013b). Multiple studies using different algorithms have also noted an overrepresentation of the canonical DBE and its variants in the *C. elegans* genome (van Helden *et al.*, 1998, Bussemaker *et al.*, 2000, Furuyama *et al.*, 2000, Lee *et al.*, 2003, McElwee *et al.*, 2003, Murphy *et al.*, 2003). 78% of all *C. elegans* promoters were initially found to contain the DBE within 5 kb upstream regions despite only few of these genes were DAF-16 targets (Murphy *et al.*, 2003). Following re-assessment by Kenyon and Murphy, it was reported that 88% of 514 DAF-16 target genes contain either the DBE or the DAE in the assessed 5-kb upstream regulatory regions (Kenyon and Murphy, 2006, Murphy, 2006). Thus, this suggests that the presence of the DBE alone was not sufficient to predict DAF-16-induced expression. In our motif analysis, DBE was in fact not detected by any of the four web tools we used despite numerous of the DEGs being among the list of most responsive *daf-16* targets and subsequent manual search revealed 37-44% of the common ethosuximide-responsive genes had at least one DBE located 200 bp upstream of the promoter region. It is possible that the motif analysing softwares could not find known binding motifs common to the *C. elegans* genome, and instead detected only statistically significant *de novo* motifs. However, the detection of two conserved and commonly observed core promoter elements Sp1 and TATA which are known *cis*-regulatory elements in our upstream regions by multiple motif analysing web tools are difficult to interpret. It is possible that these *cis*-regulatory elements which direct the initiation of transcription and participate in the specificity of

enhancer function are important for other mechanisms that are still largely undefined. Indeed, despite a well characterised genome, the binding specificities of most of the putative *C. elegans* TF are not known, particularly many of the zinc finger proteins. TFBS have also been identified for only a dozen of the TFs encoding genes and transcriptional regulation is understood for only a few genes. Recent advances in ChIP-chip and high-throughput ChIP-Seq technologies (Kim *et al.*, 2013) have facilitated genome-wide identification of TFBS and have already been utilised to untangle the complex developmental (Niu *et al.*, 2011) and aging (Van Nostrand and Kim, 2013) regulatory networks. Thus future work using ChIP-Seq might permit more accurate identification of novel ethosuximide regulators.

As mentioned above, several of the ageing-related and tissue-specific *C. elegans* GATA TFs such as ELT-2, ELT-3, ELT-4 were proposed to bind the DAE and cooperate with DAF-16 to regulate longevity genes in the intestine (Maduro and Rothman, 2002, Budovskaya *et al.*, 2008, Kormish *et al.*, 2010, McGee *et al.*, 2011)**,** their relation however, have been under much debate. Using a combination of computational and experimental methods, Bussemaker's lab (Tepper *et al.*, 2013) recently demonstrated that DAF-16 directly up-regulates Class I genes through the DBE, while DAE correlates with responsiveness to both Class I and II genes. Class I genes are positive targets of DAF-16 which are consistently up-regulated and are enriched for the GO categories of oxidation, reduction, and energy metabolism, whereas Class II genes are negative targets of DAF-16 that are consistently down-regulated and are enriched for biosynthesis, growth, reproduction, and development. A novel TF PQM-1 was shown to activate Class II DAF-16

down-regulated gene expression and some of the Class I DAF-16 up-regulated gene expression via binding to DAE motifs at the posttranslational level. Moreover, in response to different upstream stimuli, PQM-1 and DAF-16/FOXO were shown to be regulated reciprocally by IIS as they mutually antagonise each other with regard to localisation in the nucleus - where nuclear translocation of PQM-1 (promoted by DAF-2) results in depletion of DAF-16 from the nucleus and vice-versa. It is possible that PQM-1 TF is not involved in the regulation of ethosuximide as our analysis indicated that the expression level of Class I genes were more commonly modulated by ethosuximide than Class II genes.

Exposure to ethosuximide however did not promote the nuclear translocation of a functional DAF-16::GFP fusion protein. In previous studies, several long-lived IIS mutants showed very weak and transient nuclear localisation of DAF-16::GFP (Henderson and Johnson, 2001, Patel *et al.*, 2008). In particular, *age-1(hx546)* mutants, which are classical IIS mutants defective in the conserved phosphatidylinositol 3-kinase (PI 3-kinase)/Akt pathway and require DAF-16 for lifespan extension, did not exhibit increased nuclear DAF-16-GFP at all under normal culture conditions (Henderson and Johnson, 2001). It is possible that the effect of ethosuximide on nuclear enrichment of DAF-16::GFP or the amount of nuclear DAF-16/FOXO required for the effects on lifespan might simply be below the detection threshold in this experiment. The cytoplasmic/nuclear retention of DAF-16/FOXO upon ethosuximide treatment also does not necessarily reflect the fate of the whole DAF-16 cellular pool and protective effects of ethosuximide could be due to stimulated *daf-16* transcriptional activity without an

accompanying significant change in DAF-16 subcellular localisation or even any nuclear localisation being required. A novel conserved pathway called the EAK (enhancer-of-*akt-1*) pathway has recently been shown to act in parallel to the Akt/PKB kinases and modulate aging by regulating the transcriptional activity of DAF-16/FOXO, without modifying its nuclear abundance (Williams *et al.*, 2010). Alternatively, the effect of ethosuximide on DAF-16::GFP nuclear localisation might be negated by a role for the zinc finger TF PQM-1 in the localisation of DAF-16 (Tepper *et al.*, 2013). Studies by Tissenbaum's group also demonstrated that the subcellular localisation of *daf-16* and the kinetics of translocation are isoform and temperature-dependent (Bansal *et al.*, 2014). *daf-16* isoforms respond differently to changes in the levels of IIS. While a small decrease in IIS was able to induce rapid and strong DAF-16a nuclear localisation, the kinetics of DAF-16d/f translocation was much slower and nuclear enrichment of DAF-16d/f occurred only after substantial decreases in IIS.

Recent analyses of IIS-dependent and IIS-independent epigenetic modifications have yielded new insights into additional layers of DAF-16 regulation in the process of ageing and longevity. Hatta and Cirillo (Hatta and Cirillo, 2007) first reported that the diverse regulatory roles of FOXO could be attributed to its dynamic chromatin-remodelling ability. Riedel *et al.* (Riedel *et al.*, 2013) and several follow-up studies provided further mechanistic insights into DAF-16/FOXO-mediated transcriptional regulation by demonstrating that upon pro-longevity stimuli, unphosphorylated DAF-16/FOXO translocates to the nucleus and binds the DAE (CTTATCA) consensus sequence to recruit a BAF-like subclass of the SWI/SNF (SWItch/sucrose non-fermentable) family

of ATP-dependent chromatin remodellers to target promoters. This in turn induces local restructuring and mobilisation of nucleosomes to create a zone of low nucleosome occupancy where the *cis*-regulatory promoter elements become exposed and therefore more accessible to binding of multiple factors that coordinately act on DAF-16 to ensure proper transcriptional outcomes. Bansal *et al.* further demonstrated using a RNAi screen that the SWI/SNF complex specifically regulates the age-dependent expression of *daf-16d/f* but not *daf-16a* and that ELT-2 and ELT-4 GATA factors promote longevity by regulating intestinal *daf-16* expression (Bansal *et al.*, 2014). In line with these evidence, our microarray data have shown a marked decline in the expression of several H1 linker histone subunits which are essential stabilisers of nucleosomes and assist the chromatin condensation into higher order structure. Ethosuximide-induced changes in nucleosome composition and arrangement through changing the expression of histone gene cluster in this study were likely to have loosened the normally compact chromatin structure to create a permissive environment for transcription and expression of DAF-16/FOXO targets.

Over the past years, apart from ongoing research in elucidating the direct and indirect transcriptional targets of DAF-16/FOXO as well as functional and molecular interactions between its co-regulators (Murphy *et al.*, 2003, McElwee *et al.*, 2004), the therapeutic potential of IIS reduction, IIS-regulated TF including DAF-16/FOXO and its interactors in NDs has also been extensively explored (Cohen and Dillin, 2008, Moll *et al.*, 2014). Indeed, numerous studies, including our own repeatedly demonstrated that genetic or pharmacological modulations of various components of the IIS cascade and

other converging signalling pathways effectively countered proteotoxicity of neurodegeneration-linked aggregative proteins in multiple well-characterised worm ND models. IIS reduction by *daf-2* RNAi conferred protection against not only Aβ aggregation and Aβ-associated paralysis (Cohen *et al.*, 2006, Florez-McClure *et al.*, 2007, McColl *et al.*, 2010), but also ALS-linked mutated TDP-43 (Zhang *et al.*, 2011) and SOD-1-induced aggregations and the resulting locomotion impairments (Boccitto *et al.*, 2012). IIS reduction by *age-1* RNAi alleviated HD-associated polyQ stretches (polyQ82-YFP) aggregation in worm embryos and protected adult nematodes from polyQ aggregation-associated motility impairment (Morley *et al.*, 2002). Similarly, reducing IIS activity via *daf-2* or *age-1* depletions lessened the toxicity associated with the aggregation of MJD-linked polyQ-containing protein ATXN-3 (Teixeira-Castro *et al.*, 2011). Most of the compounds that were recently shown to alleviate proteotoxicity with counter-neurodegeneration potential are derived from natural products including blueberries (Wilson *et al.*, 2006), herbs (Wu *et al.*, 2002), green tea (Brown *et al.*, 2006, Abbas and Wink, 2009), royal jelly (Honda *et al.*, 2011) and cocoa (Martorell *et al.*, 2013). Indeed, blueberry polyphenols, caffeine (Sutphin *et al.*, 2012), EGCG, myricetin, quercetin, kaempferol, aspalathin, naringenin, fisetin, apigenin and trehalose (Koch *et al.*, 2014) were shown to enhance lifespan and protect *C. elegans* from Aβ- and/or polyQ-associated proteotoxicity by modulating the components of the IIS cascade. Parallel to our study, compounds with pre-approved indications such as the amyloid binding dye, thioflavin T (Alavez *et al.*, 2011), and anti-inflammatory drugs celecoxib (Ching *et al.*, 2011) and aspirin (Ayyadevara *et al.*, 2013, Wan *et al.*, 2013), were proposed as

potential candidates for repurposing as treatments for age-related diseases due to their ability to slow ageing, increase lifespan and protect nematodes from Aβ-and/or polyQ-mediated toxicity. Here, we demonstrated that the protective effects of ethosuximide are highly dependent on the DAF-16/FOXO TF by using both *C. elegans* and a mouse neuroblastoma cell line. Similarly, previous studies also utilised several complementary experimental platforms to corroborate that the identified compounds such as psammaplysene A and NT219 modulate proteostasis via a DAF-16/FOXO-dependent IIS pathway (Mojsilovic-Petrovic *et al.*, 2009, Calamini *et al.*, 2011, El-Ami *et al.*, 2014), while novel compounds such as choline analogs JWB1-84-1 and JAY2-22-33 protected against Aβ toxicity through a multitarget mechanism involving both DAF-16-independent but HSF-1-dependent IIS pathway as well nicotinic acetylcholine receptors (Keowkase *et al.*, 2010a).

As discussed in Chapter 4, several lines of evidence support the idea that genetic and pharmacological perturbations of chemosensory perception influence both the insulin/IGF-1-dependent and -independent components to regulate lifespan. Mutations that impair sensory neuronal structure and/ or their function, laser-ablation of ASI chemosensory neurons, or defects in neurosecretion were shown to confer longevity by activating DAF-16/FOXO. Anticonvulsants were also shown to promote longevity of invertebrate model animals as ethosuximide and trimethadione extended lifespan in *C. elegans* while lamotrigine lengthened lifespan in *Drosophila*. Inability of ethosuximide to further extend the lifespan of long-lived chemosensory mutants led to the proposal that the pro-longevity effects of ethosuximide are due to inhibition of

chemosensory neuron function, which prevents worms from sensing food, resulting in a perceived state of dietary restriction and hence lifespan increase (Collins *et al.*, 2008).

However, in this chapter, the reported chemosensory inhibition-induced longevity was not evident since *osm-3* mutants had a shorter lifespan than N2 WT. In contrast to earlier work which demonstrated that the *osm-3* mutation resulted in a small but significant increase in *daf-16* mutant lifespan (Apfeld and Kenyon, 1999, Lans and Jansen, 2007), depletion of DAF-16 here significantly decreased *osm-3* mutant lifespan. In addition, ethosuximide treatment was able to increase the mean lifespan of both *osm-3* and *osm-3* depleted of *daf-16* but failed to augment lifespan in both *daf-16* RNAi fed N2 and *dnj-14(ok237)* worms. The lifespan prolongation by ethosuximide was shown to be dependent on DAF-16 as depletion of *daf-16* completely blocked the lifespan-extending effects of the ethosuximide. In contrast, *osm-3* mutants did not show resistance to ethosuximide as previously observed, but instead lifespan extension was maintained in both *osm-3* mutants and *osm-3* mutants depleted of DAF-16. This therefore is consistent with the results presented in this work, further arguing against the mechanism that ethosuximide extend lifespan by inhibiting the function of specific chemosensory neurons. In addition, preliminary qRT-PCR analysis also found that some of the top ethosuximide-responsive genes from the microarray analysis were also induced in ethosuximide treated *osm-3* relative to those with vehicle control (data not shown).

Whilst the role of *C. elegans* DAF-16 in longevity and protein homeostasis appear to be well-characterised, to date, relatively little is known

about the therapeutic potential of FOXO network in protein quality control, protein aggregation and neurodegeneration. Whether activation or inhibition of FOXO transcriptional activity attenuate or aggravate ND pathogenesis remains a subject of debate, and the differences between FOXOs' beneficial and harmful effects have been attributed to cell-type and context dependent activation and specific posttranslational modifications (Birkenkamp and Coffer, 2003). It is possible that the beneficial net outcome might require the same FOXO activity to be modulated in opposing fashions (Cohen and Dillin, 2008)

Analogous to its roles in regulating DAF-16 target genes and modulating aggregation formation in *C. elegans*, ethosuximide was shown in this chapter to induce the transcriptional activity of a subset of mammalian FOXO target genes and conferred protection against polyQ aggregation in neuronal cells, highlighting the conservation of DAF-16/FOXO-regulated ethosuximide response pathways in mammals. DAF-16 homologue FOXO3a is highly expressed in adult brain, and recent work suggested that it could have key regulatory roles in neuronal survival under both basal and disease conditions (Kops *et al.*, 2002, Mojsilovic-Petrovic *et al.*, 2009, Peng *et al.*, 2010). FOXO3a partially mediated the neuroprotection by Sirt1 in the striatal cell model of Huntington's disease (Jiang *et al.*, 2012) and moderate FOXO3 activation was also shown to oppose α-synuclein accumulation and proteotoxicity (Pino *et al.*, 2014). Two studies further demonstrated that genetic and/or pharmacological activation of DAF-16/FOXO3a pathway could be broadly neuroprotective across phyla using both *in vitro* and *in vivo* models of motor neuron diseases (Mojsilovic-Petrovic *et al.*, 2009) and

Parkinson's disease. While erythropoietin induced the expression of phosphorylated FOXO3a (Jia *et al.*, 2014), compound psammaplysene A evoked a dose-dependent increase in FOXO-dependent transcription (Mojsilovic-Petrovic *et al.*, 2009) which is in agreement with the role of ethosuximide in increasing FOXO's ability to induce cell cycle arrest and DNA repair.

Of particular interest was the observation that ethosuximide treatment resulted in significant induction of FOXO targets in differentiated N2A cells. This response was however absent in undifferentiated N2A cells, as ethosuximide was either suppressive or had no effect on FOXO target expression. This discordance between differentiated and undifferentiated neuroblastoma cells together with the observed differential protective effects of ethosuximide on *C. elegans* aggregation models further suggests that ethosuximide is likely to act non-cell autonomously in worms and mammals and the drug response may be neuron-specific.

In conclusion, preliminary analyses of gene expression profiles obtained by using microarrays in this chapter have shed light on the potential molecular mechanisms of ethosuximide. Our work confirmed the important role of DAF-16/FOXO TF in the regulation of ethosuximide and further extended the protective activity of ethosuximide in mammalian neurons. Further studies are needed to evaluate the physiological importance of the increased or decreased levels of ethosuximide-responsive DEGs, and to assess the magnitude and complexity of expression changes elicited by ethosuximide at multiple exposure time points. As a complementary approach to the use of DNA microarrays, proteomic profiling could also be

performed in the future to identify to what extent a particular protein product is functionally altered by ethosuximide.

CHAPTER 6: CONCLUSION

6.1 SUMMARY

Age-associated neurodegenerative diseases (NDs) are increasingly common and exert large costs on society. A major goal of neurodegeneration research is therefore to identify potential new therapies for these devastating diseases. There is considerable current interest in the idea of repurposing existing medicines for the treatment of NDs, since screening pre-approved drugs with well established safety and toxicity profiles obviates the need for early toxicity trials and thus expediting translation to clinical testing (Corbett *et al.*, 2012). In this thesis, the nematode *C. elegans* was used as a pharmacological model system to identify generally neuroprotective compounds that alleviate the functional consequences of protein misfolding common to neurodegeneration. Using a combination of physiological, biochemical, and genetic tools, the research presented in this thesis demonstrated that ethosuximide, a widely prescribed anti-epileptic drug was efficacious in improving the pathological phenotypes of several worm ND models, and was further shown to induce the transcriptional activity of several mammalian FOXO target genes and conferred protection against expanded polyglutamine peptides-induced aggregation in cell culture experiments. Ethosuximide therefore is a potential candidate for repurposing as a treatment for NDs. These findings prompted further investigation into the protective effects of ethosuximide at the molecular level and have opened several directions for the future studies

The first aim of this thesis was to test the applicability of established *C. elegans* ND models and select models with robust and readily-assayable screening phenotypes that are comparable to the human NDs. Chapter 3

describes the selection and phenotypic characterisation of nine neuronal ND models, of which many have already made substantial contribution to our understanding of the molecular mechanisms underlying aggregation and proteotoxicity in many human NDs. However, utility of most of these selected models for testing chemical modifiers are limited due to their lack of penetrance, variable phenotypes, incomplete manifestations and failure to reproduce published phenotypes. AD and HD transgenic models displayed highly variant neurodegenerative phenotypes that lack robustness and penetrance, while transgenic PD models have limited and variable phenotypes. The toxin-based PD model and the SMA null mutant model exhibited moderately robust phenotypes, but their usages for screening are restricted by their technical difficulties. Our data support the utility of a *C. elegans* null mutant model of ANCL, a distinct worm FTDP-17 model and an ALS model for subsequent modifier screening since they exhibited statistically robust and reproducible phenotypes. These models involve deletion of an endogenous neuroprotective gene (*dnj-14*), and pan-neuronal transgenic expression of disease-associated mutant Tau or SOD1 proteins, respectively. Pharmacological screening using ANCL and FTDP-17 models have already uncovered promising therapeutic interventions (McCormick *et al.*, 2013, Kashyap *et al.*, 2014).

The second part of this thesis (Chapter 4) demonstrated that the AED ethosuximide is a promising general modifier of early-onset proteotoxicity since it was efficacious in three contrasting worm ND models, reducing proteotoxicity and enhancing lifespan not only in the null mutant model of ANCL, but also the FTDP-17 and a polyQ model based on pan-neuronal and

muscle-specific expression of mutant human Tau protein and aggregation-prone polyglutamine stretches, respectively. Possible mechanisms of ethosuximide protection were subsequently addressed. Our finding that the beneficial effects of ethosuximide on motility and longevity in the FTDP-17 model persist in strains harbouring a null mutation in the *C. elegans* T-type calcium channel, *cca-1*, suggests that ethosuximide's neuroprotective activity is not mediated by inhibition of T-type channels. This conclusion is supported by previous work in *C. elegans* showing that lifespan extension by ethosuximide is unaffected by a different mutant allele of *cca-1* (Collins *et al.*, 2008). Our data also revealed an imperfect correlation between the ability of ethosuximide to alter biochemical endpoints such as levels of soluble and insoluble Tau protein and polyQ aggregation and suppress proteotoxicity. We further excluded the possibility that the protective effects of ethosuximide are due to changes in the *E. coli* food source.

The third part of the thesis aimed to understand the mechanism of action of ethosuximide. An Affymetrix microarray comparing the whole genome mRNA expression of untreated to ethosuximide-treated ANCL models and N2 WT animals was performed. The major findings in this part are: 1) Gene expression profiles of all worms following ethosuximide treatment are distinctly different from their untreated counterparts. 2) Genes commonly regulated in ethosuximide-treated animals have varied roles in lipid metabolism, redox homeostatsis, longevity/ageing, cell cycle and ubiquitination. 3) DAF-16/FOXO TF contributes to the observed protective action of ethosuximide. 4) Ethosuximide induced the transcriptional activity of

a subset of mammalian FOXO target genes and conferred protection against polyQ aggregation in mammalian neuronal cells.

6.2 FUTURE DIRECTIONS

Our data, combined with other studies, support a growing field investigating existing Medicines and Healthcare products Regulatory Agency (MHRA)-approved medications for new indications. The anticonvulsant ethosuximide is clearly a potential candidate for repurposing as a treatment for NDs as demonstrated by its general neuroprotective activity in various different worm ND models which was also extended in mammalian cells. Our microarray data further substantiated that DAF-16/FOXO is a major component of the transcriptional network that regulates ethosuximide-mediated protection. Many questions still await to be addressed, and there are a number of possibilities to be followed-up in the near future.

Numerous research studies involving the structure-function analysis of known compounds such as resveratrol (Richard *et al.*, 2011), hydroxylamine (Haldimann *et al.*, 2011), icariin (Cai *et al.*, 2011) and celecoxib (Ching *et al.*, 2011) and their respective derivatives, have demonstrated their promising anti-ageing and anti-neurodegenerative activities. Polyphenols, in particular resveratrol, were shown to have neuroprotective effects in a range of worm models and also in mammalian systems (Parker *et al.*, 2005, Karuppagounder *et al.*, 2009, Bizat *et al.*, 2010, Tauffenberger *et al.*, 2013, Kashyap *et al.*, 2014), as resveratrol not only rescued Htt-polyQ toxicity in both worm and neuronal culture models (Parker *et al.*, 2005), but also protected against neurodegeneration both in a transgenic ALS model

overexpressing mutant TDP-43 (Tauffenberger *et al.*, 2013) and a *dnj-14* null mutant model of ANCL (Kashyap *et al.*, 2014). Several of the resveratrol derivatives such as scirpusin A and ε-viniferin glucoside have also been demonstrated to effectively modulate multiple mechanisms of the AD pathology (Richard *et al.*, 2011). Treating *C. elegans* muscle polyQ model with hydroxylamine, icariin and celecoxib derivatives: NG-094, Icariside II and OSU-03012 ameliorated polyQ-mediated protein aggregation and conferred protection against polyQ proteotoxicity (Cai *et al.*, 2011, Ching *et al.*, 2011, Haldimann *et al.*, 2011). Studies have also previously demonstrated that trimethadione and 3,3-diethyl-2-pyrrolidinone, which are two other succinimide anticonvulsants structurally related to ethosuximide, can extend *C. elegans* lifespan and delay age-related degenerative changes (Evason *et al.*, 2005). In this perspective, a potential next step could be to utilise both computer-assisted drug design/computer modeling methods and laboratory techniques to visualise and characterise the molecular structure of ethosuximide, and refine it to increase its specificity. This in turn could facilitate the identification of more potent and selective ethosuximide derivatives with multiple variations, as well as development of novel compounds which are currently not in clinical use, but may be screened for actions on neurodegeneration and neuronal loss associated with protein misfolding and aggregation (Caldwell *et al.*, 2008).

As previously discussed, the drawbacks of certain worm ND models include subtle, low penetrance and variable phenotypes, or phenotypes that are cumbersome to score, while others recapitulate the pathology of corresponding human NDs, but the severity of the defects make identification

of modifiers of the phenotype very demanding. Together, these limit the potential use of such models in modifier screening. During the course of my studies, not only have new worm ND models been developed (McColl *et al.*, 2012, Christie *et al.*, 2014), ways to circumvent or overcome the technical difficulties and reduce data variability of the old models have also been discovered. While automation of labour intensive and low-throughput behaviour assays facilitates precise and rapid phenotypic data acquisition, development of novel technologies such as macro-scale flow-cytometry, microfluidics and optic techniques for rapid worm immobilisation, sorting, screening and automated long-term imaging have opened the possibility for performing high throughput analyses (Hulme and Whitesides, 2011, Yanik *et al.*, 2011). Continuing refinement of high-throughput methods that require expensive or specialised equipment (Burns *et al.*, 2006, Rohde *et al.*, 2007, Doitsidou *et al.*, 2008, Boyd *et al.*, 2010, Gosai *et al.*, 2010, Swierczek *et al.*, 2011) have led to the development of affordable systems that automate accurate and high-throughput scoring of a greater range of phenotypic endpoints of *C. elegans* (Mathew *et al.*, 2012). In one recent report, a semi-automated motion tracking analysis was applied on the neuronal AD model which allowed for a more efficient, accurate and detailed assessment of the behaviour deficits of strain CL2355 (Machino *et al.*, 2014). Therefore, these platforms could potentially overcome some of the limitations associated with ND models as discussed above, to allow accurate analysis and quantification of behaviour defects and other neurological phenotypes that can be potentially rescued by ethosuximide with high-throughput.

It was demonstrated that the worm *dnj-14* phenotype is reminiscent of *dnajc5* KO mice which are relatively normal at birth, but have a short lifespan associated with progressive sensorimotor defects and neurodegeneration (Fernandez-Chacon *et al.*, 2004). *dnj-14* mutants also develop profound chemosensory neuron impairments with increasing age (Kashyap *et al.*, 2014), and this selectivity in the types of neurons affected bears a striking similarity with the selective vulnerability of photoreceptors and GABAergic neurons (Schmitz *et al.*, 2006, Garcia-Junco-Clemente *et al.*, 2010) observed in CSPα null models and ANCL patients. Therefore, the efficacy of ethosuximide would be further evaluated in the *dnajc5* KO mouse model of ANCL to see if the treatment can abrogate the motor impairments, lethality and neurodegeneration caused by the loss of CSPα function.

In line with previous work, we have shown in Chapter 4 that ethosuximide-mediated protection is independent of CCA-1, the sole worm orthologue of mammalian T-type calcium channel. Given that the *C. elegans* genome does not encode voltage-sensitive sodium channels or display typical voltage-gated sodium currents (Bargmann, 1998), it seems likely that ethosuximide ameliorates neurodegeneration via a novel ion-channel-independent mechanism. To validate this experimentally, we should proceed to investigate the role of other voltage-gated calcium channels such as UNC-2 (CaV2 or N/P/Q-type), EGL-19 (CaV1 or L-type), and non-selective cation channels NCA-1 and NCA-2 channels (Liu *et al.*, 2011a) in ethosuximide action by generating and analysing the responses of respective double mutants to ethosuximide exposure. To determine whether K^+ channels are important in ethosuximide action, functional analyses of double mutants with

deletions in the voltage-gated channels SHL-1 and SHK-1, and the Ca^{2+}/Cl^{-}-gated channel SLO-2 should be performed.

Our studies also did not address the functioning of the nervous system beyond gross behavioural experiments. Further experiments could include a more in-depth observation of the neurotransmitter systems that were not quantitatively assessed in these studies, such as assessing ND models treated with ethosuximide for sensitivity to acetylcholinesterase inhibitor aldicarb and nicotinic agonist levamisole, which could reveal potential impact of ethosuximide on synaptic transmission.

Our microarray analysis in Chapter 5 has laid an excellent foundation for the discovery of therapeutic targets of ethosuximide as well as future explorations into the regulation of gene transcription and the exact molecular alterations that occur with ND processes. PQM-1, a novel TF was recently discovered to regulate Class II (down-regulated) DAF-16/FOXO targets by binding to the DAE located in the promoter of these genes, whereas DAF-16 regulates Class I (up-regulated) DAF-16/FOXO targets by binding to the DBE (Tepper *et al.*, 2013). However, the common ethosuximide-regulated gene set with a significant enrichment in DAE consists more of the most responsive Class I than Class II genes. Therefore whether PQM-1 TF has a regulatory role in ethosuximide-mediated protection awaits future studies. As experimental follow-up, the effect of ethosuximide treatment on *pqm-1*$^{-/-}$, double mutant involving *pqm-1* deletion, and nuclear localisation of PQM-1::GFP worms would be investigated. Fully exploring whether the DAE binding to either DAF-16 or PQM-1 is direct or indirect is also a high priority. As noted by Tepper *et al*.(Tepper *et al.*, 2013), there are several other DAE-

binding TFs over-represented in Class I and Class II targets and ones that are of potential interest include PHA-4, a FoxA TF required for dietary-restriction-mediated longevity (Panowski *et al.*, 2007) with similar consensus site as DAF-16 (DAF-16: TTGTTTAC and PHA-4: T(A/G)TT(T/G)(A/G)(T/C) (Gaudet and Mango, 2002, Lee and Batzoglou, 2003); NHR-28, a nuclear hormone receptor and UNC-62, a developmental regulator (He *et al.*, 2014). They have all been identified as putative aging regulatory TFs in a recent ChIP-seq screen (Van Nostrand and Kim, 2013). Their potential roles in regulating ethosuximide-mediated protection could be explored in a similar way as DAF-16.

Our microarray work has concentrated on DEGs commonly regulated by ethosuximide. Additional experiments should further address the contributions of these genes in ethosuximide-mediated protection and test whether knocking them down by RNAi affect the phenotypes of untreated and treated *dnj-14* mutants. DEGs which are of particular interest include individual significant genes (*ttr-44*, *asm-3*), downstream targets of DAF-16/FOXO (*cyp-34A9, cyp-35B1, dod-6, dod-3, ftn-1*) and F-box proteins (*fbxb-11, fbxb-41, fbxb-63* and *fbxb-66*). Since F-box proteins were also enriched in our analysis for common DEGs down-regulated in response to ethosuximide, the effect of ethosuximide on the regulation of polyubiquitination and proteasome-mediated proteolysis should be addressed. To achieve this, a *sur-5*::*UbV-GFP* reporter strain that expresses ubiquitin with an C-terminal glycine to valine mutation fused to GFP under the control of the *sur-5* promoter in various somatic tissues (Segref *et al.*, 2011)

would be used and through assessing its GFP expression and protein levels, the ubiquitin proteasome system (UPS) activity would be monitored.

An interesting extension of this work would be to investigate the effects of ethosuximide on various ages. Likewise, complex analyses of expression profile changes between other genotypes, several ethosuximide treatment regimes and incorporation of previously published datasets and whole genome transcriptome analyses with newer technologies such as ChIP-seq and RNA-Seq could also be performed. This combinatory approach would be more informative than any one approach alone. In addition, functional proteomics could also be utilised to define the network of protein components whose synthesis and degradation are regulated by ethosuximide.

APPENDIX

NDs	Model	Strain/transgene name/(plasmid)	Expression in *C. elegans*	Phenotypes	Efficacious compounds identified/validated	References
Transgenic overexpression of human neurodegeneration-associated protein/peptide						
AD	P_{unc-54}::$A\beta_{1-42}$ (wild type); Dimer $A\beta_{1-42}$ or Met^{35}Cys $A\beta_{1-42}$	CL2005, CL2006, CL1019, CL1118, CL1119, CL1120, CL1121, CL2120; CL2109, CL3109; CL3115	Constitutive muscles	Age-dependent progressive paralysis; forms amyloid deposits; increased oxidative stress. CL2109, CL3109 and CL3115: no formation of amyloid deposits and no increase in oxidative stress	CL2006: caffeine, tannic acid and bacitracin; epigallocatechin gallate; reserpine; *Ginkgo biloba* extract EGb 761; soya isoflavone glycitein; rifampicin; thioflavin T; curcumin; ferulic acid; fluoxetine; JWB1-84-1 and JAY2-22-33; NT219 CL2120: PBT2	(Link, 1995, Fay *et al.*, 1998, Yatin *et al.*, 1999, Link *et al.*, 2001)
	dvIs100 [pCL354(*unc-54*:DA-$A\beta_{1-42}$) + pCL26(*mtl-2*: GFP)].	GMC101		Severe and fully penetrant paralysis within 48 hours after temperature shift	PBT2	(McColl *et al.*, 2012)
	smg-1(cc546);Is [P_{myo-3}::$A\beta_{1-42}$::let UTR) + *(rol-6(su1006)*]	CL4176	Inducible body wall muscles	Rapid paralysis; oxidative stress precedes amyloid deposition; autophagosome accumulation	coffee extracts, tetracycline and related analogs; copper; *Ginkgo biloba* extract EGb 761 and Ginkgolide A and J; Liuwei Dihuang (LWDH); galanthamine; icariside II; cocoa peptide	(Drake *et al.*, 2003, Link *et al.*, 2003, Florez-McClure *et al.*, 2007)
	smg-1(cc546); Is[P_{myo-3}::GFP::degron + P_{mtl-2}::GFP]	CL2337		Rapid paralysis; formation of stable perinuclear deposits		(Link, 2006)
	smg-1(cc546); Is[P_{snb-1}::$A\beta_{1-42}$ + P_{mtl-2}::GFP]	CL2241, CL2355	Inducible pan-neuronal	CL2241 exhibit WT movement. CL2355 is defective in chemotaxis toward benzaldehyde, associative learning, and thrashing in liquid; hypersensitive to serotonin; forms amyloid deposits; has partial sterility due to germline proliferation defects and embryonic lethality	CL2355: *Ginkgo biloba* extract EGb 761	(Link, 2006, Wu *et al.*, 2006, Dosanjh *et al.*, 2010)
	N2; *Is* [P_{eat-4}::ss$A\beta_{1-42}$(N-terminus) + P_{eat-4}::*gfp* + P_{myo-2}::*mCherry*]	UA166	Glutamatergic neurons	Loss of GFP-marked glutamatergic neurons in an age-related manner; at day 3 only 48% of worms had five intact glutamatergic neurons, and at day 7 only 25% did	clioquinol	(Treusch *et al.*, 2011)
	N2; *ynIs13*[P_{snb-1}::APL-1] N2; *ynIs104*[P_{rab-3}::*apl-1*::GFP]	LGIII, LGV, LGX	Constitutive pan-neuronal	Defects in brood size, movement, and viability; severe chemotaxis defects and diminished touch habituation		(Hornsten et al., 2007, Ewald et al., 2012)
ALS	N2; *Is*[$P_{hsp-16.2}$::*SOD-1 (WT, A4V, G37R, G93A)* + P_{myo-3}::*SOD-1 (WT, A4V)*::GFP + *rol-6(su1006)*]		Heat shock inducible body wall muscles	Paraquat hypersensitivity; formation of aggregates under oxidative stress		(Oeda *et al.*, 2001)

NDs	Model	Strain/transgene name/(plasmid)	Expression in *C. elegans*	Phenotypes	Efficacious compounds identified/validated	References
ALS	*P_{snb-1}::SOD1(WT,G85R) -YFP*	*iwIs8gf*	Constitutive pan-neuronal	G85R and G85R-YFP: severely reduced forward crawling, thrashings and strong resistance to aldicarb. H46R/H48Q-YFP produced a movement defect less prominent than that seen in G85R-YFP		(Wang *et al.*, 2009b)
	N2; *Is* [P_{sng-1}*::SOD-1 (WT, A4V, G37R , G93C)*– EGFP]			Increased aggregation formaton; SOD1(G85R) heterodimeric worms have significantly impaired locomotion and reduced lifespan		(Witan *et al.*, 2008)
	lin -15(n765ts); [P_{rgef-1}*::FUS (WT, R514G, R521G, R522G, R524S and P525L)* + P_{pab-1}:: *mcherry; lin-15(+)*]	*pJH897*		Formation of cytoplasmic FUS aggregates; R522G, P525L, FUS513 and FUS501: significantly shorter lifespan. P525L, FUS513 and FUS501: partially or completely paralysed, severely shrunken by 8 days of age		(Murakami *et al.*, 2002)
	P_{unc-54}::*SOD1(WT, G85R, G93A, G127insTGGGstop)*::YFP	AM263; AM265	Constitutive muscles	Accumulation of mutant SOD1 causes 25-30% decrease in motility on day 2 of adulthood, and further decrease by approx. 10% on day 6 of adulthood		(Gidalevitz *et al.*, 2009, Silva *et al.*, 2011a)
	unc-119(ed3);Is[P_{unc-47}::TDP-43-(WT, A315T) + unc-119(+)] unc-119(ed3); Is[P_{unc-47}::FUS-(WT, S57Δ) + unc-119(+)]	*xqIs132, xqIs133, xqIs173, xqIs98*	GABAergic motor neurons	Have normal lifespan, but displayed adult-onset, age-dependent loss of motility, progressive paralysis, neuronal degeneration, accumulation of highly insoluble TDP-43 and FUS proteins	methylene blue, salubrinal, guanabenz, and phenazine; resveratrol, rolipram, reserpine, trolox, propyl gallate, and ethosuximide	(Vaccaro *et al.*, 2012)
	[P_{snb-1}*::TDP-43-YFP WT(iwIs26)*], [P_{snb-1}*::TDP-C25-YFP(iwIs22)*], [P_{snb-1}*::TDP-43-YFP Q331K(iwEx20)*], [P_{snb-1}*::TDP-43-YFP M337V(iwEx28)*], [P_{snb-1}*::SOD1-YFP WT(iwIs27)*] and [P_{snb-1}*::SOD1-YFP G85R(iwIs8)*]	IW63, IW33, IW20, IW46, IW31, IW8	Constitutive pan-neuronal	Transgenic models developed robust locomotion defects and protein aggregation		(Zhang *et al.*, 2011)
	P_{unc-25}*::G93A SOD1-GFP*		GABAergic motor neurons	Age-dependent paralysis; G93A SOD1 aggregates in neural cell bodies and causes axon guidance defects		(Li *et al.*, 2013)
ALS/ FTLD-U	N2; *Is*[P_{snb-1}*::TDP-43 (WT, G290A, A315T, M337V)* + P_{snb-1}::GFP]	CK405, CK406, CK410; CK422; CK423; CK426	Constitutive pan-neuronal	Mutant TDP-43: significantly impaired locomotion; degeneration of GABAergic motor neurons	PHA767491; LDN-0130436	(Liachko *et al.*, 2010)
ALS/ FTLD-U	*Is*[P_{unc-25}::SNB-1::GFP] + *Ex*[P_{snb-1}::TDP-43*;* P_{regf-1}:: DsRed2; $P_{unc--122}$::RFP]	CL2609, CL1681, CL1682		Unc and abnormal motor neuron synapses		(Ash *et al.*, 2010)

NDs	Model	Strain/transgene name/(plasmid)	Expression in *C. elegans*	Phenotypes	Efficacious compounds identified/validated	References
FTDP-17	*N2; Is*[P_{aex-3}:: *4R1N human tau (WT, V337M , P301L)* + P_{myo-2}*::GFP*]	CK10, CK49, CK1301, CK1310	Constitutive pan-neuronal	Mutant tau: strong age-dependent progressive uncoordination and accumulation of insoluble tau; neurodegeneration; presynaptic cholinergic transmission defect; reduced lifespan	azaperone, clofazimine, isoniazid, lorglumide, nefopam, and trazodone	(Kraemer *et al.*, 2003)
	Pro-aggregant lines: *N2; Is*[P_{rab-3}::*F3ΔK280* + P_{myo-2}::mCherry]	BR5270, BR5485, BR5944, BR5706		Strongly defective locomotion at day 1 of adulthood, accelerated aggregation of insoluble Tau, severe developmental defects of nervous syetem, impaired presynaptic transmission	methylene blue, BSc3094, bb14 and cmp16	(Fatouros *et al.*, 2012)
	Anti-aggregant lines: *N2; Is*[P_{rab-3}::*F3ΔK280(I277P)(I308P)* + P_{myo-2}::mCherry]	BR5271, BR5486, BR6516, BR6427		No obvious locomotion defects and minimum perturbation of the development of the nervous system		
	N2; Is [P_{mec-7}::*tau WT(0N4R, 0N3R)* + *rol-6(su1006)*]	*tmIs82, tmIs83, tmIs84, tmIs85, tmIs171; tmIs110, tmIs173*	Touch neurons (ALML/R, AVM, PLML/R, PVM); weak in FLP, PVD, BDU	Age-dependent progressive impairment in touch response; neurodegeneration; tau WT4R: little tau accumulation in PLM neuron		(Miyasaka *et al.*, 2005)
	N2; Is [P_{mec-7}:: *tau (P301L, R406W)* + *rol-6(su1006)*]	*tmIs81, tmIs178, tmIs179; tmIs146, tmIs147, tmIs148, tmIs149*		Strong age-dependent progressive impairment in touch response; neurodegeneration; strong tau accumulation in PLM neuron		
	pha-1(e2123ts); *Ex*[P_{rgef-1}:: Tau_{352} *(WT, PHP, Ala10)* + *pha-1(+)*]	VH255, VH1016, VH1018; VH254, VH1014, VH1015; VH418, VH421	Constitutive pan-neuronal	Both WT and PHP tau_{352} showed age-dependent progressive uncoordination and neurodegeneration; no change in motor neuron viability. Mutant PHP tau: altered motor neuron development. Ala10 tau: early onset of movement defects and reduced lifespan		(Brandt *et al.*, 2009)
HD	P_{unc-54}*::polyQ*-GFP/YFP/CFP	*pEGFP-N1-Q19, pEGFP-N1-Q82*	Constitutive muscles	Length-dependent formation of aggregates; growth rates slowed down; reduced motility	icariside II; NG-094; aspirin	(Satyal *et al.*, 2000, Morley *et al.*, 2002, Wang *et al.*, 2006)
	P_{unc-54}*::DRPLAP-Q(32, 40, 56, 79)*-GFP	*pCKX2004, pCKX2003, pCKX2002, pCKX2001*		Q>40: formation of cytoplasmic aggregates		(Yamanaka *et al.*, 2004)
	P_{mec-3}*::htt57Q(19, 88, 128)*-GFP P_{mec-3}*::htt57Q(19, 88, 128)* ::CFP + P_{mec-7}::YFP	ID24, ID1	Mechanosensory neurons	Highly penetrant posterior touch insensitivity, significant anterior Mec phenotype; significant deposits and morphological abnormalities in PLM cell axons	resveratrol	(Parker *et al.*, 2001, Lejeune *et al.*, 2012)

NDs	Model	Strain/transgene name/(plasmid)	Expression in *C. elegans*	Phenotypes	Efficacious compounds identified/validated	References
HD	N2; *rmEx*[P_{rgef-1}*::HttQ (0,19,35,40,67,86)*-CFP/YFP]	CFP lines: (Q35) AM303; (Q40) AM305; (Q67) AM308; (Q86) AM313. YFP lines: (Q35) AM78 and AM80; (Q40) AM85 and AM87; (Q67) AM81 and AM83; (Q86) AM322 and AM324	Constitutive pan-neuronal	PolyQ length-dependent aggregation; overt neuronal dysfunction; polyQ length-dependent decrease of thrashing, pharyngeal pumping and erratic defecation cycle	β-lapachone	(Brignull *et al.*, 2006b)
	rtIs11[P_{osm-10}::GFP + P_{osm-10}*::HttQ150 +Dpy-20*(+)]	HA659	Chemosensory neurons	Severe defect in the nose touch response		(Faber *et al.*, 2002)
	pqe-1(rt13) III; *rtIs11*[P_{osm-10}::GFP + P_{osm-10}*::HttQ150 + Dpy-20*(+)]	HA759		Accelerated polyQ mediated neurodegeneration. Vast majority (>90%) of ASH neurons undergo cell death in less than three days	lithium chloride, mithramycin, trichostatin; rotenone, oligomycin and 4-dinitrophenol; *D. officinarum* extracts; salidroside	(Varma *et al.*, 2007, Voisine *et al.*, 2007)
	N2; rmIs[P_{unc-54}*::polyQ(0, 24, 35, 37, 40)::YFP]*	(Q35) AM140*; (*Q37) AM470; *(*Q40) AM141	Constitutive muscles	Q35 and Q37 aggregation in muscle cells causes a significant motility defect	AM140: ML346; celecoxib; NT219 AM141: salidroside	(Silva *et al.*, 2011a)
MJD	Full-length ATXN-3 expressing lines: P_{rgef-1}*::AT3q14, AT3q75, AT3q130::*YFP	AM491, AM513, AM509, AM494, AM519, AM520, AM666, AM685, AM599	Constitutive pan-neuronal	PolyQ length-dependent aggregation and motor dysfunction	17-(allylamino)-17-demethoxygeldanamycin (17-AAG), valproic acid	(Teixeira-Castro *et al.*, 2011)
	C-terminal ATXN-3 expressing lines: P_{rgef-1}*::257cAT3q14, 257cAT3q75, 257cAT3q80, 257cAT3q128::*YFP	AM396, AM416, AM422, AM391, AM428, AM419, AM420, AM684, AM683, AM702		Worms with truncated ATXN3 expression have similar aggregation profiles in their neurons and have more severe motility defects		
	N2; [P_{unc-54}*257cAT3(Q45)*::YFP] or P_{unc-54}*257cAT3(Q63)*::YFP		Constitutive muscles	PolyQ length-dependent toxicity; aggregation and toxicity are not significantly modulated by aging		(Christie *et al.*, 2014)
PD	N2; *Is*[P_{unc-54}*::α-syn::*GFP + *rol-6(su1006)*]	UA49	Constitutive muscles	α-syn misfolding and accumulation		(Hamamichi *et al.*, 2008)
	Is[P_{unc-54}*::α-syn::*YFP + *unc-119(+)*]	NL5901		Formation of inclusions	10-*O-trans-p*-Coumaroylcatalpol	(van Ham *et al.*, 2008)
	P_{aex-3}*::α-syn (WT, A53T)* + P_{aex-3}::GFP/P_{dat-1}::GFP		Constitutive pan-neuronal	Motility deficits, significant dopaminergic neuron loss and dendritic breaks		(Lakso *et al.*, 2003)
	$P_{(acr-2, unc-30)}$*::α-syn (WT, A53T)* + P_{aex-3}::GFP/P_{dat-1}::GFP		Motor neurons			

NDs	Model	Strain/transgene name/(plasmid)	Expression in *C. elegans*	Phenotypes	Efficacious compounds identified/validated	References
PD	N2; *Is*[$P_{unc-119}$::*α-syn (WT, A53T, β-syn)* + *pDPSU006*-GFP]		Constitutive pan-neuronal	A53T: greater vulnerability to rotenone-induced toxicity, exhibiting 68.4% lower survival after 4 days of 50 μM rotenone treatment.		(Ved *et al.*, 2005)
	P_{dat-1}::*α-syn (WT, A53T)* + P_{dat-1}::GFP	BY273, UA18, UA31, UA44	Dopaminergic neuron	Mean life span was similar among the non-Tg, WT, and A53T α-synuclein-expressing strains; significant DAergic neuron loss and dendritic breaks	acetaminophen; bromocriptine and quinpirole;valproic acid	(Lakso *et al.*, 2003, Cao *et al.*, 2005, Kuwahara *et al.*, 2006, Settivari *et al.*, 2009)
	P_{dat-1}::*α-syn (A30P, A53T, A56P)* + P_{dat-1}::*mCherry*		Dopaminergic neuron	Increased neurodegeneration; A30P or A53T: failure in modulation of locomotory rate in response to food and markedly reduced DA content (~1 ng/g vs N2 ~5 ng/g). A56P: more impaired in DA-dependent behaviour		(Karpinar *et al.*, 2009)
	N2; *Is*[P_{unc-51}::*α-syn (WT, A53T, A30P)* + P_{unc-51}::EGFP]		Constitutive pan-neuronal	No motor deterioration or retardation in growth		(Kuwahara *et al.*, 2008)
	N2; *Is*[P_{mec-7}::*α-syn (WT, A53T)* + *rol-6 (su1006)*]		Mechanosensory neurons	Moderate impairments in touch response		
	P_{unc-51}::*S129A or S129D α-syn* + P_{unc-51}::EGFP P_{unc-51}::*S129A or S129D α-syn* + P_{unc-25}:: SNB-1::GFP		Constitutive pan-neuronal	Strikingly severe motor defects throughout development and aging, growth retardation, and synaptic abnormality. SNB-1::GFP fluorescence was broadly diminished in the nerve cord.		(Kuwahara *et al.*, 2012)
	lin-15(n765ts); Is[P_{snb-1}::*LRRK2 (WT, G2019S, R1441C, KD, R1441C/KD*) + P_{mec-4}::GFP; *lin-15 (+)*]	*wIzIs1-7*	Constitutive pan-neuronal	G2019S LRRK2 increased vulnerability of dopaminergic neurons to mitochondrial stress. Reduced lifespan in mutant LRRK2 (G2019S or R1441C)		(Saha *et al.*, 2009)
	N2; *baIn20* [P_{dat-1}::*LRRK2 (G2019S)* + P_{dat-1}::GFP]	UA118	Dopaminergic neuron	Age-dependent degeneration of DAergic neurons, behavioural deficit, locomotor dysfunction and depletion of dopamine(~72% loss). G2019S causes more rapid progression of behavioural deficits than others	GW5074 indoline; sorafenib	(Liu *et al.*, 2011b)
	BY250*; baEx129*[P_{dat-1}::LRRK2(G2019S/D1994A)]	UA215, UA216				
	lin-15(n765ts) X; Is[P_{dat-1}::*LRRK2 (WT,R1441C, G2019S, K1347A)* + P_{dat-1}::GFP + *lin-15 (+)*]	SGC722, SGC851, SGC856, SGC862			TTT-3002 and LRRK2-IN1	(Yao *et al.*, 2010, Yao *et al.*, 2012)
	lin-15(n765ts) X; cwrEx900 [P_{dat}-1::GFP, P_{dat}-1::*LRRK2(R1441C/A2016T), lin-15(+)*]	SG900, SGC910,		Double mutants displayed DAergic defects and neurodegeneration similar to R1441C- and G2019S-LRRK2 models.		(Yao *et al.*, 2012)

NDs	Model	Strain/transgene name/(plasmid)	Expression in *C. elegans*	Phenotypes	Efficacious compounds identified/validated	References
Prion	*lin-15(n765ts);* [P_{mec-7}*::PrP(WT, PG13)* + P_{Str-1}*::* GFP; P_{mec-7}*::*GFP + *lin-15 (+)*]		Mechanosensory neurons	Progressive loss of response to touch at the tail caused by mutant (PG13-PrP) PrP expression without causing cell death	quinacrine, resveratrol	(Bizat *et al.*, 2010)
	P_{ric-19}*::*PrP + P_{ric-19}*::*GFP	*cgIs51, cgIs52, cgIs53*	Constitutive pan-neuronal	High PrP levels cause abnormal morphology, striking neuropathogenic phenotypes and remarkable reductions in lifespan		(Park and Li, 2011)
	rmIs319[P_{unc-54}*::*sup35(rΔ2-5, *nm, r2e2*)::yfp],	AM801, AM803, AM806	Constitutive muscles	Profound cell autonomous and cell non-autonomous disruption of mitochondrial integrity, embryonic and larval arrest, developmental delay, widespread tissue defects, and loss of organismal proteostasis		(Nussbaum-Krammer *et al.*, 2013)
Mutant/RNAi						
AD	*apl-1(yn10)*			Larval lethality, defects in molting and morphogenesis		(Lakowski and Hekimi, 1998)
	*apl-1(*RNAi)			Reduced body size, with some worms exhibiting L4 molting problems		(Hornsten *et al.*, 2007)
	sel-12(ar131) and *(ar171)*	GS1894		Exhibit thermotaxis defects		(Levitan and Greenwald, 1998, Wittenburg *et al.*, 2000)
ANCL	*dnj-14(ok237)* *dnj-14(tm3223)*	RM2754 TM3223		Age-dependent progressive impairment in locomotion, severe progressive chemosensory defects which precede neurodegeneration of sensory neurons and significantly shorter lifespan	resveratrol	(Kashyap *et al.*, 2014)
PD	*lrk-1(km17), (km41), (tm1898) and (RNAi)*			Mitochondrial stress, ER stress sensitive		(Saha *et al.*, 2009)
	pdr-1(lg103), (XY1046, Parkin KO3) and (RNAi)			Display severe developmental defects and lethality at early larval stages in presence of ER stressors. Majority died or arrested at, or prior to, the larval L3 stage. 15.4% shorter life span than that of non-Tg strain		(Springer *et al.*, 2005, Ved *et al.*, 2005)
	pink-1(tm1779)			Increased sensitivity to a 3-day exposure to 150 mM paraquat		(Sämann *et al.*, 2009)
	djr-1.1(RNAi)			Significantly more sensitive to rotenone treatment than control nematodes		(Ved *et al.*, 2005)

NDs	Model	Strain/transgene name/(plasmid)	Expression in *C. elegans*	Phenotypes	Efficacious compounds identified/validated	References
SMA	*smn-1(ok355) I/hT2*[*bli-4(e937) let-?(q782) qIs48*] *(I;III)*	LM99		Thrashing rate progressively declined and almost completely ceased after 5 days post-L1. Pharyngeal pumping rates showed a rapid and progressive decline. Mean lifespan is 6.0 days Vs 17.7 days for N2	riluzole	(Briese *et al.*, 2009)
	smn-1(cb131)I	LL2073		Body length and lifespan was significantly shorter than that of the WT; defective motility, egg-laying and hatching	4-aminopyridine, gaboxadol hydrochloride, N-acetylneuraminic acid	(Sleigh *et al.*, 2011)
Chemical treatment						
PD	*vtIs7*[P_{dat-1}::GFP] subjected to 6-hydroxydopamine (6-OHDA)	BY250, BY200		Neuronal process blebbing, cell body rounding with process loss and cell body loss reproducibly appear in this order within a few hours.	bromocriptine, quinpirole and memantine; acetaminophen	(Nass *et al.*, 2001, Cao *et al.*, 2005, Ruan *et al.*, 2010)
	N2; [P_{cat-2}::GFP], *egIs1*[P_{dat-1}::GFP] subjected to 1-methyl-4-phenyl-1,2,3,6-tetrahydropyridine (MPTP)	BZ555		Reduced mobility, increased lethality and DA neurodegeneration,	lisuride, apomorphine and rottlerin; P7C3, P7C3A20; polysaccharides from *Chaenomeles speciosa;* acetylcorynoline; *n*-butylidenephthalide	(Braungart *et al.*, 2004)
	N2; [P_{dat-1}::α-syn+ P_{dat-1}::GFP] subjected to Manganese (Mn^{2+})			Oxidative stress, mitochondrial stress, enhanced DA neurodegeneration, reduced DA levels		(Settivari *et al.*, 2009)
	pink-1(tm1779) subjected to Paraquat			Oxidative stress		(Sämann *et al.*, 2009)
	pdr-1(XY1046), P_{snb-1}*::α-syn WT,* $P_{unc-119}$*::α-syn A53T*, N2, *lrk-1(km17),* P_{snb-1}*::LRRK2 (WT, R1441C, G2019S)* subjected to Rotenone			Mitochondrial stress, reduced viability	D-α-hydroxybutyrate in combination with tauroursodeoxycholic acid	(Ved *et al.*, 2005, Saha *et al.*, 2009)
	P_{dat-1}::GFP subjected to *Streptomyces venezuelae* secondary metabolite			DA neurodegeneration		(Caldwell *et al.*, 2009)

Table A1: An inclusive list of published *C. elegans* models of human neurodegenerative diseases that were utilised to study specific neurodegenerative diseases. Potential drugs that were shown to confer neuroprotection are also listed. Human neuorodegenerative diseases (NDs): AD, Alzheimer's disease; ANCL, Adult-onset neuronal ceroid lipofuscinosis; ALS, Amyotrophic lateral sclerosis; CJD, Creutzfeldt-Jakob disease; FTDP-17, Frontotemporal dementia with parkinsonism-17; FTLD-U,frontotemporal lobar degeneration with ubiquitinated inclusions; HD, Huntington's disease, MJD, Machado–Joseph disease (or spinocerebellar ataxia type 3); PD, Parkinson's disease, SMA, Spinal muscular atrophy

Strains	Drug treatments$^{\Delta}$ (mg/ml)	Mean lifespan ± S.E.M (days)	% Change in mean lifespan§	*p*-value	75% mortality (days)	90% mortality (days)	Maximum (days)	Total number of worms analysed
N2	PBS control	19.69 ± 1.05	-	-	27	29	31	53
	Juglone (40 µM)	16.43 ± 0.55**	-16.56%	0.0021	18†††	23†	25	52
	Succinimide (1)	15.91 ± 0.57**	-19.20%	0.0003	18†††	21†	25	52
	Ethosuximide (1)	20.39 ± 1.02	3.56%	0.3966	27	29	33	54
	PBS control	18.55 ± 0.64	-	-	22	24	25	52
	Ethosuximide (2)	18.79 ± 1.06	1.29%	0.5061	24	25	29	52
	Ethosuximide (4)	17.12 ± 0.98	-7.71%	0.5000	21	23	26	52
N2; *L4440* (RNAi)	PBS control	19.48 ± 0.30	-	-	22	25	27	131
	Ethosuximide (1)	19.08 ± 0.38	-2.05%	0.9164	22	25	27	130
N2; *hsp-1* (RNAi)	PBS control	12.19 ± 0.24***	-	0.0e+00	14†††	15	17	116
	Ethosuximide (1)	14.35 ± 0.38***	17.72%	2.2e-08	17†††	20	25	118
N2; *daf-16a* (RNAi)	PBS control	15.73 ± 0.33***	-	0.0e+00	18†††	20††	22	128
	Ethosuximide (1)	15.90 ± 0.33	1.08%	0.8868	18	20	25	128
dnj-14(ok237)	PBS control	15.87 ± 0.62	-	-	18	21	23	56
	Juglone (40 µM)	18.01 ± 0.57*	13.48%	0.0070	21	23	25	58
	Succinimide (1)	16.71 ± 0.51	5.29%	0.3586	18	21	25	54
	Ethosuximide (1)	21.56 ± 0.79***	35.85%	1.1e-07	21	23	25	58
	PBS control	15.76 ± 0.61	-	-	17	21	27	52
	Ethosuximide (0.0001)	16.66 ± 0.76	5.71%	0.4174	19†	23†	24	52
	Ethosuximide (0.001)	18.40 ± 0.84*	16.75%	0.0217	21††	24††	26	52
	Ethosuximide (0.01)	16.59 ± 0.60	5.27%	0.3757	19	22	25	50
	Ethosuximide (0.1)	17.46 ± 0.78	10.79%	0.1722	21	25†	26	53
	Ethosuximide (0.2)	19.27 ± 0.78**	22.27%	0.0017	23†	24	29	52
	Ethosuximide (0.5)	20.15 ± 0.98**	27.86%	0.0005	24††	26††	32	52
	Ethosuximide (1)	22.26 ± 1.25***	41.24%	2.6e-06	29††	32†	34	112
	Ethosuximide (2)	21.11 ± 1.21**	33.95%	0.0002	26††	32†	33	52
	Ethosuximide (4)	18.73 ± 0.75**	18.85%	0.0038	22††	24	26	55
dnj-14(ok237); *L4440* (RNAi)	PBS control	16.81 ± 0.32***	-	3.5e-09	20†††	22†	25	118
	Ethosuximide (1)	21.23 ± 0.44***	26.29%	1.2e-06	25††	27†	31	125
dnj-14(ok237); *hsp-1* (RNAi)	PBS control	14.16 ± 0.28***	-	0.0e+00	15†††	17††	22	120
	Ethosuximide (1)	17.39 ± 0.39***	22.81%	0.0e+00	20†††	25†††	27	119
dnj-14(ok237); *daf-16a* (RNAi)	PBS control	15.37 ± 0.37*	-	0.0113	18	20	22	114
	Ethosuximide (1)	16.23 ± 0.33	5.60%	0.1518	18	20	22	126
osm-3(p802); *L4440* (RNAi)	PBS control	17.84 ± 0.63	-	-	22	25	29	68

Strains	Drug treatments$^{\Delta}$ (mg/ml)	Mean lifespan ± S.E.M (days)	% Change in mean lifespan§	*p*-value	75% mortality (days)	90% mortality (days)	Maximum (days)	Total number of worms analysed
	Ethosuximide (1)	20.51 ± 0.63**	14.97%	0.0046	22	25	31	65
osm-3(p802); *hsp-1* (RNAi)	PBS control	13.33 ± 0.41***	-	6.3e-08	15†††	17†	22	60
	Ethosuximide (1)	19.13 ± 0.81***	43.51%	0.0e+00	22†††	27†††	29	60
osm-3(p802); *daf-16a* (RNAi)	PBS control	15.06 ± 0.46***	-	0.0e+00	17†	20	22	60
	Ethosuximide (1)	17.03 ± 0.58*	13.08%	0.0102	20	22	25	60
lin-25(n756)X; *juIs76*[P_{unc-25}::GFP + *lin-15(+)*]	PBS control	15.28 ± 0.41	-	-	18	20	22	102
	Ethosuximide (0.1)	16.02 ± 0.59	4.84%	0.1813	19	20	22	50
	Ethosuximide (0.2)	14.53 ± 0.58	-4.91%	0.5148	18	20	22	50
	Ethosuximide (0.5)	14.99 ± 0.79	-1.90%	0.8618	20	21	22	50
	Ethosuximide (1)	14.61 ± 0.65	-4.38%	0.8320	18	20	22	52
	Ethosuximide (2)	14.56 ± 0.76	-4.71%	0.5504	18†	19†	22	52
bkIs10 [P_{aex-3}::*h4R1N TauV337M* + P_{myo-2}::*GFP*]	PBS control	10.94 ± 0.27	-	-	13	14	16	102
	Ethosuximide (0.0001)	13.18 ± 0.49**	20.48%	0.0002	16	17	20	52
	Ethosuximide (0.001)	13.51± 0.27***	23.49%	1.1e-06	15†	16	17	52
	Ethosuximide (0.01)	13.80 ± 0.52***	26.14%	5.6e-06	15†	20	21	52
	Ethosuximide (0.1)	13.79 ± 0.36***	26.05%	8.8e-09	16†††	18†	20	102
	Ethosuximide (0.2)	14.04 ± 0.36***	28.34%	2.4e-09	16†††	17†	20	102
	Ethosuximide (0.5)	13.76 ± 0.34***	25.78%	5.6e-09	15†††	16†	19	102
	Ethosuximide (1)	14.17 ± 0.37***	29.52%	0.0e+00	16††	19	20	102
	Ethosuximide (2)	15.50 ± 0.40***	41.68%	0.0e+00	18†††	20†	21	102
	PBS control	11.28 ± 0.30	-	-	13	14	17	92
	PBS control + Kanamycin	15.50 ± 0.46***	37.41%	0.0e+00	17†††	19†	25	81
	Ethosuximide (1)	16.71 ± 0.51***	48.14%	0.0e+00	21	23	25	80
	Ethosuximide (1) + Kanamycin	19.41 ± 0.60***	72.07%	0.0e+00	23	25	29	80
cca-1(ad1650)	PBS control	17.50 ± 0.55	-	-	21	24	27	108
	Ethosuximide (1)	17.82 ± 0.57	1.83%	0.5423	21	26	27	107
bkIs10 [P_{aex-3}::*h4R1N TauV337M* + P_{myo-2}::*GFP*]	PBS control	11.45 ± 0.33	-	-	14	15	17	116
	Ethosuximide (1)	14.80 ± 0.43***	29.26%	6.5e-09	17††	19†	22	116
CK10; *cca-1(ad1650)*	PBS control	11.27 ± 0.31	-	-	14	15	19	114
	Ethosuximide (1)	14.27 ± 0.35***	26.62%	2.2e-09	16	17††	23	112
rmIs126 [Punc-54::Q0::YFP::unc-54 3'-UTR]	PBS control	18.60 ± 0.43	-	-	21	23	27	81
	Ethosuximide (1)	17.25 ± 0.67	-7.26%	0.2014	20	21	25	60
rmIs130 [Punc-54::Q24::YFP::unc-54 3'-UTR]	PBS control	17.12 ± 0.54	-	-	20	23	25	62
	Ethosuximide (1)	20.57 ± 0.70***	20.15%	0.0005	23††	25††	27	50

Strains	Drug treatments$^{\Delta}$ (mg/ml)	Mean lifespan ± S.E.M (days)	% Change in mean lifespan§	*p*-value	75% mortality (days)	90% mortality (days)	Maximum (days)	Total number of worms analysed
rmIs132 [Punc-54::Q35::YFP::unc-54 3'-UTR]	PBS control	12.21 ± 0.31	-	-	14	16	18	66
	Ethosuximide (1)	14.80 ± 0.50***	21.21%	9.1e-06	16††	20	21	51
rmIs133 [Punc-54::Q40::YFP::unc-54 3'-UTR]	PBS control	14.06 ± 0.24	-	-	16	18	20	77
	Ethosuximide (1)	15.87 ± 0.34***	12.87%	4.0e-05	18††	20	25	88

Table A2: Statistical analysis of lifespan extension in *C. elegans*. Adult mean lifespan ± SEM in days observed in lifespan analysis. The strains and concentrations of the drugs tested were indicated. Lifespan experiments were carried out at 20°C. We used Online Application for the Survival Analysis of Lifespan Assays (OASIS; http://sbi.postech.ac.kr/oasis/introduction/) (Yang *et al.*, 2011) for statistical analysis and to determine means and percentiles. Mean lifespans were compared using the log-rank (Mantel-Cox) test (**p*<0.05; ***p*<0.005;****p*<0.0001), and mortality at more specific time points was compared using Fisher's exact test ($^{\dagger}p$<0.05 $^{\dagger\dagger}p$<0.005; $^{\dagger\dagger\dagger}p$<0.0001). ΔDrug treatments were from conception until death. PBS was used to solubilise ethosuximide, and PBS alone was the control treatment for ethosuximide. For the antibiotic kanamycin treatment of OP50 *E.coli*, 80 µl of 10 mM kanamycin solubilised by water was added after 24 hours of bacterial growth as described, kanamycin alone was the control treatment for kanamycin + ethosuximide combined treatment. §The percentage change and the statistical significance of this change were determined by comparing the experimental ethosuximide treatments to PBS control. The experimental treatment kanamycin + ethosuximide was compared to kanamycin.

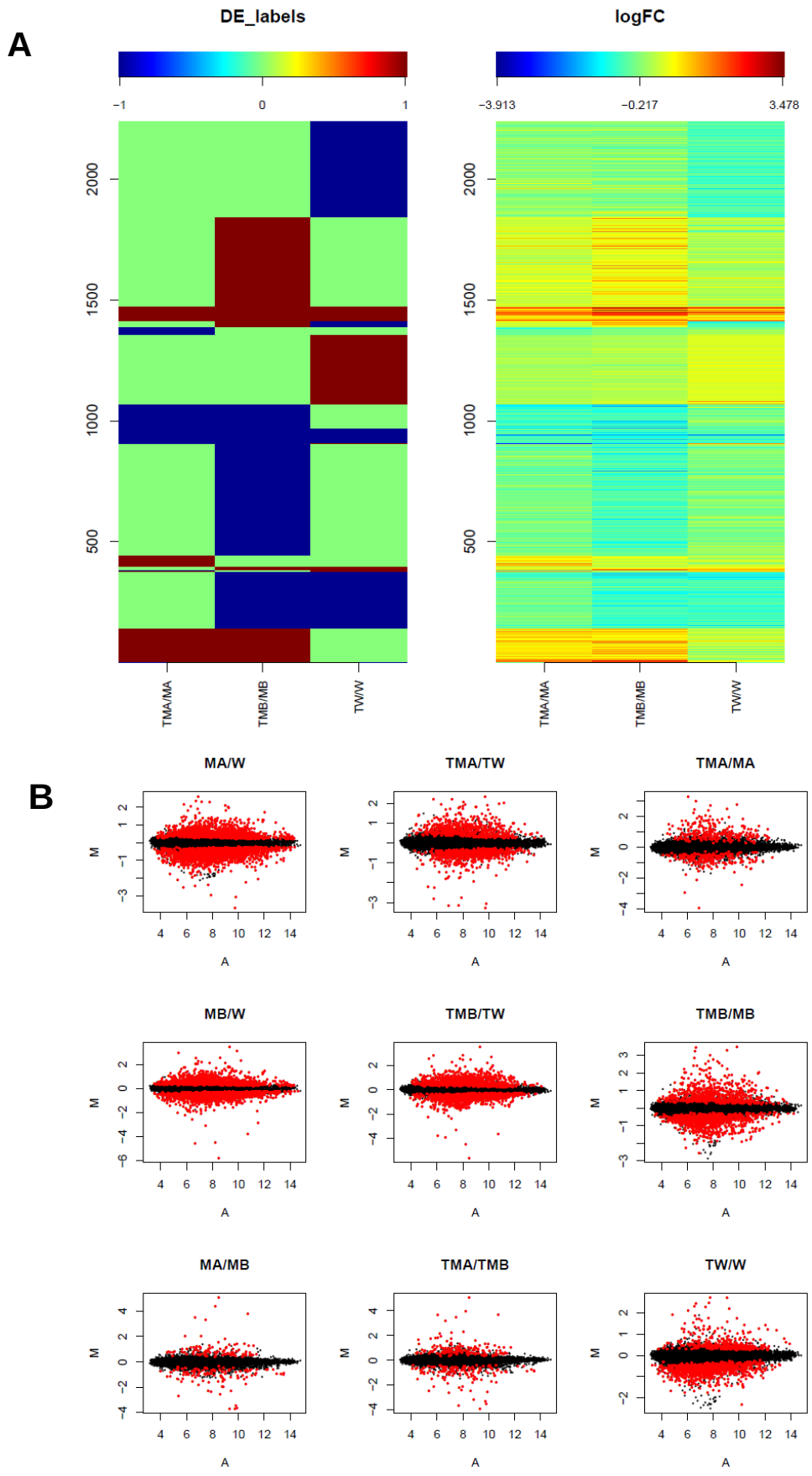

Figure S5.1 A) Heatmap for contrast between ethosuximide-treated group with corresponding untreated sample groups. B) The M-A plot illustrates the estimated log_2FC values for 9 contrasts. Log_2 FC (M) vs mean log_2 expression (A) plot for each contrast. The DEGs are highlighted as red colour.

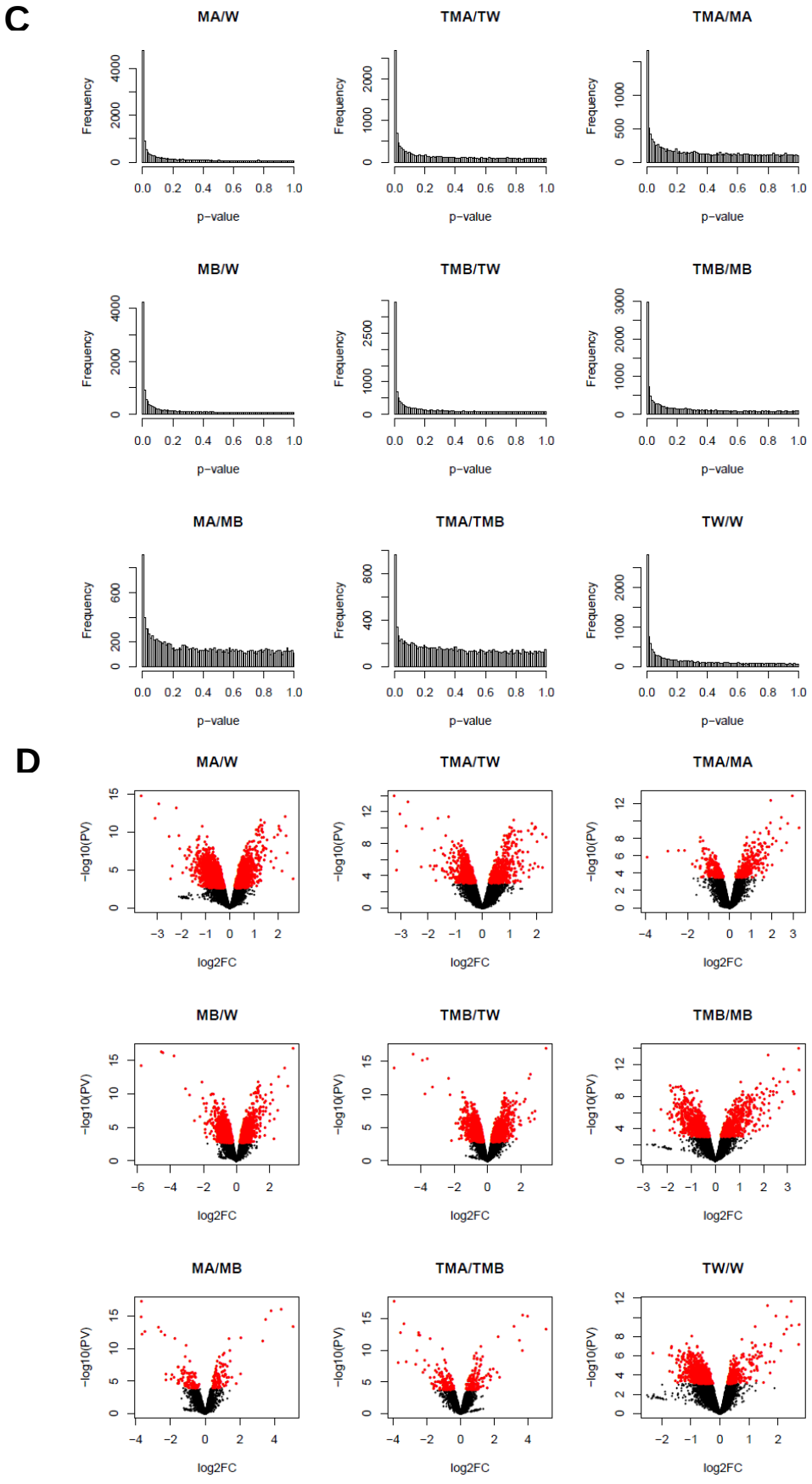

Figure S5.1 C) Histogram of *p*-values. The plot shows the significance test results of estimated logFC for each contrast. Each panel is for one contrast. The first bar in the left end in each panel shows how many probe-set are with *p*-value < 0.01, in corresponding contrast. D) Volcano scatter plot of -$\log_{10}$ *p*-values vs $\log_2$ FC. The DEGs are highlighted as red colour.

E

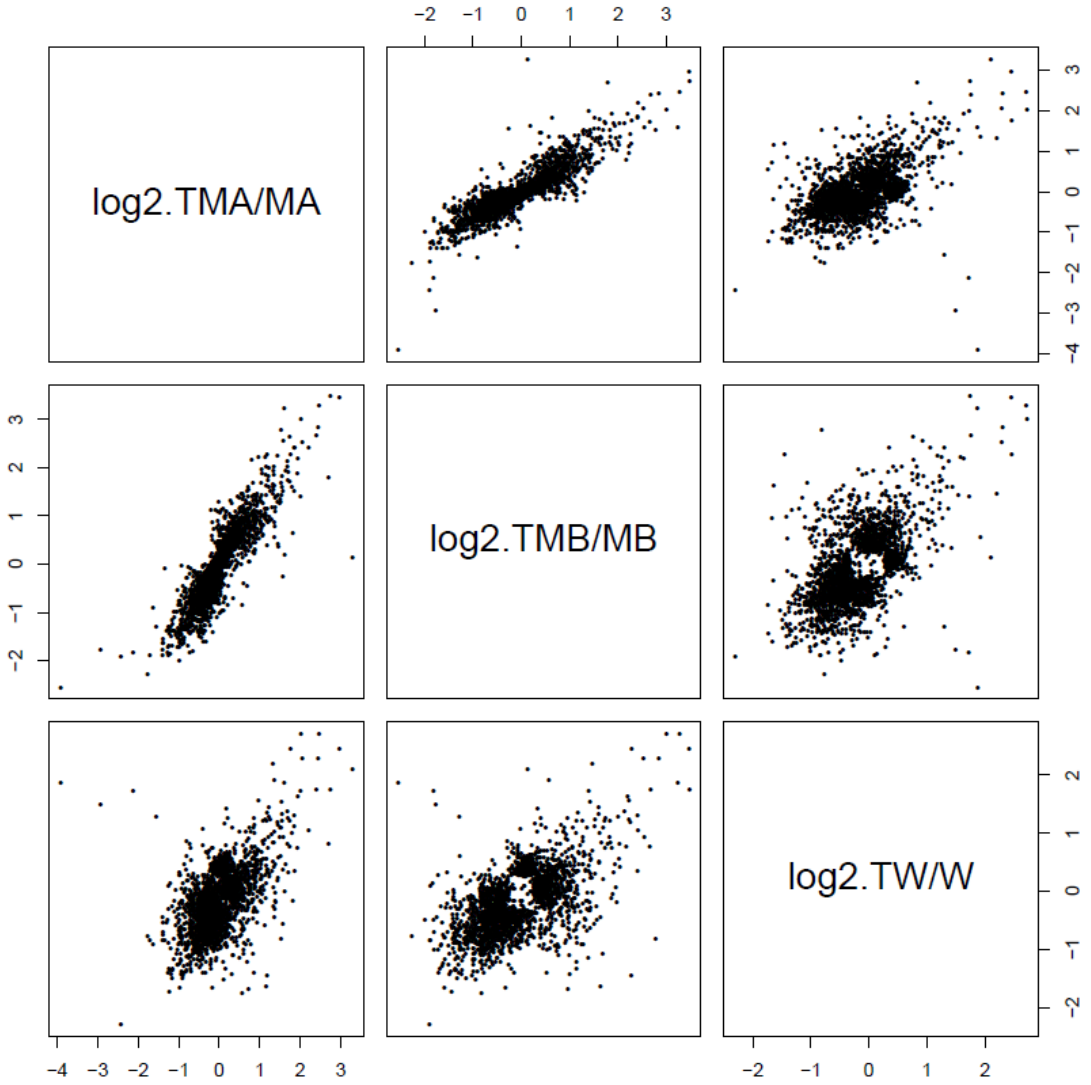

Figure S5.1 E) Pairwise scatter plot of log_2FC of DE probe-set identified from contrasts of sample groups.

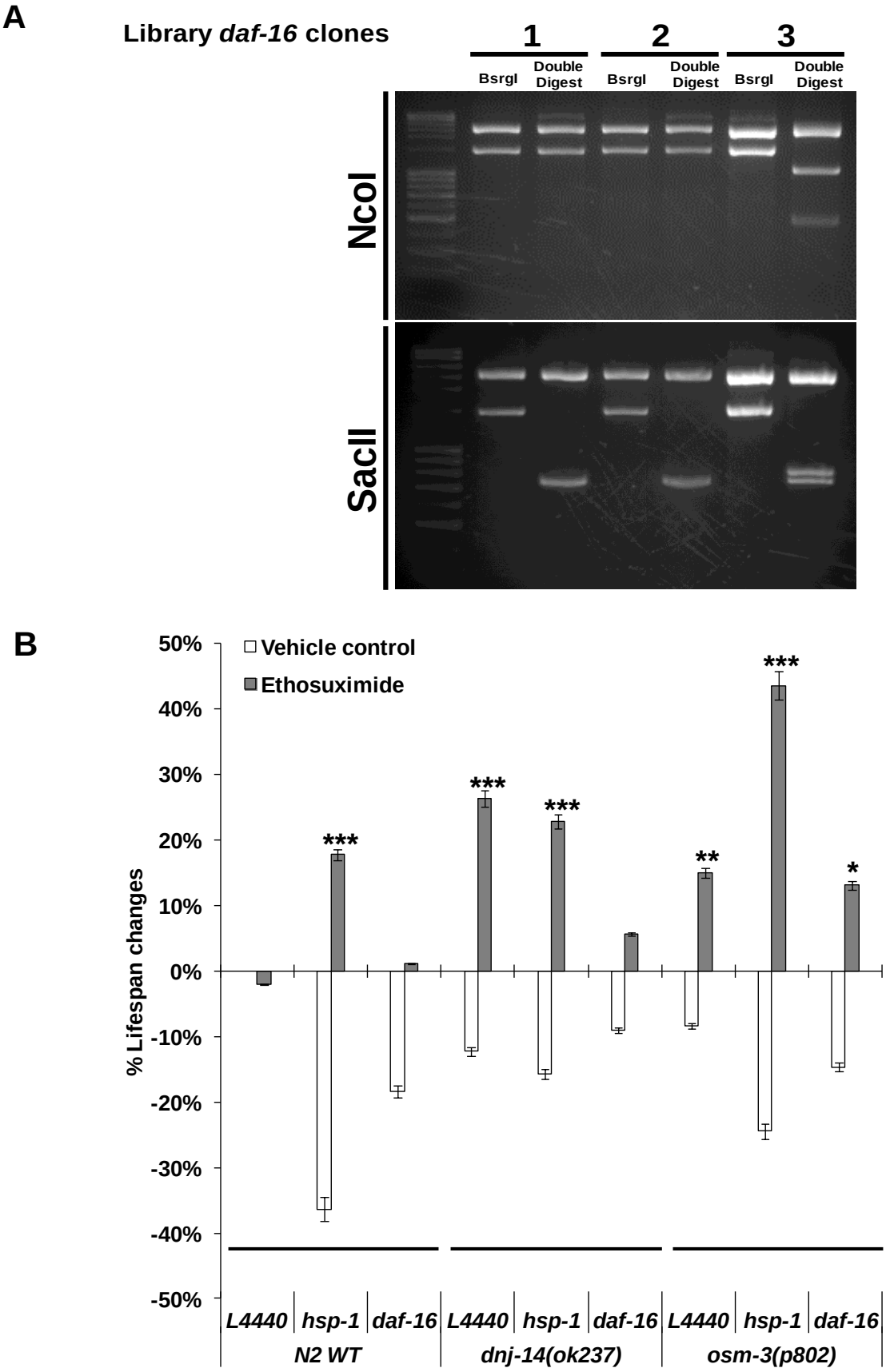

Figure S5.2 A) Restriction analysis identified one of the 3 *daf-16* clones in Vidal *C. elegans* ORF RNAi Library as *daf-16* isoform a (*daf-16a*). B) Percent mean lifespan differences between RNAi fed mutants and WT control worms treated with either vehicle control or ethosuximide. Bars represent the degree of lifespan shortening or extension relative to control (*p<0.05; **p<0.005;***p<0.0001).

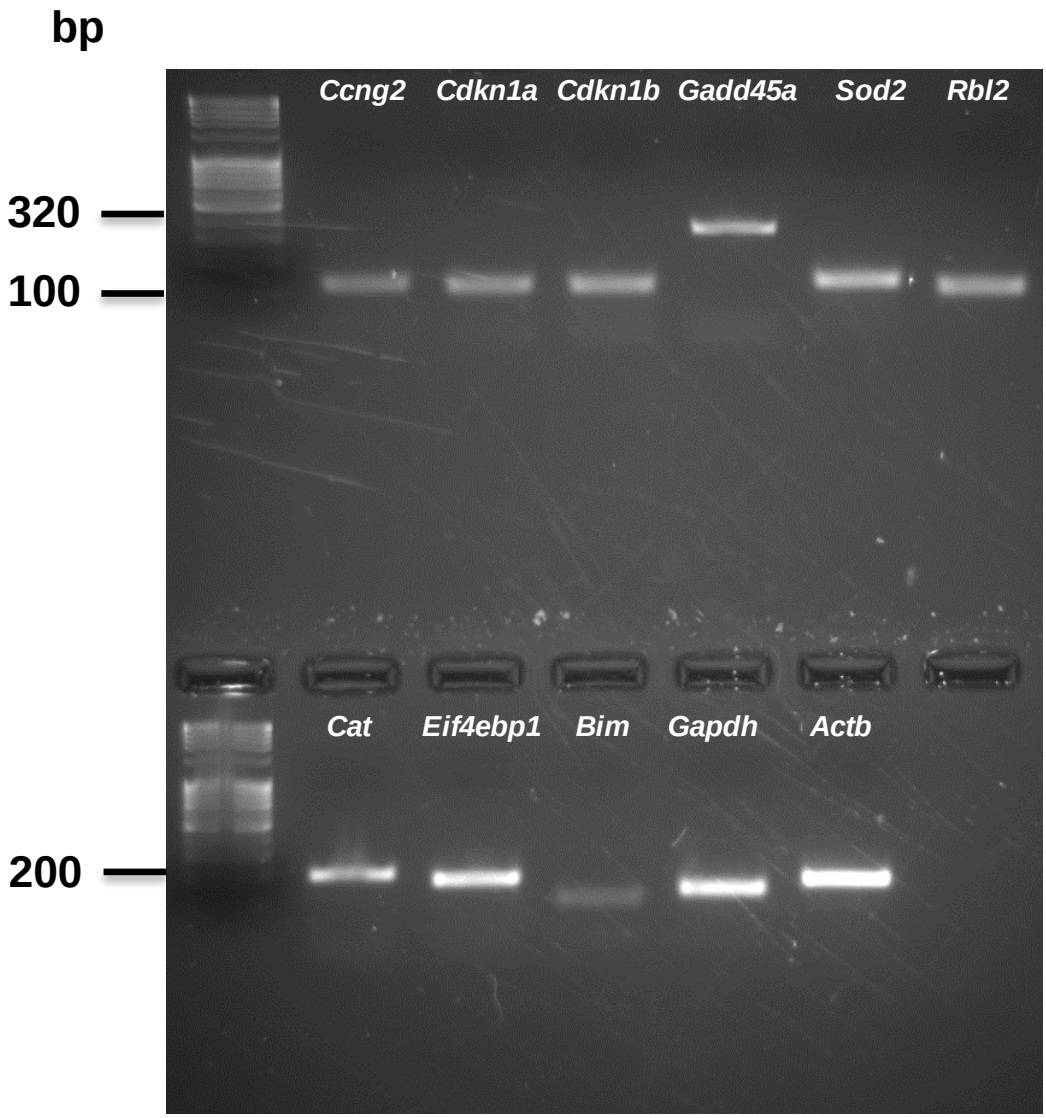

Figure S5.3 Mouse qRT-PCR primers obtained from PrimerBank were validated by RT-PCR and gel electrophoresis (Table 2.2)

BIBLIOGRAPHY

ABBAS, S. & WINK, M. 2009. Epigallocatechin gallate from green tea (Camellia sinensis) increases lifespan and stress resistance in *Caenorhabditis elegans*. *Planta Med,* 75**,** 216-21.

ABBAS, S. & WINK, M. 2010. Epigallocatechin gallate inhibits beta amyloid oligomerization in *Caenorhabditis elegans* and affects the daf-2/insulin-like signaling pathway. *Phytomedicine,* 17**,** 902-909.

ACKERMAN, D. & GEMS, D. 2012. Insulin/IGF-1 and hypoxia signaling act in concert to regulate iron homeostasis in *Caenorhabditis elegans*. *PLoS Genet,* 8**,** e1002498.

AITLHADJ, L., AVILA, D. S., BENEDETTO, A., ASCHNER, M. & STURZENBAUM, S. R. 2011. Environmental exposure, obesity, and Parkinson's disease: lessons from fat and old worms. *Environ Health Perspect,* 119**,** 20-8.

AITLHADJ, L. & STUERZENBAUM, S. R. 2010. The use of FUdR can cause prolonged longevity in mutant nematodes. *Mechanisms of Ageing and Development,* 131**,** 364-365.

ALAVEZ, S., VANTIPALLI, M. C., ZUCKER, D. J., KLANG, I. M. & LITHGOW, G. J. 2011. Amyloid-binding compounds maintain protein homeostasis during ageing and extend lifespan. *Nature,* 472**,** 226-9.

ALTAR, C. A., VAWTER, M. P. & GINSBERG, S. D. 2008. Target identification for CNS diseases by transcriptional profiling. *Neuropsychopharmacology,* 34**,** 18-54.

ANTEBI, A. 2007. Genetics of aging in *Caenorhabditis elegans*. *PLoS Genet,* 3**,** 1565-71.

APFELD, J. & KENYON, C. 1999. Regulation of lifespan by sensory perception in *Caenorhabditis elegans*. *Nature,* 402**,** 804-9.

ARLT, A., BAUER, I., SCHAFMAYER, C., TEPEL, J., MUERKOSTER, S. S., BROSCH, M., RODER, C., KALTHOFF, H., HAMPE, J., MOYER, M. P., FOLSCH, U. R. & SCHAFER, H. 2009. Increased proteasome subunit protein expression and proteasome activity in colon cancer relate to an enhanced activation of nuclear factor E2-related factor 2 (Nrf2). *Oncogene,* 28**,** 3983-96.

ARRASATE, M., MITRA, S., SCHWEITZER, E. S., SEGAL, M. R. & FINKBEINER, S. 2004. Inclusion body formation reduces levels of mutant huntingtin and the risk of neuronal death. *Nature,* 431**,** 805-10.

ARTAL-SANZ, M., DE JONG, L. & TAVERNARAKIS, N. 2006. *Caenorhabditis elegans*: a versatile platform for drug discovery. *Biotechnol J,* 1**,** 1405-18.

ARYA, U., DWIVEDI, H. & SUBRAMANIAM, J. R. 2009. Reserpine ameliorates Abeta toxicity in the Alzheimer's disease model in *Caenorhabditis elegans*. *Exp Gerontol,* 44**,** 462-6.

ASCHNER, M., CHEN, P., MARTINEZ-FINLEY, E. J., BORNHORST, J. & CHAKRABORTY, S. 2013. Metal-induced neurodegeneration in *C. elegans*. *Frontiers in Aging Neuroscience,* 5.

ASH, P. E., BIENIEK, K. F., GENDRON, T. F., CAULFIELD, T., LIN, W. L., DEJESUS-HERNANDEZ, M., VAN BLITTERSWIJK, M. M., JANSEN-WEST, K., PAUL, J. W., 3RD, RADEMAKERS, R., BOYLAN, K. B., DICKSON, D. W. & PETRUCELLI, L. 2013. Unconventional translation of C9ORF72 GGGGCC expansion generates insoluble polypeptides specific to c9FTD/ALS. *Neuron,* 77**,** 639-46.

ASH, P. E., ZHANG, Y. J., ROBERTS, C. M., SALDI, T., HUTTER, H., BURATTI, E., PETRUCELLI, L. & LINK, C. D. 2010. Neurotoxic effects of TDP-43 overexpression in *C. elegans*. *Hum Mol Genet,* 19**,** 3206-18.

AYYADEVARA, S., BHARILL, P., DANDAPAT, A., HU, C., KHAIDAKOV, M., MITRA, S., SHMOOKLER REIS, R. J. & MEHTA, J. L. 2013. Aspirin inhibits oxidant stress, reduces age-associated functional declines, and extends lifespan of *Caenorhabditis elegans*. *Antioxid Redox Signal,* 18**,** 481-90.

BANSAL, A., KWON, E.-S., CONTE, D., LIU, H., GILCHRIST, M., MACNEIL, L. & TISSENBAUM, H. 2014. Transcriptional regulation of *Caenorhabditis elegans* FOXO/DAF-16 modulates lifespan. *Longevity & Healthspan,* 3**,** 5.

BARBER, S. C. & SHAW, P. J. 2010. Oxidative stress in ALS: key role in motor neuron injury and therapeutic target. *Free Radic Biol Med,* 48**,** 629-41.

BARGMANN, C. I. 1998. Neurobiology of the *Caenorhabditis elegans* genome. *Science,* 282**,** 2028-33.

BASSILANA, F., MACE, N., LI, Q., STUTZMANN, J. M., GROSS, C. E., PRADIER, L., BENAVIDES, J., MÉNAGER, J. & BEZARD, E. 2005. Unraveling substantia nigra sequential gene expression in a progressive MPTP-lesioned macaque model of Parkinson's disease. *Neurobiology of Disease,* 20**,** 93-103.

BATES, E. A., VICTOR, M., JONES, A. K., SHI, Y. & HART, A. C. 2006. Differential contributions of *Caenorhabditis elegans* histone deacetylases to huntingtin polyglutamine toxicity. *J Neurosci,* 26**,** 2830-8.

BENITEZ, B. A., ALVARADO, D., CAI, Y., MAYO, K., CHAKRAVERTY, S., NORTON, J., MORRIS, J. C., SANDS, M. S., GOATE, A. & CRUCHAGA, C. 2011. Exome-sequencing confirms *DNAJC5* mutations as cause of Adult Neuronal Ceroid-Lipofuscinosis. *PLoS ONE,* 6**,** e26741.

BENJAMINI, Y. & HOCHBERG, Y. 1995. Controlling the False Discovery Rate: a practical and powerful approach to multiple testing. *Journal of the Royal Statistical Society. Series B (Methodological),* 57**,** 289-300.

BERGER, Z., TTOFI, E. K., MICHEL, C. H., PASCO, M. Y., TENANT, S., RUBINSZTEIN, D. C. & O'KANE, C. J. 2005. Lithium rescues toxicity of aggregate-prone proteins in *Drosophila* by perturbing Wnt pathway. *Human Molecular Genetics,* 14**,** 3003-3011.

BERTRAM, L., LILL, C. M. & TANZI, R. E. 2010. The genetics of Alzheimer disease: back to the future. *Neuron,* 68**,** 270-81.

BETARBET, R., CANET-AVILES, R. M., SHERER, T. B., MASTROBERARDINO, P. G., MCLENDON, C., KIM, J. H., LUND, S., NA, H. M., TAYLOR, G., BENCE, N. F., KOPITO, R., SEO, B. B., YAGI, T., YAGI, A., KLINEFELTER, G., COOKSON, M. R. & GREENAMYRE, J. T. 2006. Intersecting pathways to neurodegeneration in Parkinson's disease: effects of the pesticide rotenone on DJ-1, alpha-synuclein, and the ubiquitin-proteasome system. *Neurobiol Dis,* 22**,** 404-20.

BIRKENKAMP, K. U. & COFFER, P. J. 2003. Regulation of cell survival and proliferation by the FOXO (Forkhead box, class O) subfamily of Forkhead transcription factors. *Biochem Soc Trans,* 31**,** 292-7.

BIZAT, N., PEYRIN, J.-M., HAÏK, S., COCHOIS, V., BEAUDRY, P., LAPLANCHE, J.-L. & NÉRI, C. 2010. Neuron dysfunction is induced by prion protein with an insertional mutation via a Fyn kinase and reversed by Sirtuin activation in *Caenorhabditis elegans*. *The Journal of Neuroscience,* 30**,** 5394-5403.

BOCCITTO, M., LAMITINA, T. & KALB, R. G. 2012. Daf-2 signaling modifies mutant SOD1 toxicity in *C. elegans*. *PLoS One,* 7**,** e33494.

BOEHLER, C. J., RAINES, A. M. & SUNDE, R. A. 2014. Toxic-selenium and low-selenium transcriptomes in *Caenorhabditis elegans*: toxic selenium up-regulates oxidoreductase and down-regulates cuticle-associated genes. *PLoS One,* 9**,** e101408.

BOILLÉE, S., VANDE VELDE, C. & CLEVELAND, DON W. 2006. ALS: A disease of motor neurons and their nonneuronal neighbors. *Neuron,* 52**,** 39-59.

BOND, M., HOLTHAUS, S.-M. K., TAMMEN, I., TEAR, G. & RUSSELL, C. 2013. Use of model organisms for the study of neuronal ceroid lipofuscinosis. *Biochimica et Biophysica Acta (BBA) - Molecular Basis of Disease,* 1832**,** 1842-1865.

BONIN, M., POTHS, S., OSAKA, H., WANG, Y. L., WADA, K. & RIESS, O. 2004. Microarray expression analysis of gad mice implicates involvement of Parkinson's disease associated UCH-L1 in multiple metabolic pathways. *Molecular Brain Research,* 126**,** 88-97.

BOROVECKI, F., LOVRECIC, L., ZHOU, J., JEONG, H., THEN, F., ROSAS, H. D., HERSCH, S. M., HOGARTH, P., BOUZOU, B., JENSEN, R. V. & KRAINC, D. 2005. Genome-wide expression profiling of human blood reveals biomarkers for Huntington's disease. *Proc Natl Acad Sci U S A,* 102**,** 11023-8.

BOUSTANY, R. M. 2013. Lysosomal storage diseases--the horizon expands. *Nat Rev Neurol,* 9**,** 583-98.

BOYD, W. A., SMITH, M. V., KISSLING, G. E. & FREEDMAN, J. H. 2010. Medium- and high-throughput screening of neurotoxicants using *C. elegans*. *Neurotoxicol Teratol,* 32**,** 68-73.

BRANDT, R., GERGOU, A., WACKER, I., FATH, T. & HUTTER, H. 2009. A *Caenorhabditis elegans* model of tau hyperphosphorylation: induction of developmental defects by transgenic overexpression of Alzheimer's disease-like modified tau. *Neurobiol Aging,* 30**,** 22-33.

BRAS, J., VERLOES, A., SCHNEIDER, S. A., MOLE, S. E. & GUERREIRO, R. J. 2012. Mutation of the parkinsonism gene ATP13A2 causes neuronal ceroid-lipofuscinosis. *Hum Mol Genet,* 21**,** 2646-50.

BRAUNGART, E., GERLACH, M., RIEDERER, P., BAUMEISTER, R. & HOENER, M. C. 2004. *Caenorhabditis elegans* MPP+ model of Parkinson's disease for high-throughput drug screenings. *Neurodegener Dis,* 1**,** 175-83.

BRENNER, S. 1974. The genetics of *Caenorhabditis elegans*. *Genetics,* 77**,** 71-94.

BRIESE, M., ESMAEILI, B., FRABOULET, S., BURT, E. C., CHRISTODOULOU, S., TOWERS, P. R., DAVIES, K. E. & SATTELLE, D. B. 2009. Deletion of smn-1, the *Caenorhabditis elegans* ortholog of the spinal muscular atrophy gene, results in locomotor dysfunction and reduced lifespan. *Hum Mol Genet,* 18**,** 97-104.

BRIGNULL, H., MORLEY, J. & MORIMOTO, R. 2007. The stress of misfolded proteins: *C. elegans* models for neurodegenerative disease and aging. *Adv Exp Med Biol,* 594**,** 167 - 189.

BRIGNULL, H. R., MOORE, F. E., TANG, S. J. & MORIMOTO, R. I. 2006a. Polyglutamine proteins at the pathogenic threshold display neuron-specific aggregation in a pan-neuronal *Caenorhabditis elegans* model. *The Journal of Neuroscience,* 26**,** 7597-7606.

BRIGNULL, H. R., MORLEY, J. F., GARCIA, S. M. & MORIMOTO, R. I. 2006b. Modeling polyglutamine pathogenesis in *C. elegans*. *Methods Enzymol,* 412**,** 256-82.

BROWN, M. K., EVANS, J. L. & LUO, Y. 2006. Beneficial effects of natural antioxidants EGCG and alpha-lipoic acid on life span and age-dependent behavioral declines in *Caenorhabditis elegans*. *Pharmacol Biochem Behav,* 85**,** 620-8.

BUDOVSKAYA, Y., WU, K., SOUTHWORTH, L., JIANG, M., TEDESCO, P., JOHNSON, T. & KIM, S. 2008. An elt-3/elt-5/elt-6 GATA transcription circuit guides aging in *C. elegans*. *Cell,* 134**,** 291 - 303.

BURNEO, J. G., ARNOLD, T., PALMER, C. A., KUZNIECKY, R. I., OH, S. J. & FAUGHT, E. 2003. Adult-onset neuronal ceroid lipofuscinosis (Kufs disease) with autosomal dominant inheritance in Alabama. *Epilepsia,* 44**,** 841-6.

BURNS, A. R., KWOK, T. C., HOWARD, A., HOUSTON, E., JOHANSON, K., CHAN, A., CUTLER, S. R., MCCOURT, P. & ROY, P. J. 2006. High-throughput screening of small molecules for bioactivity and target identification in *Caenorhabditis elegans*. *Nat Protoc,* 1**,** 1906-14.

BURNS, A. R., WALLACE, I. M., WILDENHAIN, J., TYERS, M., GIAEVER, G., BADER, G. D., NISLOW, C., CUTLER, S. R. & ROY, P. J. 2010. A predictive model for drug bioaccumulation and bioactivity in *Caenorhabditis elegans*. *Nat Chem Biol,* 6**,** 549-57.

BUSSEMAKER, H. J., LI, H. & SIGGIA, E. D. 2000. Building a dictionary for genomes: identification of presumptive regulatory sites by statistical analysis. *Proc Natl Acad Sci U S A,* 97**,** 10096-100.

CABREIRO, F., AU, C., LEUNG, K. Y., VERGARA-IRIGARAY, N., COCHEME, H. M., NOORI, T., WEINKOVE, D., SCHUSTER, E., GREENE, N. D. & GEMS, D. 2013. Metformin retards aging in *C. elegans* by altering microbial folate and methionine metabolism. *Cell,* 153**,** 228-39.

CÁCERES, I. D. C., VALMAS, N., HILLIARD, M. A. & LU, H. 2012. Laterally orienting *C. elegans* using geometry at microscale for high-throughput visual screens in neurodegeneration and neuronal development studies. *PLoS One,* 7**,** e35037.

CADIEUX-DION, M., ANDERMANN, E., LACHANCE-TOUCHETTE, P., ANSORGE, O., MELOCHE, C., BARNABE, A., KUZNIECKY, R. I., ANDERMANN, F., FAUGHT, E., LEONBERG, S., DAMIANO, J. A., BERKOVIC, S. F., ROULEAU, G. A. & COSSETTE, P. 2013. Recurrent mutations in DNAJC5 cause autosomal dominant Kufs disease. *Clin Genet,* 83**,** 571-5.

CAI, W. J., HUANG, J. H., ZHANG, S. Q., WU, B., KAPAHI, P., ZHANG, X. M. & SHEN, Z. Y. 2011. Icariin and its derivative Icariside II extend healthspan via Insulin/IGF-1 pathway in *C. elegans*. *Plos One,* 6.

CAITO, S., FRETHAM, S., MARTINEZ-FINLEY, E., CHAKRABORTY, S., AVILA, D., CHEN, P. & ASCHNER, M. 2012. Genome-wide analyses of metal responsive genes in *Caenorhabditis elegans*. *Front Genet,* 3**,** 52.

CALAMINI, B., SILVA, M., MADOUX, F., HUTT, D., KHANNA, S., CHALFANT, M., SALDANHA, S., HODDER, P., TAIT, B. & GARZA, D. 2011. Small-molecule proteostasis regulators for protein conformational diseases. *Nat Chem Biol,* 8**,** 185 - 196.

CALDWELL, G. A., CALDWELL, K. A. & CAO, S. 2008. Methods of using small molecule compounds for neuroprotection. Google Patents.

CALDWELL, K. A., HARRINGTON, A. J., HAMAMICHI, S. & CALDWELL, G. A. 2010. *C. elegans* as a model organism to investigate molecular pathways involved with Parkinson's disease. *Developmental Dynamics,* 239**,** 1282-1295.

CALDWELL, K. A., TUCCI, M. L., ARMAGOST, J., HODGES, T. W., CHEN, J., MEMON, S. B., BLALOCK, J. E., DELEON, S. M., FINDLAY, R. H., RUAN, Q., WEBBER, P. J., STANDAERT, D. G., OLSON, J. B. & CALDWELL, G. A. 2009. Investigating bacterial sources of toxicity as an environmental contributor to dopaminergic neurodegeneration. *PLoS One,* 4**,** e7227.

CAMPION, D., DUMANCHIN, C., HANNEQUIN, D., DUBOIS, B., BELLIARD, S., PUEL, M., THOMAS-ANTERION, C., MICHON, A., MARTIN, C., CHARBONNIER, F., RAUX, G., CAMUZAT, A., PENET, C., MESNAGE, V., MARTINEZ, M., CLERGET-DARPOUX, F., BRICE, A. & FREBOURG, T. 1999. Early-onset autosomal dominant Alzheimer disease: prevalence, genetic heterogeneity, and mutation spectrum. *Am J Hum Genet,* 65**,** 664-70.

CAO, S., GELWIX, C. C., CALDWELL, K. A. & CALDWELL, G. A. 2005. Torsin-mediated protection from cellular stress in the dopaminergic neurons of *Caenorhabditis elegans*. *J Neurosci,* 25**,** 3801-3812.

CARMICHAEL, J., SUGARS, K. L., BAO, Y. P. & RUBINSZTEIN, D. C. 2002. Glycogen synthase kinase-3β inhibitors prevent cellular polyglutamine toxicity caused by the Huntington's disease mutation. *Journal of Biological Chemistry,* 277**,** 33791-33798.

CHAMBERLAIN, L. H. & BURGOYNE, R. D. 2000. Cysteine-string protein: the chaperone at the synapse. *J Neurochem,* 74**,** 1781-9.
CHAN, E. Y., LUTHI-CARTER, R., STRAND, A., SOLANO, S. M., HANSON, S. A., DEJOHN, M. M., KOOPERBERG, C., CHASE, K. O., DIFIGLIA, M., YOUNG, A. B., LEAVITT, B. R., CHA, J. H., ARONIN, N., HAYDEN, M. R. & OLSON, J. M. 2002. Increased huntingtin protein length reduces the number of polyglutamine-induced gene expression changes in mouse models of Huntington's disease. *Hum Mol Genet,* 11**,** 1939-51.
CHANDRA, S., GALLARDO, G., FERNANDEZ-CHACON, R., SCHLUTER, O. M. & SUDHOF, T. C. 2005. Alpha-synuclein cooperates with CSPalpha in preventing neurodegeneration. *Cell,* 123**,** 383-96.
CHAUDHURI, K. R., HEALY, D. G. & SCHAPIRA, A. H. 2006. Non-motor symptoms of Parkinson's disease: diagnosis and management. *Lancet Neurol,* 5**,** 235-45.
CHEGE, P. M. & MCCOLL, G. 2014. *Caenorhabditis elegans*: a model to investigate oxidative stress and metal dyshomeostasis in Parkinson's disease. *Front Aging Neurosci,* 6**,** 89.
CHEN, J., QUAN, Q. Y., YANG, F., WANG, Y., WANG, J. C., ZHAO, G. & JIANG, W. 2010. Effects of lamotrigine and topiramate on hippocampal neurogenesis in experimental temporal-lobe epilepsy. *Brain Res,* 1313**,** 270-82.
CHEN, S., SAYANA, P., ZHANG, X. & LE, W. 2013. Genetics of amyotrophic lateral sclerosis: an update. *Molecular Neurodegeneration,* 8**,** 28.
CHEN, X. & BURGOYNE, R. 2012. Identification of common genetic modifiers of neurodegenerative diseases from an integrative analysis of diverse genetic screens in model organisms. *BMC Genomics,* 13**,** 71.
CHENGALVALA, M. V., CHENNATHUKUZHI, V. M., JOHNSTON, D. S., STEVIS, P. E. & KOPF, G. S. 2007. Gene expression profiling and its practice in drug development. *Curr Genomics,* 8**,** 262-70.
CHERNY, R. A., AYTON, S., FINKELSTEIN, D. I., BUSH, A. I., MCCOLL, G. & MASSA, S. M. 2012. PBT2 reduces toxicity in a *C. elegans* model of polyQ aggregation and extends lifespan, reduces striatal atrophy and improves motor performance in the R6/2 mouse model of Huntington's disease. *Journal of Huntington's Disease,* 1**,** 211-219.
CHESSELET, M. F., FLEMING, S., MORTAZAVI, F. & MEURERS, B. 2008. Strengths and limitations of genetic mouse models of Parkinson's disease. *Parkinsonism Relat Disord,* 14 Suppl 2**,** S84-7.
CHEW, Y. L., FAN, X., GOTZ, J. & NICHOLAS, H. R. 2013. PTL-1 regulates neuronal integrity and lifespan in *C. elegans*. *J Cell Sci,* 126**,** 2079-91.
CHEW, Y. L., FAN, X., GOTZ, J. & NICHOLAS, H. R. 2014. Regulation of age-related structural integrity in neurons by protein with tau-like repeats (PTL-1) is cell autonomous. *Sci Rep,* 4**,** 5185.
CHING, T. T., CHIANG, W. C., CHEN, C. S. & HSU, A. L. 2011. Celecoxib extends *C. elegans* lifespan via inhibition of insulin-like signaling but not cyclooxygenase-2 activity. *Aging Cell,* 10**,** 506-19.
CHOI, H., SCHNEIDER, H., KLUM, S., CHANDLER-BROWN, D., KAEBERLEIN, M. & SHAMIEH, L. 2013. UV-photoconversion of ethosuximide from a longevity-promoting compound to a potent toxin. *PLoS One,* 8**,** e82543.
CHOPRA, V., FOX, J. H., LIEBERMAN, G., DORSEY, K., MATSON, W., WALDMEIER, P., HOUSMAN, D. E., KAZANTSEV, A., YOUNG, A. B. & HERSCH, S. 2007. A small-molecule therapeutic lead for Huntington's disease: preclinical pharmacology and efficacy of C2-8 in the R6/2 transgenic mouse. *Proc Natl Acad Sci U S A,* 104**,** 16685-9.

CHRISTIE, N. T., LEE, A. L., FAY, H. G., GRAY, A. A. & KIKIS, E. A. 2014. Novel polyglutamine model uncouples proteotoxicity from aging. *PLoS One,* 9**,** e96835.

CINAR, H., KELES, S. & JIN, Y. 2005. Expression profiling of GABAergic motor neurons in *Caenorhabditis elegans*. *Curr Biol,* 15**,** 340-6.

CIOSK, R., DEPALMA, M. & PRIESS, J. R. 2004. ATX-2, the *C. elegans* ortholog of ataxin 2, functions in translational regulation in the germline. *Development,* 131**,** 4831-41.

COHEN, E., BIESCHKE, J., PERCIAVALLE, R., KELLY, J. & DILLIN, A. 2006. Opposing activities protect against age-onset proteotoxicity. *Science,* 313**,** 1604 - 1610.

COHEN, E. & DILLIN, A. 2008. The insulin paradox: aging, proteotoxicity and neurodegeneration. *Nat Rev Neurosci,* 9**,** 759-67.

COLANGELO, V., SCHURR, J., BALL, M. J., PELAEZ, R. P., BAZAN, N. G. & LUKIW, W. J. 2002. Gene expression profiling of 12633 genes in Alzheimer hippocampal CA1: transcription and neurotrophic factor down-regulation and up-regulation of apoptotic and pro-inflammatory signaling. *J Neurosci Res,* 70**,** 462-73.

COLLINS, J. J., EVASON, K., PICKETT, C. L., SCHNEIDER, D. L. & KORNFELD, K. 2008. The anticonvulsant ethosuximide disrupts sensory function to extend *C. elegans* lifespan. *PLoS Genet,* 4**,** e1000230.

COLOSIMO, M. E., BROWN, A., MUKHOPADHYAY, S., GABEL, C., LANJUIN, A. E., SAMUEL, A. D. & SENGUPTA, P. 2004. Identification of thermosensory and olfactory neuron-specific genes via expression profiling of single neuron types. *Curr Biol,* 14**,** 2245-51.

CONTRINO, S., SMITH, R. N., BUTANO, D., CARR, A., HU, F., LYNE, R., RUTHERFORD, K., KALDERIMIS, A., SULLIVAN, J., CARBON, S., KEPHART, E. T., LLOYD, P., STINSON, E. O., WASHINGTON, N. L., PERRY, M. D., RUZANOV, P., ZHA, Z., LEWIS, S. E., STEIN, L. D. & MICKLEM, G. 2012. modMine: flexible access to modENCODE data. *Nucleic Acids Research,* 40**,** D1082-D1088.

COOKSON, M. R. 2010. The role of leucine-rich repeat kinase 2 (LRRK2) in Parkinson's disease. *Nat Rev Neurosci,* 11**,** 791-797.

COOPER, A., GITLER, A., CASHIKAR, A., HAYNES, C., HILL, K., BHULLAR, B., LIU, K., XU, K., STRATHEARN, K. & LIU, F. 2006. Alpha-synuclein blocks ER-Golgi traffic and Rab1 rescues neuron loss in Parkinson's models. *Science,* 313**,** 324 - 328.

CORBETT, A., PICKETT, J., BURNS, A., CORCORAN, J., DUNNETT, S. B., EDISON, P., HAGAN, J. J., HOLMES, C., JONES, E., KATONA, C., KEARNS, I., KEHOE, P., MUDHER, A., PASSMORE, A., SHEPHERD, N., WALSH, F. & BALLARD, C. 2012. Drug repositioning for Alzheimer's disease. *Nat Rev Drug Discov,* 11**,** 833-846.

COULTER, D. A., HUGUENARD, J. R. & PRINCE, D. A. 1989a. Characterization of ethosuximide reduction of low-threshold calcium current in thalamic neurons. *Ann Neurol,* 25**,** 582-93.

COULTER, D. A., HUGUENARD, J. R. & PRINCE, D. A. 1989b. Specific petit mal anticonvulsants reduce calcium currents in thalamic neurons. *Neuroscience Letters,* 98**,** 74-78.

COULTER, D. A., HUGUENARD, J. R. & PRINCE, D. A. 1990. Differential effects of petit mal anticonvulsants and convulsants on thalamic neurones: calcium current reduction. *Br J Pharmacol,* 100**,** 800-6.

CRAWFORD, T. O. & PARDO, C. A. 1996. The neurobiology of childhood spinal muscular atrophy. *Neurobiol Dis,* 3**,** 97-110.

CRUNELLI, V. & LERESCHE, N. 2002. Block of thalamic T-type Ca^{2+} channels by ethosuximide is not the whole story. *Epilepsy Curr,* 2**,** 53-56.

CUI, Y., MCBRIDE, S., BOYD, W., ALPER, S. & FREEDMAN, J. 2007. Toxicogenomic analysis of *Caenorhabditis elegans* reveals novel genes and pathways involved in the resistance to cadmium toxicity. *Genome Biology,* 8**,** R122.

DANGOND, F., HWANG, D., CAMELO, S., PASINELLI, P., FROSCH, M. P., STEPHANOPOULOS, G., BROWN, R. H., JR. & GULLANS, S. R. 2004. Molecular signature of late-stage human ALS revealed by expression profiling of postmortem spinal cord gray matter. *Physiol Genomics,* 16**,** 229-39.

DANIELSON, P. B. 2002. The cytochrome P450 superfamily: biochemistry, evolution and drug metabolism in humans. *Curr Drug Metab,* 3**,** 561-97.

DAVID, D. C., OLLIKAINEN, N., TRINIDAD, J. C., CARY, M. P., BURLINGAME, A. L. & KENYON, C. 2010. Widespread protein aggregation as an inherent part of aging in *C. elegans*. *PLoS Biol,* 8**,** e1000450.

DAVIES, S. K., LEROI, A. M. & BUNDY, J. G. 2012. Fluorodeoxyuridine affects the identification of metabolic responses to *daf-2* status in *Caenorhabditis elegans*. *Mech Ageing Dev,* 133**,** 46-9.

DE JESUS-CORTES, H., XU, P., DRAWBRIDGE, J., ESTILL, S. J., HUNTINGTON, P., TRAN, S., BRITT, J., TESLA, R., MORLOCK, L., NAIDOO, J., MELITO, L. M., WANG, G., WILLIAMS, N. S., READY, J. M., MCKNIGHT, S. L. & PIEPER, A. A. 2012. Neuroprotective efficacy of aminopropyl carbazoles in a mouse model of Parkinson disease. *Proc Natl Acad Sci U S A,* 109**,** 17010-5.

DE VOER, G., PETERS, D. & TASCHNER, P. E. M. 2008. *Caenorhabditis elegans* as a model for lysosomal storage disorders. *Biochimica et Biophysica Acta (BBA) - Molecular Basis of Disease,* 1782**,** 433-446.

DEJESUS-HERNANDEZ, M., MACKENZIE, I. R., BOEVE, B. F., BOXER, A. L., BAKER, M., RUTHERFORD, N. J., NICHOLSON, A. M., FINCH, N. A., FLYNN, H., ADAMSON, J., KOURI, N., WOJTAS, A., SENGDY, P., HSIUNG, G. Y., KARYDAS, A., SEELEY, W. W., JOSEPHS, K. A., COPPOLA, G., GESCHWIND, D. H., WSZOLEK, Z. K., FELDMAN, H., KNOPMAN, D. S., PETERSEN, R. C., MILLER, B. L., DICKSON, D. W., BOYLAN, K. B., GRAFF-RADFORD, N. R. & RADEMAKERS, R. 2011. Expanded GGGGCC hexanucleotide repeat in noncoding region of C9ORF72 causes chromosome 9p-linked FTD and ALS. *Neuron,* 72**,** 245-56.

DENNIS, G., SHERMAN, B., HOSACK, D., YANG, J., GAO, W., LANE, H. & LEMPICKI, R. 2003. DAVID: Database for Annotation, Visualization, and Integrated Discovery. *Genome Biol,* 4**,** P3.

DI DOMENICO, F., SULTANA, R., FERREE, A., SMITH, K., BARONE, E., PERLUIGI, M., COCCIA, R., PIERCE, W., CAI, J., MANCUSO, C., SQUILLACE, R., WIENGELE, M., DALLE-DONNE, I., WOLOZIN, B. & BUTTERFIELD, D. A. 2012. Redox proteomics analyses of the influence of co-expression of wild-type or mutated LRRK2 and Tau on *C. elegans* protein expression and oxidative modification: relevance to Parkinson disease. *Antioxid Redox Signal*.

DICKEY, C. A., YUE, M., LIN, W.-L., DICKSON, D. W., DUNMORE, J. H., LEE, W. C., ZEHR, C., WEST, G., CAO, S., CLARK, A. M. K., CALDWELL, G. A., CALDWELL, K. A., ECKMAN, C., PATTERSON, C., HUTTON, M. & PETRUCELLI, L. 2006. Deletion of the ubiquitin ligase CHIP leads to the accumulation, but not the aggregation, of both endogenous phospho- and caspase-3-cleaved Tau species. *The Journal of Neuroscience,* 26**,** 6985-6996.

DIMITRIADI, M. & HART, A. C. 2010. Neurodegenerative disorders: insights from the nematode *Caenorhabditis elegans*. *Neurobiol Dis,* 40**,** 4-11.

DIMITRIADI, M., KYE, M. J., KALLOO, G., YERSAK, J. M., SAHIN, M. & HART, A. C. 2013. The neuroprotective drug riluzole acts via small conductance Ca^{2+}-activated K^+ channels to ameliorate defects in spinal muscular atrophy models. *J Neurosci,* 33**,** 6557-62.

DIOMEDE, L., CASSATA, G., FIORDALISO, F., SALIO, M., AMI, D., NATALELLO, A., DOGLIA, S. M., DE LUIGI, A. & SALMONA, M. 2010. Tetracycline and its analogues protect *Caenorhabditis elegans* from beta amyloid-induced toxicity by targeting oligomers. *Neurobiol Dis,* 40**,** 424-31.

DIOMEDE, L., RIGACCI, S., ROMEO, M., STEFANI, M. & SALMONA, M. 2013. Oleuropein aglycone protects transgenic *C. elegans* strains expressing Abeta42 by reducing plaque load and motor deficit. *PLoS One,* 8**,** e58893.

DIOMEDE, L., SORIA, C., ROMEO, M., GIORGETTI, S., MARCHESE, L., MANGIONE, P. P., PORCARI, R., ZORZOLI, I., SALMONA, M., BELLOTTI, V. & STOPPINI, M. 2012. *C. elegans* expressing human β_2-microglobulin: a novel model for studying the relationship between the molecular assembly and the toxic phenotype. *PLoS One,* 7**,** e52314.

DOITSIDOU, M., FLAMES, N., LEE, A. C., BOYANOV, A. & HOBERT, O. 2008. Automated screening for mutants affecting dopaminergic-neuron specification in *C. elegans*. *Nat Meth,* 5**,** 869-872.

DOLZHANSKAYA, N., GONZALEZ, M. A., SPERZIANI, F., STEFL, S., MESSING, J., WEN, G. Y., ALEXOV, E., ZUCHNER, S. & VELINOV, M. 2014. A novel p.Leu(381)Phe mutation in presenilin 1 is associated with very early onset and unusually fast progressing dementia as well as lysosomal inclusions typically seen in Kufs disease. *Journal of Alzheimer's Disease,* 39**,** 23-27.

DONNELIER, J. & BRAUN, J. E. A. 2014. CSPα—chaperoning presynaptic proteins. *Frontiers in Cellular Neuroscience,* 8.

DOONAN, R., MCELWEE, J. J., MATTHIJSSENS, F., WALKER, G. A., HOUTHOOFD, K., BACK, P., MATSCHESKI, A., VANFLETEREN, J. R. & GEMS, D. 2008. Against the oxidative damage theory of aging: superoxide dismutases protect against oxidative stress but have little or no effect on life span in *Caenorhabditis elegans*. *Genes & Development,* 22**,** 3236-3241.

DORMANN, D., RODDE, R., EDBAUER, D., BENTMANN, E., FISCHER, I., HRUSCHA, A., THAN, M. E., MACKENZIE, I. R., CAPELL, A., SCHMID, B., NEUMANN, M. & HAASS, C. 2010. ALS-associated fused in sarcoma (FUS) mutations disrupt Transportin-mediated nuclear import. *EMBO J,* 29**,** 2841-57.

DOSANJH, L. E., BROWN, M. K., RAO, G., LINK, C. D. & LUO, Y. 2010. Behavioral phenotyping of a transgenic *Caenorhabditis elegans* expressing neuronal amyloid-β. *Journal of Alzheimer's Disease,* 19**,** 681-690.

DOSTAL, V., ROBERTS, C. M. & LINK, C. D. 2010. Genetic mechanisms of coffee extract protection in a *Caenorhabditis elegans* model of beta-amyloid peptide toxicity. *Genetics,* 186**,** 857-66.

DRAKE, J., LINK, C. D. & BUTTERFIELD, D. A. 2003. Oxidative stress precedes fibrillar deposition of Alzheimer's disease amyloid beta-peptide (1-42) in a transgenic *Caenorhabditis elegans* model. *Neurobiol Aging,* 24**,** 415-20.

DUAN, Z. & SESTI, F. 2013. A *Caenorhabditis elegans* model system for amylopathy study. *J Vis Exp***,** e50435.

DUKE, D. C., MORAN, L. B., KALAITZAKIS, M. E., DEPREZ, M., DEXTER, D. T., PEARCE, R. K. B. & GRAEBER, M. B. 2006. Transcriptome analysis reveals link between proteasomal and mitochondrial pathways in Parkinson's disease. *Neurogenetics,* 7**,** 139-148.

ECKDAHL, T., BROWN, A., HART, S., MALLOY, K., SHOTT, M., YIU, G., HOOPES, L. & HEYER, L. 2008. Microarray analysis of the in vivo sequence preferences of a minor groove binding drug. *BMC Genomics,* 9**,** 32.

EDENS, B. M., AJROUD-DRISS, S., MA, L. & MA, Y. C. 2014. Molecular mechanisms and animal models of spinal muscular atrophy. *Biochim Biophys Acta*.

EHRNHOEFER, D. E., WONG, B. K. & HAYDEN, M. R. 2011. Convergent pathogenic pathways in Alzheimer's and Huntington's diseases: shared targets for drug development. *Nat Rev Drug Discov,* 10**,** 853-67.

EKINS, S. & WILLIAMS, A. J. 2011. Finding promiscuous old drugs for new uses. *Pharm Res,* 28**,** 1785-91.

EL-AMI, T., MOLL, L., CARVALHAL MARQUES, F., VOLOVIK, Y., REUVENI, H. & COHEN, E. 2014. A novel inhibitor of the insulin/IGF signaling pathway protects from age-onset, neurodegeneration-linked proteotoxicity. *Aging Cell,* 13**,** 165-74.

EVANS, E. A., KAWLI, T. & TAN, M. W. 2008. Pseudomonas aeruginosa suppresses host immunity by activating the DAF-2 insulin-like signaling pathway in *Caenorhabditis elegans*. *PLoS Pathog,* 4**,** e1000175.

EVASON, K., COLLINS, J. J., HUANG, C., HUGHES, S. & KORNFELD, K. 2008. Valproic acid extends *Caenorhabditis elegans* lifespan. *Aging Cell,* 7**,** 305-17.

EVASON, K., HUANG, C., YAMBEN, I., COVEY, D. F. & KORNFELD, K. 2005. Anticonvulsant medications extend worm life-span. *Science,* 307**,** 258-62.

EWALD, C. & LI, C. 2012. *Caenorhabditis elegans* as a model organism to study APP function. *Experimental Brain Research,* 217**,** 397-411.

EWALD, C. Y., CHENG, R., TOLEN, L., SHAH, V., GILLANI, A., NASRIN, A. & LI, C. 2012. Pan-neuronal expression of APL-1, an APP-related protein, disrupts olfactory, gustatory, and touch plasticity in *Caenorhabditis elegans*. *J Neurosci,* 32**,** 10156-69.

EYAL, S., YAGEN, B., SOBOL, E., ALTSCHULER, Y., SHMUEL, M. & BIALER, M. 2004. The activity of antiepileptic drugs as histone deacetylase inhibitors. *Epilepsia,* 45**,** 737-744.

FABER, P. W., ALTER, J. R., MACDONALD, M. E. & HART, A. C. 1999. Polyglutamine-mediated dysfunction and apoptotic death of a *Caenorhabditis elegans* sensory neuron. *Proc Natl Acad Sci U S A,* 96**,** 179-84.

FABER, P. W., VOISINE, C., KING, D. C., BATES, E. A. & HART, A. C. 2002. Glutamine/proline-rich PQE-1 proteins protect *Caenorhabditis elegans* neurons from huntingtin polyglutamine neurotoxicity. *Proc Natl Acad Sci U S A,* 99**,** 17131-6.

FALKENBURGER, B. H. & SCHULZ, J. B. 2006. Limitations of cellular models in Parkinson's disease research. *J Neural Transm Suppl***,** 261-8.

FARBER, N. B., JIANG, X. P., HEINKEL, C. & NEMMERS, B. 2002. Antiepileptic drugs and agents that inhibit voltage-gated sodium channels prevent NMDA antagonist neurotoxicity. *Molecular Psychiatry,* 7**,** 726-733.

FATOUROS, C., PIR, G. J., BIERNAT, J., KOUSHIKA, S. P., MANDELKOW, E., MANDELKOW, E.-M., SCHMIDT, E. & BAUMEISTER, R. 2012. Inhibition of tau aggregation in a novel *Caenorhabditis elegans* model of tauopathy mitigates proteotoxicity. *Human Molecular Genetics,* 21**,** 3587-3603.

FAY, D. S., FLUET, A., JOHNSON, C. J. & LINK, C. D. 1998. In vivo aggregation of beta-amyloid peptide variants. *J Neurochem,* 71**,** 1616-25.

FERNANDEZ-CHACON, R., WOLFEL, M., NISHIMUNE, H., TABARES, L., SCHMITZ, F., CASTELLANO-MUNOZ, M., ROSENMUND, C., MONTESINOS, M. L., SANES, J. R., SCHNEGGENBURGER, R. & SUDHOF, T. C. 2004. The synaptic vesicle protein CSP alpha prevents presynaptic degeneration. *Neuron,* 42**,** 237-51.

FERRANTE, R. J., RYU, H., KUBILUS, J. K., D'MELLO, S., SUGARS, K. L., LEE, J., LU, P., SMITH, K., BROWNE, S., BEAL, M. F., KRISTAL, B. S., STAVROVSKAYA, I. G., HEWETT, S., RUBINSZTEIN, D. C., LANGLEY, B.

& RATAN, R. R. 2004. Chemotherapy for the brain: the antitumor antibiotic mithramycin prolongs survival in a mouse model of Huntington's disease. *J Neurosci,* 24**,** 10335-42.
FIESEL, F. C., WEBER, S. S., SUPPER, J., ZELL, A. & KAHLE, P. J. 2012. TDP-43 regulates global translational yield by splicing of exon junction complex component SKAR. *Nucleic Acids Res,* 40**,** 2668-82.
FIGIEL, M., SZLACHCIC, W. J., SWITONSKI, P. M., GABKA, A. & KRZYZOSIAK, W. J. 2012. Mouse models of polyglutamine diseases: review and data table. Part I. *Mol Neurobiol,* 46**,** 393-429.
FISZER, A. & KRZYZOSIAK, W. J. 2013. RNA toxicity in polyglutamine disorders: concepts, models, and progress of research. *J Mol Med (Berl),* 91**,** 683-91.
FLEMING, C. E., NUNES, A. F. & SOUSA, M. M. 2009. Transthyretin: More than meets the eye. *Progress in Neurobiology,* 89**,** 266-276.
FLOREZ-MCCLURE, M. L., HOHSFIELD, L. A., FONTE, G., BEALOR, M. T. & LINK, C. D. 2007. Decreased insulin-receptor signaling promotes the autophagic degradation of beta-amyloid peptide in *C. elegans*. *Autophagy,* 3**,** 569-580.
FONTE, V., DOSTAL, V., ROBERTS, C., GONZALES, P., LACOR, P., MAGRANE, J., DINGWELL, N., FAN, E., SILVERMAN, M., STEIN, G. & LINK, C. 2011. A glycine zipper motif mediates the formation of toxic beta-amyloid oligomers in vitro and in vivo. *Molecular Neurodegeneration,* 6**,** 61.
FONTE, V., KAPULKIN, V., TAFT, A., FLUET, A., FRIEDMAN, D. & LINK, C. D. 2002. Interaction of intracellular beta amyloid peptide with chaperone proteins. *Proc Natl Acad Sci U S A,* 99**,** 9439-44.
FONTE, V., KIPP, D. R., YERG, J., 3RD, MERIN, D., FORRESTAL, M., WAGNER, E., ROBERTS, C. M. & LINK, C. D. 2008. Suppression of in vivo beta-amyloid peptide toxicity by overexpression of the HSP-16.2 small chaperone protein. *J Biol Chem,* 283**,** 784-91.
FOX, R. M., VON STETINA, S. E., BARLOW, S. J., SHAFFER, C., OLSZEWSKI, K. L., MOORE, J. H., DUPUY, D., VIDAL, M. & MILLER, D. M., 3RD 2005. A gene expression fingerprint of *C. elegans* embryonic motor neurons. *BMC Genomics,* 6**,** 42.
FU, R.-H., HARN, H.-J., LIU, S.-P., CHEN, C.-S., CHANG, W.-L., CHEN, Y.-M., HUANG, J.-E., LI, R.-J., TSAI, S.-Y., HUNG, H.-S., SHYU, W.-C., LIN, S.-Z. & WANG, Y.-C. 2014a. *n*-Butylidenephthalide protects against dopaminergic neuron degeneration and α-synuclein accumulation in *Caenorhabditis elegans* models of Parkinson's Disease. *PLoS ONE,* 9**,** e85305.
FU, R.-H., WANG, Y.-C., CHEN, C.-S., TSAI, R.-T., LIU, S.-P., CHANG, W.-L., LIN, H.-L., LU, C.-H., WEI, J.-R., WANG, Z.-W., SHYU, W.-C. & LIN, S.-Z. 2014b. Acetylcorynoline attenuates dopaminergic neuron degeneration and α-synuclein aggregation in animal models of Parkinson's disease. *Neuropharmacology,* 82**,** 108-120.
FUJIWARA, H., HASEGAWA, M., DOHMAE, N., KAWASHIMA, A., MASLIAH, E., GOLDBERG, M. S., SHEN, J., TAKIO, K. & IWATSUBO, T. 2002. alpha-Synuclein is phosphorylated in synucleinopathy lesions. *Nat Cell Biol,* 4**,** 160-164.
FURUYAMA, T., NAKAZAWA, T., NAKANO, I. & MORI, N. 2000. Identification of the differential distribution patterns of mRNAs and consensus binding sequences for mouse DAF-16 homologues. *Biochem J,* 349**,** 629 - 634.
GAMI, M. S. & WOLKOW, C. A. 2006. Studies of *Caenorhabditis elegans* DAF-2/insulin signaling reveal targets for pharmacological manipulation of lifespan. *Aging Cell,* 5**,** 31-7.
GANDHI, S. & WOOD, N. W. 2010. Genome-wide association studies: the key to unlocking neurodegeneration? *Nat Neurosci,* 13**,** 789-94.

GARCIA-ALCOVER, I., LOPEZ CASTEL, A., PEREZ-ALONSO, M. & ARTERO, R. 2013. In vivo strategies for drug discovery in myotonic dystrophy disorders. *Drug Discov Today Technol,* 10**,** e97-102.

GARCIA-JUNCO-CLEMENTE, P., CANTERO, G., GOMEZ-SANCHEZ, L., LINARES-CLEMENTE, P., MARTINEZ-LOPEZ, J. A., LUJAN, R. & FERNANDEZ-CHACON, R. 2010. Cysteine string protein-alpha prevents activity-dependent degeneration in GABAergic synapses. *J Neurosci,* 30**,** 7377-91.

GARIGAN, D., HSU, A. L., FRASER, A. G., KAMATH, R. S., AHRINGER, J. & KENYON, C. 2002. Genetic analysis of tissue aging in *Caenorhabditis elegans*: A role for heat-shock factor and bacterial proliferation. *Genetics,* 161**,** 1101-1112.

GAUDET, J. & MANGO, S. E. 2002. Regulation of organogenesis by the *Caenorhabditis elegans* FoxA protein PHA-4. *Science,* 295**,** 821-5.

GEMS, D. & RIDDLE, D. L. 2000. Defining wild-type life span in *Caenorhabditis elegans*. *J Gerontol A Biol Sci Med Sci,* 55**,** B215-9.

GERHOLD, D., LU, M., XU, J., AUSTIN, C., CASKEY, C. T. & RUSHMORE, T. 2001. Monitoring expression of genes involved in drug metabolism and toxicology using DNA microarrays. *Physiol Genomics,* 5**,** 161-70.

GERHOLD, D. L., JENSEN, R. V. & GULLANS, S. R. 2002. Better therapeutics through microarrays. *Nat Genet,* 32 Suppl**,** 547-51.

GIDALEVITZ, T., BEN-ZVI, A., HO, K. H., BRIGNULL, H. R. & MORIMOTO, R. I. 2006. Progressive disruption of cellular protein folding in models of polyglutamine diseases. *Science,* 311**,** 1471-4.

GIDALEVITZ, T., KRUPINSKI, T., GARCIA, S. & MORIMOTO, R. I. 2009. Destabilizing protein polymorphisms in the genetic background direct phenotypic expression of mutant SOD1 toxicity. *PLoS Genet,* 5**,** e1000399.

GIDALEVITZ, T., WANG, N., DERAVAJ, T., ALEXANDER-FLOYD, J. & MORIMOTO, R. 2013. Natural genetic variation determines susceptibility to aggregation or toxicity in a *C. elegans* model for polyglutamine disease. *BMC Biology,* 11**,** 100.

GITLER, A. D., BEVIS, B. J., SHORTER, J., STRATHEARN, K. E., HAMAMICHI, S., SU, L. J., CALDWELL, K. A., CALDWELL, G. A., ROCHET, J. C., MCCAFFERY, J. M., BARLOWE, C. & LINDQUIST, S. 2008. The Parkinson's disease protein alpha-synuclein disrupts cellular Rab homeostasis. *Proc Natl Acad Sci U S A,* 105**,** 145-50.

GOEBEL, H. H., KOHNECKE, B. & KOPPANG, N. 1982. Ultrastructural studies on the retina in human and canine neuronal ceroid-lipofuscinoses and other lysosomal disorders. *Birth Defects Orig Artic Ser,* 18**,** 241-53.

GOEDERT, M. 1996. Tau protein and the neurofibrillary pathology of Alzheimer's disease. *Ann N Y Acad Sci,* 777**,** 121-31.

GOLDEN, T. R., HUBBARD, A., DANDO, C., HERREN, M. A. & MELOV, S. 2008. Age-related behaviors have distinct transcriptional profiles in *Caenorhabditis elegans*. *Aging Cell,* 7**,** 850-865.

GOLDEN, T. R. & MELOV, S. 2004. Microarray analysis of gene expression with age in individual nematodes. *Aging Cell,* 3**,** 111-24.

GÓMEZ-SUAGA, P., FDEZ, E., FERNÁNDEZ, B., MARTÍNEZ-SALVADOR, M., BLANCA RAMÍREZ, M., MADERO-PÉREZ, J., RIVERO-RÍOS, P., FUENTES, J. M. & HILFIKER, S. 2014. Novel insights into the neurobiology underlying LRRK2-linked Parkinson's disease. *Neuropharmacology,* 85**,** 45-56.

GOMORA, J. C., DAUD, A. N., WEIERGRABER, M. & PEREZ-REYES, E. 2001. Block of cloned human T-type calcium channels by succinimide antiepileptic drugs. *Mol Pharmacol,* 60**,** 1121-32.

GOREN, M. Z. & ONAT, F. 2007. Ethosuximide: from bench to bedside. *CNS Drug Rev,* 13**,** 224-39.

GOSAI, S. J., KWAK, J. H., LUKE, C. J., LONG, O. S., KING, D. E., KOVATCH, K. J., JOHNSTON, P. A., SHUN, T. Y., LAZO, J. S., PERLMUTTER, D. H., SILVERMAN, G. A. & PAK, S. C. 2010. Automated high-content live animal drug screening using *C. elegans* expressing the aggregation prone serpin α1-antitrypsin Z. *PLoS ONE,* 5**,** e15460.

GREAVES, J., LEMONIDIS, K., GORLEKU, O. A., CRUCHAGA, C., GREFEN, C. & CHAMBERLAIN, L. H. 2012. Palmitoylation-induced aggregation of cysteine-string protein mutants that cause Neuronal ceroid lipofuscinosis. *Journal of Biological Chemistry,* 287**,** 37330-37339.

GROS-LOUIS, F., GASPAR, C. & ROULEAU, G. A. 2006. Genetics of familial and sporadic amyotrophic lateral sclerosis. *Biochim Biophys Acta,* 1762**,** 956-72.

GRÜNBLATT, E., MANDEL, S., JACOB-HIRSCH, J., ZELIGSON, S., AMARIGLO, N., RECHAVI, G., LI, J., RAVID, R., ROGGENDORF, W., RIEDERER, P. & YOUDIM, M. B. H. 2004. Gene expression profiling of parkinsonian substantia nigra pars compacta; alterations in ubiquitin-proteasome, heat shock protein, iron and oxidative stress regulated proteins, cell adhesion/cellular matrix and vesicle trafficking genes. *Journal of Neural Transmission,* 111**,** 1543-1573.

GUHATHAKURTA, D., PALOMAR, L., STORMO, G. D., TEDESCO, P., JOHNSON, T. E., WALKER, D. W., LITHGOW, G., KIM, S. & LINK, C. D. 2002. Identification of a novel cis-regulatory element involved in the heat shock response in *Caenorhabditis elegans* using microarray gene expression and computational methods. *Genome Res,* 12**,** 701-12.

GULBINS, E., PALMADA, M., REICHEL, M., LUTH, A., BOHMER, C., AMATO, D., MULLER, C. P., TISCHBIREK, C. H., GROEMER, T. W., TABATABAI, G., BECKER, K. A., TRIPAL, P., STAEDTLER, S., ACKERMANN, T. F., VAN BREDERODE, J., ALZHEIMER, C., WELLER, M., LANG, U. E., KLEUSER, B., GRASSME, H. & KORNHUBER, J. 2013. Acid sphingomyelinase-ceramide system mediates effects of antidepressant drugs. *Nat Med,* 19**,** 934-938.

GUSELLA, J. F. & MACDONALD, M. E. 2000. Molecular genetics: unmasking polyglutamine triggers in neurodegenerative disease. *Nat Rev Neurosci,* 1**,** 109-15.

GUTHRIE, C., SCHELLENBERG, G. & KRAEMER, B. 2009. SUT-2 potentiates tau-induced neurotoxicity in *Caenorhabditis elegans*. *Hum Mol Genet,* 18**,** 1825 - 1838.

GUTIERREZ-ZEPEDA, A., SANTELL, R., WU, Z., BROWN, M., WU, Y., KHAN, I., LINK, C. D., ZHAO, B. & LUO, Y. 2005. Soy isoflavone glycitein protects against beta amyloid-induced toxicity and oxidative stress in transgenic *Caenorhabditis elegans*. *BMC Neurosci,* 6**,** 54.

HAEUSLER, A. R., DONNELLY, C. J., PERIZ, G., SIMKO, E. A., SHAW, P. G., KIM, M. S., MARAGAKIS, N. J., TRONCOSO, J. C., PANDEY, A., SATTLER, R., ROTHSTEIN, J. D. & WANG, J. 2014. C9orf72 nucleotide repeat structures initiate molecular cascades of disease. *Nature,* 507**,** 195-200.

HALDIMANN, P., MURISET, M., VIGH, L. & GOLOUBINOFF, P. 2011. The novel hydroxylamine derivative NG-094 suppresses polyglutamine protein toxicity in *Caenorhabditis elegans*. *J Biol Chem,* 286**,** 18784-94.

HALL, D. & RUSSELL, R. 1991. The posterior nervous system of the nematode *Caenorhabditis elegans*: serial reconstruction of identified neurons and complete pattern of synaptic interactions. *The Journal of Neuroscience,* 11**,** 1-22.

HALL, G. F. & YAO, J. 2005. Modeling tauopathy: a range of complementary approaches. *Biochim Biophys Acta,* 1739**,** 224-39.

HALTIA, M. 2006. The neuronal ceroid-lipofuscinoses: from past to present. *Biochim Biophys Acta,* 1762**,** 850-6.
HAMAMICHI, S., RIVAS, R. N., KNIGHT, A. L., CAO, S., CALDWELL, K. A. & CALDWELL, G. A. 2008. Hypothesis-based RNAi screening identifies neuroprotective genes in a Parkinson's disease model. *Proc Natl Acad Sci U S A,* 105**,** 728-33.
HAMILTON, G. & GILLINGWATER, T. H. 2013. Spinal muscular atrophy: going beyond the motor neuron. *Trends Mol Med,* 19**,** 40-50.
HANOVER, J. A. & WANG, P. 2013. O-GlcNAc cycling shows neuroprotective potential in *C. elegans* models of neurodegenerative disease. *Worm,* 2**,** e27043.
HARDAWAY, J. A., HARDIE, S. L., WHITAKER, S. M., BAAS, S. R., ZHANG, B., BERMINGHAM, D. P., LICHTENSTEIN, A. J. & BLAKELY, R. D. 2012. Forward genetic analysis to identify determinants of dopamine signaling in *Caenorhabditis elegans* using swimming-induced paralysis. *G3: Genes|Genomes|Genetics,* 2**,** 961-975.
HARDIMAN, O. 2011. Amyotrophic Lateral Sclerosis. *In:* HARDIMAN, O. & DOHERTY, C. P. (eds.) *Neurodegenerative Disorders.* Springer London.
HASEGAWA, K., MIWA, S., ISOMURA, K., TSUTSUMIUCHI, K., TANIGUCHI, H. & MIWA, J. 2008. Acrylamide-responsive genes in the nematode *Caenorhabditis elegans*. *Toxicol Sci,* 101**,** 215-25.
HASSAN, W. M., MERIN, D. A., FONTE, V. & LINK, C. D. 2009. AIP-1 ameliorates beta-amyloid peptide toxicity in a *Caenorhabditis elegans* Alzheimer's disease model. *Hum Mol Genet,* 18**,** 2739-47.
HATTA, M. & CIRILLO, L. A. 2007. Chromatin opening and stable perturbation of core histone:DNA contacts by FoxO1. *Journal of Biological Chemistry,* 282**,** 35583-35593.
HE, K., ZHOU, T., SHAO, J., REN, X., ZHAO, Z. & LIU, D. 2014. Dynamic regulation of genetic pathways and targets during aging in *Caenorhabditis elegans*. *Aging (Albany NY),* 6**,** 215-30.
HELMCKE, K. J., AVILA, D. S. & ASCHNER, M. 2010. Utility of *Caenorhabditis elegans* in high throughput neurotoxicological research. *Neurotoxicology and Teratology,* 32**,** 62-67.
HENDERSON, S. T. & JOHNSON, T. E. 2001. *daf-16* integrates developmental and environmental inputs to mediate aging in the nematode *Caenorhabditis elegans*. *Current Biology,* 11**,** 1975-1980.
HERNDON, L. A., SCHMEISSNER, P. J., DUDARONEK, J. M., BROWN, P. A., LISTNER, K. M., SAKANO, Y., PAUPARD, M. C., HALL, D. H. & DRISCOLL, M. 2002. Stochastic and genetic factors influence tissue-specific decline in ageing *C. elegans*. *Nature,* 419**,** 808-14.
HIBBS, M. A., HESS, D. C., MYERS, C. L., HUTTENHOWER, C., LI, K. & TROYANSKAYA, O. G. 2007. Exploring the functional landscape of gene expression: directed search of large microarray compendia. *Bioinformatics,* 23**,** 2692-2699.
HIGASHI, M., MARUTA, N., BERNSTEIN, A., IKENAKA, K. & HITOSHI, S. 2008. Mood stabilizing drugs expand the neural stem cell pool in the adult brain through activation of notch signaling. *Stem Cells,* 26**,** 1758-67.
HILL, A. A., HUNTER, C. P., TSUNG, B. T., TUCKER-KELLOGG, G. & BROWN, E. L. 2000. Genomic analysis of gene expression in *C. elegans*. *Science,* 290**,** 809-12.
HISAHARA, S. & SHIMOHAMA, S. 2010. Toxin-induced and genetic animal models of Parkinson's disease. *Parkinsons Dis,* 2011**,** 951709.
HOBERT, O., JOHNSTON, R. J., JR. & CHANG, S. 2002. Left-right asymmetry in the nervous system: the *Caenorhabditis elegans* model. *Nat Rev Neurosci,* 3**,** 629-40.

HONDA, Y., FUJITA, Y., MARUYAMA, H., ARAKI, Y., ICHIHARA, K., SATO, A., KOJIMA, T., TANAKA, M., NOZAWA, Y., ITO, M. & HONDA, S. 2011. Lifespan-extending effects of royal jelly and its related substances on the nematode *Caenorhabditis elegans*. *PLoS One,* 6**,** e23527.

HONDA, Y., TANAKA, M. & HONDA, S. 2010. Trehalose extends longevity in the nematode *Caenorhabditis elegans*. *Aging Cell,* 9**,** 558-69.

HORNSTEN, A., LIEBERTHAL, J., FADIA, S., MALINS, R., HA, L., XU, X., DAIGLE, I., MARKOWITZ, M., O'CONNOR, G., PLASTERK, R. & LI, C. 2007. APL-1, a *Caenorhabditis elegans* protein related to the human beta-amyloid precursor protein, is essential for viability. *Proc Natl Acad Sci U S A,* 104**,** 1971-6.

HSU, A., MURPHY, C. & KENYON, C. 2003. Regulation of aging and age-related disease by DAF-16 and heat-shock factor. *Science,* 300**,** 1142 - 1145.

HUANG, D. W., SHERMAN, B. T. & LEMPICKI, R. A. 2008. Systematic and integrative analysis of large gene lists using DAVID bioinformatics resources. *Nat. Protocols,* 4**,** 44-57.

HUGUENARD, J. R. 1999. Neuronal circuitry of thalamocortical epilepsy and mechanisms of antiabsence drug action. *Adv Neurol,* 79**,** 991-9.

HULME, S. E. & WHITESIDES, G. M. 2011. Chemistry and the worm: *Caenorhabditis elegans* as a platform for integrating chemical and biological research. *Angewandte Chemie International Edition,* 50**,** 4774-4807.

HUNT, P. R., SON, T. G., WILSON, M. A., YU, Q. S., WOOD, W. H., ZHANG, Y., BECKER, K. G., GREIG, N. H., MATTSON, M. P., CAMANDOLA, S. & WOLKOW, C. A. 2011. Extension of lifespan in *C. elegans* by naphthoquinones that act through stress hormesis mechanisms. *PLoS One,* 6**,** e21922.

HUSSON, S. J., GOTTSCHALK, A. & LEIFER, A. M. 2013. Optogenetic manipulation of neural activity in *C. elegans*: from synapse to circuits and behaviour. *Biol Cell,* 105**,** 235-50.

HUTTON, M., LENDON, C. L., RIZZU, P., BAKER, M., FROELICH, S., HOULDEN, H., PICKERING-BROWN, S., CHAKRAVERTY, S., ISAACS, A., GROVER, A., HACKETT, J., ADAMSON, J., LINCOLN, S., DICKSON, D., DAVIES, P., PETERSEN, R. C., STEVENS, M., DE GRAAFF, E., WAUTERS, E., VAN BAREN, J., HILLEBRAND, M., JOOSSE, M., KWON, J. M., NOWOTNY, P., CHE, L. K., NORTON, J., MORRIS, J. C., REED, L. A., TROJANOWSKI, J., BASUN, H., LANNFELT, L., NEYSTAT, M., FAHN, S., DARK, F., TANNENBERG, T., DODD, P. R., HAYWARD, N., KWOK, J. B., SCHOFIELD, P. R., ANDREADIS, A., SNOWDEN, J., CRAUFURD, D., NEARY, D., OWEN, F., OOSTRA, B. A., HARDY, J., GOATE, A., VAN SWIETEN, J., MANN, D., LYNCH, T. & HEUTINK, P. 1998. Association of missense and 5'-splice-site mutations in tau with the inherited dementia FTDP-17. *Nature,* 393**,** 702-5.

ICHIBANGASE, T., SAIMARU, H., TAKAMURA, N., KUWAHARA, T., KOYAMA, A., IWATSUBO, T. & IMAI, K. 2008. Proteomics of *Caenorhabditis elegans* over-expressing human α-synuclein analyzed by fluorogenic derivatization–liquid chromatography/tandem mass spectrometry: identification of actin and several ribosomal proteins as negative markers at early Parkinson's disease stages. *Biomedical Chromatography,* 22**,** 232-234.

INGRAM, E. M. & SPILLANTINI, M. G. 2002. Tau gene mutations: dissecting the pathogenesis of FTDP-17. *Trends Mol Med,* 8**,** 555-62.

IRIZARRY, R. A., HOBBS, B., COLLIN, F., BEAZER-BARCLAY, Y. D., ANTONELLIS, K. J., SCHERF, U. & SPEED, T. P. 2003. Exploration, normalization, and summaries of high density oligonucleotide array probe level data. *Biostatistics,* 4**,** 249-64.

ISHIGURO, H., YASUDA, K., ISHII, N., IHARA, K., OHKUBO, T., HIYOSHI, M., ONO, K., SENOO-MATSUDA, N., SHINOHARA, O., YOSSHII, F., MURAKAMI, M., HARTMAN, P. S. & TSUDA, M. 2001. Enhancement of oxidative damage to cultured cells and *Caenorhabditis elegans* by mitochondrial electron transport inhibitors. *IUBMB Life,* 51**,** 263-8.

ISHIHARA, T., HONG, M., ZHANG, B., NAKAGAWA, Y., LEE, M. K., TROJANOWSKI, J. Q. & LEE, V. M. Y. 1999. Age-dependent emergence and progression of a Tauopathy in transgenic mice overexpressing the shortest human Tau isoform. *Neuron,* 24**,** 751-762.

IVAN, C. S., SAINT-HILAIRE, M. H., CHRISTENSEN, T. G. & MILUNSKY, J. M. 2005. Adult-onset neuronal ceroid lipofuscinosis type B in an African-American. *Mov Disord,* 20**,** 752-4.

JACKSON, G. R., WIEDAU-PAZOS, M., SANG, T. K., WAGLE, N., BROWN, C. A., MASSACHI, S. & GESCHWIND, D. H. 2002. Human wild-type tau interacts with wingless pathway components and produces neurofibrillary pathology in Drosophila. *Neuron,* 34**,** 509-19.

JAGOTA, S. & RAJADAS, J. 2012. Effect of phenolic compounds against Abeta aggregation and Abeta-induced toxicity in transgenic *C. elegans*. *Neurochem Res,* 37**,** 40-8.

JALANKO, A. & BRAULKE, T. 2009. Neuronal ceroid lipofuscinoses. *Biochim Biophys Acta,* 1793**,** 697-709.

JEONG, H., THEN, F., MELIA, T. J., JR., MAZZULLI, J. R., CUI, L., SAVAS, J. N., VOISINE, C., PAGANETTI, P., TANESE, N., HART, A. C., YAMAMOTO, A. & KRAINC, D. 2009. Acetylation targets mutant huntingtin to autophagosomes for degradation. *Cell,* 137**,** 60-72.

JEONG, S., KIM, H. & SEO, Y. 2011. Microarray analysis of global gene expression in *Caenorhabditis elegans* exposed to potassium dichromate. *BioChip Journal,* 5**,** 151-157.

JIA, Y., MO, S.-J., FENG, Q.-Q., ZHAN, M.-L., OUYANG, L.-S., CHEN, J.-C., MA, Y.-X., WU, J.-J. & LEI, W.-L. 2014. EPO-dependent activation of PI3K/Akt/FoxO3a signalling mediates neuroprotection in in vitro and in vivo models of Parkinson's Disease. *Journal of Molecular Neuroscience,* 53**,** 117-124.

JIANG, M., RYU, J., KIRALY, M., DUKE, K., REINKE, V. & KIM, S. K. 2001. Genome-wide analysis of developmental and sex-regulated gene expression profiles in *Caenorhabditis elegans*. *Proc Natl Acad Sci U S A,* 98**,** 218-23.

JIANG, M., WANG, J., FU, J., DU, L., JEONG, H., WEST, T., XIANG, L., PENG, Q., HOU, Z., CAI, H., SEREDENINA, T., ARBEZ, N., ZHU, S., SOMMERS, K., QIAN, J., ZHANG, J., MORI, S., YANG, X. W., TAMASHIRO, K. L. K., AJA, S., MORAN, T. H., LUTHI-CARTER, R., MARTIN, B., MAUDSLEY, S., MATTSON, M. P., CICHEWICZ, R. H., ROSS, C. A., HOLTZMAN, D. M., KRAINC, D. & DUAN, W. 2012. Neuroprotective role of Sirt1 in mammalian models of Huntington's disease through activation of multiple Sirt1 targets. *Nat Med,* 18**,** 153-158.

JIN, Y., JORGENSEN, E., HARTWIEG, E. & HORVITZ, H. R. 1999. The *Caenorhabditis elegans* gene *unc-25* encodes glutamic acid decarboxylase and is required for synaptic transmission but not synaptic development. *J Neurosci,* 19**,** 539-48.

JOHNSON, J., JENN, R., BARCLAY, J., BURGOYNE, R. & MORGAN, A. 2010. *Caenorhabditis elegans*: a useful tool to decipher neurodegenerative pathways. *Biochem Soc Trans,* 38**,** 559 - 563.

JONES, L. M., RAYSON, S. J., FLEMMING, A. J. & URWIN, P. E. 2013. Adaptive and specialised transcriptional responses to xenobiotic stress in *Caenorhabditis elegans* are regulated by nuclear hormone receptors. *PLoS One,* 8**,** e69956.

KAHN, N. W., REA, S. L., MOYLE, S., KELL, A. & JOHNSON, T. E. 2008. Proteasomal dysfunction activates the transcription factor SKN-1 and produces a selective oxidative-stress response in *Caenorhabditis elegans*. *Biochem J,* 409**,** 205-13.

KAKIZUKA, A. 1998. Protein precipitation: a common etiology in neurodegenerative disorders? *Trends Genet,* 14**,** 396-402.

KAMP, F., EXNER, N., LUTZ, A. K., WENDER, N., HEGERMANN, J., BRUNNER, B., NUSCHER, B., BARTELS, T., GIESE, A., BEYER, K., EIMER, S., WINKLHOFER, K. F. & HAASS, C. 2010. Inhibition of mitochondrial fusion by alpha-synuclein is rescued by PINK1, Parkin and DJ-1. *EMBO J,* 29**,** 3571-89.

KANG, M., KWON, J. & KIM, M. 2013. Induction of neuronal differentiation of rat muscle-derived stem cells in vitro using basic fibroblast growth factor and ethosuximide. *International Journal of Molecular Sciences,* 14**,** 6614-6623.

KAO, C.-Y., LOS, F. C. O., HUFFMAN, D. L., WACHI, S., KLOFT, N., HUSMANN, M., KARABRAHIMI, V., SCHWARTZ, J.-L., BELLIER, A., HA, C., SAGONG, Y., FAN, H., GHOSH, P., HSIEH, M., HSU, C.-S., CHEN, L. & AROIAN, R. V. 2011. Global functional analyses of cellular responses to pore-forming toxins. *PLoS Pathog,* 7**,** e1001314.

KAPETA, S., CHONDROGIANNI, N. & GONOS, E. S. 2010. Nuclear erythroid factor 2-mediated proteasome activation delays senescence in human fibroblasts. *J Biol Chem,* 285**,** 8171-84.

KAPLAN, J. M. & HORVITZ, H. R. 1993. A dual mechanosensory and chemosensory neuron in *Caenorhabditis elegans*. *Proc Natl Acad Sci U S A,* 90**,** 2227-31.

KARPINAR, D. P., BALIJA, M. B., KUGLER, S., OPAZO, F., REZAEI-GHALEH, N., WENDER, N., KIM, H. Y., TASCHENBERGER, G., FALKENBURGER, B. H., HEISE, H., KUMAR, A., RIEDEL, D., FICHTNER, L., VOIGT, A., BRAUS, G. H., GILLER, K., BECKER, S., HERZIG, A., BALDUS, M., JACKLE, H., EIMER, S., SCHULZ, J. B., GRIESINGER, C. & ZWECKSTETTER, M. 2009. Pre-fibrillar alpha-synuclein variants with impaired beta-structure increase neurotoxicity in Parkinson's disease models. *EMBO J,* 28**,** 3256-68.

KARUPPAGOUNDER, S. S., PINTO, J. T., XU, H., CHEN, H. L., BEAL, M. F. & GIBSON, G. E. 2009. Dietary supplementation with resveratrol reduces plaque pathology in a transgenic model of Alzheimer's disease. *Neurochem Int,* 54**,** 111-8.

KASHYAP, S. S., JOHNSON, J. R., MCCUE, H. V., CHEN, X., EDMONDS, M. J., AYALA, M., GRAHAM, M. E., JENN, R. C., BARCLAY, J. W., BURGOYNE, R. D. & MORGAN, A. 2014. *Caenorhabditis elegans dnj-14*, the orthologue of the *DNAJC5* gene mutated in adult onset neuronal ceroid lipofuscinosis, provides a new platform for neuroprotective drug screening and identifies a SIR-2.1-independent action of resveratrol. *Human Molecular Genetics*.

KAUTU, B. B., CARRASQUILLA, A., HICKS, M. L., CALDWELL, K. A. & CALDWELL, G. A. 2013. Valproic acid ameliorates *C. elegans* dopaminergic neurodegeneration with implications for ERK-MAPK signaling. *Neuroscience Letters,* 541**,** 116-119.

KEARNEY, J. 2011. Genetic modifiers of neurological disease. *Current Opinion in Genetics & Development,* 21**,** 349 - 353.

KENYON, C. & MURPHY, C. T. 2006. Enrichment of regulatory motifs upstream of predicted DAF-16 targets. *Nat Genet,* 38**,** 397-8; author reply 398.

KEOWKASE, R., ABOUKHATWA, M., ADAM, B.-L., BEACH, J. W., TERRY, A., BUCCAFUSSCO, J. & LUO, Y. 2010a. Neuroprotective effects and mechanism of cognitive-enhancing choline analogs JWB 1-84-1 and JAY 2-22-33 in neuronal culture and *Caenorhabditis elegans*. *Molecular Neurodegeneration,* 5**,** 59.

KEOWKASE, R., ABOUKHATWA, M. & LUO, Y. 2010b. Fluoxetine protects against amyloid-beta toxicity, in part via *daf-16* mediated cell signaling pathway, in *Caenorhabditis elegans*. *Neuropharmacology,* 59**,** 358-65.

KIEHL, T.-R., SHIBATA, H. & PULST, S.-M. 2000. The ortholog of human ataxin-2 is essential for early embryonic patterning in *C. elegans*. *Journal of Molecular Neuroscience,* 15**,** 231-241.

KIM, D. 2008. Studying host-pathogen interactions and innate immunity in *Caenorhabditis elegans*. *Disease Models & Mechanisms,* 1**,** 205-208.

KIM, N., JAYATILLAKE, R. & SPOUGE, J. 2013. NEXT-peak: a normal-exponential two-peak model for peak-calling in ChIP-seq data. *BMC Bioinforma,* 14**,** 349.

KIM, Y. & SUN, H. 2007. Functional genomic approach to identify novel genes involved in the regulation of oxidative stress resistance and animal lifespan. *Aging Cell,* 6**,** 489-503.

KIM, Y. & SUN, H. 2012. ASM-3 acid sphingomyelinase functions as a positive regulator of the DAF-2/AGE-1 signaling pathway and serves as a novel anti-aging target. *PLoS ONE,* 7**,** e45890.

KIRKITADZE, M. D., BITAN, G. & TEPLOW, D. B. 2002. Paradigm shifts in Alzheimer's disease and other neurodegenerative disorders: the emerging role of oligomeric assemblies. *J Neurosci Res,* 69**,** 567-77.

KMOCH, S., STRANECKY, V., EMES, R. D. & MITCHISON, H. M. 2013. Bioinformatic perspectives in the neuronal ceroid lipofuscinoses. *Biochim Biophys Acta,* 1832**,** 1831-41.

KOBAYASHI, T., HIRAI, H., IINO, M., FUSE, I., MITSUMURA, K., WASHIYAMA, K., KASAI, S. & IKEDA, K. 2009. Inhibitory effects of the antiepileptic drug ethosuximide on G protein-activated inwardly rectifying K+ channels. *Neuropharmacology,* 56**,** 499-506.

KOCH, K., HAVERMANN, S., BÜCHTER, C. & WÄTJEN, W. 2014. *Caenorhabditis elegans* as model system in pharmacology and toxicology: effects of flavonoids on redox-sensitive signalling pathways and ageing. *The Scientific World Journal,* 2014**,** 15.

KOIKE, M., NAKANISHI, H., SAFTIG, P., EZAKI, J., ISAHARA, K., OHSAWA, Y., SCHULZ-SCHAEFFER, W., WATANABE, T., WAGURI, S., KAMETAKA, S., SHIBATA, M., YAMAMOTO, K., KOMINAMI, E., PETERS, C., VON FIGURA, K. & UCHIYAMA, Y. 2000. Cathepsin D deficiency induces lysosomal storage with ceroid lipofuscin in mouse CNS neurons. *J Neurosci,* 20**,** 6898-906.

KOPITO, R. R. & RON, D. 2000. Conformational disease. *Nat Cell Biol,* 2**,** E207-9.

KOPS, G. J., DANSEN, T. B., POLDERMAN, P. E., SAARLOOS, I., WIRTZ, K. W., COFFER, P. J., HUANG, T. T., BOS, J. L., MEDEMA, R. H. & BURGERING, B. M. 2002. Forkhead transcription factor FOXO3a protects quiescent cells from oxidative stress. *Nature,* 419**,** 316-21.

KORMISH, J. D., GAUDET, J. & MCGHEE, J. D. 2010. Development of the *C. elegans* digestive tract. *Curr Opin Genet Dev,* 20**,** 346-54.

KOSTYUK, P. G., MOLOKANOVA, E. A., PRONCHUK, N. F., SAVCHENKO, A. N. & VERKHRATSKY, A. N. 1992. Different action of ethosuximide on low- and high-threshold calcium currents in rat sensory neurons. *Neuroscience,* 51**,** 755-8.

KOUSI, M., SIINTOLA, E., DVORAKOVA, L., VLASKOVA, H., TURNBULL, J., TOPCU, M., YUKSEL, D., GOKBEN, S., MINASSIAN, B. A., ELLEDER, M., MOLE, S. E. & LEHESJOKI, A. E. 2009. Mutations in CLN7/MFSD8 are a common cause of variant late-infantile neuronal ceroid lipofuscinosis. *Brain,* 132**,** 810-9.

KRAEMER, B. C., BURGESS, J. K., CHEN, J. H., THOMAS, J. H. & SCHELLENBERG, G. D. 2006. Molecular pathways that influence human

tau-induced pathology in *Caenorhabditis elegans*. *Hum Mol Genet,* 15**,** 1483-1496.
KRAEMER, B. C. & SCHELLENBERG, G. D. 2007. SUT-1 enables tau-induced neurotoxicity in *C. elegans*. *Hum Mol Genet,* 16**,** 1959-1971.
KRAEMER, B. C., ZHANG, B., LEVERENZ, J. B., THOMAS, J. H., TROJANOWSKI, J. Q. & SCHELLENBERG, G. D. 2003. Neurodegeneration and defective neurotransmission in a *Caenorhabditis elegans* model of tauopathy. *Proc Natl Acad Sci U S A,* 100**,** 9980-5.
KUNITOMO, H., UESUGI, H., KOHARA, Y. & IINO, Y. 2005. Identification of ciliated sensory neuron-expressed genes in *Caenorhabditis elegans* using targeted pull-down of poly(A) tails. *Genome Biol,* 6**,** R17.
KUWABARA, P. E. & O'NEIL, N. 2001. The use of functional genomics in *C. elegans* for studying human development and disease. *Journal of Inherited Metabolic Disease,* 24**,** 127-138.
KUWAHARA, T., KOYAMA, A., GENGYO-ANDO, K., MASUDA, M., KOWA, H., TSUNODA, M., MITANI, S. & IWATSUBO, T. 2006. Familial Parkinson mutant alpha-synuclein causes dopamine neuron dysfunction in transgenic *Caenorhabditis elegans*. *J Biol Chem,* 281**,** 334-40.
KUWAHARA, T., KOYAMA, A., KOYAMA, S., YOSHINA, S., REN, C.-H., KATO, T., MITANI, S. & IWATSUBO, T. 2008. A systematic RNAi screen reveals involvement of endocytic pathway in neuronal dysfunction in α-synuclein transgenic *C. elegans*. *Hum Mol Genet,* 17**,** 2997-3009.
KUWAHARA, T., TONEGAWA, R., ITO, G., MITANI, S. & IWATSUBO, T. 2012. Phosphorylation of α-synuclein protein at Ser-129 reduces neuronal dysfunction by lowering its membrane binding property in *Caenorhabditis elegans*. *Journal of Biological Chemistry,* 287**,** 7098-7109.
KWON, D. Y., DIMITRIADI, M., TERZIC, B., CABLE, C., HART, A. C., CHITNIS, A., FISCHBECK, K. H. & BURNETT, B. G. 2013. The E3 ubiquitin ligase mind bomb 1 ubiquitinates and promotes the degradation of survival of motor neuron protein. *Mol Biol Cell,* 24**,** 1863-71.
KYLE, B. D., AHRENDT, E., BRAUN, A. P. & BRAUN, J. E. 2013. The large conductance, calcium-activated K+ (BK) channel is regulated by cysteine string protein. *Sci Rep,* 3**,** 2447.
LA SPADA, A. R., WEYDT, P. & PINEDA, V. V. 2011. Huntington's disease pathogenesis: mechanisms and pathways. *In:* LO, D. C. & HUGHES, R. E. (eds.) *Neurobiology of Huntington's Disease: Applications to Drug Discovery.* Boca Raton (FL).
LAENG, P., PITTS, R. L., LEMIRE, A. L., DRABIK, C. E., WEINER, A., TANG, H., THYAGARAJAN, R., MALLON, B. S. & ALTAR, C. A. 2004. The mood stabilizer valproic acid stimulates GABA neurogenesis from rat forebrain stem cells. *J Neurochem,* 91**,** 238-51.
LAING, S. T., IVENS, A., BUTLER, V., RAVIKUMAR, S. P., LAING, R., WOODS, D. J. & GILLEARD, J. S. 2012. The transcriptional response of *Caenorhabditis elegans* to Ivermectin exposure identifies novel genes involved in the response to reduced food intake. *PLoS One,* 7**,** e31367.
LAKOWSKI, B., EIMER, S., GÖBEL, C., BÖTTCHER, A., WAGLER, B. & BAUMEISTER, R. 2003. Two suppressors of sel-12 encode C2H2 zinc-finger proteins that regulate presenilin transcription in *Caenorhabditis elegans*. *Development,* 130**,** 2117-2128.
LAKOWSKI, B. & HEKIMI, S. 1998. The genetics of caloric restriction in *Caenorhabditis elegans*. *Proc Natl Acad Sci U S A,* 95**,** 13091-6.
LAKSO, M., VARTIAINEN, S., MOILANEN, A. M., SIRVIO, J., THOMAS, J. H., NASS, R., BLAKELY, R. D. & WONG, G. 2003. Dopaminergic neuronal loss and motor deficits in *Caenorhabditis elegans* overexpressing human alpha-synuclein. *Journal of Neurochemistry,* 86**,** 165-72.

LANS, H. & JANSEN, G. 2007. Multiple sensory G proteins in the olfactory, gustatory and nociceptive neurons modulate longevity in *Caenorhabditis elegans*. *Developmental Biology,* 303**,** 474-482.
LEE, J. K., JIN, H. K., PARK, M. H., KIM, B. R., LEE, P. H., NAKAUCHI, H., CARTER, J. E., HE, X., SCHUCHMAN, E. H. & BAE, J. S. 2014. Acid sphingomyelinase modulates the autophagic process by controlling lysosomal biogenesis in Alzheimer's disease. *J Exp Med,* 211**,** 1551-70.
LEE, S. I. & BATZOGLOU, S. 2003. Application of independent component analysis to microarrays. *Genome Biol,* 4**,** R76.
LEE, S. S., KENNEDY, S., TOLONEN, A. C. & RUVKUN, G. 2003. DAF-16 target genes that control *C. elegans* life-span and metabolism. *Science,* 300**,** 644-647.
LEHMANN, S., SHEPHARD, F., JACOBSON, L. & SZEWCZYK, N. J. 2012. Integrated control of protein degradation in *C. elegans* muscle. *Worm,* 1**,** 0-9.
LEIBOLD, E. A. & ANDERSON, C. P. 2014. Mechanisms of iron metabolism in *Caenorhabditis elegans*. *Frontiers in Pharmacology,* 5.
LEJEUNE, F.-X., MESROB, L., PARMENTIER, F., BICEP, C., VAZQUEZ-MANRIQUE, R., PARKER, J. A., VERT, J.-P., TOURETTE, C. & NERI, C. 2012. Large-scale functional RNAi screen in *C. elegans* identifies genes that regulate the dysfunction of mutant polyglutamine neurons. *BMC Genomics,* 13**,** 91.
LERESCHE, N., PARRI, H. R., ERDEMLI, G., GUYON, A., TURNER, J. P., WILLIAMS, S. R., ASPRODINI, E. & CRUNELLI, V. 1998. On the action of the anti-absence drug ethosuximide in the rat and cat thalamus. *J Neurosci,* 18**,** 4842-53.
LESAGE, S. & BRICE, A. 2009. Parkinson's disease: from monogenic forms to genetic susceptibility factors. *Hum Mol Genet,* 18**,** R48-59.
LEUNG, C. K., DEONARINE, A., STRANGE, K. & CHOE, K. P. 2011. High-throughput screening and biosensing with fluorescent *C. elegans* strains. *J Vis Exp*.
LEUNG, C. K., WANG, Y., MALANY, S., DEONARINE, A., NGUYEN, K., VASILE, S. & CHOE, K. P. 2013. An ultra high-throughput, whole-animal screen for small molecule modulators of a specific genetic pathway in *Caenorhabditis elegans*. *PLoS One,* 8**,** e62166.
LEUNG, M. C. K., WILLIAMS, P. L., BENEDETTO, A., AU, C., HELMCKE, K. J., ASCHNER, M. & MEYER, J. N. 2008. *Caenorhabditis elegans*: an emerging model in biomedical and environmental toxicology. *Toxicological Sciences,* 106**,** 5-28.
LEVITAN, D. & GREENWALD, I. 1998. Effects of SEL-12 presenilin on LIN-12 localization and function in *Caenorhabditis elegans*. *Development,* 125**,** 3599-606.
LEWIS, J., GEHMAN, E., BAER, C. & JACKSON, D. 2013. Alterations in gene expression in *Caenorhabditis elegans* associated with organophosphate pesticide intoxication and recovery. *BMC Genomics,* 14**,** 291.
LI, J., HUANG, K. X. & LE, W. D. 2013. Establishing a novel *C. elegans* model to investigate the role of autophagy in amyotrophic lateral sclerosis. *Acta Pharmacol Sin,* 34**,** 644-50.
LI, X. & BUXBAUM, J. N. 2011. Transthyretin and the brain re-visited: is neuronal synthesis of transthyretin protective in Alzheimer's disease? *Mol Neurodegener,* 6**,** 79.
LIACHKO, N. F., GUTHRIE, C. R. & KRAEMER, B. C. 2010. Phosphorylation promotes neurotoxicity in a *Caenorhabditis elegans* model of TDP-43 proteinopathy. *J Neurosci,* 30**,** 16208-19.

LIACHKO, N. F., MCMILLAN, P. J., GUTHRIE, C. R., BIRD, T. D., LEVERENZ, J. B. & KRAEMER, B. C. 2013. CDC7 inhibition blocks pathological TDP-43 phosphorylation and neurodegeneration. *Ann Neurol,* 74**,** 39-52.

LIN, K., HSIN, H., LIBINA, N. & KENYON, C. 2001. Regulation of the *Caenorhabditis elegans* longevity protein DAF-16 by insulin/IGF-1 and germline signaling. *Nat Genet,* 28**,** 139 - 145.

LING, K. K. Y., GIBBS, R. M., FENG, Z. & KO, C.-P. 2012. Severe neuromuscular denervation of clinically relevant muscles in a mouse model of spinal muscular atrophy. *Human Molecular Genetics,* 21**,** 185-195.

LINK, C. D. 1995. Expression of human beta-amyloid peptide in transgenic *Caenorhabditis elegans*. *Proc Natl Acad Sci U S A,* 92**,** 9368-72.

LINK, C. D. 2006. *C. elegans* models of age-associated neurodegenerative diseases: lessons from transgenic worm models of Alzheimer's disease. *Exp Gerontol,* 41**,** 1007-13.

LINK, C. D., JOHNSON, C. J., FONTE, V., PAUPARD, M.-C., HALL, D. H., STYREN, S., MATHIS, C. A. & KLUNK, W. E. 2001. Visualization of fibrillar amyloid deposits in living, transgenic *Caenorhabditis elegans* animals using the sensitive amyloid dye, X-34. *Neurobiology of Aging,* 22**,** 217-226.

LINK, C. D., TAFT, A., KAPULKIN, V., DUKE, K., KIM, S., FEI, Q., WOOD, D. E. & SAHAGAN, B. G. 2003. Gene expression analysis in a transgenic *Caenorhabditis elegans* Alzheimer's disease model. *Neurobiol Aging,* 24**,** 397-413.

LIU, J., ZHANG, B., LEI, H., FENG, Z., LIU, J., HSU, A. L. & XU, X. Z. 2013. Functional aging in the nervous system contributes to age-dependent motor activity decline in *C. elegans*. *Cell Metab,* 18**,** 392-402.

LIU, P., GE, Q., CHEN, B., SALKOFF, L., KOTLIKOFF, M. I. & WANG, Z. W. 2011a. Genetic dissection of ion currents underlying all-or-none action potentials in *C. elegans* body-wall muscle cells. *J Physiol,* 589**,** 101-17.

LIU, Y., YU, J. T., ZONG, Y., ZHOU, J. & TAN, L. 2014. C9ORF72 mutations in neurodegenerative diseases. *Mol Neurobiol,* 49**,** 386-98.

LIU, Z., HAMAMICHI, S., LEE, B. D., YANG, D., RAY, A., CALDWELL, G. A., CALDWELL, K. A., DAWSON, T. M., SMITH, W. W. & DAWSON, V. L. 2011b. Inhibitors of LRRK2 kinase attenuate neurodegeneration and Parkinson-like phenotypes in *Caenorhabditis elegans* and *Drosophila* Parkinson's disease models. *Hum Mol Genet,* 20**,** 3933-42.

LOCKE, C. J., FOX, S. A., CALDWELL, G. A. & CALDWELL, K. A. 2008. Acetaminophen attenuates dopamine neuron degeneration in animal models of Parkinson's disease. *Neurosci Lett,* 439**,** 129-33.

LORING, J. F., WEN, X., LEE, J. M., SEILHAMER, J. & SOMOGYI, R. 2001. A gene expression profile of Alzheimer's disease. *DNA Cell Biol,* 20**,** 683-95.

LU, T., ARON, L., ZULLO, J., PAN, Y., KIM, H., CHEN, Y., YANG, T.-H., KIM, H.-M., DRAKE, D., LIU, X. S., BENNETT, D. A., COLAIACOVO, M. P. & YANKNER, B. A. 2014. REST and stress resistance in ageing and Alzheimer's disease. *Nature,* 507**,** 448-454.

LUBLIN, A., ISODA, F., PATEL, H., YEN, K., NGUYEN, L., HAJJE, D., SCHWARTZ, M. & MOBBS, C. 2011. FDA-approved drugs that protect mammalian neurons from glucose toxicity slow aging dependent on Cbp and protect against proteotoxicity. *PLoS One,* 6**,** e27762.

LUBLIN, A. L. & LINK, C. D. 2013. Alzheimer's disease drug discovery: in vivo screening using *Caenorhabditis elegans* as a model for β-amyloid peptide-induced toxicity. *Drug Discovery Today: Technologies*.

LUND, J., TEDESCO, P., DUKE, K., WANG, J., KIM, S. K. & JOHNSON, T. E. 2002. Transcriptional profile of aging in *C. elegans*. *Curr Biol,* 12**,** 1566-73.

MACHINO, K., LINK, C. D., WANG, S., MURAKAMI, H. & MURAKAMI, S. 2014. A semi-automated motion-tracking analysis of locomotion speed in the *C.*

elegans transgenics overexpressing beta-amyloid in neurons. *Front Genet,* 5**,** 202.

MADURO, M. F. & ROTHMAN, J. H. 2002. Making worm guts: the gene regulatory network of the *Caenorhabditis elegans* endoderm. *Dev Biol,* 246**,** 68-85.

MAIOLI, S., PUERTA, E., MERINO-SERRAIS, P., FUSARI, L., GIL-BEA, F., RIMONDINI, R. & CEDAZO-MINGUEZ, A. 2012. Combination of apolipoprotein e4 and high carbohydrate diet reduces hippocampal BDNF and arc levels and impairs memory in young mice. *J Alzheimers Dis,* 32**,** 341-55.

MANDEL, S., WEINREB, O. & YOUDIM, M. B. H. 2003. Using cDNA microarray to assess Parkinson's disease models and the effects of neuroprotective drugs. *Trends in Pharmacological Sciences,* 24**,** 184-191.

MANDELKOW, E. M. & MANDELKOW, E. 1998. Tau in Alzheimer's disease. *Trends Cell Biol,* 8**,** 425-7.

MANNING, J. P., RICHARDS, D. A. & BOWERY, N. G. 2003. Pharmacology of absence epilepsy. *Trends Pharmacol Sci,* 24**,** 542-9.

MARTIN, I., DAWSON, V. L. & DAWSON, T. M. 2011. Recent advances in the genetics of Parkinson's disease. *Annu Rev Genomics Hum Genet,* 12**,** 301-25.

MARTORELL, P., BATALLER, E., LLOPIS, S., GONZALEZ, N., ÁLVAREZ, B., MONTÓN, F., ORTIZ, P., RAMÓN, D. & GENOVÉS, S. 2013. A cocoa peptide protects *Caenorhabditis elegans* from oxidative stress and β-amyloid peptide toxicity. *PLoS One,* 8**,** e63283.

MARVANOVA, M. & NICHOLS, C. D. 2007. Identification of neuroprotective compounds of *Caenorhabditis elegans* dopaminergic neurons against 6-OHDA. *J Mol Neurosci,* 31**,** 127-37.

MATHEW, M. D., MATHEW, N. D. & EBERT, P. R. 2012. WormScan: a technique for high-throughput phenotypic analysis of *Caenorhabditis elegans*. *PLoS ONE,* 7**,** e33483.

MATLACK, K. E., TARDIFF, D. F., NARAYAN, P., HAMAMICHI, S., CALDWELL, K. A., CALDWELL, G. A. & LINDQUIST, S. 2014. Clioquinol promotes the degradation of metal-dependent amyloid-beta (Abeta) oligomers to restore endocytosis and ameliorate Abeta toxicity. *Proc Natl Acad Sci U S A,* 111**,** 4013-8.

MAYHEW, I. G., JOLLY, R. D., PICKETT, B. T. & SLACK, P. M. 1985. Ceroid-lipofuscinosis (Batten's disease): pathogenesis of blindness in the ovine model. *Neuropathol Appl Neurobiol,* 11**,** 273-90.

MCCOLL, G., KILLILEA, D. W., HUBBARD, A. E., VANTIPALLI, M. C., MELOV, S. & LITHGOW, G. J. 2008. Pharmacogenetic analysis of lithium-induced delayed aging in *Caenorhabditis elegans*. *J Biol Chem,* 283**,** 350-7.

MCCOLL, G., ROBERTS, B. R., PUKALA, T. L., KENCHE, V. B., ROBERTS, C. M., LINK, C. D., RYAN, T. M., MASTERS, C. L., BARNHAM, K. J., BUSH, A. I. & CHERNY, R. A. 2012. Utility of an improved model of amyloid-beta ($A\beta_{1-42}$) toxicity in *Caenorhabditis elegans* for drug screening for Alzheimer's disease. *Mol Neurodegener,* 7**,** 57.

MCCOLL, G., ROGERS, A. N., ALAVEZ, S., HUBBARD, A. E., MELOV, S., LINK, C. D., BUSH, A. I., KAPAHI, P. & LITHGOW, G. J. 2010. Insulin-like signaling determines survival during stress via posttranscriptional mechanisms in *C. elegans*. *Cell Metab,* 12**,** 260-72.

MCCORMICK, A. V., WHEELER, J. M., GUTHRIE, C. R., LIACHKO, N. F. & KRAEMER, B. C. 2013. Dopamine D2 receptor antagonism suppresses tau aggregation and neurotoxicity. *Biol Psychiatry,* 73**,** 464-71.

MCDERMOTT, J. B., AAMODT, S. & AAMODT, E. 1996. ptl-1, a *Caenorhabditis elegans* gene whose products are homologous to the tau microtubule-associated proteins. *Biochemistry,* 35**,** 9415-23.

MCDONALD, P. W., HARDIE, S. L., JESSEN, T. N., CARVELLI, L., MATTHIES, D. S. & BLAKELY, R. D. 2007. Vigorous motor activity in *Caenorhabditis elegans* requires efficient clearance of dopamine mediated by synaptic localization of the dopamine transporter DAT-1. *The Journal of Neuroscience,* 27**,** 14216-14227.

MCELWEE, J., BUBB, K. & THOMAS, J. H. 2003. Transcriptional outputs of the *Caenorhabditis elegans* forkhead protein DAF-16. *Aging Cell,* 2**,** 111-21.

MCELWEE, J. J., SCHUSTER, E., BLANC, E., THOMAS, J. H. & GEMS, D. 2004. Shared transcriptional signature in *Caenorhabditis elegans* Dauer larvae and long-lived daf-2 mutants implicates detoxification system in longevity assurance. *J Biol Chem,* 279**,** 44533-43.

MCGEE, M. D., WEBER, D., DAY, N., VITELLI, C., CRIPPEN, D., HERNDON, L. A., HALL, D. H. & MELOV, S. 2011. Loss of intestinal nuclei and intestinal integrity in aging *C. elegans*. *Aging Cell,* 10**,** 699-710.

MCGOUGH, IAN J., STEINBERG, F., JIA, D., BARBUTI, PETER A., MCMILLAN, KIRSTY J., HEESOM, KATE J., WHONE, ALAN L., CALDWELL, MAEVE A., BILLADEAU, DANIEL D., ROSEN, MICHAEL K. & CULLEN, PETER J. 2014. Retromer binding to FAM21 and the WASH complex is perturbed by the Parkinson disease-linked VPS35(D620N) mutation. *Current Biology,* 24**,** 1670-1676.

MENZEL, R., MENZEL, S., SWAIN, S. C., PIETSCH, K., TIEDT, S., WITCZAK, J., STURZENBAUM, S. R. & STEINBERG, C. E. 2012. The nematode *Caenorhabditis elegans*, stress and aging: identifying the complex interplay of genetic pathways following the treatment with humic substances. *Front Genet,* 3**,** 50.

MENZEL, R., SWAIN, S., HOESS, S., CLAUS, E., MENZEL, S., STEINBERG, C., REIFFERSCHEID, G. & STURZENBAUM, S. 2009. Gene expression profiling to characterize sediment toxicity - a pilot study using *Caenorhabditis elegans* whole genome microarrays. *BMC Genomics,* 10**,** 160.

MIGUEL-ALIAGA, I., CULETTO, E., WALKER, D. S., BAYLIS, H. A., SATTELLE, D. B. & DAVIES, K. E. 1999. The *Caenorhabditis elegans* orthologue of the human gene responsible for spinal muscular atrophy is a maternal product critical for germline maturation and embryonic viability. *Hum Mol Genet,* 8**,** 2133-43.

MILLER, L. C., SWAYNE, L. A., CHEN, L., FENG, Z. P., WACKER, J. L., MUCHOWSKI, P. J., ZAMPONI, G. W. & BRAUN, J. E. 2003. Cysteine string protein (CSP) inhibition of N-type calcium channels is blocked by mutant huntingtin. *J Biol Chem,* 278**,** 53072-81.

MILLER, R. M., CALLAHAN, L. M., CASACELI, C., CHEN, L., KISER, G. L., CHUI, B., KAYSSER-KRANICH, T. M., SENDERA, T. J., PALANIAPPAN, C. & FEDEROFF, H. J. 2004. Dysregulation of gene expression in the 1-methyl-4-phenyl-1,2,3,6-tetrahydropyridine-lesioned mouse substantia nigra. *The Journal of Neuroscience,* 24**,** 7445-7454.

MIMURA, Y., JOHNOSONO, M., IZUMO, S., KURIYAMA, M. & OSAME, M. 1992. Adult-onset neuronal ceroid lipofuscinosis--a case report with biological study. *Rinsho Shinkeigaku,* 32**,** 771-3.

MITCHISON, H. M. & MOLE, S. E. 2001. Neurodegenerative disease: the neuronal ceroid lipofuscinoses (Batten disease). *Curr Opin Neurol,* 14**,** 795-803.

MITRPANT, C., PORENSKY, P., ZHOU, H., PRICE, L., MUNTONI, F., FLETCHER, S., WILTON, S. D. & BURGHES, A. H. M. 2013. Improved antisense oligonucleotide design to suppress aberrant *SMN2* gene transcript processing: towards a treatment for spinal muscular atrophy. *PLoS ONE,* 8**,** e62114.

MIYASAKA, T., DING, Z., GENGYO-ANDO, K., OUE, M., YAMAGUCHI, H., MITANI, S. & IHARA, Y. 2005. Progressive neurodegeneration in *C. elegans* model of tauopathy. *Neurobiol Dis,* 20**,** 372-83.

MOCKO, J. B., KERN, A., MOOSMANN, B., BEHL, C. & HAJIEVA, P. 2010. Phenothiazines interfere with dopaminergic neurodegeneration in *Caenorhabditis elegans* models of Parkinson's disease. *Neurobiol Dis,* 40**,** 120-9.

MOJSILOVIC-PETROVIC, J., NEDELSKY, N., BOCCITTO, M., MANO, I., GEORGIADES, S. N., ZHOU, W., LIU, Y., NEVE, R. L., TAYLOR, J. P., DRISCOLL, M., CLARDY, J., MERRY, D. & KALB, R. G. 2009. FOXO3a is broadly neuroprotective in vitro and in vivo against insults implicated in motor neuron diseases. *The Journal of Neuroscience,* 29**,** 8236-8247.

MOLL, L., EL-AMI, T. & COHEN, E. 2014. Selective manipulation of aging: a novel strategy for the treatment of neurodegenerative disorders. *Swiss Med Wkly,* 144**,** w13917.

MORLEY, J. & MORIMOTO, R. 2004. Regulation of longevity in *Caenorhabditis elegans* by heat shock factor and molecular chaperones. *Mol Biol Cell,* 15**,** 657 - 64.

MORLEY, J. F., BRIGNULL, H. R., WEYERS, J. J. & MORIMOTO, R. I. 2002. The threshold for polyglutamine-expansion protein aggregation and cellular toxicity is dynamic and influenced by aging in *Caenorhabditis elegans*. *Proceedings of the National Academy of Sciences,* 99**,** 10417-10422.

MUCHOWSKI, P. J. 2002. Protein misfolding, amyloid formation, and neurodegeneration: a critical role for molecular chaperones? *Neuron,* 35**,** 9-12.

MUNOZ-LOBATO, F., RODRIGUEZ-PALERO, M. J., NARANJO-GALINDO, F. J., SHEPHARD, F., GAFFNEY, C. J., SZEWCZYK, N. J., HAMAMICHI, S., CALDWELL, K. A., CALDWELL, G. A., LINK, C. D. & MIRANDA-VIZUETE, A. 2013. Protective role of DNJ-27/ERdj5 in *Caenorhabditis elegans* models of human neurodegenerative diseases. *Antioxid Redox Signal*.

MURAKAMI, A., KOJIMA, K., OHYA, K., IMAMURA, K. & TAKASAKI, Y. 2002. A new conformational epitope generated by the binding of recombinant 70-kd protein and U1 RNA to anti-U1 RNP autoantibodies in sera from patients with mixed connective tissue disease. *Arthritis Rheum,* 46**,** 3273-82.

MURATA, M., HASEGAWA, K. & KANAZAWA, I. 2007. Zonisamide improves motor function in Parkinson disease: a randomized, double-blind study. *Neurology,* 68**,** 45-50.

MURPHY, C. T. 2006. The search for DAF-16/FOXO transcriptional targets: approaches and discoveries. *Exp Gerontol,* 41**,** 910-21.

MURPHY, C. T., MCCARROLL, S. A., BARGMANN, C. I., FRASER, A., KAMATH, R. S., AHRINGER, J., LI, H. & KENYON, C. 2003. Genes that act downstream of DAF-16 to influence the lifespan of *Caenorhabditis elegans*. *Nature,* 424**,** 277-283.

NAPOLITANO, M., CENTONZE, D., CALCE, A., PICCONI, B., SPIEZIA, S., GULINO, A., BERNARDI, G. & CALABRESI, P. 2002. Experimental parkinsonism modulates multiple genes involved in the transduction of dopaminergic signals in the striatum. *Neurobiology of Disease,* 10**,** 387-395.

NASS, R., HAHN, M. K., JESSEN, T., MCDONALD, P. W., CARVELLI, L. & BLAKELY, R. D. 2005. A genetic screen in *Caenorhabditis elegans* for dopamine neuron insensitivity to 6-hydroxydopamine identifies dopamine transporter mutants impacting transporter biosynthesis and trafficking. *Journal of Neurochemistry,* 94**,** 774-785.

NASS, R. & HAMZA, I. 2001. The nematode *C. elegans* as an animal model to explore toxicology in vivo: solid and axenic growth culture conditions and

compound exposure parameters. *Current Protocols in Toxicology.* John Wiley & Sons, Inc.

NASS, R., MILLER, D. M. & BLAKELY, R. D. 2001. *C. elegans*: a novel pharmacogenetic model to study Parkinson's disease. *Parkinsonism & Related Disorders,* 7**,** 185-191.

NIU, W., LU, Z. J., ZHONG, M., SAROV, M., MURRAY, J. I., BRDLIK, C. M., JANETTE, J., CHEN, C., ALVES, P., PRESTON, E., SLIGHTHAM, C., JIANG, L., HYMAN, A. A., KIM, S. K., WATERSTON, R. H., GERSTEIN, M., SNYDER, M. & REINKE, V. 2011. Diverse transcription factor binding features revealed by genome-wide ChIP-seq in *C. elegans*. *Genome Research,* 21**,** 245-254.

NOLLEN, E. A., GARCIA, S. M., VAN HAAFTEN, G., KIM, S., CHAVEZ, A., MORIMOTO, R. I. & PLASTERK, R. H. 2004. Genome-wide RNA interference screen identifies previously undescribed regulators of polyglutamine aggregation. *Proc Natl Acad Sci U S A,* 101**,** 6403-8.

NOSKOVA, L., STRANECKY, V., HARTMANNOVA, H., PRISTOUPILOVA, A., BARESOVA, V., IVANEK, R., HULKOVA, H., JAHNOVA, H., VAN DER ZEE, J., STAROPOLI, J. F., SIMS, K. B., TYYNELA, J., VAN BROECKHOVEN, C., NIJSSEN, P. C., MOLE, S. E., ELLEDER, M. & KMOCH, S. 2011. Mutations in *DNAJC5*, encoding cysteine-string protein alpha, cause autosomal-dominant adult-onset neuronal ceroid lipofuscinosis. *Am J Hum Genet,* 89**,** 241-52.

NUSSBAUM-KRAMMER, C. I. & MORIMOTO, R. I. 2014. *Caenorhabditis elegans* as a model system for studying non-cell-autonomous mechanisms in protein-misfolding diseases. *Disease Models & Mechanisms,* 7**,** 31-39.

NUSSBAUM-KRAMMER, C. I., PARK, K.-W., LI, L., MELKI, R. & MORIMOTO, R. I. 2013. Spreading of a prion domain from cell-to-cell by vesicular transport in *Caenorhabditis elegans*. *PLoS Genet,* 9**,** e1003351.

O'REILLY, L. P., LUKE, C. J., PERLMUTTER, D. H., SILVERMAN, G. A. & PAK, S. C. 2014. *C. elegans* in high-throughput drug discovery. *Adv Drug Deliv Rev,* 69-70**,** 247-53.

OEDA, T., SHIMOHAMA, S., KITAGAWA, N., KOHNO, R., IMURA, T., SHIBASAKI, H. & ISHII, N. 2001. Oxidative stress causes abnormal accumulation of familial amyotrophic lateral sclerosis-related mutant SOD1 in transgenic *Caenorhabditis elegans*. *Hum Mol Genet,* 10**,** 2013-23.

OLIVEIRA, R. P., PORTER ABATE, J., DILKS, K., LANDIS, J., ASHRAF, J., MURPHY, C. T. & BLACKWELL, T. K. 2009. Condition-adapted stress and longevity gene regulation by *Caenorhabditis elegans* SKN-1/Nrf. *Aging Cell,* 8**,** 524-41.

OMIECINSKI, C. J., VANDEN HEUVEL, J. P., PERDEW, G. H. & PETERS, J. M. 2011. Xenobiotic metabolism, disposition, and regulation by receptors: from biochemical phenomenon to predictors of major toxicities. *Toxicol Sci,* 120 Suppl 1**,** S49-75.

ONKEN, B. & DRISCOLL, M. 2010. Metformin induces a dietary restriction-like state and the oxidative stress response to extend *C. elegans* Healthspan via AMPK, LKB1, and SKN-1. *PLoS One,* 5**,** e8758.

ORR, H. T. & ZOGHBI, H. Y. 2007. Trinucleotide repeat disorders. *Annu Rev Neurosci,* 30**,** 575-621.

PALGUNOW, D., KLAPPER, M. & DORING, F. 2012. Dietary restriction during development enlarges intestinal and hypodermal lipid droplets in *Caenorhabditis elegans*. *PLoS One,* 7**,** e46198.

PALMER, D. N., BARRY, L. A., TYYNELA, J. & COOPER, J. D. 2013. NCL disease mechanisms. *Biochim Biophys Acta,* 1832**,** 1882-93.

PANOWSKI, S. H., WOLFF, S., AGUILANIU, H., DURIEUX, J. & DILLIN, A. 2007. PHA-4/Foxa mediates diet-restriction-induced longevity of *C. elegans*. *Nature,* 447**,** 550-555.

PARDO, C. A., RABIN, B. A., PALMER, D. N. & PRICE, D. L. 1994. Accumulation of the adenosine triphosphate synthase subunit C in the mnd mutant mouse. A model for neuronal ceroid lipofuscinosis. *Am J Pathol,* 144**,** 829-35.

PARK, H. M., KIM, J. A. & KWAK, M. K. 2009a. Protection against amyloid beta cytotoxicity by sulforaphane: role of the proteasome. *Arch Pharm Res,* 32**,** 109-15.

PARK, K.-W. & LI, L. 2011. Prion protein in *Caenorhabditis elegans*: Distinct models of anti-BAX and neuropathology. *Prion,* 5**,** 28-38.

PARK, S.-K., TEDESCO, P. M. & JOHNSON, T. E. 2009b. Oxidative stress and longevity in *Caenorhabditis elegans* as mediated by SKN-1. *Aging Cell,* 8**,** 258-269.

PARK, S. H., KUKUSHKIN, Y., GUPTA, R., CHEN, T., KONAGAI, A., HIPP, M. S., HAYER-HARTL, M. & HARTL, F. U. 2013. PolyQ proteins interfere with nuclear degradation of cytosolic proteins by sequestering the Sis1p chaperone. *Cell,* 154**,** 134-45.

PARKER, J., ARANGO, M., ABDERRAHMANE, S., LAMBERT, E., TOURETTE, C., CATOIRE, H. & NERI, C. 2005. Resveratrol rescues mutant polyglutamine cytotoxicity in nematode and mammalian neurons. *Nat Genet,* 37**,** 349 - 350.

PARKER, J., CONNOLLY, J., WELLINGTON, C., HAYDEN, M., DAUSSET, J. & NERI, C. 2001. Expanded polyglutamines in *Caenorhabditis elegans* cause axonal abnormalities and severe dysfunction of PLM mechanosensory neurons without cell death. *Proc Natl Acad Sci USA,* 98**,** 13318 - 13323.

PARKER, J., METZLER, M., GEORGIOU, J., MAGE, M., RODER, J., ROSE, A., HAYDEN, M. & NERI, C. 2007. Huntingtin-interacting protein 1 influences worm and mouse presynaptic function and protects *Caenorhabditis elegans* neurons against mutant polyglutamine toxicity. *J Neurosci,* 27**,** 11056 - 11064.

PASINELLI, P. & BROWN, R. H. 2006. Molecular biology of amyotrophic lateral sclerosis: insights from genetics. *Nat Rev Neurosci,* 7**,** 710-23.

PATEL, D. S., FANG, L. L., SVY, D. K., RUVKUN, G. & LI, W. 2008. Genetic identification of HSD-1, a conserved steroidogenic enzyme that directs larval development in *Caenorhabditis elegans*. *Development,* 135**,** 2239-2249.

PELTONEN, L., SAVUKOSKI, M. & VESA, J. 2000. Genetics of the neuronal ceroid lipofuscinoses. *Curr Opin Genet Dev,* 10**,** 299-305.

PENG, K., LI, Y., LONG, L., LI, D., JIA, Q., WANG, Y., SHEN, Q., TANG, Y., WEN, L., KUNG, H. F. & PENG, Y. 2010. Knockdown of FoxO3a induces increased neuronal apoptosis during embryonic development in zebrafish. *Neurosci Lett,* 484**,** 98-103.

PETRASCHECK, M., YE, X. & BUCK, L. B. 2007. An antidepressant that extends lifespan in adult *Caenorhabditis elegans*. *Nature,* 450**,** 553-556.

PICKETT, C. B. & LU, A. Y. 1989. Glutathione S-transferases: gene structure, regulation, and biological function. *Annu Rev Biochem,* 58**,** 743-64.

PIETSCH, K., SAUL, N., SWAIN, S., MENZEL, R., STEINBERG, C. E. W. & STURZENBAUM, S. 2012. Meta-analysis of global transcriptomics reveals conserved genetic pathways of Quercetin and Tannic acid mediated longevity in *C. elegans*. *Frontiers in Genetics,* 3.

PINO, E., AMAMOTO, R., ZHENG, L., CACQUEVEL, M., SARRIA, J.-C., KNOTT, G. W. & SCHNEIDER, B. L. 2014. FOXO3 determines the accumulation of α-synuclein and controls the fate of dopaminergic neurons in the substantia nigra. *Human Molecular Genetics,* 23**,** 1435-1452.

PITKANEN, A. 2002. Efficacy of current antiepileptics to prevent neurodegeneration in epilepsy models. *Epilepsy Research,* 50**,** 141-60.

PLANT, K. E., ANDERSON, E., SIMECEK, N., BROWN, R., FORSTER, S., SPINKS, J., TOMS, N., GIBSON, G. G., LYON, J. & PLANT, N. 2009. The neuroprotective action of the mood stabilizing drugs lithium chloride and sodium valproate is mediated through the up-regulation of the homeodomain protein Six1. *Toxicology and Applied Pharmacology,* 235**,** 124-134.

PORTER, M. Y., TURMAINE, M. & MOLE, S. E. 2005. Identification and characterization of *Caenorhabditis elegans* palmitoyl protein thioesterase1. *Journal of Neuroscience Research,* 79**,** 836-848.

PORTMAN, D. S. & EMMONS, S. W. 2004. Identification of *C. elegans* sensory ray genes using whole-genome expression profiling. *Developmental Biology,* 270**,** 499-512.

POUYA, R., SANGEENA, S., SELVAGANAPATHY, P. & BHAGWATI, G. 2011. Microfluidic systems to study the biology of human diseases and identify potential therapeutic targets in *Caenorhabditis elegans*. *Integrated Microsystems.* CRC Press.

PRZYBYSZ, A. J., CHOE, K. P., ROBERTS, L. J. & STRANGE, K. 2009. Increased age reduces DAF-16 and SKN-1 signaling and the hormetic response of *Caenorhabditis elegans* to the xenobiotic juglone. *Mech Ageing Dev,* 130**,** 357-69.

PULAK, R. 2006. Techniques for analysis, sorting, and dispensing of *C. elegans* on the COPAS flow-sorting system. *Methods Mol Biol,* 351**,** 275-86.

QING, H., HE, G., LY, P. T., FOX, C. J., STAUFENBIEL, M., CAI, F., ZHANG, Z., WEI, S., SUN, X., CHEN, C. H., ZHOU, W., WANG, K. & SONG, W. 2008. Valproic acid inhibits Abeta production, neuritic plaque formation, and behavioral deficits in Alzheimer's disease mouse models. *J Exp Med,* 205**,** 2781-9.

RAND, J. B. & JOHNSON, C. D. 1995. Genetic pharmacology: interactions between drugs and gene products in *Caenorhabditis elegans*. *Methods Cell Biol,* 48**,** 187-204.

REICHERT, K. & MENZEL, R. 2005. Expression profiling of five different xenobiotics using a *Caenorhabditis elegans* whole genome microarray. *Chemosphere,* 61**,** 229-237.

REINKE, V., SMITH, H. E., NANCE, J., WANG, J., VAN DOREN, C., BEGLEY, R., JONES, S. J. M., DAVIS, E. B., SCHERER, S., WARD, S. & KIM, S. K. 2000. A global profile of germline gene expression in *C. elegans*. *Molecular Cell,* 6**,** 605-616.

RENTON, A. E., MAJOUNIE, E., WAITE, A., SIMON-SANCHEZ, J., ROLLINSON, S., GIBBS, J. R., SCHYMICK, J. C., LAAKSOVIRTA, H., VAN SWIETEN, J. C., MYLLYKANGAS, L., KALIMO, H., PAETAU, A., ABRAMZON, Y., REMES, A. M., KAGANOVICH, A., SCHOLZ, S. W., DUCKWORTH, J., DING, J., HARMER, D. W., HERNANDEZ, D. G., JOHNSON, J. O., MOK, K., RYTEN, M., TRABZUNI, D., GUERREIRO, R. J., ORRELL, R. W., NEAL, J., MURRAY, A., PEARSON, J., JANSEN, I. E., SONDERVAN, D., SEELAAR, H., BLAKE, D., YOUNG, K., HALLIWELL, N., CALLISTER, J. B., TOULSON, G., RICHARDSON, A., GERHARD, A., SNOWDEN, J., MANN, D., NEARY, D., NALLS, M. A., PEURALINNA, T., JANSSON, L., ISOVIITA, V. M., KAIVORINNE, A. L., HOLTTA-VUORI, M., IKONEN, E., SULKAVA, R., BENATAR, M., WUU, J., CHIO, A., RESTAGNO, G., BORGHERO, G., SABATELLI, M., CONSORTIUM, I., HECKERMAN, D., ROGAEVA, E., ZINMAN, L., ROTHSTEIN, J. D., SENDTNER, M., DREPPER, C., EICHLER, E. E., ALKAN, C., ABDULLAEV, Z., PACK, S. D., DUTRA, A., PAK, E., HARDY, J., SINGLETON, A., WILLIAMS, N. M., HEUTINK, P., PICKERING-BROWN, S., MORRIS, H. R., TIENARI, P. J. & TRAYNOR, B. J. 2011. A hexanucleotide repeat expansion in C9ORF72 is the cause of chromosome 9p21-linked ALS-FTD. *Neuron,* 72**,** 257-68.

RICCIARELLI, R., D'ABRAMO, C., MASSONE, S., MARINARI, U. M., PRONZATO, M. A. & TABATON, M. 2004. Microarray analysis in Alzheimer's disease and normal aging. *IUBMB Life,* 56**,** 349-354.

RICHARD, T., PAWLUS, A. D., IGLESIAS, M. L., PEDROT, E., WAFFO-TEGUO, P., MERILLON, J. M. & MONTI, J. P. 2011. Neuroprotective properties of resveratrol and derivatives. *Ann N Y Acad Sci,* 1215**,** 103-8.

RIDGE, P. G., MUKHERJEE, S., CRANE, P. K., KAUWE, J. S. & ALZHEIMER'S DISEASE GENETICS, C. 2013. Alzheimer's disease: analyzing the missing heritability. *PLoS One,* 8**,** e79771.

RIEDEL, C. G., DOWEN, R. H., LOURENCO, G. F., KIRIENKO, N. V., HEIMBUCHER, T., WEST, J. A., BOWMAN, S. K., KINGSTON, R. E., DILLIN, A., ASARA, J. M. & RUVKUN, G. 2013. DAF-16 employs the chromatin remodeller SWI/SNF to promote stress resistance and longevity. *Nat Cell Biol,* 15**,** 491-501.

RODRIGUES, A. J., NEVES-CARVALHO, A., TEIXEIRA-CASTRO, A., ROKKA, A., CORTHALS, G., LOGARINHO, E. & MACIEL, P. 2011. Absence of Ataxin-3 leads to enhanced stress response in *C. elegans*. *PLoS One,* 6**,** e18512.

RODRIGUEZ, A., MCKAY, K., GRAHAM, M., DITTRICH, J. & HOLGADO, A. M. 2014. Analysis of differential gene expression profiles in *Caenorhabditis elegans* knockouts for the v-SNARE master protein 1. *Journal of Neuroscience Research,* 92**,** 772-782.

ROHDE, C. B., ZENG, F., GONZALEZ-RUBIO, R., ANGEL, M. & YANIK, M. F. 2007. Microfluidic system for on-chip high-throughput whole-animal sorting and screening at subcellular resolution. *Proc Natl Acad Sci U S A,* 104**,** 13891-5.

ROSEN, D. R., SIDDIQUE, T., PATTERSON, D., FIGLEWICZ, D. A., SAPP, P., HENTATI, A., DONALDSON, D., GOTO, J., O'REGAN, J. P., DENG, H.-X., RAHMANI, Z., KRIZUS, A., MCKENNA-YASEK, D., CAYABYAB, A., GASTON, S. M., BERGER, R., TANZI, R. E., HALPERIN, J. J., HERZFELDT, B., VAN DEN BERGH, R., HUNG, W.-Y., BIRD, T., DENG, G., MULDER, D. W., SMYTH, C., LAING, N. G., SORIANO, E., PERICAK-VANCE, M. A., HAINES, J., ROULEAU, G. A., GUSELLA, J. S., HORVITZ, H. R. & BROWN, R. H. 1993. Mutations in Cu/Zn superoxide dismutase gene are associated with familial amyotrophic lateral sclerosis. *Nature,* 362**,** 59-62.

ROSS, C. A. & POIRIER, M. A. 2005. What is the role of protein aggregation in neurodegeneration? *Nat Rev Mol Cell Biol,* 6**,** 891-898.

RUAL, J.-F., CERON, J., KORETH, J., HAO, T., NICOT, A.-S., HIROZANE-KISHIKAWA, T., VANDENHAUTE, J., ORKIN, S. H., HILL, D. E., VAN DEN HEUVEL, S. & VIDAL, M. 2004. Toward improving *Caenorhabditis elegans* phenome mapping with an ORFeome-based RNAi library. *Genome Research,* 14**,** 2162-2168.

RUAN, Q., HARRINGTON, A. J., CALDWELL, K. A., CALDWELL, G. A. & STANDAERT, D. G. 2010. VPS41, a protein involved in lysosomal trafficking, is protective in *Caenorhabditis elegans* and mammalian cellular models of Parkinson's disease. *Neurobiology of Disease,* 37**,** 330-338.

RUSHMORE, T. H. & PICKETT, C. B. 1993. Glutathione S-transferases, structure, regulation, and therapeutic implications. *J Biol Chem,* 268**,** 11475-8.

SAHA, S., GUILLILY, M. D., FERREE, A., LANCETA, J., CHAN, D., GHOSH, J., HSU, C. H., SEGAL, L., RAGHAVAN, K., MATSUMOTO, K., HISAMOTO, N., KUWAHARA, T., IWATSUBO, T., MOORE, L., GOLDSTEIN, L., COOKSON, M. & WOLOZIN, B. 2009. LRRK2 modulates vulnerability to mitochondrial dysfunction in *Caenorhabditis elegans*. *J Neurosci,* 29**,** 9210-8.

SAHARIA, K., ARYA, U., KUMAR, R., SAHU, R., DAS, C. K., GUPTA, K., DWIVEDI, H. & SUBRAMANIAM, J. R. 2012. Reserpine modulates neurotransmitter

release to extend lifespan and alleviate age-dependent Abeta proteotoxicity in *Caenorhabditis elegans*. *Exp Gerontol,* 47**,** 188-97.
SALIH, D. A. & BRUNET, A. 2008. FoxO transcription factors in the maintenance of cellular homeostasis during aging. *Curr Opin Cell Biol,* 20**,** 126-36.
SÄMANN, J., HEGERMANN, J., VON GROMOFF, E., EIMER, S., BAUMEISTER, R. & SCHMIDT, E. 2009. *Caenorhabditits elegans* LRK-1 and PINK-1 act antagonistically in stress response and neurite outgrowth. *Journal of Biological Chemistry,* 284**,** 16482-16491.
SANCHEZ, P. E., ZHU, L., VERRET, L., VOSSEL, K. A., ORR, A. G., CIRRITO, J. R., DEVIDZE, N., HO, K., YU, G. Q., PALOP, J. J. & MUCKE, L. 2012. Levetiracetam suppresses neuronal network dysfunction and reverses synaptic and cognitive deficits in an Alzheimer's disease model. *Proc Natl Acad Sci U S A,* 109**,** E2895-903.
SANGHA, J. S., SUN, X., WALLY, O. S. D., ZHANG, K., JI, X., WANG, Z., WANG, Y., ZIDICHOUSKI, J., PRITHIVIRAJ, B. & ZHANG, J. 2012. Liuwei Dihuang (LWDH), a traditional Chinese medicinal formula, protects against β-Amyloid toxicity in transgenic *Caenorhabditis elegans*. *PLoS One,* 7**,** e43990.
SATYAL, S. H., SCHMIDT, E., KITAGAWA, K., SONDHEIMER, N., LINDQUIST, S., KRAMER, J. M. & MORIMOTO, R. I. 2000. Polyglutamine aggregates alter protein folding homeostasis in *Caenorhabditis elegans*. *Proc Natl Acad Sci U S A,* 97**,** 5750-5.
SAYED, A. A. 2011. Ferulsinaic acid attenuation of advanced glycation end products extends the lifespan of *Caenorhabditis elegans*. *J Pharm Pharmacol,* 63**,** 423-8.
SCHIRMER, R. H., ADLER, H., PICKHARDT, M. & MANDELKOW, E. 2011. "Lest we forget you — methylene blue …". *Neurobiology of Aging,* 32**,** 2325.e7-2325.e16.
SCHMITZ, F., TABARES, L., KHIMICH, D., STRENZKE, N., DE LA VILLA-POLO, P., CASTELLANO-MUÑOZ, M., BULANKINA, A., MOSER, T., FERNÁNDEZ-CHACÓN, R. & SÜDHOF, T. C. 2006. CSPα-deficiency causes massive and rapid photoreceptor degeneration. *Proceedings of the National Academy of Sciences of the United States of America,* 103**,** 2926-2931.
SCHOBER, A. 2004. Classic toxin-induced animal models of Parkinson's disease: 6-OHDA and MPTP. *Cell Tissue Res,* 318**,** 215-24.
SCHULZ, A., KOHLSCHUTTER, A., MINK, J., SIMONATI, A. & WILLIAMS, R. 2013. NCL diseases - clinical perspectives. *Biochim Biophys Acta,* 1832**,** 1801-6.
SEGREF, A., TORRES, S. & HOPPE, T. 2011. A screenable in vivo assay to study proteostasis networks in *Caenorhabditis elegans*. *Genetics,* 187**,** 1235-40.
SEO, J., HOWELL, M. D., SINGH, N. N. & SINGH, R. N. 2013. Spinal muscular atrophy: an update on therapeutic progress. *Biochim Biophys Acta,* 1832**,** 2180-90.
SETTIVARI, R., LEVORA, J. & NASS, R. 2009. The divalent metal transporter homologues SMF-1/2 mediates dopamine neuron sensitivity in *Caenorhabditis elegans* models of manganism and Parkinson's disease. *J. Biol. Chem.***,** M109.051409.
SHAPIRA, M. & TAN, M. W. 2008. Genetic analysis of *Caenorhabditis elegans* innate immunity. *Methods Mol Biol,* 415**,** 429-42.
SHARMA, M., BURRE, J. & SUDHOF, T. C. 2011. CSPalpha promotes SNARE-complex assembly by chaperoning SNAP-25 during synaptic activity. *Nat Cell Biol,* 13**,** 30-9.
SHARMA, M., BURRE, J. & SUDHOF, T. C. 2012. Proteasome inhibition alleviates SNARE-dependent neurodegeneration. *Sci Transl Med,* 4**,** 147ra113.
SHASTRY, B. S. 1998. Molecular genetics of familial Alzheimer disease. *Am J Med Sci,* 315**,** 266-72.

SHAW, W. M., LUO, S., LANDIS, J., ASHRAF, J. & MURPHY, C. T. 2007. The *C. elegans* TGF-β dauer pathway regulates longevity via insulin signaling. *Current Biology,* 17**,** 1635-1645.

SHIN, B. H., LIM, Y., OH, H. J., PARK, S. M., LEE, S.-K., AHNN, J., KIM, D. H., SONG, W. K., KWAK, T. H. & PARK, W. J. 2013. Pharmacological activation of Sirt1 ameliorates polyglutamine-induced toxicity through the regulation of autophagy. *PLoS ONE,* 8**,** e64953.

SIINTOLA, E., LEHESJOKI, A. E. & MOLE, S. E. 2006a. Molecular genetics of the NCLs -- status and perspectives. *Biochim Biophys Acta,* 1762**,** 857-64.

SIINTOLA, E., PARTANEN, S., STROMME, P., HAAPANEN, A., HALTIA, M., MAEHLEN, J., LEHESJOKI, A. E. & TYYNELA, J. 2006b. Cathepsin D deficiency underlies congenital human neuronal ceroid-lipofuscinosis. *Brain,* 129**,** 1438-45.

SILVA, D. F., ESTEVES, A. R., OLIVEIRA, C. R. & CARDOSO, S. M. 2011a. Mitochondria: the common upstream driver of amyloid-beta and tau pathology in Alzheimer's disease. *Curr Alzheimer Res,* 8**,** 563-72.

SILVA, M., FOX, S., BEAM, M., THAKKAR, H., AMARAL, M. & MORIMOTO, R. 2011b. A genetic screening strategy identifies novel regulators of the proteostasis network. *PLoS Genet,* 7**,** e1002438.

SIMMER, F., MOORMAN, C., VAN DER LINDEN, A., KUIJK, E., VAN DEN BERGHE, P., KAMATH, R., FRASER, A., AHRINGER, J. & PLASTERK, R. 2003. Genome-wide RNAi of *C. elegans* using the hypersensitive *rrf-3* strain reveals novel gene functions. *PLoS Biol,* 1**,** E12.

SINGH, P., MOHAMMAD, F. & SHARMA, A. 2011. Transcriptomic analysis in a *Drosophila* model identifies previously implicated and novel pathways in the therapeutic mechanism in neuropsychiatric disorders. *Frontiers in Neuroscience,* 5.

SLEIGH, J. & SATTELLE, D. 2010. *C. elegans* models of neuromuscular diseases expedite translational research. *Translational Neuroscience,* 1**,** 214-227.

SLEIGH, J. N., BUCKINGHAM, S. D., ESMAEILI, B., VISWANATHAN, M., CUPPEN, E., WESTLUND, B. M. & SATTELLE, D. B. 2011. A novel *Caenorhabditis elegans* allele, *smn-1(cb131)*, mimicking a mild form of spinal muscular atrophy, provides a convenient drug screening platform highlighting new and pre-approved compounds. *Hum Mol Genet,* 20**,** 245-60.

SMITH, E. L. & SCHUCHMAN, E. H. 2008. The unexpected role of acid sphingomyelinase in cell death and the pathophysiology of common diseases. *FASEB J,* 22**,** 3419-31.

SMITH, J. V. & LUO, Y. 2003. Elevation of oxidative free radicals in Alzheimer's disease models can be attenuated by Ginkgo biloba extract EGb 761. *Journal of Alzheimer's Disease,* 5**,** 287-300.

SMITH, K. R., DAHL, H. H., CANAFOGLIA, L., ANDERMANN, E., DAMIANO, J., MORBIN, M., BRUNI, A. C., GIACCONE, G., COSSETTE, P., SAFTIG, P., GROTZINGER, J., SCHWAKE, M., ANDERMANN, F., STAROPOLI, J. F., SIMS, K. B., MOLE, S. E., FRANCESCHETTI, S., ALEXANDER, N. A., COOPER, J. D., CHAPMAN, H. A., CARPENTER, S., BERKOVIC, S. F. & BAHLO, M. 2013. Cathepsin F mutations cause Type B Kufs disease, an adult-onset neuronal ceroid lipofuscinosis. *Hum Mol Genet,* 22**,** 1417-23.

SMITH, K. R., DAMIANO, J., FRANCESCHETTI, S., CARPENTER, S., CANAFOGLIA, L., MORBIN, M., ROSSI, G., PAREYSON, D., MOLE, S. E., STAROPOLI, J. F., SIMS, K. B., LEWIS, J., LIN, W. L., DICKSON, D. W., DAHL, H. H., BAHLO, M. & BERKOVIC, S. F. 2012a. Strikingly different clinicopathological phenotypes determined by progranulin-mutation dosage. *Am J Hum Genet,* 90**,** 1102-7.

SMITH, R. N., ALEKSIC, J., BUTANO, D., CARR, A., CONTRINO, S., HU, F., LYNE, M., LYNE, R., KALDERIMIS, A., RUTHERFORD, K., STEPAN, R.,

SULLIVAN, J., WAKELING, M., WATKINS, X. & MICKLEM, G. 2012b. InterMine: a flexible data warehouse system for the integration and analysis of heterogeneous biological data. *Bioinformatics,* 28**,** 3163-5.

SONDOSSI, K., MAJDZADEH, M., GHAELI, P., GHAHREMANI, M. H., SHAFAROODI, H., PAKNEJAD, B. & OSTAD, S. N. 2014. Analysis of the antiepileptic, ethosuximide impacts on neurogenesis of rat forebrain stem cells. *Fundamental & Clinical Pharmacology***,** n/a-n/a.

SOTO, C. & ESTRADA, L. D. 2008. Protein misfolding and neurodegeneration. *Arch Neurol,* 65**,** 184-9.

SPRINGER, W., HOPPE, T., SCHMIDT, E. & BAUMEISTER, R. 2005. A *Caenorhabditis elegans* Parkin mutant with altered solubility couples alpha-synuclein aggregation to proteotoxic stress. *Hum Mol Genet,* 14**,** 3407-23.

SREEDHARAN, J., BLAIR, I. P., TRIPATHI, V. B., HU, X., VANCE, C., ROGELJ, B., ACKERLEY, S., DURNALL, J. C., WILLIAMS, K. L., BURATTI, E., BARALLE, F., DE BELLEROCHE, J., MITCHELL, J. D., LEIGH, P. N., AL-CHALABI, A., MILLER, C. C., NICHOLSON, G. & SHAW, C. E. 2008. TDP-43 mutations in familial and sporadic Amyotrophic Lateral Sclerosis. *Science,* 319**,** 1668-1672.

SRIVAREERAT, M., TRAN, T., SALIM, S., ALEISA, A. & ALKADHI, K. 2009. Chronic nicotine restores normal Abeta levels and prevents short-term memory and E-LTP impairment in Abeta rat model of Alzheimer's disease. *Neurobiol Aging,* 4**,** 15.

STAROPOLI, J. F., KARAA, A., LIM, E. T., KIRBY, A., ELBALALESY, N., ROMANSKY, S. G., LEYDIKER, K. B., COPPEL, S. H., BARONE, R., XIN, W., MACDONALD, M. E., ABDENUR, J. E., DALY, M. J., SIMS, K. B. & COTMAN, S. L. 2012. A homozygous mutation in KCTD7 links neuronal ceroid lipofuscinosis to the ubiquitin-proteasome system. *Am J Hum Genet,* 91**,** 202-8.

STEFANI, M. & DOBSON, C. M. 2003. Protein aggregation and aggregate toxicity: new insights into protein folding, misfolding diseases and biological evolution. *J Mol Med (Berl),* 81**,** 678-99.

STEGER, K. A., SHTONDA, B. B., THACKER, C., SNUTCH, T. P. & AVERY, L. 2005. The *C. elegans* T-type calcium channel CCA-1 boosts neuromuscular transmission. *J Exp Biol,* 208**,** 2191-203.

STEINKRAUS, K. A., SMITH, E. D., DAVIS, C., CARR, D., PENDERGRASS, W. R., SUTPHIN, G. L., KENNEDY, B. K. & KAEBERLEIN, M. 2008. Dietary restriction suppresses proteotoxicity and enhances longevity by an *hsf-1*-dependent mechanism in *Caenorhabditis elegans*. *Aging Cell,* 7**,** 394-404.

STRAND, A. D., ARAGAKI, A. K., SHAW, D., BIRD, T., HOLTON, J., TURNER, C., TAPSCOTT, S. J., TABRIZI, S. J., SCHAPIRA, A. H., KOOPERBERG, C. & OLSON, J. M. 2005. Gene expression in Huntington's disease skeletal muscle: a potential biomarker. *Hum Mol Genet,* 14**,** 1863-76.

SUTPHIN, G., BISHOP, E., YANOS, M., MOLLER, R. & KAEBERLEIN, M. 2012. Caffeine extends life span, improves healthspan, and delays age-associated pathology in *Caenorhabditis elegans*. *Longevity & Healthspan,* 1**,** 1-12.

SWARUP, V., PHANEUF, D., DUPRE, N., PETRI, S., STRONG, M., KRIZ, J. & JULIEN, J. P. 2011. Deregulation of TDP-43 in amyotrophic lateral sclerosis triggers nuclear factor kappaB-mediated pathogenic pathways. *J Exp Med,* 208**,** 2429-47.

SWIERCZEK, N. A., GILES, A. C., RANKIN, C. H. & KERR, R. A. 2011. High-throughput behavioral analysis in *C. elegans*. *Nat Methods,* 8**,** 592-8.

SYNTICHAKI, P., XU, K., DRISCOLL, M. & TAVERNARAKIS, N. 2002. Specific aspartyl and calpain proteases are required for neurodegeneration in *C. elegans*. *Nature,* 419**,** 939-944.

TAKASUGI, N., TOMITA, T., HAYASHI, I., TSURUOKA, M., NIIMURA, M., TAKAHASHI, Y., THINAKARAN, G. & IWATSUBO, T. 2003. The role of presenilin cofactors in the gamma-secretase complex. *Nature,* 422**,** 438-41.

TANK, E. M., RODGERS, K. E. & KENYON, C. 2011. Spontaneous age-related neurite branching in *Caenorhabditis elegans*. *J Neurosci,* 31**,** 9279-88.

TARDIFF, D. F., TUCCI, M. L., CALDWELL, K. A., CALDWELL, G. A. & LINDQUIST, S. 2012. Different 8-hydroxyquinolines protect models of TDP-43 protein, alpha-synuclein, and polyglutamine proteotoxicity through distinct mechanisms. *J Biol Chem,* 287**,** 4107-20.

TAUFFENBERGER, A., CHITRAMUTHU, B. P., BATEMAN, A., BENNETT, H. P. & PARKER, J. A. 2012. Reduction of polyglutamine toxicity by TDP-43, FUS and progranulin in Huntington's disease models. *Human Molecular Genetics*.

TAUFFENBERGER, A., JULIEN, C. & PARKER, J. A. 2013. Evaluation of longevity enhancing compounds against transactive response DNA-binding protein-43 neuronal toxicity. *Neurobiology of Aging,* 34**,** 2175-2182.

TAYLOR, J. P., HARDY, J. & FISCHBECK, K. H. 2002. Toxic proteins in neurodegenerative disease. *Science,* 296**,** 1991-5.

TEIXEIRA-CASTRO, A., AILION, M., JALLES, A., BRIGNULL, H. R., VILAÇA, J. L., DIAS, N., RODRIGUES, P., OLIVEIRA, J. F., NEVES-CARVALHO, A., MORIMOTO, R. I. & MACIEL, P. 2011. Neuron-specific proteotoxicity of mutant ataxin-3 in *C. elegans*: rescue by the DAF-16 and HSF-1 pathways. *Human Molecular Genetics*.

TEPPER, RONALD G., ASHRAF, J., KALETSKY, R., KLEEMANN, G., MURPHY, COLEEN T. & BUSSEMAKER, HARMEN J. 2013. PQM-1 complements DAF-16 as a key transcriptional regulator of DAF-2-mediated development and longevity. *Cell,* 154**,** 676-690.

TESCHENDORF, D. & LINK, C. 2009. What have worm models told us about the mechanisms of neuronal dysfunction in human neurodegenerative diseases? *Mol Neurodegener,* 4**,** 1-13.

TEULING, E., BOURGONJE, A., VEENJE, S., THIJSSEN, K., DE BOER, J., VAN DER VELDE, J., SWERTZ, M. & NOLLEN, E. 2011. Modifiers of mutant huntingtin aggregation: functional conservation of *C. elegans*-modifiers of polyglutamine aggregation. *PLoS Curr,* 3**,** RRN1255.

THAN, M. T., KUDLOW, B. A. & HAN, M. 2013. Functional analysis of neuronal microRNAs in *Caenorhabditis elegans* dauer formation by combinational genetics and neuronal miRISC immunoprecipitation. *PLoS Genet,* 9**,** e1003592.

THERRIEN, M. & PARKER, J. A. 2014. Worming forward: amyotrophic lateral sclerosis toxicity mechanisms and genetic interactions in *Caenorhabditis elegans*. *Frontiers in Genetics,* 5.

THERRIEN, M., ROULEAU, G. A., DION, P. A. & PARKER, J. A. 2013. Deletion of C9ORF72 results in motor neuron degeneration and stress sensitivity in *C. elegans*. *PLoS ONE,* 8**,** e83450.

THOMAS-CHOLLIER, M., DARBO, E., HERRMANN, C., DEFRANCE, M., THIEFFRY, D. & VAN HELDEN, J. 2012a. A complete workflow for the analysis of full-size ChIP-seq (and similar) data sets using peak-motifs. *Nat. Protocols,* 7**,** 1551-1568.

THOMAS-CHOLLIER, M., DEFRANCE, M., MEDINA-RIVERA, A., SAND, O., HERRMANN, C., THIEFFRY, D. & VAN HELDEN, J. 2011. RSAT 2011: regulatory sequence analysis tools. *Nucleic Acids Res,* 29**,** W86 - W91.

THOMAS-CHOLLIER, M., HERRMANN, C., DEFRANCE, M., SAND, O., THIEFFRY, D. & VAN HELDEN, J. 2012b. RSAT peak-motifs: motif analysis in full-size ChIP-seq datasets. *Nucleic Acids Research,* 40**,** e31.

THOMAS-CHOLLIER, M., SAND, O., TURATSINZE, J.-V., JANKY, R. S., DEFRANCE, M., VERVISCH, E., BROHÉE, S. & VAN HELDEN, J. 2008.

RSAT: regulatory sequence analysis tools. *Nucleic Acids Research,* 36**,** W119-W127.

TIMCHALK, C., NOLAN, R. J., MENDRALA, A. L., DITTENBER, D. A., BRZAK, K. A. & MATTSSON, J. L. 2002. A Physiologically based pharmacokinetic and pharmacodynamic (PBPK/PD) model for the organophosphate insecticide chlorpyrifos in rats and humans. *Toxicol Sci,* 66**,** 34-53.

TIMMONS, L., COURT, D. & FIRE, A. 2001. Ingestion of bacterially expressed dsRNAs can produce specific and potent genetic interference in *Caenorhabditis elegans*. *Gene,* 263**,** 103 - 112.

TIMMONS, L., TABARA, H., MELLO, C. C. & FIRE, A. Z. 2003. Inducible systemic RNA silencing in *Caenorhabditis elegans*. *Molecular Biology of the Cell,* 14**,** 2972-2983.

TOTH, M. L., MELENTIJEVIC, I., SHAH, L., BHATIA, A., LU, K., TALWAR, A., NAJI, H., IBANEZ-VENTOSO, C., GHOSE, P., JEVINCE, A., XUE, J., HERNDON, L. A., BHANOT, G., RONGO, C., HALL, D. H. & DRISCOLL, M. 2012. Neurite sprouting and synapse deterioration in the aging *Caenorhabditis elegans* nervous system. *J Neurosci,* 32**,** 8778-90.

TRAN, N. T. & HUANG, C.-H. 2014. A survey of motif finding Web tools for detecting binding site motifs in ChIP-Seq data. *Biology Direct,* 9**,** 4.

TREUSCH, S., CYR, D. M. & LINDQUIST, S. 2009. Amyloid deposits: protection against toxic protein species? *Cell Cycle,* 8**,** 1668-74.

TREUSCH, S., HAMAMICHI, S., GOODMAN, J. L., MATLACK, K. E. S., CHUNG, C. Y., BARU, V., SHULMAN, J. M., PARRADO, A., BEVIS, B. J., VALASTYAN, J. S., HAN, H., LINDHAGEN-PERSSON, M., REIMAN, E. M., EVANS, D. A., BENNETT, D. A., OLOFSSON, A., DEJAGER, P. L., TANZI, R. E., CALDWELL, K. A., CALDWELL, G. A. & LINDQUIST, S. 2011. Functional links between Aβ toxicity, endocytic trafficking, and Alzheimer's disease risk factors in yeast. *Science,* 334**,** 1241-1245.

TRINH, J. & FARRER, M. 2013. Advances in the genetics of Parkinson disease. *Nat Rev Neurol,* 9**,** 445-54.

TROEMEL, E. R., CHU, S. W., REINKE, V., LEE, S. S., AUSUBEL, F. M. & KIM, D. H. 2006. p38 MAPK regulates expression of immune response genes and contributes to longevity in *C. elegans*. *PLoS Genet,* 2**,** e183.

TURATSINZE, J.-V., THOMAS-CHOLLIER, M., DEFRANCE, M. & VAN HELDEN, J. 2008. Using RSAT to scan genome sequences for transcription factor binding sites and cis-regulatory modules. *Nat. Protocols,* 3**,** 1578-1588.

TURNER, P. R., O'CONNOR, K., TATE, W. P. & ABRAHAM, W. C. 2003. Roles of amyloid precursor protein and its fragments in regulating neural activity, plasticity and memory. *Prog Neurobiol,* 70**,** 1-32.

USENOVIC, M., KNIGHT, A. L., RAY, A., WONG, V., BROWN, K. R., CALDWELL, G. A., CALDWELL, K. A., STAGLJAR, I. & KRAINC, D. 2012. Identification of novel ATP13A2 interactors and their role in α-synuclein misfolding and toxicity. *Human Molecular Genetics*.

VACCARO, A., PATTEN, S. A., CIURA, S., MAIOS, C., THERRIEN, M., DRAPEAU, P., KABASHI, E. & PARKER, J. A. 2012. Methylene Blue protects against TDP-43 and FUS neuronal toxicity in *C. elegans* and *D. rerio*. *PLoS One,* 7**,** e42117.

VAN GILST, M. R., HADJIVASSILIOU, H. & YAMAMOTO, K. R. 2005. A *Caenorhabditis elegans* nutrient response system partially dependent on nuclear receptor NHR-49. *Proc Natl Acad Sci U S A,* 102**,** 13496-501.

VAN HAM, T., BREITLING, R., SWERTZ, M. & NOLLEN, E. 2009. Neurodegenerative diseases: Lessons from genome-wide screens in small model organisms. *EMBO Molecular Medicine,* 1**,** 360 - 370.

VAN HAM, T. J., THIJSSEN, K. L., BREITLING, R., HOFSTRA, R. M. W., PLASTERK, R. H. A. & NOLLEN, E. A. A. 2008. *C. elegans* model identifies

genetic modifiers of α-Synuclein inclusion formation during aging. *PLoS Genet,* 4**,** e1000027.

VAN HELDEN, J., ANDRE, B. & COLLADO-VIDES, J. 1998. Extracting regulatory sites from the upstream region of yeast genes by computational analysis of oligonucleotide frequencies. *J Mol Biol,* 281**,** 827 - 842.

VAN NOSTRAND, E. L. & KIM, S. K. 2013. Integrative analysis of *C. elegans* modENCODE ChIP-seq data sets to infer gene regulatory interactions. *Genome Research,* 23**,** 941-953.

VARMA, H., CHENG, R., VOISINE, C., HART, A. C. & STOCKWELL, B. R. 2007. Inhibitors of metabolism rescue cell death in Huntington's disease models. *Proceedings of the National Academy of Sciences,* 104**,** 14525-14530.

VARTIAINEN, S., PEHKONEN, P., LAKSO, M., NASS, R. & WONG, G. 2006. Identification of gene expression changes in transgenic *C. elegans* overexpressing human alpha-synuclein. *Neurobiol Dis,* 22**,** 477-86.

VED, R., SAHA, S., WESTLUND, B., PERIER, C., BURNAM, L., SLUDER, A., HOENER, M., RODRIGUES, C. M., ALFONSO, A., STEER, C., LIU, L., PRZEDBORSKI, S. & WOLOZIN, B. 2005. Similar patterns of mitochondrial vulnerability and rescue induced by genetic modification of alpha-synuclein, parkin, and DJ-1 in *Caenorhabditis elegans*. *J Biol Chem,* 280**,** 42655-68.

VELINOV, M., DOLZHANSKAYA, N., GONZALEZ, M., POWELL, E., KONIDARI, I., HULME, W., STAROPOLI, J. F., XIN, W., WEN, G. Y., BARONE, R., COPPEL, S. H., SIMS, K., BROWN, W. T. & ZUCHNER, S. 2012. Mutations in the gene *DNAJC5* cause autosomal dominant Kufs disease in a proportion of cases: study of the Parry family and 8 other families. *PLoS One,* 7**,** e29729.

VESA, J., HELLSTEN, E., VERKRUYSE, L. A., CAMP, L. A., RAPOLA, J., SANTAVUORI, P., HOFMANN, S. L. & PELTONEN, L. 1995. Mutations in the palmitoyl protein thioesterase gene causing infantile neuronal ceroid lipofuscinosis. *Nature,* 376**,** 584-7.

VILARINO-GUELL, C., WIDER, C., ROSS, O. A., DACHSEL, J. C., KACHERGUS, J. M., LINCOLN, S. J., SOTO-ORTOLAZA, A. I., COBB, S. A., WILHOITE, G. J., BACON, J. A., BEHROUZ, B., MELROSE, H. L., HENTATI, E., PUSCHMANN, A., EVANS, D. M., CONIBEAR, E., WASSERMAN, W. W., AASLY, J. O., BURKHARD, P. R., DJALDETTI, R., GHIKA, J., HENTATI, F., KRYGOWSKA-WAJS, A., LYNCH, T., MELAMED, E., RAJPUT, A., RAJPUT, A. H., SOLIDA, A., WU, R. M., UITTI, R. J., WSZOLEK, Z. K., VINGERHOETS, F. & FARRER, M. J. 2011. VPS35 mutations in Parkinson disease. *Am J Hum Genet,* 89**,** 162-7.

VIÑUELA, A., SNOEK, L. B., RIKSEN, J. A. G. & KAMMENGA, J. E. 2010. Genome-wide gene expression analysis in response to organophosphorus pesticide Chlorpyrifos and Diazinon in *C. elegans*. *PLoS One,* 5**,** e12145.

VISWANATHAN, M., KIM, S. K., BERDICHEVSKY, A. & GUARENTE, L. 2005. A role for SIR-2.1 regulation of ER stress response genes in determining *C. elegans* life span. *Dev Cell,* 9**,** 605-15.

VOISINE, C., VARMA, H., WALKER, N., BATES, E. A., STOCKWELL, B. R. & HART, A. C. 2007. Identification of potential therapeutic drugs for huntington's disease using *Caenorhabditis elegans*. *PLoS One,* 2**,** e504.

VOßFELDT, H., BUTZLAFF, M., PRÜßING, K., NÍ CHÁRTHAIGH, R.-A., KARSTEN, P., LANKES, A., HAMM, S., SIMONS, M., ADRYAN, B., SCHULZ, J. B. & VOIGT, A. 2012. Large-scale screen for modifiers of ataxin-3-derived polyglutamine-induced toxicity in *Drosophila*. *PLoS ONE,* 7**,** e47452.

WAINWRIGHT, M. & AMARAL, L. 2005. The phenothiazinium chromophore and the evolution of antimalarial drugs. *Trop Med Int Health,* 10**,** 501-11.

WAN, Q. L., ZHENG, S. Q., WU, G. S. & LUO, H. R. 2013. Aspirin extends the lifespan of *Caenorhabditis elegans* via AMPK and DAF-16/FOXO in dietary restriction pathway. *Exp Gerontol,* 48**,** 499-506.

WANG, H., LIM, P. J., KARBOWSKI, M. & MONTEIRO, M. J. 2009a. Effects of overexpression of huntingtin proteins on mitochondrial integrity. *Hum Mol Genet,* 18**,** 737-52.

WANG, H., LIM, P. J., YIN, C., RIECKHER, M., VOGEL, B. E. & MONTEIRO, M. J. 2006. Suppression of polyglutamine-induced toxicity in cell and animal models of Huntington's disease by ubiquilin. *Human Molecular Genetics,* 15**,** 1025-1041.

WANG, J., FARR, G. W., HALL, D. H., LI, F., FURTAK, K., DREIER, L. & HORWICH, A. L. 2009b. An ALS-linked mutant SOD1 produces a locomotor defect associated with aggregation and synaptic dysfunction when expressed in neurons of *Caenorhabditis elegans*. *PLoS Genet,* 5**,** e1000350.

WANG, P., LAZARUS, B. D., FORSYTHE, M. E., LOVE, D. C., KRAUSE, M. W. & HANOVER, J. A. 2012. O-GlcNAc cycling mutants modulate proteotoxicity in *Caenorhabditis elegans* models of human neurodegenerative diseases. *Proceedings of the National Academy of Sciences*.

WANG, X., CATTANEO, F., RYNO, L., HULLEMAN, J., REIXACH, N. & BUXBAUM, J. N. 2014. The systemic amyloid precursor transthyretin (TTR) behaves as a neuronal stress protein regulated by HSF1 in SH-SY5Y human neuroblastoma cells and APP23 Alzheimer's disease model mice. *The Journal of Neuroscience,* 34**,** 7253-7265.

WEINBERG, M. S. & WOOD, M. J. 2009. Short non-coding RNA biology and neurodegenerative disorders: novel disease targets and therapeutics. *Hum Mol Genet,* 18**,** R27-39.

WEINREB, O., DRIGUES, N., SAGI, Y., REZNICK, A. Z., AMIT, T. & YOUDIM, M. B. 2007. The application of proteomics and genomics to the study of age-related neurodegeneration and neuroprotection. *Antioxid Redox Signal,* 9**,** 169-79.

WHITE, J. G., SOUTHGATE, E., THOMSON, J. N. & BRENNER, S. 1976. The structure of the ventral nerve cord of *Caenorhabditis elegans*. *Philos Trans R Soc Lond B Biol Sci,* 275**,** 327-48.

WHITE, J. G., SOUTHGATE, E., THOMSON, J. N. & BRENNER, S. 1986. The structure of the nervous system of the nematode *Caenorhabditis elegans*. *Philos Trans R Soc Lond B Biol Sci,* 314**,** 1-340.

WIESE, M., ANTEBI, A. & ZHENG, H. 2010. Intracellular trafficking and synaptic function of APL-1 in *Caenorhabditis elegans*. *PLoS One,* 5**,** e12790.

WILLIAMS, T. W., DUMAS, K. J. & HU, P. J. 2010. EAK proteins: novel conserved regulators of *C. elegans* lifespan. *Aging (Albany NY),* 2**,** 742-7.

WILLMORE, L. J. 2005. Antiepileptic drugs and neuroprotection: current status and future roles. *Epilepsy Behav,* 7 Suppl 3**,** S25-8.

WILSON, M. A., SHUKITT-HALE, B., KALT, W., INGRAM, D. K., JOSEPH, J. A. & WOLKOW, C. A. 2006. Blueberry polyphenols increase lifespan and thermotolerance in *Caenorhabditis elegans*. *Aging Cell,* 5**,** 59-68.

WINDERICKX, J., DELAY, C., DE VOS, A., KLINGER, H., PELLENS, K., VANHELMONT, T., VAN LEUVEN, F. & ZABROCKI, P. 2008. Protein folding diseases and neurodegeneration: lessons learned from yeast. *Biochim Biophys Acta,* 1783**,** 1381-95.

WITAN, H., KERN, A., KOZIOLLEK-DRECHSLER, I., WADE, R., BEHL, C. & CLEMENT, A. M. 2008. Heterodimer formation of wild-type and amyotrophic lateral sclerosis-causing mutant Cu/Zn-superoxide dismutase induces toxicity independent of protein aggregation. *Hum Mol Genet,* 17**,** 1373-85.

WITTENBURG, N., EIMER, S., LAKOWSKI, B., ROHRIG, S., RUDOLPH, C. & BAUMEISTER, R. 2000. Presenilin is required for proper morphology and function of neurons in *C. elegans*. *Nature,* 406**,** 306-309.

WOLOZIN, B., GABEL, C., FERREE, A., GUILLILY, M. & EBATA, A. 2011. Watching worms whither: modeling neurodegeneration in *C. elegans*. *Prog Mol Biol Transl Sci,* 100**,** 499-514.

WOOD, J. G., ROGINA, B., LAVU, S., HOWITZ, K., HELFAND, S. L., TATAR, M. & SINCLAIR, D. 2004. Sirtuin activators mimic caloric restriction and delay ageing in metazoans. *Nature,* 430**,** 686-9.

WU, Y., CAO, Z., KLEIN, W. L. & LUO, Y. 2010. Heat shock treatment reduces beta amyloid toxicity in vivo by diminishing oligomers. *Neurobiol Aging,* 31**,** 1055-8.

WU, Y., WU, Z., BUTKO, P., CHRISTEN, Y., LAMBERT, M. P., KLEIN, W. L., LINK, C. D. & LUO, Y. 2006. Amyloid-beta-induced pathological behaviors are suppressed by Ginkgo biloba extract EGb 761 and ginkgolides in transgenic *Caenorhabditis elegans*. *J Neurosci,* 26**,** 13102-13.

WU, Z., SMITH, J. V., PARAMASIVAM, V., BUTKO, P., KHAN, I., CYPSER, J. R. & LUO, Y. 2002. Ginkgo biloba extract EGb 761 increases stress resistance and extends life span of *Caenorhabditis elegans*. *Cell Mol Biol (Noisy-le-grand),* 48**,** 725-31.

XIAO, L., LI, H., ZHANG, J., YANG, F., HUANG, A., DENG, J., LIANG, M., MA, F., HU, M. & HUANG, Z. 2014. Salidroside protects *Caenorhabditis elegans* neurons from polyglutamine-mediated toxicity by reducing oxidative stress. *Molecules,* 19**,** 7757-7769.

YAMANAKA, K., OKUBO, Y., SUZAKI, T. & OGURA, T. 2004. Analysis of the two p97/VCP/Cdc48p proteins of *Caenorhabditis elegans* and their suppression of polyglutamine-induced protein aggregation. *J Struct Biol,* 146**,** 242-250.

YANG, J. S., NAM, H. J., SEO, M., HAN, S. K., CHOI, Y., NAM, H. G., LEE, S. J. & KIM, S. 2011. OASIS: online application for the survival analysis of lifespan assays performed in aging research. *PLoS One,* 6**,** e23525.

YANG, X., ZHANG, P., WU, J., XIONG, S., JIN, N. & HUANG, Z. 2012. The neuroprotective and lifespan-extension activities of *Damnacanthus officinarum* extracts in *Caenorhabditis elegans*. *Journal of Ethnopharmacology,* 141**,** 41-47.

YANIK, M. F., ROHDE, C. B. & PARDO-MARTIN, C. 2011. Technologies for micromanipulating, imaging, and phenotyping small invertebrates and vertebrates. *Annu Rev Biomed Eng,* 13**,** 185-217.

YAO, C., EL KHOURY, R., WANG, W., BYRD, T. A., PEHEK, E. A., THACKER, C., ZHU, X., SMITH, M. A., WILSON-DELFOSSE, A. L. & CHEN, S. G. 2010. LRRK2-mediated neurodegeneration and dysfunction of dopaminergic neurons in a *Caenorhabditis elegans* model of Parkinson's disease. *Neurobiol Dis,* 40**,** 73-81.

YAO, C., JOHNSON, W. M., GAO, Y., WANG, W., ZHANG, J., DEAK, M., ALESSI, D. R., ZHU, X., MIEYAL, J. J., RODER, H., WILSON-DELFOSSE, A. L. & CHEN, S. G. 2012. Kinase inhibitors arrest neurodegeneration in cell and *C. elegans* models of LRRK2 toxicity. *Hum Mol Genet*.

YATIN, S. M., YATIN, M., AULICK, T., AIN, K. B. & BUTTERFIELD, D. A. 1999. Alzheimer's amyloid beta-peptide associated free radicals increase rat embryonic neuronal polyamine uptake and ornithine decarboxylase activity: protective effect of vitamin E. *Neurosci Lett,* 263**,** 17-20.

YUEN, T., WURMBACH, E., PFEFFER, R. L., EBERSOLE, B. J. & SEALFON, S. C. 2002. Accuracy and calibration of commercial oligonucleotide and custom cDNA microarrays. *Nucleic Acids Res,* 30**,** e48.

ZHANG, H., PAN, N., XIONG, S., ZOU, S., LI, H., XIAO, L., CAO, Z., TUNNACLIFFE, A. & HUANG, Z. 2012a. Inhibition of polyglutamine-

mediated proteotoxicity by Astragalus membranaceus polysaccharide through the DAF-16/FOXO transcription factor in *Caenorhabditis elegans*. *Biochemical Journal,* 441**,** 417-424.

ZHANG, K. Y., YANG, S., WARRAICH, S. T. & BLAIR, I. P. 2014. Ubiquilin 2: A component of the ubiquitin-proteasome system with an emerging role in neurodegeneration. *Int J Biochem Cell Biol,* 50C**,** 123-126.

ZHANG, M., LUO, G., ZHOU, Y., WANG, S. & ZHONG, Z. 2013a. Phenotypic screens targeting neurodegenerative diseases. *J Biomol Screen*.

ZHANG, P., JUDY, M., LEE, S.-J. & KENYON, C. 2013b. Direct and indirect gene regulation by a life-extending FOXO protein in *C. elegans*: roles for GATA factors and lipid gene regulators. *Cell Metabolism,* 17**,** 85-100.

ZHANG, T., HWANG, H.-Y., HAO, H., TALBOT, C. & WANG, J. 2012b. *Caenorhabditis elegans* RNA-processing protein TDP-1 regulates protein homeostasis and life span. *Journal of Biological Chemistry,* 287**,** 8371-8382.

ZHANG, T., MULLANE, P. C., PERIZ, G. & WANG, J. 2011. TDP-43 neurotoxicity and protein aggregation modulated by heat shock factor and Insulin/IGF-1 signaling. *Human Molecular Genetics*.

ZHANG, X., SMITH, D. L., MERIIN, A. B., ENGEMANN, S., RUSSEL, D. E., ROARK, M., WASHINGTON, S. L., MAXWELL, M. M., MARSH, J. L., THOMPSON, L. M., WANKER, E. E., YOUNG, A. B., HOUSMAN, D. E., BATES, G. P., SHERMAN, M. Y. & KAZANTSEV, A. G. 2005. A potent small molecule inhibits polyglutamine aggregation in Huntington's disease neurons and suppresses neurodegeneration in vivo. *Proc Natl Acad Sci U S A,* 102**,** 892-7.

ZHANG, Y.-Q., HENDERSON, MICHAEL X., COLANGELO, CHRISTOPHER M., GINSBERG, STEPHEN D., BRUCE, C., WU, T. & CHANDRA, SREEGANGA S. 2012c. Identification of CSPα clients reveals a role in dynamin 1 regulation. *Neuron,* 74**,** 136-150.

ZHANG, Y., CHEN, D., SMITH, M. A., ZHANG, B. & PAN, X. 2012d. Selection of reliable reference genes in *Caenorhabditis elegans* for analysis of nanotoxicity. *PLoS One,* 7**,** e31849.

ZHAO, Y.-L. & WANG, D.-Y. 2012. Formation and regulation of adaptive response in nematode *Caenorhabditis elegans*. *Oxidative Medicine and Cellular Longevity,* 2012**,** 6.

ZHOU, R., YUAN, P., WANG, Y., HUNSBERGER, J. G., ELKAHLOUN, A., WEI, Y., DAMSCHRODER-WILLIAMS, P., DU, J., CHEN, G. & MANJI, H. K. 2008. Evidence for selective microRNAs and their effectors as common long-term targets for the actions of mood stabilizers. *Neuropsychopharmacology,* 34**,** 1395-1405.

ZIMPRICH, A., BENET-PAGES, A., STRUHAL, W., GRAF, E., ECK, S. H., OFFMAN, M. N., HAUBENBERGER, D., SPIELBERGER, S., SCHULTE, E. C., LICHTNER, P., ROSSLE, S. C., KLOPP, N., WOLF, E., SEPPI, K., PIRKER, W., PRESSLAUER, S., MOLLENHAUER, B., KATZENSCHLAGER, R., FOKI, T., HOTZY, C., REINTHALER, E., HARUTYUNYAN, A., KRALOVICS, R., PETERS, A., ZIMPRICH, F., BRUCKE, T., POEWE, W., AUFF, E., TRENKWALDER, C., ROST, B., RANSMAYR, G., WINKELMANN, J., MEITINGER, T. & STROM, T. M. 2011. A mutation in VPS35, encoding a subunit of the retromer complex, causes late-onset Parkinson disease. *Am J Hum Genet,* 89**,** 168-75.

ZIMPRICH, A., BISKUP, S., LEITNER, P., LICHTNER, P., FARRER, M., LINCOLN, S., KACHERGUS, J., HULIHAN, M., UITTI, R. J., CALNE, D. B., STOESSL, A. J., PFEIFFER, R. F., PATENGE, N., CARBAJAL, I. C., VIEREGGE, P., ASMUS, F., MULLER-MYHSOK, B., DICKSON, D. W., MEITINGER, T., STROM, T. M., WSZOLEK, Z. K. & GASSER, T. 2004. Mutations in LRRK2

cause autosomal-dominant parkinsonism with pleomorphic pathology. *Neuron,* 44**,** 601-7.
ZINSMAIER, K., EBERLE, K., BUCHNER, E., WALTER, N. & BENZER, S. 1994. Paralysis and early death in cysteine string protein mutants of *Drosophila*. *Science,* 263**,** 977-980.
ZOGHBI, H. Y. & ORR, H. T. 2000. Glutamine repeats and neurodegeneration. *Annu Rev Neurosci,* 23**,** 217-47.